UNIVERSIDAD DE ANTIOQUIA

1803

Occurrence of hot, dry, and compound dry-hot events in Tropical South America: observational analysis, historical simulations and climate change projections

Juliana Benjumea Garcés

Tesis de maestría presentada para optar al título de Magíster en Ingeniería Ambiental

Directora

Paola Andrea Arias Gómez, PhD

Universidad de Antioquia

Facultad de Ingeniería, Escuela Ambiental

Maestría en Ingeniería Ambiental

Medellín, Antioquia, Colombia

2026

UNIVERSIDAD DE ANTIOQUIA

Cita	(Benjumea, 2026)
Referencia **Estilo APA 7 (2020)**	Benjumea, J. (2026). *Occurrence of hot, dry, and compound dry-hot events in Tropical South America: observational analysis, historical simulations and climate change projections* [Tesis de maestría]. Universidad de Antioquia, Medellín, Colombia.

Maestría en Ingeniería Ambiental

Grupo de Investigación en Ingeniería y Gestión Ambiental – GIGA

CENDOI - Centro de Documentación de Ingeniería

Repositorio Institucional: http://bibliotecadigital.udea.edu.co

Universidad de Antioquia - www.udea.edu.co

El contenido de esta obra corresponde al derecho de expresión de los autores y no compromete el pensamiento institucional de la Universidad de Antioquia ni desata su responsabilidad frente a terceros. Los autores asumen la responsabilidad por los derechos de autor y conexos.

Occurrence of hot, dry, and compound dry-hot events in Tropical South America: observational analysis, historical simulations and climate change projections

Juliana Benjumea Garcés

A thesis submitted in partial fulfillment of the requirements for the degree of:
M.Sc in Environmental Engineering

Advisor:
Paola Andrea Arias Gómez, PhD.

University of Antioquia
Faculty of Engineering, Environmental School
Medellín, Colombia
2026

Agradecimientos

Esta investigación fue financiada por la Universidad de Antioquia mediante el proyecto CODI 2022-55390 - “Seguridad hídrica en Suramérica tropical bajo escenarios de cambio climático” y el Fondo de Becas de Maestría.

Quiero agradecer a mi directora, la profesora Paola Andrea Arias, por su acompañamiento desde el pregrado. Gracias por compartir su conocimiento, por su paciencia y apoyo, y por brindarme la oportunidad de llevar a cabo esta maestría. Al profesor John Alejandro Martínez, por su disposición para atender las múltiples dudas que surgieron a lo largo del proceso y porque sus cursos fueron herramientas valiosas para el desarrollo de este trabajo de investigación.

Agradezco a mi familia por su apoyo incondicional. En especial a mis padres, Lucía y Carlos Mario, por creer en mí y por apoyarme siempre en todos mis proyectos y sueños.

También agradezco a mis colegas, amigos y amigas del SIATA. No tengo duda que este proceso hubiera sido muy diferente de no haber contado con el apoyo de personas que compartieron su conocimiento, brindaron ideas para este trabajo, fueron soporte emocional y me escucharon en mis momentos de incertidumbre. Especialmente, quiero agradecer a Julián Sepúlveda, Isabel Correa, Carolina Cruz, Juan Diego Mantilla, Duvan Nieves, Santiago Hernández, Andrés Bilbao, Juliana Sánchez y Luisa Gutiérrez.

Finalmente, agradezco a las evaluadoras, las doctoras Soledad Collazo y Ana María Durán, por sus valiosos comentarios y sugerencias, que contribuyeron a mejorar el trabajo, así como por el tiempo dedicado a revisarlo con detalle.

Abstract

Extreme hydroclimatic events have increased in frequency and intensity due to climate change, generating risks for natural and human systems, especially in vulnerable regions such as South America. Hot and dry extremes have attracted growing scientific interest due to their negative impacts, which are intensified when they occur simultaneously. In this work, we characterize the occurrence of hot events (HEs), dry events (DEs), and compound dry and hot events (CDHEs) in tropical South America (TSA) during 1983–2024. We evaluate the ability of a set of CMIP6/HighResMIP models to reproduce their main characteristics (number of events, median duration, median gap between events, and median intensity), and analyze projected changes under different emission scenarios in the near and long term. During the observational period (1983-2024), a seasonal pattern was identified in HEs, with higher frequency in northern South America during December-May and in the Amazon during June–August. Meteorological droughts were more frequent, but agricultural and ecological droughts were longer in duration. CDHEs occurred less frequently than HEs, but with longer duration, increasing in frequency in recent decades. Temperature was the dominant factor during CDHEs in most of the TSA. Individual models and the ensemble median showed limitations in adequately reproducing the number, duration, and gap between events of observed extreme events. In contrast, they better reproduced the temperature intensity associated with HEs and CDHEs. The main limitations included overestimation of the number and duration of events and underestimation of the gap between events in much of TSA, with high agreement between models ($> 80\%$) in some regions. Projections throughout the 21st century indicate that HEs and CDHEs will be more frequent, longer-lasting, and more intense in TSA under all scenarios, especially in the long term and under higher emissions. Increases in CDHEs are primarily driven by increases in HEs, even though the frequency of DEs decreases in some areas, particularly between December and May. The observation-based analysis showed that the northern Andes, Orinoco, Brazilian Amazon, and northern Cerrado were among the regions with the largest increases in the frequency of HEs, DEs, and CDHEs. For these regions, an increase in the number of hot and dry days, longer event durations, higher maximum temperature intensity, and more severe droughts is expected by the end of the century, especially under the high-emission scenario.

Keywords: Drought; Hot extremes; Compound events; CMIP6; Tropical South America.

Contents

1 Introduction **21**

2 Objectives **24**
2.1 General Objective 24
2.2 Specific Objectives 24

3 Occurrence of hot, dry, and compound dry and hot events in Tropical South America: Observational Analysis (1981–2024) **25**
3.1 Introduction 25
3.2 Data and methodology 27
3.2.1 Study region 27
3.2.2 Gridded data 29
3.2.3 Events identification 29
3.2.4 Dominant factor in CDHEs 31
3.2.5 Trend Analysis 31
3.3 Results 31
3.3.1 Hot events 31
3.3.2 Dry events 36
3.3.3 Compound dry and hot events 40
3.3.4 Hot, dry, and compound events in the TSA regions with the largest changes . 46
3.4 Summary and discussion 50

4 Assessing the performance of CMIP6/HighResMIP models in simulating hot, dry, and compound dry and hot events in Tropical South America (1983–2014) **53**
4.1 Introduction 53
4.2 Data and methodology 54
4.2.1 CMIP6/HighResMIP simulations 54
4.2.2 Gridded data 57
4.2.3 Model evaluation 57
4.3 Results 58
4.3.1 Performance of CMIP6/HighResMIP models in the simulation of maximum temperature and precipitation 58
4.3.2 Performance of CMIP6/HighResMIP models in the simulation of hot events . 61
4.3.3 Performance of CMIP6/HighResMIP models in the simulation of Dry events 65
4.3.4 Performance of CMIP6/HighResMIP models in the simulation of compound dry and hot events 70
4.4 Summary and discussion 76

5 Projected changes in the characteristics of hot, dry, and compound dry-hot events under different climate change scenarios 78
5.1 Introduction . . . 78
5.2 Data and methodology . . . 80
5.2.1 CMIP6/HighResMIP simulations . . . 80
5.2.2 Events identification . . . 82
5.2.3 Projected changes and temporal evolution of HEs, DEs, and CDHEs . . . 82
5.3 Results . . . 83
5.3.1 Projected changes of hot events . . . 83
5.3.2 Trends in the characteristics of HEs in the TSA regions under climate change scenarios . . . 91
5.3.3 Projected changes of dry events . . . 96
5.3.4 Trends in the characteristics of DEs in the TSA regions under climate change scenarios . . . 104
5.3.5 Projected changes of compound dry and hot events . . . 109
5.3.6 Trends in the characteristics of CDHEs in the TSA regions under climate change scenarios . . . 120
5.4 Summary and discussion . . . 125

6 General conclusions and future research 129

References 131

Supplementary material 145

A Occurrence of hot, dry, and compound dry and hot events in Tropical South America: Observational Analysis (1981–2024) 145

B Assessing the performance of CMIP6/HighResMIP models in simulating hot, dry, and compound dry and hot events in Tropical South America (1983–2014) 154

C Projected changes in the characteristics of hot, dry, and compound dry-hot events under different climate change scenarios 170

List of Figures

1.1 Changes observed in the frequency and intensity of hot extremes (top panel) and agricultural and ecological droughts (bottom panel) from 1950 to 2019. The red hexagons indicate changes in hot extremes, while yellow hexagons indicate changes in agricultural and ecological droughts, showing a medium to high level of confidence in the increase in the frequency and intensity of these extremes in the corresponding region. The green hexagons (bottom panel) indicate medium to high confidence in the decrease in the frequency and intensity of agricultural and ecological droughts. Striped hexagons (white and light-grey) indicate low agreement on the type of change, while the gray hexagons indicate limited information to detect changes. The filled dots within each hexagon represent the level of confidence in human contribution to the observed changes, ranging from high confidence (three dots) to low confidence due to limited evidence (one unfilled dot). Adapted from Arias et al. (2021a). 22

3.1 Land cover over Tropical South America (TSA) according to the Copernicus Global Land Service (`https://land.copernicus.eu/en`). The black boxes indicate the four regions where the largest changes in the occurrence of HEs, DEs, and CDHEs were observed during 1981-2024: (A) northern Andes, (B) Orinoco, (C) Brazilian Amazon, and (D) northern Cerrado. 28

3.2 Seasonal count of Hot Events (number of HEs) based on CPC and ERA5 datasets over tropical South America during the 1981–2024 period. Events were identified using the 90th (P90) and 95th (P95) percentile thresholds. White areas indicate regions where no HEs were recorded in these datasets. 33

3.3 Seasonal median gap (days) between Hot Events (HEs) based on CPC and ERA5 datasets over tropical South America during the 1981–2024 period. The panel shows the median time gap between events identified using the 90th (P90) and 95th (P95) percentile thresholds. White areas indicate regions where no HEs were recorded in these datasets. 33

3.4 Seasonal median duration (days) of Hot Events (HEs) based on CPC and ERA5 datasets over tropical South America during the 1981–2024 period. Events were identified using the 90th (P90) and 95th (P95) percentile thresholds. White areas indicate regions where no HEs were recorded in these datasets. 34

3.5 Seasonal median intensity (°C) of Hot Events (HEs) based on CPC and ERA5 datasets over tropical South America during the 1981–2024 period. Events were identified using the 90th (P90) and 95th (P95) percentile thresholds. White areas indicate regions where no HEs were recorded in these datasets. 34

3.6 Changes in the characteristics of Hot Events (HEs) between 1981–2002 and 2003–2024 over tropical South America, based on CPC and ERA5 datasets using the 90th (P90) and 95th (P95) percentile thresholds. Dots denote statistically significant differences based on the Wilcoxon test ($p < 0.05$). 36
3.7 Seasonal count of Dry Events (DEs) based on CHIRPS v2 and ERA5 datasets over tropical South America during the 1981–2024 period. DEs were identified using SPI3 and SPI6. 37
3.8 Seasonal median gap (months) between Dry Events (DEs) based on CHIRPS v2 and ERA5 datasets over tropical South America during the 1981–2024 period. The panel shows the median time gap between events identified using SPI3 and SPI6. 37
3.9 Seasonal median duration (months) of Dry Events (DEs) based on CHIRPS v2 and ERA5 datasets over tropical South America during the 1981–2024 period. DEs were identified using SPI3 and SPI6. 38
3.10 Seasonal median SPI intensity of Dry Events (DEs) based on CHIRPS v2 and ERA5 datasets over tropical South America during the 1981–2024 period. DEs were identified using SPI3 and SPI6. The drought category (McKee et al., 1993) is shown: Moderate ($-1.5 \leq \text{SPI} < -1.0$) and Severe ($-2.0 \leq \text{SPI} < -1.5$). 38
3.11 Changes in the characteristics of Dry Events (DEs) between 1981–2002 and 2003–2024 over tropical South America, based on CHIRPS v2 and ERA5 datasets using SPI3 and SPI6 indices. Dots denote statistically significant differences based on the Wilcoxon test ($p < 0.05$). 40
3.12 Seasonal count of Compound Dry and Hot Events (CDHEs) based on CHIRPSv2-CPC and ERA5 datasets over tropical South America during the 1981–2024 period. CDHEs were identified by the concurrent occurrence of SPI3-P90 and SPI3-P95 events. White areas indicate regions where no CDHEs were recorded in these datasets. 41
3.13 Seasonal median gap (days) between Compound Dry and Hot Events (CDHEs) based on CHIRPSv2/CPC and ERA5 datasets over tropical South America during the 1981–2024 period. The panel shows the median number of days between CDHEs, identified by the concurrent occurrence of SPI3-P90 and SPI3-P95 events. White areas indicate regions where no CDHEs were recorded in these datasets. 42
3.14 Seasonal median duration (days) of Compound Dry and Hot Events (CDHEs) based on CHIRPSv2/CPC and ERA5 datasets over tropical South America during the 1981–2024 period. CDHEs were identified by the concurrent occurrence of SPI3-P90 and SPI3-P95 events. White areas indicate regions where no CDHEs were recorded in these datasets. 42
3.15 Difference in Seasonal median intensity (°C) between Compound Dry and Hot Events (CDHEs) and Hot Events (HEs) based on CPC and ERA5 datasets over tropical South America. White areas indicate regions where no CDHEs were recorded in these datasets. 43
3.16 Difference in seasonal median SPI3 intensity between Compound Dry and Hot Events (CDHEs) and Dry Events (DEs) based on CHIRPS v2 and ERA5 datasets over tropical South America. White areas indicate regions where no CDHEs were recorded in these datasets. 43
3.17 Changes in the characteristics of Compound Dry and Hot Events (CDHEs) (SPI3/P90 and SPI3/P95) between 1981–2002 and 2003–2024 over tropical South America, based on CPC/CHIRPSv2 and ERA5 datasets. Dots denote statistically significant differences based on the Wilcoxon test ($p < 0.05$). 44

3.18 Dominant seasonal factor of Compound Dry and Hot Events (CDHEs) (SPI3-P90 and SPI3-P95) based on CHIRPSv2/CPC and ERA5 datasets over tropical South America. 45
3.19 Temporal Evolution of Hot Events (HEs) based on CPC and ERA5 datasets in a) northern Andes, b) Orinoco, c) Brazilian Amazon, and d) northern Cerrado during 1981–2024. The panel shows the HEs identified using the 90th (P90) percentile threshold. 47
3.20 Temporal Evolution of Dry Events (DEs) based on CHIRPS v2 and ERA5 datasets in a) northern Andes, b) Orinoco, c) Brazilian Amazon, and d) northern Cerrado during 1981–2024. The panel shows the DEs identified using SPI3. 48
3.21 Temporal Evolution of Compound Dry and Hot Events (CDHEs) based on CHIRPSv2/CPC and ERA5 datasets in a) northern Andes, b) Orinoco, c) Brazilian Amazon, and d) northern Cerrado during 1981–2024. The panel shows the events identified using SPI3-P90. 49

4.1 Seasonal evaluation of daily maximum temperature over tropical South America. (a–d) Taylor diagrams. (e–h) Seasonal climatology for CHIRTS (reference). (i–l) Multimodel seasonal median. (m–p) Multimodel seasonal median biases. Dots indicate where at least 80 % of the CMIP6/HighResMIP models agree on the sign of the multimodel median bias. All spatial fields (e–p) are shown at a common resolution of 1° × 1°. 59
4.2 Seasonal evaluation of daily precipitation over tropical South America. (a–d) Taylor diagrams. (e–h) Seasonal climatology for CHIRPS v2 (reference). (i–l) Multimodel seasonal median. (m–p) Multimodel seasonal median biases. Dots indicate where at least 80 % of the CMIP6/HighResMIP models agree on the sign of the multimodel median bias. All spatial fields (e–p) are shown at a common resolution of 1° × 1°. . 60
4.3 Seasonal evaluation of count of Hot Events (number of HEs) over tropical South America. (a–d) Taylor diagrams. (e–h) Seasonal climatology for CHIRTS (reference). (i–l) Multimodel seasonal median. (m–p) Multimodel seasonal median biases. Dots indicate where at least 80 % of the CMIP6/HighResMIP models agree on the sign of the multimodel median bias. All spatial fields (e–p) are shown at a common resolution of 1° × 1°. 61
4.4 Seasonal evaluation of median duration of Hot Events (HEs) over tropical South America. (a–d) Taylor diagrams. (e–h) Seasonal climatology for CHIRTS (reference). (i–l) Multimodel seasonal median. (m–p) Multimodel seasonal median biases. Dots indicate where at least 80 % of the CMIP6/HighResMIP models agree on the sign of the multimodel median bias. All spatial fields (e–p) are shown at a common resolution of 1° × 1°. 62
4.5 Seasonal evaluation of median gap between Hot Events (HEs) over tropical South America. (a–d) Taylor diagrams. (e–h) Seasonal climatology for CHIRTS (reference). (i–l) Multimodel seasonal median. (m–p) Multimodel seasonal median biases. Dots indicate where at least 80 % of the CMIP6/HighResMIP models agree on the sign of the multimodel median bias. All spatial fields (e–p) are shown at a common resolution of 1° × 1°. 63

4.6 Seasonal evaluation of median intensity of Hot Events (HEs) over tropical South America. (a–d) Taylor diagrams. (e–h) Seasonal climatology for CHIRTS (reference). (i–l) Multimodel seasonal median. (m–p) Multimodel seasonal median biases. Dots indicate where at least 80 % of the CMIP6/HighResMIP models agree on the sign of the multimodel median bias. All spatial fields (e–p) are shown at a common resolution of 1° × 1°. 64
4.7 Seasonal evaluation of count of Dry Events (number of DEs) over tropical South America. (a–d) Taylor diagrams. (e–h) Seasonal climatology for CHIRPS v2 (reference). (i–l) Multimodel seasonal median. (m–p) Multimodel seasonal median biases. Dots indicate where at least 80 % of the CMIP6/HighResMIP models agree on the sign of the multimodel median bias. All spatial fields (e–p) are shown at a common resolution of 1° × 1°. 66
4.8 Seasonal evaluation of median duration of Dry Events (DEs) over tropical South America. (a–d) Taylor diagrams. (e–h) Seasonal climatology for CHIRPS v2 (reference). (i–l) Multimodel seasonal median. (m–p) Multimodel seasonal median biases. Dots indicate where at least 80 % of the CMIP6/HighResMIP models agree on the sign of the multimodel median bias. All spatial fields (e–p) are shown at a common resolution of 1° × 1°. 67
4.9 Seasonal evaluation of median gap between Dry Events (DEs) over tropical South America. (a–d) Taylor diagrams. (e–h) Seasonal climatology for CHIRPS v2 (reference). (i–l) Multimodel seasonal median. (m–p) Multimodel seasonal median biases. Dots indicate where at least 80 % of the CMIP6/HighResMIP models agree on the sign of the multimodel median bias. All spatial fields (e–p) are shown at a common resolution of 1° × 1°. 68
4.10 Seasonal evaluation of median intensity of Dry Events (DEs) over tropical South America. (a–d) Taylor diagrams. (e–h) Seasonal climatology for CHIRPS v2 (reference). (i–l) Multimodel seasonal median. (m–p) Multimodel seasonal median biases. Dots indicate where at least 80 % of the CMIP6/HighResMIP models agree on the sign of the multimodel median bias. All spatial fields (e–p) are shown at a common resolution of 1° × 1°. 69
4.11 Seasonal evaluation of count of Compound Dry and Hot Events (number of CDHEs) over tropical South America. (a–d) Taylor diagrams. (e–h) Seasonal climatology for CHIRPS v2/CHIRTS (reference). (i–l) Multimodel seasonal median. (m–p) Multimodel seasonal median biases. Dots indicate where at least 80 % of the CMIP6/HighResMIP models agree on the sign of the multimodel median bias. All spatial fields (e–p) are shown at a common resolution of 1° × 1°. 71
4.12 Seasonal evaluation of median duration of Compound Dry and Hot Events (CDHEs) over tropical South America. (a–d) Taylor diagrams. (e–h) Seasonal climatology for CHIRPS v2/CHIRTS (reference). (i–l) Multimodel seasonal median. (m–p) Multimodel seasonal median biases. Dots indicate where at least 80 % of the CMIP6/HighResMIP models agree on the sign of the multimodel median bias. All spatial fields (e–p) are shown at a common resolution of 1° × 1°. 72
4.13 Seasonal evaluation of median gap between Compound Dry and Hot Events (CDHEs) over tropical South America. (a–d) Taylor diagrams. (e–h) Seasonal climatology for CHIRPS v2/CHIRTS (reference). (i–l) Multimodel seasonal median. (m–p) Multimodel seasonal median biases. Dots indicate where at least 80 % of the CMIP6/HighResMIP models agree on the sign of the multimodel median bias. All spatial fields (e–p) are shown at a common resolution of 1° × 1°. 73

4.14 Seasonal evaluation of median intensity (SPI) of Compound Dry and Hot Events (CDHEs) over tropical South America. (a–d) Taylor diagrams. (e–h) Seasonal climatology for CHIRPS v2 (reference). (i–l) Multimodel seasonal median. (m–p) Multimodel seasonal median biases. Dots indicate where at least 80 % of the CMIP6/HighResMIP models agree on the sign of the multimodel median bias. All spatial fields (e–p) are shown at a common resolution of 1° × 1°. 74
4.15 Seasonal evaluation of median intensity (°C) of Compound Dry and Hot Events (CDHEs) over tropical South America. (a–d) Taylor diagrams. (e–h) Seasonal climatology for CHIRTS (reference). (i–l) Multimodel seasonal median. (m–p) Multimodel seasonal median biases. Dots indicate where at least 80 % of the CMIP6/HighResMIP models agree on the sign of the multimodel median bias. All spatial fields (e–p) are shown at a common resolution of 1° × 1°. 75

5.1 Projected changes in the seasonal number of Hot Events (HEs) for the near-term period (2021–2040) based on the ensemble median under different emission scenarios: SSP1-2.6 (a–d), SSP2-4.5 (e–h), SSP3-7.0 (i–l), and SSP5-8.5 (m–p) from CMIP6, and HighresFuture (HighresFuture) (q–t) from HighResMIP. Dots indicate grid points where at least 80 % of the CMIP6 or HighResMIP models agree on the sign of the projected change. Black rectangles highlight the four subregions: (A) northern Andes, (B) Orinoco, (C) Brazilian Amazon, and (D) northern Cerrado. All spatial fields are shown at a common resolution of 1° × 1°. 83
5.2 Projected changes in the seasonal number of Hot Events (HEs) for the long-term period (2081–2100) based on the ensemble median under different emission scenarios: SSP1-2.6 (a–d), SSP2-4.5 (e–h), SSP3-7.0 (i–l), and SSP5-8.5 (m–p) from CMIP6. Dots indicate grid points where at least 80 % of the CMIP6 models agree on the sign of the projected change. Black rectangles highlight the four regions: (A) northern Andes, (B) Orinoco, (C) Brazilian Amazon, and (D) northern Cerrado. All spatial fields are shown at a common resolution of 1° × 1°. 84
5.3 Projected changes in the seasonal median duration (days) of Hot Events (HEs) for the near-term period (2021–2040) based on the ensemble median under different emission scenarios: SSP1-2.6 (a–d), SSP2-4.5 (e–h), SSP3-7.0 (i–l), and SSP5-8.5 (m–p) from CMIP6, and HighresFuture (HighresFuture) (q–t) from HighResMIP. Dots indicate grid points where at least 80 % of the CMIP6 or HighResMIP models agree on the sign of the projected change. Black rectangles highlight the four regions: (A) northern Andes, (B) Orinoco, (C) Brazilian Amazon, and (D) northern Cerrado. All spatial fields are shown at a common resolution of 1° × 1°. 85
5.4 Projected changes in the seasonal median duration (days) of Hot Events (HEs) for the long-term period (2081–2100) based on the ensemble median under different emission scenarios: SSP1-2.6 (a–d), SSP2-4.5 (e–h), SSP3-7.0 (i–l), and SSP5-8.5 (m–p) from CMIP6. Dots indicate grid points where at least 80 % of the CMIP6 models agree on the sign of the projected change. Black rectangles highlight the four regions: (A) northern Andes, (B) Orinoco, (C) Brazilian Amazon, and (D) northern Cerrado. All spatial fields are shown at a common resolution of 1° × 1°. 86

5.5 Projected changes in the seasonal median gap (days) between Hot Events (HEs) for the near-term period (2021–2040) based on the ensemble median under different emission scenarios: SSP1-2.6 (a–d), SSP2-4.5 (e–h), SSP3-7.0 (i–l), and SSP5-8.5 (m–p) from CMIP6, and HighresFuture (HighresFuture) (q–t) from HighResMIP. Dots indicate grid points where at least 80 % of the CMIP6 or HighResMIP models agree on the sign of the projected change. Black rectangles highlight the four regions: (A) northern Andes, (B) Orinoco, (C) Brazilian Amazon, and (D) northern Cerrado. All spatial fields are shown at a common resolution of 1° × 1°. 87
5.6 Projected changes in the seasonal median gap (days) between Hot Events (HEs) for the long-term period (2081–2100) based on the ensemble median under different emission scenarios: SSP1-2.6 (a–d), SSP2-4.5 (e–h), SSP3-7.0 (i–l), and SSP5-8.5 (m–p) from CMIP6. Dots indicate grid points where at least 80 % of the CMIP6 models agree on the sign of the projected change. Black rectangles highlight the four regions: (A) northern Andes, (B) Orinoco, (C) Brazilian Amazon, and (D) northern Cerrado. All spatial fields are shown at a common resolution of 1° × 1°. 88
5.7 Projected changes in the seasonal median intensity (°C) of Hot Events (HEs) for the near-term period (2021–2040) based on the ensemble median under different emission scenarios: SSP1-2.6 (a–d), SSP2-4.5 (e–h), SSP3-7.0 (i–l), and SSP5-8.5 (m–p) from CMIP6, and HighresFuture (HighresFuture) (q–t) from HighResMIP. Dots indicate grid points where at least 80 % of the CMIP6 or HighResMIP models agree on the sign of the projected change. Black rectangles highlight the four regions: (A) northern Andes, (B) Orinoco, (C) Brazilian Amazon, and (D) northern Cerrado. All spatial fields are shown at a common resolution of 1° × 1°. 89
5.8 Projected changes in the seasonal median intensity (°C) of Hot Events (HEs) for the long-term period (2081–2100) based on the ensemble median under different emission scenarios: SSP1-2.6 (a–d), SSP2-4.5 (e–h), SSP3-7.0 (i–l), and SSP5-8.5 (m–p) from CMIP6. Dots indicate grid points where at least 80 % of the CMIP6 models agree on the sign of the projected change. Black rectangles highlight the four regions: (A) northern Andes, (B) Orinoco, (C) Brazilian Amazon, and (D) northern Cerrado. All spatial fields are shown at a common resolution of 1° × 1°. 90
5.9 Time series of hot events (HEs) characteristics for the northern Andes region, based on the ensemble median. The 1983–2014 series corresponds to the multimodel median of the historical simulations (gray line). For the 2015–2100 period (2015–2050 for the HighresFuture scenario), the ensemble median for each of the scenarios considered are shown: SSP1-2.6 (blue line), SSP2-4.5 (yellow line), SSP3-7.0 (orange line), SSP5-8.5 (red line), and HighresFuture (purple line). The shaded areas indicate the spread associated with the historical simulation or each scenario, calculated from the minimum and maximum values of the multimodel ensemble. 91
5.10 Time series of hot events (HEs) characteristics for the Orinoco region based on the ensemble median. The 1983–2014 series corresponds to the multimodel median of the historical simulations (gray line). For the 2015–2100 period (2015–2050 for the HighresFuture scenario), the ensemble median for each of the scenarios considered are shown: SSP1-2.6 (blue line), SSP2-4.5 (yellow line), SSP3-7.0 (orange line), SSP5-8.5 (red line), and HighresFuture (purple line). The shaded areas indicate the spread associated with the historical simulation or each scenario, calculated from the minimum and maximum values of the multimodel ensemble. 92

5.11 Time series of hot events (HEs) characteristics for the Brazilian Amazon region based on the ensemble median. The 1983–2014 series corresponds to the multimodel median of the historical simulations (gray line). For the 2015–2100 period (2015–2050 for the HighresFuture scenario), the ensemble median for each of the scenarios considered are shown: SSP1-2.6 (blue line), SSP2-4.5 (yellow line), SSP3-7.0 (orange line), SSP5-8.5 (red line), and HighresFuture (purple line). The shaded areas indicate the spread associated with the historical simulation or each scenario, calculated from the minimum and maximum values of the multimodel ensemble. 93
5.12 Time series of hot events (HEs) characteristics for the northern Cerrado region based on the ensemble median. The 1983–2014 series corresponds to the multimodel median of the historical simulations (gray line). For the 2015–2100 period (2015–2050 for the HighresFuture scenario), the ensemble median for each of the scenarios considered are shown: SSP1-2.6 (blue line), SSP2-4.5 (yellow line), SSP3-7.0 (orange line), SSP5-8.5 (red line), and HighresFuture (purple line). The shaded areas indicate the spread associated with the historical simulation or each scenario, calculated from the minimum and maximum values of the multimodel ensemble. 94
5.13 Projected changes in the seasonal count of Dry Events (DEs) for the near-term period (2021–2040) based on the ensemble median under different emission scenarios: SSP1-2.6 (a–d), SSP2-4.5 (e–h), SSP3-7.0 (i–l), and SSP5-8.5 (m–p) from CMIP6, and HighresFuture (HighresFuture) (q–t) from HighResMIP. Dots indicate grid points where at least 80 % of the CMIP6 or HighResMIP models agree on the sign of the projected change. Black rectangles highlight the four subregions: (A) northern Andes, (B) Orinoco, (C) Brazilian Amazon, and (D) northern Cerrado. All spatial fields are shown at a common resolution of 1° × 1°. 96
5.14 Projected changes in the seasonal count of Dry Events (DEs) for the long-term period (2081–2100) based on the ensemble median under different emission scenarios: SSP1-2.6 (a–d), SSP2-4.5 (e–h), SSP3-7.0 (i–l), and SSP5-8.5 (m–p) from CMIP6. Dots indicate grid points where at least 80 % of the CMIP6 models agree on the sign of the projected change. Black rectangles highlight the four regions: (A) northern Andes, (B) Orinoco, (C) Brazilian Amazon, and (D) northern Cerrado. All spatial fields are shown at a common resolution of 1° × 1°. 97
5.15 Projected changes in the seasonal median duration (months) of Dry Events (DEs) for the near-term period (2021–2040) based on the ensemble median under different emission scenarios: SSP1-2.6 (a–d), SSP2-4.5 (e–h), SSP3-7.0 (i–l), and SSP5-8.5 (m–p) from CMIP6, and HighresFuture (HighresFuture) (q–t) from HighResMIP. Dots indicate grid points where at least 80 % of the CMIP6 or HighResMIP models agree on the sign of the projected change. Black rectangles highlight the four subregions: (A) northern Andes, (B) Orinoco, (C) Brazilian Amazon, and (D) northern Cerrado. All spatial fields are shown at a common resolution of 1° × 1°. 98
5.16 Projected changes in the seasonal median duration (months) of Dry Events (DEs) for the long-term period (2081–2100) based on the ensemble median under different emission scenarios: SSP1-2.6 (a–d), SSP2-4.5 (e–h), SSP3-7.0 (i–l), and SSP5-8.5 (m–p) from CMIP6. Dots indicate grid points where at least 80 % of the CMIP6 models agree on the sign of the projected change. Black rectangles highlight the four regions: (A) northern Andes, (B) Orinoco, (C) Brazilian Amazon, and (D) northern Cerrado. All spatial fields are shown at a common resolution of 1° × 1°. 99

5.17 Projected changes in the seasonal median gap (months) between Dry Events (DEs) for the near-term period (2021–2040) based on the ensemble median under different emission scenarios: SSP1-2.6 (a–d), SSP2-4.5 (e–h), SSP3-7.0 (i–l), and SSP5-8.5 (m–p) from CMIP6, and HighresFuture (HighresFuture) (q–t) from HighResMIP. Dots indicate grid points where at least 80 % of the CMIP6 or HighResMIP models agree on the sign of the projected change. Black rectangles highlight the four subregions: (A) northern Andes, (B) Orinoco, (C) Brazilian Amazon, and (D) northern Cerrado. All spatial fields are shown at a common resolution of 1° × 1°. 100
5.18 Projected changes in the seasonal median gap (months) between Dry Events (DEs) for the long-term period (2081–2100) based on the ensemble median under different emission scenarios: SSP1-2.6 (a–d), SSP2-4.5 (e–h), SSP3-7.0 (i–l), and SSP5-8.5 (m–p) from CMIP6. Dots indicate grid points where at least 80 % of the CMIP6 models agree on the sign of the projected change. Black rectangles highlight the four regions: (A) northern Andes, (B) Orinoco, (C) Brazilian Amazon, and (D) northern Cerrado. All spatial fields are shown at a common resolution of 1° × 1°. 101
5.19 Projected changes in the seasonal median intensity (SPI) of Dry Events (DEs) for the near-term period (2021–2040) based on the ensemble median under different emission scenarios: SSP1-2.6 (a–d), SSP2-4.5 (e–h), SSP3-7.0 (i–l), and SSP5-8.5 (m–p) from CMIP6, and HighresFuture (HighresFuture) (q–t) from HighResMIP. Dots indicate grid points where at least 80 % of the CMIP6 or HighResMIP models agree on the sign of the projected change. Black rectangles highlight the four regions: (A) northern Andes, (B) Orinoco, (C) Brazilian Amazon, and (D) northern Cerrado. All spatial fields are shown at a common resolution of 1° × 1°. 102
5.20 Projected changes in the seasonal median intensity (SPI) of Dry Events (DEs) for the long-term period (2081–2100) based on the ensemble median under different emission scenarios: SSP1-2.6 (a–d), SSP2-4.5 (e–h), SSP3-7.0 (i–l), and SSP5-8.5 (m–p) from CMIP6. Dots indicate grid points where at least 80 % of the CMIP6 models agree on the sign of the projected change. Black rectangles highlight the four regions: (A) northern Andes, (B) Orinoco, (C) Brazilian Amazon, and (D) northern Cerrado. All spatial fields are shown at a common resolution of 1° × 1°. 103
5.21 Time series of dry events (DEs) characteristics for the northern Andes region based on the ensemble median. The 1983–2014 series corresponds to the multimodel median of the historical simulations (gray line). For the 2015–2100 period (2015–2050 for the HighresFuture scenario), the ensemble median for each of the scenarios considered are shown: SSP1-2.6 (blue line), SSP2-4.5 (yellow line), SSP3-7.0 (orange line), SSP5-8.5 (red line), and HighresFuture (purple line). The shaded areas indicate the spread associated with the historical simulation or each scenario, calculated from the minimum and maximum values of the multimodel ensemble. 105
5.22 Time series of dry events (DEs) characteristics for the Orinoco region based on the ensemble median. The 1983–2014 series corresponds to the multimodel median of the historical simulations (gray line). For the 2015–2100 period (2015–2050 for the HighresFuture scenario), the ensemble median for each of the scenarios considered are shown: SSP1-2.6 (blue line), SSP2-4.5 (yellow line), SSP3-7.0 (orange line), SSP5-8.5 (red line), and HighresFuture (purple line). The shaded areas indicate the spread associated with the historical simulation or each scenario, calculated from the minimum and maximum values of the multimodel ensemble. 106

5.23 Time series of dry events (DEs) characteristics for the Brazilian Amazon region based on the ensemble median. The 1983–2014 series corresponds to the multimodel median of the historical simulations (gray line). For the 2015–2100 period (2015–2050 for the HighresFuture scenario), the ensemble median for each of the scenarios considered are shown: SSP1-2.6 (blue line), SSP2-4.5 (yellow line), SSP3-7.0 (orange line), SSP5-8.5 (red line), and HighresFuture (purple line). The shaded areas indicate the spread associated with the historical simulation or each scenario, calculated from the minimum and maximum values of the multimodel ensemble. 107
5.24 Time series of dry events (DEs) characteristics for the northern Cerrado region based on the ensemble median. The 1983–2014 series corresponds to the multimodel median of the historical simulations (gray line). For the 2015–2100 period (2015–2050 for the HighresFuture scenario), the ensemble median for each of the scenarios considered are shown: SSP1-2.6 (blue line), SSP2-4.5 (yellow line), SSP3-7.0 (orange line), SSP5-8.5 (red line), and HighresFuture (purple line). The shaded areas indicate the spread associated with the historical simulation or each scenario, calculated from the minimum and maximum values of the multimodel ensemble. 108
5.25 Projected changes in the seasonal count of Compound Dry and Hot Events (CDHEs) for the near-term period (2021–2040) based on the ensemble median under different emission scenarios: SSP1-2.6 (a–d), SSP2-4.5 (e–h), SSP3-7.0 (i–l), and SSP5-8.5 (m–p) from CMIP6, and HighresFuture (HighresFuture) (q–t) from HighResMIP. Dots indicate grid points where at least 80 % of the CMIP6 or HighResMIP models agree on the sign of the projected change. Black rectangles highlight the four subregions: (A) northern Andes, (B) Orinoco, (C) Brazilian Amazon, and (D) northern Cerrado. All spatial fields are shown at a common resolution of 1° × 1°. 109
5.26 Projected changes in the seasonal count of Compound Dry and Hot Events (CDHEs) for the long-term period (2081–2100) based on the ensemble median under different emission scenarios: SSP1-2.6 (a–d), SSP2-4.5 (e–h), SSP3-7.0 (i–l), and SSP5-8.5 (m–p) from CMIP6. Dots indicate grid points where at least 80 % of the CMIP6 models agree on the sign of the projected change. Black rectangles highlight the four regions: (A) northern Andes, (B) Orinoco, (C) Brazilian Amazon, and (D) northern Cerrado. All spatial fields are shown at a common resolution of 1° × 1°. 111
5.27 Projected changes in the seasonal median duration (days) of Compound Dry and Hot Events (CDHEs) for the near-term period (2021–2040) based on the ensemble median under different emission scenarios: SSP1-2.6 (a–d), SSP2-4.5 (e–h), SSP3-7.0 (i–l), and SSP5-8.5 (m–p) from CMIP6, and HighresFuture (HighresFuture) (q–t) from HighResMIP. Dots indicate grid points where at least 80 % of the CMIP6 or HighResMIP models agree on the sign of the projected change. Black rectangles highlight the four regions: (A) northern Andes, (B) Orinoco, (C) Brazilian Amazon, and (D) northern Cerrado. All spatial fields are shown at a common resolution of 1° × 1°. 112
5.28 Projected changes in the seasonal median duration (days) of Compound Dry and Hot Events (CDHEs) for the long-term period (2081–2100) based on the ensemble median under different emission scenarios: SSP1-2.6 (a–d), SSP2-4.5 (e–h), SSP3-7.0 (i–l), and SSP5-8.5 (m–p) from CMIP6. Dots indicate grid points where at least 80 % of the CMIP6 models agree on the sign of the projected change. Black rectangles highlight the four regions: (A) northern Andes, (B) Orinoco, (C) Brazilian Amazon, and (D) northern Cerrado. All spatial fields are shown at a common resolution of 1° × 1°. 113

5.29 Projected changes in the seasonal median gap (days) between Compound Dry and Hot Events (CDHEs) for the near-term period (2021–2040) based on the ensemble median under different emission scenarios: SSP1-2.6 (a–d), SSP2-4.5 (e–h), SSP3-7.0 (i–l), and SSP5-8.5 (m–p) from CMIP6, and HighresFuture (HighresFuture) (q–t) from HighResMIP. Dots indicate grid points where at least 80 % of the CMIP6 or HighResMIP models agree on the sign of the projected change. Black rectangles highlight the four regions: (A) northern Andes, (B) Orinoco, (C) Brazilian Amazon, and (D) northern Cerrado. All spatial fields are shown at a common resolution of 1° × 1°. 114
5.30 Projected changes in the seasonal median gap (days) between Compound Dry and Hot Events (CDHEs) for the long-term period (2081–2100) based on the ensemble median under different emission scenarios: SSP1-2.6 (a–d), SSP2-4.5 (e–h), SSP3-7.0 (i–l), and SSP5-8.5 (m–p) from CMIP6. Dots indicate grid points where at least 80 % of the CMIP6 models agree on the sign of the projected change. Black rectangles highlight the four regions: (A) northern Andes, (B) Orinoco, (C) Brazilian Amazon, and (D) northern Cerrado. All spatial fields are shown at a common resolution of 1° × 1°. 115
5.31 Projected changes in the seasonal median intensity (°C) of Compound Dry and Hot Events (CDHEs) for the near-term period (2021–2040) based on the ensemble median under different emission scenarios: SSP1-2.6 (a–d), SSP2-4.5 (e–h), SSP3-7.0 (i–l), and SSP5-8.5 (m–p) from CMIP6, and HighresFuture (HighresFuture) (q–t) from HighResMIP. Dots indicate grid points where at least 80 % of the CMIP6 or HighResMIP models agree on the sign of the projected change. Black rectangles highlight the four regions: (A) northern Andes, (B) Orinoco, (C) Brazilian Amazon, and (D) northern Cerrado. All spatial fields are shown at a common resolution of 1° × 1°. 116
5.32 Projected changes in the seasonal median intensity (°C) of Compound Dry and Hot Events (CDHEs) for the long-term period (2081–2100) based on the ensemble median under different emission scenarios: SSP1-2.6 (a–d), SSP2-4.5 (e–h), SSP3-7.0 (i–l), and SSP5-8.5 (m–p) from CMIP6. Dots indicate grid points where at least 80 % of the CMIP6 models agree on the sign of the projected change. Black rectangles highlight the four regions: (A) northern Andes, (B) Orinoco, (C) Brazilian Amazon, and (D) northern Cerrado. All spatial fields are shown at a common resolution of 1° × 1°. 117
5.33 Projected changes in the seasonal median intensity (SPI) of Compound Dry and Hot Events (CDHEs) for the near-term period (2021–2040) based on the ensemble median under different emission scenarios: SSP1-2.6 (a–d), SSP2-4.5 (e–h), SSP3-7.0 (i–l), and SSP5-8.5 (m–p) from CMIP6, and HighresFuture (HighresFuture) (q–t) from HighResMIP. Dots indicate grid points where at least 80 % of the CMIP6 or HighResMIP models agree on the sign of the projected change. Black rectangles highlight the four regions: (A) northern Andes, (B) Orinoco, (C) Brazilian Amazon, and (D) northern Cerrado. All spatial fields are shown at a common resolution of 1° × 1°. 118

5.34 Projected changes in the seasonal median intensity (SPI) of Compound Dry and Hot Events (CDHEs) for the long-term period (2081–2100) based on the ensemble median under different emission scenarios: SSP1-2.6 (a–d), SSP2-4.5 (e–h), SSP3-7.0 (i–l), and SSP5-8.5 (m–p) from CMIP6. Dots indicate grid points where at least 80 % of the CMIP6 models agree on the sign of the projected change. Black rectangles highlight the four regions: (A) northern Andes, (B) Orinoco, (C) Brazilian Amazon, and (D) northern Cerrado. All spatial fields are shown at a common resolution of 1° × 1°. 119
5.35 Time series of compound dry and hot events (CDHEs) characteristics for the northern Andes region based on the ensemble median. The 1983–2014 series corresponds to the multimodel median of the historical simulations (gray line). For the 2015–2100 period (2015–2050 for the HighresFuture scenario), the multimodel medians for each of the scenarios considered are shown: SSP1-2.6 (blue line), SSP2-4.5 (yellow line), SSP3-7.0 (orange line), SSP5-8.5 (red line), and HighresFuture (purple line). The shaded areas indicate the spread associated with the historical simulation or each scenario, calculated from the minimum and maximum values of the multimodel ensemble. . . 121
5.36 Time series of compound dry and hot events (CDHEs) characteristics for the Orinoco region based on the ensemble median. The 1983–2014 series corresponds to the multimodel median of the historical simulations (gray line). For the 2015–2100 period (2015–2050 for the HighresFuture scenario), the multimodel medians for each of the scenarios considered are shown: SSP1-2.6 (blue line), SSP2-4.5 (yellow line), SSP3-7.0 (orange line), SSP5-8.5 (red line), and HighresFuture (purple line). The shaded areas indicate the spread associated with the historical simulation or each scenario, calculated from the minimum and maximum values of the multimodel ensemble. . . 122
5.37 Time series of compound dry and hot events (CDHEs) characteristics for the Brazilian Amazon region based on the ensemble median. The 1983–2014 series corresponds to the multimodel median of the historical simulations (gray line). For the 2015–2100 period (2015–2050 for the HighresFuture scenario), the multimodel medians for each of the scenarios considered are shown: SSP1-2.6 (blue line), SSP2-4.5 (yellow line), SSP3-7.0 (orange line), SSP5-8.5 (red line), and HighresFuture (purple line). The shaded areas indicate the spread associated with the historical simulation or each scenario, calculated from the minimum and maximum values of the multimodel ensemble. 123
5.38 Time series of compound dry and hot events (CDHEs) characteristics for the northern Cerrado region based on the ensemble median. The 1983–2014 series corresponds to the multimodel median of the historical simulations (gray line). For the 2015–2100 period (2015–2050 for the HighresFuture scenario), the multimodel medians for each of the scenarios considered are shown: SSP1-2.6 (blue line), SSP2-4.5 (yellow line), SSP3-7.0 (orange line), SSP5-8.5 (red line), and HighresFuture (purple line). The shaded areas indicate the spread associated with the historical simulation or each scenario, calculated from the minimum and maximum values of the multimodel ensemble. 124

A.1 Trends in the characteristics of Hot Events (HEs) over tropical South America during 1981–2024, based on CPC and ERA5 datasets using the 90th (P90) and 95th (P95) percentile thresholds. Statistically significant trends ($p < 0.05$) are marked with black dots. 146

A.2 Trends in the characteristics of Dry Events (DEs) over tropical South America during 1981–2024, based on CHIRPS and ERA5 datasets using the SPI3 and SPI6. Statistically significant trends ($p < 0.05$) are marked with black dots. 147
A.3 Changes in the characteristics of Compound Dry and Hot Events (CDHEs) (SPI6-P90 and SPI6-P95) between 1981–2002 and 2003–2024 over tropical South America, based on CPC/CHIRPS and ERA5 datasets. 148
A.4 Temporal Evolution of Hot Events (HEs) based on CPC and ERA5 datasets in a) northern Andes, b) Orinoco, c) Brazilian Amazon, and d) northern Cerrado during 1981–2024. The panel shows the HEs identified using the 95th (P95) percentile threshold. 149
A.5 Temporal Evolution of Dry Events (DEs) based on CHIRPS v2 and ERA5 datasets in a) northern Andes, b) Orinoco, c) Brazilian Amazon, and d) northern Cerrado during 1981–2024. The panel shows the DEs identified using SPI6. 150
A.6 Temporal Evolution of Compound Dry and Hot Events (CDHEs) based on CHIRPSv2/CPC and ERA5 datasets in a) northern Andes, b) Orinoco, c) Brazilian Amazon, and d) northern Cerrado during 1981–2024. The panel shows the events identified using SPI3-P95. 151
A.7 Temporal Evolution of Compound Dry and Hot Events (CDHEs) based on CHIRPSv2/CPC and ERA5 datasets in a) northern Andes, b) Orinoco, c) Brazilian Amazon, and d) northern Cerrado during 1981–2024. The panel shows the events identified using SPI6-P90. 152
A.8 Temporal Evolution of Compound Dry and Hot Events (CDHEs) based on CHIRPSv2/CPC and ERA5 datasets in a) northern Andes, b) Orinoco, c) Brazilian Amazon, and d) northern Cerrado during 1981–2024. The panel shows the events identified using SPI6-P95. 153

B.1 Taylor Skill Score (TS) for the seasonal patterns of daily maximum temperature. Scores are shown for observational databases (CPC), ERA5, ensemble median, HighResMIP models, and CMIP6 models with respect to the reference dataset (CHIRTS). Higher values (green) indicate better model performance. Dark green (dark purple) indicates the best (worst) models. 155
B.2 Taylor Skill Score (TS) for the seasonal patterns of daily precipitation. Scores are shown for observational databases (CHIRPS v3), ERA5, ensemble median, HighResMIP models, and CMIP6 models with respect to the reference dataset (CHIRTS). Higher values (green) indicate better model performance. Dark green (dark purple) indicates the best (worst) models. 156
B.3 Taylor Skill Score (TS) for the seasonal patterns of the number of hot events (HEs). Scores are shown for observational databases (CPC), ERA5, ensemble median, HighResMIP models, and CMIP6 models with respect to the reference dataset (CHIRTS). Higher values (green) indicate better model performance. Dark green (dark purple) indicates the best (worst) models. 157
B.4 Taylor Skill Score (TS) for the seasonal patterns of the median duration of hot events (HEs). Scores are shown for observational databases (CPC), ERA5, ensemble median, HighResMIP models, and CMIP6 models with respect to the reference dataset (CHIRTS). Higher values (green) indicate better model performance. Dark green (dark purple) indicates the best (worst) models. 158

B.5 Taylor Skill Score (TS) for the seasonal patterns of the median gap between hot events (HEs). Scores are shown for observational databases (CPC), ERA5, ensemble median, HighResMIP models, and CMIP6 models with respect to the reference dataset (CHIRTS). Higher values (green) indicate better model performance. Dark green (dark purple) indicates the best (worst) models. 159
B.6 Taylor Skill Score (TS) for the seasonal patterns of the median intensity of hot events (HEs). Scores are shown for observational databases (CPC), ERA5, ensemble median, HighResMIP models, and CMIP6 models with respect to the reference dataset (CHIRTS). Higher values (green) indicate better model performance. Dark green (dark purple) indicates the best (worst) models. 160
B.7 Taylor Skill Score (TS) for the seasonal patterns of the number of dry events (DEs). Scores are shown for observational databases (CHIRPS v3), ERA5, ensemble median, HighResMIP models, and CMIP6 models with respect to the reference dataset (CHIRPS v2). Higher values (green) indicate better model performance. Dark green (dark purple) indicates the best (worst) models. 161
B.8 Taylor Skill Score (TS) for the seasonal patterns of the median duration of dry events (DEs). Scores are shown for observational databases (CHIRPS v3), ERA5, ensemble median, HighResMIP models, and CMIP6 models with respect to the reference dataset (CHIRPS v2). Higher values (green) indicate better model performance. Dark green (dark purple) indicates the best (worst) models. 162
B.9 Taylor Skill Score (TS) for the seasonal patterns of the median gap between dry events (DEs). Scores are shown for observational databases (CHIRPS v3), ERA5, ensemble median, HighResMIP models, and CMIP6 models with respect to the reference dataset (CHIRPS v2). Higher values (green) indicate better model performance. Dark green (dark purple) indicates the best (worst) models. 163
B.10 Taylor Skill Score (TS) for the seasonal patterns of the median intensity of dry events (DEs). Scores are shown for observational databases (CHIRPS v3), ERA5, ensemble median, HighResMIP models, and CMIP6 models with respect to the reference dataset (CHIRPS v2). Higher values (green) indicate better model performance. Dark green (dark purple) indicates the best (worst) models. 164
B.11 Taylor Skill Score (TS) for the seasonal patterns of the number of compound dry and hot events (CDHEs). Scores are shown for ERA5, ensemble median, HighResMIP models, and CMIP6 models with respect to the reference dataset (CHIRPS v2/CHIRTS). Higher values (green) indicate better model performance. Dark green (dark purple) indicates the best (worst) models. 165
B.12 Taylor Skill Score (TS) for the seasonal patterns of the median duration of compound dry and hot events (CDHEs). Scores are shown for ERA5, ensemble median, HighResMIP models, and CMIP6 models with respect to the reference dataset (CHIRPS v2/CHIRTS). Higher values (green) indicate better model performance. Dark green (dark purple) indicates the best (worst) models. 166
B.13 Taylor Skill Score (TS) for the seasonal patterns of the median gap between compound dry and hot events (CDHEs). Scores are shown for ERA5, ensemble median, HighResMIP models, and CMIP6 models with respect to the reference dataset (CHIRPS v2/CHIRTS). Higher values (green) indicate better model performance. Dark green (dark purple) indicates the best (worst) models. 167

B.14 Taylor Skill Score (TS) for the seasonal patterns of the median intensity of drought of compound dry and hot events (CDHEs). Scores are shown for ERA5, ensemble median, HighResMIP models, and CMIP6 models with respect to the reference dataset (CHIRPS v2/CHIRTS). Higher values (green) indicate better model performance. Dark green (dark purple) indicates the best (worst) models. 168
B.15 Taylor Skill Score (TS) for the seasonal patterns of the median intensity of maximum temperature of compound dry and hot events (CDHEs). Scores are shown for ERA5, ensemble median, HighResMIP models, and CMIP6 models with respect to the reference dataset (CHIRPS v2/CHIRTS). Higher values (green) indicate better model performance. Dark green (dark purple) indicates the best (worst) models. . . 169

C.1 Projected changes in the seasonal count of Dry Events (DEs) for the near-term period (2021–2040) based on the ensemble median under different emission scenarios: SSP1-2.6 (a–d), SSP2-4.5 (e–h), SSP3-7.0 (i–l), and SSP5-8.5 (m–p) from CMIP6, and HighresFuture (HighresFuture) (q–t) from HighResMIP. Dots indicate grid points where at least 80 % of the CMIP6 or HighResMIP models agree on the sign of the projected change. Black rectangles highlight the four subregions: (A) northern Andes, (B) Orinoco, (C) Brazilian Amazon, and (D) northern Cerrado. All spatial fields are shown at a common resolution of 1° × 1° (based on the second methodology (subsection 5.2.2)). 173
C.2 Projected changes in the seasonal count of Dry Events (DEs) for the long-term period (2081–2100) based on the ensemble median under different emission scenarios: SSP1-2.6 (a–d), SSP2-4.5 (e–h), SSP3-7.0 (i–l), and SSP5-8.5 (m–p) from CMIP6. Dots indicate grid points where at least 80 % of the CMIP6 models agree on the sign of the projected change. Black rectangles highlight the four regions: (A) northern Andes, (B) Orinoco, (C) Brazilian Amazon, and (D) northern Cerrado. All spatial fields are shown at a common resolution of 1° × 1° (based on the second methodology (subsection 5.2.2)). 174
C.3 Projected changes in the seasonal median duration (months) of Dry Events (DEs) for the near-term period (2021–2040) based on the ensemble median under different emission scenarios: SSP1-2.6 (a–d), SSP2-4.5 (e–h), SSP3-7.0 (i–l), and SSP5-8.5 (m–p) from CMIP6, and HighresFuture (HighresFuture) (q–t) from HighResMIP. Dots indicate grid points where at least 80 % of the CMIP6 or HighResMIP models agree on the sign of the projected change. Black rectangles highlight the four subregions: (A) northern Andes, (B) Orinoco, (C) Brazilian Amazon, and (D) northern Cerrado. All spatial fields are shown at a common resolution of 1° × 1° (based on the second methodology (subsection 5.2.2)). 175
C.4 Projected changes in the seasonal median duration (months) of Dry Events (DEs) for the long-term period (2081–2100) based on the ensemble median under different emission scenarios: SSP1-2.6 (a–d), SSP2-4.5 (e–h), SSP3-7.0 (i–l), and SSP5-8.5 (m–p) from CMIP6. Dots indicate grid points where at least 80 % of the CMIP6 models agree on the sign of the projected change. Black rectangles highlight the four regions: (A) northern Andes, (B) Orinoco, (C) Brazilian Amazon, and (D) northern Cerrado. All spatial fields are shown at a common resolution of 1° × 1° (based on the second methodology (subsection 5.2.2)). 176

C.5 Projected changes in the seasonal median gap (months) between Dry Events (DEs) for the near-term period (2021–2040) based on the ensemble median under different emission scenarios: SSP1-2.6 (a–d), SSP2-4.5 (e–h), SSP3-7.0 (i–l), and SSP5-8.5 (m–p) from CMIP6, and HighresFuture (HighresFuture) (q–t) from HighResMIP. Dots indicate grid points where at least 80 % of the CMIP6 or HighResMIP models agree on the sign of the projected change. Black rectangles highlight the four subregions: (A) northern Andes, (B) Orinoco, (C) Brazilian Amazon, and (D) northern Cerrado. All spatial fields are shown at a common resolution of 1° × 1° (based on the second methodology (subsection 5.2.2)). 177
C.6 Projected changes in the seasonal median gap (months) between Dry Events (DEs) for the long-term period (2081–2100) based on the ensemble median under different emission scenarios: SSP1-2.6 (a–d), SSP2-4.5 (e–h), SSP3-7.0 (i–l), and SSP5-8.5 (m–p) from CMIP6. Dots indicate grid points where at least 80 % of the CMIP6 models agree on the sign of the projected change. Black rectangles highlight the four regions: (A) northern Andes, (B) Orinoco, (C) Brazilian Amazon, and (D) northern Cerrado. All spatial fields are shown at a common resolution of 1° × 1° (based on the second methodology (subsection 5.2.2)). 178
C.7 Projected changes in the seasonal median intensity (SPI) of Dry Events (DEs) for the near-term period (2021–2040) based on the ensemble median under different emission scenarios: SSP1-2.6 (a–d), SSP2-4.5 (e–h), SSP3-7.0 (i–l), and SSP5-8.5 (m–p) from CMIP6, and HighresFuture (HighresFuture) (q–t) from HighResMIP. Dots indicate grid points where at least 80 % of the CMIP6 or HighResMIP models agree on the sign of the projected change. Black rectangles highlight the four regions: (A) northern Andes, (B) Orinoco, (C) Brazilian Amazon, and (D) northern Cerrado. All spatial fields are shown at a common resolution of 1° × 1° (based on the second methodology (subsection 5.2.2)). 179
C.8 Projected changes in the seasonal median intensity (SPI) of Dry Events (DEs) for the long-term period (2081–2100) based on the ensemble median under different emission scenarios: SSP1-2.6 (a–d), SSP2-4.5 (e–h), SSP3-7.0 (i–l), and SSP5-8.5 (m–p) from CMIP6. Dots indicate grid points where at least 80 % of the CMIP6 models agree on the sign of the projected change. Black rectangles highlight the four regions: (A) northern Andes, (B) Orinoco, (C) Brazilian Amazon, and (D) northern Cerrado. All spatial fields are shown at a common resolution of 1° × 1° (based on the second methodology (subsection 5.2.2)). 180
C.9 Projected changes in the seasonal count of Compound Dry and Hot Events (CDHEs) for the near-term period (2021–2040) based on the ensemble median under different emission scenarios: SSP1-2.6 (a–d), SSP2-4.5 (e–h), SSP3-7.0 (i–l), and SSP5-8.5 (m–p) from CMIP6, and HighresFuture (HighresFuture) (q–t) from HighResMIP. Dots indicate grid points where at least 80 % of the CMIP6 or HighResMIP models agree on the sign of the projected change. Black rectangles highlight the four subregions: (A) northern Andes, (B) Orinoco, (C) Brazilian Amazon, and (D) northern Cerrado. All spatial fields are shown at a common resolution of 1° × 1° (based on the second methodology (subsection 5.2.2)). 183

C.10 Projected changes in the seasonal count of Compound Dry and Hot Events (CDHEs) for the long-term period (2081–2100) based on the ensemble median under different emission scenarios: SSP1-2.6 (a–d), SSP2-4.5 (e–h), SSP3-7.0 (i–l), and SSP5-8.5 (m–p) from CMIP6. Dots indicate grid points where at least 80 % of the CMIP6 models agree on the sign of the projected change. Black rectangles highlight the four regions: (A) northern Andes, (B) Orinoco, (C) Brazilian Amazon, and (D) northern Cerrado. All spatial fields are shown at a common resolution of 1° × 1° (based on the second methodology (subsection 5.2.2)). 184
C.11 Projected changes in the seasonal median duration (days) of Compound Dry and Hot Events (CDHEs) for the near-term period (2021–2040) based on the ensemble median under different emission scenarios: SSP1-2.6 (a–d), SSP2-4.5 (e–h), SSP3-7.0 (i–l), and SSP5-8.5 (m–p) from CMIP6, and HighresFuture (HighresFuture) (q–t) from HighResMIP. Dots indicate grid points where at least 80 % of the CMIP6 or HighResMIP models agree on the sign of the projected change. Black rectangles highlight the four regions: (A) northern Andes, (B) Orinoco, (C) Brazilian Amazon, and (D) northern Cerrado. All spatial fields are shown at a common resolution of 1° × 1° (based on the second methodology (subsection 5.2.2)). 185
C.12 Projected changes in the seasonal median duration (days) of Compound Dry and Hot Events (CDHEs) for the long-term period (2081–2100) based on the ensemble median under different emission scenarios: SSP1-2.6 (a–d), SSP2-4.5 (e–h), SSP3-7.0 (i–l), and SSP5-8.5 (m–p) from CMIP6. Dots indicate grid points where at least 80 % of the CMIP6 models agree on the sign of the projected change. Black rectangles highlight the four regions: (A) northern Andes, (B) Orinoco, (C) Brazilian Amazon, and (D) northern Cerrado. All spatial fields are shown at a common resolution of 1° × 1° (based on the second methodology (subsection 5.2.2)). 186
C.13 Projected changes in the seasonal median gap (days) between Compound Dry and Hot Events (CDHEs) for the near-term period (2021–2040) based on the ensemble median under different emission scenarios: SSP1-2.6 (a–d), SSP2-4.5 (e–h), SSP3-7.0 (i–l), and SSP5-8.5 (m–p) from CMIP6, and HighresFuture (HighresFuture) (q–t) from HighResMIP. Dots indicate grid points where at least 80 % of the CMIP6 or HighResMIP models agree on the sign of the projected change. Black rectangles highlight the four regions: (A) northern Andes, (B) Orinoco, (C) Brazilian Amazon, and (D) northern Cerrado. All spatial fields are shown at a common resolution of 1° × 1° (based on the second methodology (subsection 5.2.2)). 187
C.14 Projected changes in the seasonal median gap (days) between Compound Dry and Hot Events (CDHEs) for the long-term period (2081–2100) based on the ensemble median under different emission scenarios: SSP1-2.6 (a–d), SSP2-4.5 (e–h), SSP3-7.0 (i–l), and SSP5-8.5 (m–p) from CMIP6. Dots indicate grid points where at least 80 % of the CMIP6 models agree on the sign of the projected change. Black rectangles highlight the four regions: (A) northern Andes, (B) Orinoco, (C) Brazilian Amazon, and (D) northern Cerrado. All spatial fields are shown at a common resolution of 1° × 1° (based on the second methodology (subsection 5.2.2)). 188

C.15 Projected changes in the seasonal median intensity (°C) of Compound Dry and Hot Events (CDHEs) for the near-term period (2021–2040) based on the ensemble median under different emission scenarios: SSP1-2.6 (a–d), SSP2-4.5 (e–h), SSP3-7.0 (i–l), and SSP5-8.5 (m–p) from CMIP6, and HighresFuture (HighresFuture) (q–t) from HighResMIP. Dots indicate grid points where at least 80 % of the CMIP6 or HighResMIP models agree on the sign of the projected change. Black rectangles highlight the four regions: (A) northern Andes, (B) Orinoco, (C) Brazilian Amazon, and (D) northern Cerrado. All spatial fields are shown at a common resolution of 1° × 1° (based on the second methodology (subsection 5.2.2)). 189
C.16 Projected changes in the seasonal median intensity (°C) of Compound Dry and Hot Events (CDHEs) for the long-term period (2081–2100) based on the ensemble median under different emission scenarios: SSP1-2.6 (a–d), SSP2-4.5 (e–h), SSP3-7.0 (i–l), and SSP5-8.5 (m–p) from CMIP6. Dots indicate grid points where at least 80 % of the CMIP6 models agree on the sign of the projected change. Black rectangles highlight the four regions: (A) northern Andes, (B) Orinoco, (C) Brazilian Amazon, and (D) northern Cerrado. All spatial fields are shown at a common resolution of 1° × 1° (based on the second methodology (subsection 5.2.2)). 190
C.17 Projected changes in the seasonal median intensity (SPI) of Compound Dry and Hot Events (CDHEs) for the near-term period (2021–2040) based on the ensemble median under different emission scenarios: SSP1-2.6 (a–d), SSP2-4.5 (e–h), SSP3-7.0 (i–l), and SSP5-8.5 (m–p) from CMIP6, and HighresFuture (HighresFuture) (q–t) from HighResMIP. Dots indicate grid points where at least 80 % of the CMIP6 or HighResMIP models agree on the sign of the projected change. Black rectangles highlight the four regions: (A) northern Andes, (B) Orinoco, (C) Brazilian Amazon, and (D) northern Cerrado. All spatial fields are shown at a common resolution of 1° × 1° (based on the second methodology (subsection 5.2.2)). 191
C.18 Projected changes in the seasonal median intensity (SPI) of Compound Dry and Hot Events (CDHEs) for the long-term period (2081–2100) based on the ensemble median under different emission scenarios: SSP1-2.6 (a–d), SSP2-4.5 (e–h), SSP3-7.0 (i–l), and SSP5-8.5 (m–p) from CMIP6. Dots indicate grid points where at least 80 % of the CMIP6 models agree on the sign of the projected change. Black rectangles highlight the four regions: (A) northern Andes, (B) Orinoco, (C) Brazilian Amazon, and (D) northern Cerrado. All spatial fields are shown at a common resolution of 1° × 1° (based on the second methodology (subsection 5.2.2)). 192

List of Tables

3.1 Drought intensity categories for the SPI (McKee et al., 1993). 30

4.1 CMIP6 and HighResMIP models used in this study for the historical experiment. . . 55

5.1 Projections from CMIP6 and HighResMIP models used in this study under different greenhouse gas (GHG) emission scenarios. The number of models used was 17 for SSP1-2.6, 21 for SSP2-4.5 and SSP5-8.5, 19 for SSP3-7.0, and 5 for HighresFuture. SSP: Shared Socioeconomic Pathway, CMIP6. Differences in the number of models with respect to chapter 4 are due to data availability per scenario. 80

C.1 Trends in characteristics of hot events (HEs) for the northern Andes, Orinoco, Brazilian Amazon, and northern Cerrado regions. Bold values with asterisk (*) denote statistically significant trends (Mann-Kendall test, $p < 0.05$). Negative values indicate decreasing trends. Trends were calculated for all scenarios over the period 2015–2100, except for highres-future, for which the analysis covers the period 2015–2050 due to its shorter temporal extent. 171

C.2 Uncertainty in the estimated slopes of hot events (HEs) characteristics for the northern Andes, Orinoco, Brazilian Amazon, and northern Cerrado regions. 172

C.3 Trends in characteristics of dry events (DEs) for the northern Andes, Orinoco, Brazilian Amazon, and northern Cerrado regions. Bold values with asterisk (*) denote statistically significant trends (Mann-Kendall test, $p < 0.05$). Negative values indicate decreasing trends. Trends were calculated for all scenarios over the period 2015–2100, except for highres-future, for which the analysis covers the period 2015–2050 due to its shorter temporal extent. 181

C.4 Uncertainty in the estimated slopes of dry events (DEs) characteristics for the northern Andes, Orinoco, Brazilian Amazon, and northern Cerrado regions. 182

C.5 Trends in characteristics of compound dry and hot events (CDHEs) for the northern Andes, Orinoco, Brazilian Amazon, and northern Cerrado regions. Bold values with asterisk (*) denote statistically significant trends (Mann-Kendall test, $p < 0.05$). Negative values indicate decreasing trends. Trends were calculated for all scenarios over the period 2015–2100, except for highres-future, for which the analysis covers the period 2015–2050 due to its shorter temporal extent. 193

C.6 Uncertainty in the estimated slopes of compound dry and hot events (CDHEs) characteristics for the northern Andes, Orinoco, Brazilian Amazon, and northern Cerrado regions. 194

Chapter 1

Introduction

Extreme hydrometeorological events, such as heatwaves, droughts, or floods, are becoming more frequent and intense due to global warming (Seneviratne et al., 2021), posing risks to water availability, agriculture, ecosystems, public health, among others. South America is highly vulnerable to these extreme events because of the low socioeconomic development of most countries in the region and the low adaptive capacity of human systems (Castellanos et al., 2022; Cavazos et al., 2024). According to Nagy et al. (2018), between 2000 and 2015, nearly 74 million people in South America were affected by floods, landslides, and extreme temperatures, resulting in the displacement of thousands due to adverse environmental conditions.

In 2021, much of South America was affected by high-impact extreme events, such as intense rainfall in southern and northeastern Brazil, the Brazilian Amazon, and French Guiana, and floods such as those that affected Colombia and the Peruvian Amazon (OMM, 2022). In addition, severe droughts were recorded in Chile, Paraguay, and the Paraná–Plata basin in Brazil and Argentina, as well as heatwaves and forest fires in the Brazilian Amazon and the Pantanal (OMM, 2022). During 2023, extreme weather and climate events with serious socioeconomic impacts were recorded on all continents (WMO, 2024). In central and southern South America, the persistent drought experienced since 2020 intensified, especially in northern Argentina and Uruguay, where rainfall between January and August 2023 was 20 % to 50 % below average. This resulted in crop losses and low water storage levels. Most continental areas experienced warmer-than-average temperatures between 1991 and 2020, with unusually high records in large areas of Central and South America (WMO, 2024). Furthermore, the temperatures recorded during the months between June 2023 and March 2024 are the highest on record (`https://www.courthousenews.com/copernicus-february-marked-9-months-of-record-temperatures-globally/`). The year 2024 was the hottest in 175 years of observational records, reaching an annual mean surface temperature of 1.55 °C (±0.13 °C) above pre-industrial levels (WMO, 2025). El Niño conditions prevailed in early 2024, contributing to increases of global temperature but also to droughts in northern South America. In addition, the Amazon basin experienced a severe drought that intensified between April and June and peaked between July and September (WMO, 2025).

The Sixth Assessment Report of the Intergovernmental Panel on Climate Change (IPCC) discusses projections of increased intensity and frequency of hot extremes for the South American region, with the exception of southern South America, where there is insufficient evidence to identify changes in this variable (Figure 1.1, upper panel). Regarding droughts (Figure 1.1, lower panel), the IPCC analyzes projections of increased frequency and intensity of agricultural and ecological

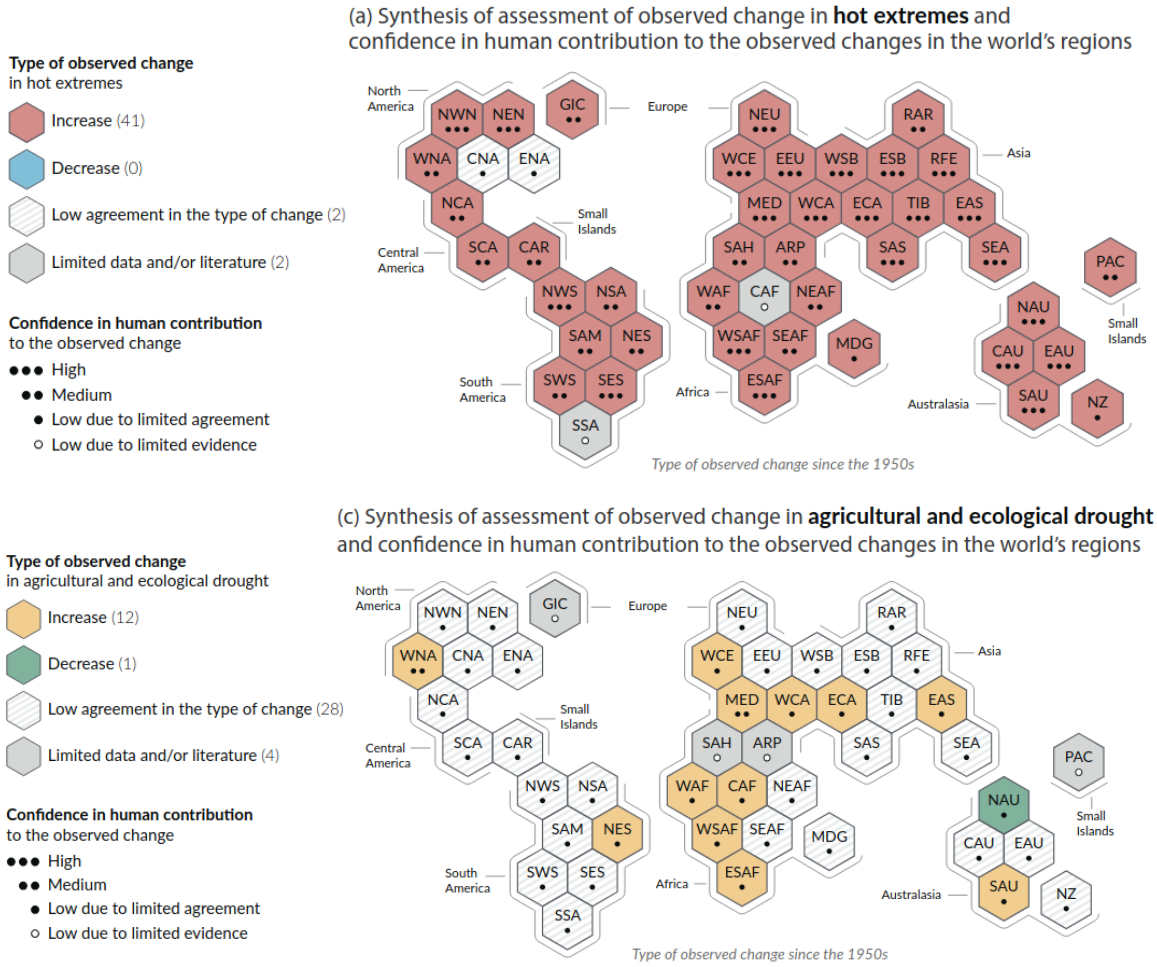

Figure 1.1: Changes observed in the frequency and intensity of hot extremes (top panel) and agricultural and ecological droughts (bottom panel) from 1950 to 2019. The red hexagons indicate changes in hot extremes, while yellow hexagons indicate changes in agricultural and ecological droughts, showing a medium to high level of confidence in the increase in the frequency and intensity of these extremes in the corresponding region. The green hexagons (bottom panel) indicate medium to high confidence in the decrease in the frequency and intensity of agricultural and ecological droughts. Striped hexagons (white and light-grey) indicate low agreement on the type of change, while the gray hexagons indicate limited information to detect changes. The filled dots within each hexagon represent the level of confidence in human contribution to the observed changes, ranging from high confidence (three dots) to low confidence due to limited evidence (one unfilled dot). Adapted from Arias et al. (2021a).

droughts for northeastern South America, while for the rest of the region there is low agreement on the type of change identified by different published studies (Arias et al., 2021a). Figure 1.1 (lower panel) does not imply that there are no changes in the frequency and intensity of these droughts in the region, but rather that the scientific studies considered do not allow reaching a level of agreement with medium or high confidence. However, several recent studies suggest increases in these extremes in various regions of South America (e.g., Avila-Diaz et al., 2020; Cerón et al., 2021; Garcia et al., 2018; Marengo & Espinoza, 2016; Wainwright et al., 2022).

In particular, hot extremes and droughts have become an increasing concern within the scientific community due to their adverse impacts on natural and socioeconomic systems. These impacts are often more severe when both extremes occur simultaneously (AghaKouchak et al., 2020; Seneviratne et al., 2021; Zhao et al., 2023). However, a geographic imbalance has been observed in the number of studies published on hot and drought extremes and the regions on which they focus, as reflected by Afroz et al. (2023). Moreover, most of the studies available for regions of South America examine only one of these extremes, underestimating the effects of their co-occurrence (Leonard et al., 2014; Zscheischler et al., 2018). According to the latest IPCC report, research on projected changes in droughts in South America remains ongoing, highlighting the importance of analyzing changes in the occurrence of compound dry and hot events (CDHEs), as suggested by various studies (e.g., Arias et al., 2024; Hao et al., 2018a; Manning et al., 2019). In this context, this work addresses the following question: How does the occurrence of CDHEs in Tropical South America vary in historical simulations and in projections under different climate change scenarios?

This work is developed as follows. Chapter 3 presents an observational analysis of the occurrence of hot events (HEs), dry events (DEs), and their combination (CDHEs) during the period 1981–2024. Chapter 4 evaluates the ability of different CMIP6/HighResMIP models to simulate the characteristics of HEs, DEs and CDHEs. Chapter 5 analyzes the projections of HEs, DEs and CDHEs by CMIP6/HighResMIP models under different greenhouse gas (GHG) emissions scenarios throughout the 21st century. Finally, Chapter 6 discusses the main conclusions of this work. Chapters 3 to 5 are structured as individual papers, so the theoretical framework, as well as the data and methodology considered, are presented within each chapter.

Chapter 2

Objectives

2.1 General Objective

To identify changes in the combined occurrence of extreme hot and dry events in Tropical South America according to historical simulations and projections under different climate change scenarios.

2.2 Specific Objectives

- To characterize changes in the frequency, duration and intensity of compound dry-hot events, based on maximum temperature and standardized precipitation index (SPI), in Tropical South America using different observational databases (e.g., CHIRPS, CPC, ERA5) for the historical period (1981-2024).
- To evaluate the performance of CMIP6/HighResMIP in simulating compound dry-hot events in Tropical South America during the historical period (1983-2014) using Taylor diagrams and Taylor Skill Score (TS).
- To identify projected changes in the frequency, duration and intensity of compound dry-hot events in Tropical South America during the near-term (2021–2040) and long-term (2081–2100) periods, under SSP1-2.6, SSP2-4.5, SSP3-7.0, SSP5-8.5 and highres-future scenarios.

Chapter 3

Occurrence of hot, dry, and compound dry and hot events in Tropical South America: Observational Analysis (1981–2024)

3.1 Introduction

Numerous studies have addressed the analysis of changes in the frequency and intensity of droughts in various regions of South America. For instance, the Amazon basin has experienced severe droughts since the late 20th century (Garcia et al., 2018; Marengo & Espinoza, 2016; Panisset et al., 2018); in particular, the 2005 and 2010 events were characterized by their large spatial extent and severity (Panisset et al., 2018). Additionally, more than three-quarters of the Amazon rainforest has been losing resilience since the early 2000s, with a more accelerated reduction in regions with a lower rainfall (Boulton et al., 2022). However, the effects of drought are not limited to the Amazon region. Avila-Diaz et al. (2020) and Cerón et al. (2021) have documented an increase in the duration of dry periods in the northern La Plata river basin and much of Brazil, respectively.

In a recent study, Wainwright et al. (2022) observed an increase in the duration of dry spells during the dry season in northeastern South America, with an increase of approximately 2 days/decade. This phenomenon has been linked to a warming pattern in the North Atlantic Ocean and to an amplified land surface warming in contrast to the surrounding oceans. Furthermore, these effects are expected to intensify due to the increase in global temperature (Wainwright et al., 2022). In northern South America, Arregocés et al. (2025b) analyzed drought trends and variability from 1982 to 2022. Their study showed that the coastal areas of Colombia and Venezuela experienced moderate to severe droughts between January and March. Similarly, the Orinoco region has faced severe drought-related impacts, particularly during February. The trend toward longer dry periods in South America may also be associated with deforestation, as it has been shown to significantly affect moisture recycling and reduce latent heat flux, demanding greater moisture transport and deeper convection to generate precipitation (Leite-Filho et al., 2019; Ruiz-Vásquez et al., 2020).

Central-eastern South America has also been affected by dry events (DEs). In 2020, the Pantanal region experienced major wildfires, largely driven by the combined effects of drought and heatwaves (Libonati et al., 2022). This drought also had severe impacts on the region's hydrology,

significantly lowering the water level of the Paraguay River (Marengo et al., 2021). During 2020-2023, central-eastern South America faced severe drought conditions, with substantial negative soil moisture anomalies. These anomalies were linked to internal climate variability, particularly the occurrence of the La Niña phase of the El Niño–Southern Oscillation (ENSO) (Arias et al., 2024; Geirinhas et al., 2023). Geirinhas et al. (2023) identified that the precipitation deficits and increased evaporation in east-central South America were driven by both subtropical and tropical forcing. This was associated with changes in the circulation of the Walker and Hadley cells, as well as with a Rossby wave that extended from the western South Pacific to South America.

While droughts typically persist over extended periods, recent research indicates that they can develop rapidly under extreme conditions (Zeng et al., 2023). The frequency of flash droughts has increased during recent decades in humid and vegetated regions, such as the Amazon and Congo river basins, compared to 1981-2000. In addition, Zeng et al. (2023) found that flash droughts in several regions were mainly caused by precipitation deficits and positive temperature anomalies during the 1981-2000 and 2001-2020 periods.

With respect to hot events (HEs), an increase in the proportion of extremely hot days has been observed during the last decades in northern South America for December-January-February (Feron et al., 2019). On the other hand, Rusticucci & Zazulie (2021) conducted an attribution analysis and projections of extreme temperature trends in southern South America, finding a marked warming trend in tropical nights, with a clear anthropogenic signal in the subtropical region. For example, in the subtropical Andes, a decrease in frost days and an increase in tropical night temperatures and the number of hot days have been observed, with evident anthropogenic influence. Furthermore, in the Patagonian region, there is a pronounced effect of anthropogenic forcing on the increasing frequency and intensity of temperature extremes (Rusticucci & Zazulie, 2021). Similarly, in the Brazilian Amazon basin and northeastern Brazil, an increase in temperatures has been recorded, with a higher number of hot days and nights and a lower frequency of cold days and nights (Da Silva et al., 2019).

One of the emerging threats posed by human-induced climate change is the occurrence of combined extremes, also known as compound extremes. In various parts of the world, increases in the frequency of compound dry and hot events (CDHEs) have been recorded (e.g., Alizadeh et al., 2020; Ghanbari et al., 2023; Hao et al., 2018a; Mazdiyasni & AghaKouchak, 2015; Mukherjee & Mishra, 2021; Sharma & Mujumdar, 2017; Wu et al., 2021a; Xu & Luo, 2019; Yu & Zhai, 2020). Moreover, the severity and spatial extent of CDHEs have increased globally since the 1990s (Wu et al., 2021a). The coexistence of these compound events is largely explained by land–atmosphere feedbacks, which drive and amplify these phenomena at regional and local scales (AghaKouchak et al., 2020; Miralles et al., 2019; Perkins, 2015). Shi et al. (2021) found that the intensity and duration of heatwaves increased during CDHEs, in contrast to individual heatwave events. This is attributed to land–atmosphere coupling, which acted as a key factor in amplifying the severity and frequency of compound events (Shi et al., 2021). Furthermore, Lyu et al. (2025) observed that, in northern and southeastern South America, synchronous CDHEs tend to occur primarily at a regional scale. Meanwhile, regions such as the Amazon, the Congo Basin, and the Yangtze River Valley act as key nodes within a synchronization network, capable of coordinating the occurrence of CDHEs with other nodes even at intercontinental or interhemispheric scales.

In the context of South America, Costa et al. (2022) focused on analyzing heatwaves in the Amazonia, observing that the most extreme events occurred under conditions of severe drought.

In 2023, the Amazon experienced drought conditions and hot extremes, associated with two atmospheric mechanisms: anomalies in vertically integrated moisture flux over the southwest (November 2022 - February 2023) and subsidence of warm air in the north (June - August 2023) (Espinoza et al., 2024). In the Orinoco region, Arias et al. (2025b) found a greater precipitation deficit during CDHEs compared to DEs during the period 1981-2021. The reduction in cloud cover associated with decreased precipitation increased surface solar radiation, raising land temperature and reinforcing drought impacts. In addition, they identified that these combined conditions increased the area burned in the basin.

In the Pantanal region, Costa et al. (2024) identified that the extreme event occurring between 2019 and 2021 included a prolongation of the dry season, a reduction and delay of the rainy season, and the persistent presence of heatwaves, resulting in CDHEs. In the states of São Paulo, Rio de Janeiro, and Minas Gerais, statistically significant increases in the number of CDHEs have been recorded. Specifically, the last decade was marked by two austral summer seasons (2013–2014 and 2014–2015) characterized by concurrent drought and heatwave conditions, driven by severe precipitation deficits and increased frequency of atmospheric blocking patterns (Geirinhas et al., 2021). Another notable case is the 2020-2023 drought across central and southern South America, attributed to three consecutive La Niña events (Jones, 2022) and concurrent heatwave development (Arias et al., 2024; Collazo et al., 2024; Rivera et al., 2023). Recent studies have identified that in regions particularly affected by ENSO, such as northern South America, El Niño can increase the probability of CDHEs during the dry season by approximately 60 %, while La Niña can contribute to a decrease of about 35 % in the probability of occurrence of these compound events (Feng & Hao, 2021). In southern South America, CDHEs are associated with La Niña events and the negative phase of the Pacific Decadal Oscillation (Collazo et al., 2023). This relationship between ENSO and CDHEs in South America has also been evidenced in other studies (e.g., Feron et al., 2024; Hao et al., 2018b; Zhang et al., 2023). On the other hand, studies such as those by Chiang et al. (2022), Pan et al. (2023), and Li et al. (2025) have analyzed the influence of climate change on the occurrence of CDHEs. For example, Chiang et al. (2022) found that in land areas between 60°N and 60°S, the occurrence of CDHEs is approximately 2.7 times higher under historical conditions than under historical natural-only conditions, with this difference being more pronounced in tropical and subtropical regions. Also, a solid anthropogenic influence on the intensified has been detected in the CDHEs across six continents and in over 65 % of the subcontinental regions (Pan et al., 2023).

This chapter begins by examining the occurrence of HEs, DEs, and CDHEs during the last decades using observational datasets, which provides useful context on the characteristics of these extremes in tropical South America. First, individual HEs are examined (Subsection 3.3.1). Then, subsection 3.3.2 presents the results related to DEs, while subsection 3.3.3 explores the combined occurrence of both extremes (CDHEs). Subsection 3.3.4 focuses on specific regions which experienced substantial increases in CDHEs, and finally, Section 3.4 presents the conclusions and discussion of the main findings.

3.2 Data and methodology

3.2.1 Study region

The study area (Figure 3.1) corresponds to the Northwestern South America (NWS), Northern South America (NSA), and South American Monsoon (SAM) climate regions, as defined in the Sixth Assessment Report (AR6) of the Intergovernmental Panel on Climate Change (IPCC) (Itur-

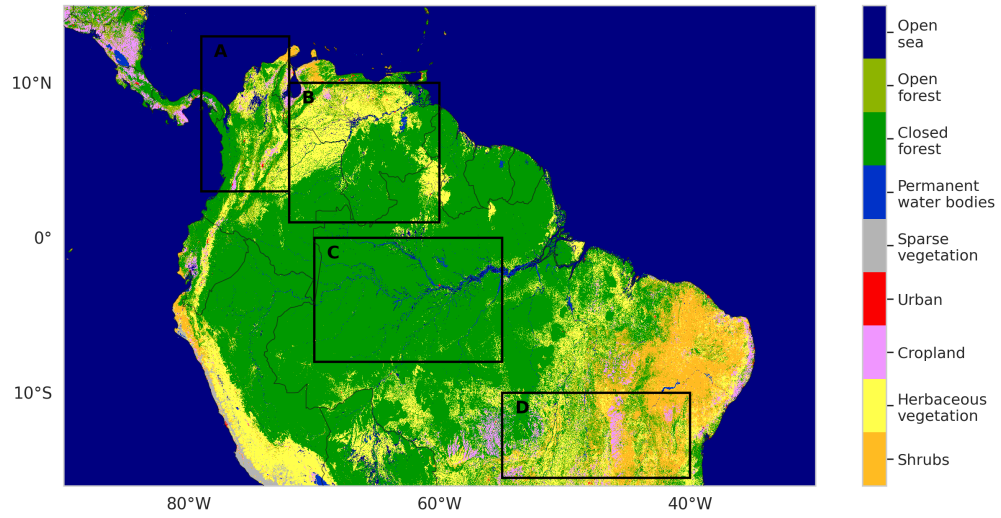

Figure 3.1: Land cover over Tropical South America (TSA) according to the Copernicus Global Land Service (`https://land.copernicus.eu/en`). The black boxes indicate the four regions where the largest changes in the occurrence of HEs, DEs, and CDHEs were observed during 1981-2024: (A) northern Andes, (B) Orinoco, (C) Brazilian Amazon, and (D) northern Cerrado.

bide et al., 2020). These three regions are collectively referred to here as Tropical South America (TSA). Colombia is included in the NWS and NSA regions. The IPCC regional classification is used here to define the TSA domain but does not inform the subsequent analysis. We selected this area due to the limited number of studies on CDHEs in this part of the continent, in contrast to the greater research focus on southern South America (e.g., Collazo et al., 2023; Geirinhas et al., 2021; Monteiro Dos Santos et al., 2024a).

The analyses presented in Chapter 3 identify four regions of TSA exhibiting the largest changes in the occurrence of HEs, DEs, and CDHEs during the 1981–2024 period, based on observational/reanalysis datasets. These regions are the northern Andes, the Orinoco, the Brazilian Amazon, and the northern Cerrado. In this section, we focus on the evolution of the different characteristics of HEs, DEs, and CDHEs in these regions. We considered the following spatial domains for each region (Figure 3.1):

- **Northern Andes** (3–13°N, 79–72°W), encompassing the Caribbean, Pacific, and Andean regions of Colombia.
- **Orinoco** (1–10°N, 72–60°W), which includes the Orinoco River basin.
- **Brazilian Amazon** (8°S–0°N, 70–55°W), covering the northwestern portion of the Brazilian Amazon.
- **Northern Cerrado** (15.5–10°S, 55–40°W), which represents the northern sector of the Cerrado biome.

3.2.2 Gridded data

To analyze the occurrence of CDHEs in TSA during the 1981–2024 period, we used daily maximum temperature data from the Climate Prediction Center (CPC) Global Unified Temperature dataset, provided by the National Oceanic and Atmospheric Administration (NOAA) Physical Science Laboratory (PSL) (Boulder, Colorado, USA), available at `https://psl.noaa.gov`. This dataset provides daily records from 1979 to the present, with a horizontal resolution of 0.5°. Additionally, we used the ERA5 reanalysis from the European Centre for Medium-Range Weather Forecasts (ECMWF) (Hersbach et al., 2023), which provides records from 1979 to the present, with a horizontal resolution of 0.25°. For monthly precipitation, we used data from the Climate Hazards Group Infrared Precipitation with Stations (CHIRPS) v2 (Funk et al., 2015), which has a horizontal resolution of 0.25° and data available from 1981 to the present.

3.2.3 Events identification

Dry and hot extremes can occur on different time scales. While temperature extremes, such as heatwaves (generally associated with low-to-mid-troposphere anticyclones), can last from weeks to months, droughts can vary in duration, ranging from days to weeks (in the case of flash droughts) and may even persist for months or years (in the case of prolonged droughts) (Hao et al., 2022).

To identify and assess the occurrence of HEs and DEs, different indices have been used to analyze changes in their frequency, duration, and intensity. Drought indices are quantitative measures that characterize drought conditions by incorporating multiple indicators, such as precipitation and evapotranspiration. Beyond the type of drought being assessed, droughts are primarily characterized along three dimensions: severity, duration, and spatial distribution, as well as two main attributes: frequency and magnitude (Zargar et al., 2011). Droughts are classified as meteorological droughts (when a precipitation deficit occurs), agricultural and ecological droughts (when a soil moisture deficit occurs), and hydrological droughts (when the deficit extends to surface runoff) (Seneviratne et al., 2021; Van Loon, 2015; Wilhite & Glantz, 1985). Similarly, warm extreme indices can be categorized into three groups: absolute indices, duration-based indices, and percentile-based indices, as proposed by the Expert Team on Climate Change Detection and Indices (ETCCDI) (`http://etccdi.pacificclimate.org/list_27_indices.shtml`).

In this work, we used the Standardized Precipitation Index (SPI) to assess meteorological drought conditions (McKee et al., 1993). The SPI has several advantages. First, it can be compared across locations and calculated over multiple time scales (Zhang et al., 2022b). Second, SPI allows differentiating between different types of drought, such as meteorological (3-months SPI; SPI3), agricultural and ecological (6-months SPI; SPI6), and hydrological (12-months SPI; SPI12) (McKee et al., 1993; Vicente-Serrano & López-Moreno, 2005). In addition, the World Meteorological Organization (WMO) has recommended this index for detecting meteorological drought (Hayes et al., 2011), and Kim et al. (2022) reported that the SPI is commonly used in regions such as Africa, Europe, South America, as well as in tropical and arid climates. However, it is important to consider its limitations: the SPI relies exclusively on precipitation data to characterize drought, and these data may face measurement and availability challenges (Feng et al., 2021). Also, this index does not consider the influence of evapotranspiration. Drought categories based on the SPI are shown in Table 3.1.

To calculate the SPI, the accumulated precipitation data (3 months - SPI3, 6 months - SPI6, and

Table 3.1: Drought intensity categories for the SPI (McKee et al., 1993).

Drought Category	**SPI Values**
Mild	$-1.0 \leq \text{SPI} < -0.5$
Moderate	$-1.5 \leq \text{SPI} < -1.0$
Severe	$-2.0 \leq \text{SPI} < -1.5$
Extreme	$\text{SPI} < -2.0$

12 months - SPI12) were fitted by the gamma distribution for each month and then transformed into a standard normal distribution (Zhang et al., 2022b). However, in regions with very low seasonal precipitation, no accumulated precipitation may be recorded, especially for short accumulation periods of 1 to 3 months (Stagge et al., 2015). In such cases, SPI values were assigned based on the historical occurrence (%) of periods with zero precipitation (Stagge et al., 2015):

$$p(x) = p_0 + (1 - p_0)\, F(x_{p>0}, \lambda) \tag{3.1}$$

Equation 3.1 describes the probability distribution of accumulated precipitation, where p denotes this distribution. The term x, p_0 indicates the historical proportion of time periods with no recorded precipitation. $F(x, \lambda)$ represents a parametric univariate distribution fitted to samples with detectable accumulated precipitation, based on parameters λ (Stagge et al., 2015).

We calculated the probability of zero precipitation using the method proposed by Stagge et al. (2015):

$$\bar{p_0} = \frac{n_{p=0} + 1}{2\,(n+1)} \tag{3.2}$$

where $\overline{p}_0$ represents the mean probability of zero precipitation events is estimated using the Weibull plotting position formula (Equation 3.2). This value is then used to calculate the SPI corresponding to the center of the probability mass for zero precipitation. $n_{p=0}$ indicates the number of zero-precipitation cases in the reference period, and n is the total number of observations in that period (Stagge et al., 2015).

Thus, the probability distribution (p) is (Stagge et al., 2015):

$$p(x) = \begin{cases} p_0 + (1 - p_0)\, F(x_{p>0}, \lambda), & x > 0, \\ \dfrac{n_{p=0} + 1}{2(n+1)}, & x = 0. \end{cases} \tag{3.3}$$

where p denotes the probability distribution, while $F(x, \lambda)$ represents the parametric univariate distribution to samples with detectable accumulated precipitation, fit with parameters λ (Equation 3.3). The methodology is described in detail by Stagge et al. (2015).

Based on the methodology used by Collazo et al. (2023), DEs were considered when the values of SPI3, SPI6, and SPI12 were less than -1.0. HEs were identified by considering at least 5 consecutive days with the daily maximum temperature values above the 90th (P90), 95th (P95), and 99th (P99) percentiles of the calendar day. These percentiles were calculated over the 1981–2010 reference period, without the application of a moving average. Because HEs may have some

days of interruption, in this work we considered the existence of gaps of up to 2 consecutive days without exceeding the threshold. The above methodology was based on the R package heatwaveR (Schlegel & Smit, 2018). Finally, a CDHE was defined when a hot event occurs during a dry event (Collazo et al., 2023). Moreover, HEs, DEs, and CDHEs over four particular regions (Figure 3.1) were identified from daily maximum temperature and precipitation time series spatially averaged over each domain.

Using these definitions, we analyzed different characteristics of HEs, DEs, and CDHEs for each climatological season (December–February, DJF; March–May, MAM; June–August, JJA; September–November, SON), The characteristics considered were:

- **Number of events:** Total count of events occurring within each season.
- **Median duration:** Median number of days for HEs and CDHEs, and median number of months for DEs.
- **Median gap between events:** Median number of days between events for HEs and CDHEs, and median number of months for DEs.
- **Median intensity:** Median anomaly of daily maximum temperature exceeding the 90th percentile threshold for HEs and CDHEs, and median SPI value below -1.0 for DEs.

3.2.4 Dominant factor in CDHEs

We also identified if the CDHEs are temperature-dominated or drought-dominated. Following the methodology proposed by Zhang et al. (2022b), the dominant factor in CDHEs was assessed by comparing drought and temperature intensities. Since the SPI is a standardized and dimensionless index, the average of standardized temperature anomalies was also computed for each event to enable a direct comparison. Accordingly, the dominant factor of the CDHEs is determined based on the following criterion (Yang et al., 2024):

$$\begin{aligned} \textit{If } Drought_{\text{Inten}} > Heat_{\text{Inten}},\ \textit{Drought dominates CDHEs} \\ \textit{If } Drought_{\text{Inten}} < Heat_{\text{Inten}},\ \textit{Heat dominates CDHEs} \end{aligned}$$

3.2.5 Trend Analysis

To analyze the temporal evolution of the characteristics of HEs, DEs, and CDHEs during the observational period, the non-parametric Mann–Kendall test (Kendall, 1948; Mann, 1945) was used to detect trends in the time series. Sen's slope estimator (Sen, 1968) was then used to quantify the magnitude of the detected trends.

3.3 Results

3.3.1 Hot events

Before analyzing CDHEs, it is essential to first characterize each type of extreme event individually. This section examines spatial frequency, median time gaps between HEs, as well as their median duration and intensity, with the aim of identifying the regions with the highest occurrence and describing their main characteristics during the 1981–2024 period. Based on the 90th percentile

(P90), CPC and ERA5 datasets indicate the occurrence of HEs across much of TSA during all seasons (Figure 3.2a-h). During December-January-February (DJF) and March-April-May (MAM), HEs are more frequent in northern South America, southern Peru and eastern and central Brazil. In June-July-August (JJA), these events are more common in central and southern Amazonia, as well as in the Guianas, according to the CPC database (Figure 3.2c). In September-October-November (SON), the highest number of HEs is observed in the eastern and southern of the study region. ERA5 shows a substantial number of HEs over northern Colombia and Venezuela during JJA and SON. Notably, both datasets identify maximum event frequencies (49 - 61 events) in central Brazil and Bolivia during JJA (Figures 3.2c and 3.2g). The number of HEs decreases across the study region when considering the 95th percentile (P95) instead of the P90 due to the stricter threshold (Figure 3.2i-p). However, the spatial distribution remains similar to that of the P90, with the highest HE frequencies occurring in the same areas. Similar to the P90, ERA5 shows a high frequency of HEs over northern Colombia and Venezuela throughout all seasons. When considering the 99th percentile (P99), results are qualitatively similar (not shown).

To complement the event frequency analysis (Figure 3.2), we examined the median time gaps between HEs (Figure 3.3). For P90, most of the study region exhibits median gaps between HEs ranging from 3 to 53 days (Figure 3.3a-h). However, some areas show longer gaps, exceeding 365 days between events. CPC and ERA5 tend to show these longer gaps in the western part of TSA during DJF and MAM. In JJA and SON, ERA5 presents a more localized pattern, covering a smaller area than CPC. For P95, the spatial extent of less frequent events increases (Figure 3.3i-p), consistent with the patterns observed in Figure 3.2. Nevertheless, a portion of TSA maintains median event gaps between 3 and 53 days. This area is largest in SON, where a greater extent of the TSA domain falls within this range (3 to 53 days) compared to the other seasons. This is also observed for the P99 (not shown).

CPC and ERA5 show the longest durations of HEs in northern South America and eastern Brazil during DJF (Figures 3.4a and 3.4e). However, ERA5 (Figure 3.4e) suggests a broader extent of events with a mean duration exceeding 9 days in northern and central Colombia and much of Venezuela. In the remaining seasons, both datasets tend to show a very similar duration pattern: in MAM (Figures 3.4b and 3.4f), the most prolonged durations are observed in northern South America, central Brazil, and western Peru; in JJA (Figures 3.4c and 3.4g), in northern and central Colombia, the Brazilian Amazon, and western Ecuador and Peru; and in SON (Figures 3.4d and 3.4h), in the northern and central parts of the study region, with CPC highlighting longer durations in the Guianas (Figure 3.4d). The HEs defined from P95 continue to exhibit substantial mean durations (Figure 3.4i-p). Although the spatial pattern of long-duration event is very similar to that observed for the events based on P90, both datasets show durations exceeding 11 days during JJA and SON in northern and central Colombia (with longer durations in CPC), in contrast to what is observed in these regions during the same seasons for P90. The P99 shows similar results (not shown).

CPC exhibits the highest HEs intensities over western and central TSA during MAM and JJA, particularly in the northern and southern parts of TSA, where the highest values are recorded (Figures 3.5b and 3.5c). During SON and DJF (Figures 3.5a and 3.5d), these high intensities extend over a broader area, with the most intense events concentrated in the southern TSA, especially during SON. ERA5 exhibits a spatial pattern similar to CPC but with generally lower intensity values (Figure 3.5e-h). In all seasons, CPC shows substantial intensities along the Colombia–Brazil border. The HEs defined by P95 (Figure 3.5i-p) exhibit greater intensity than those based on P90,

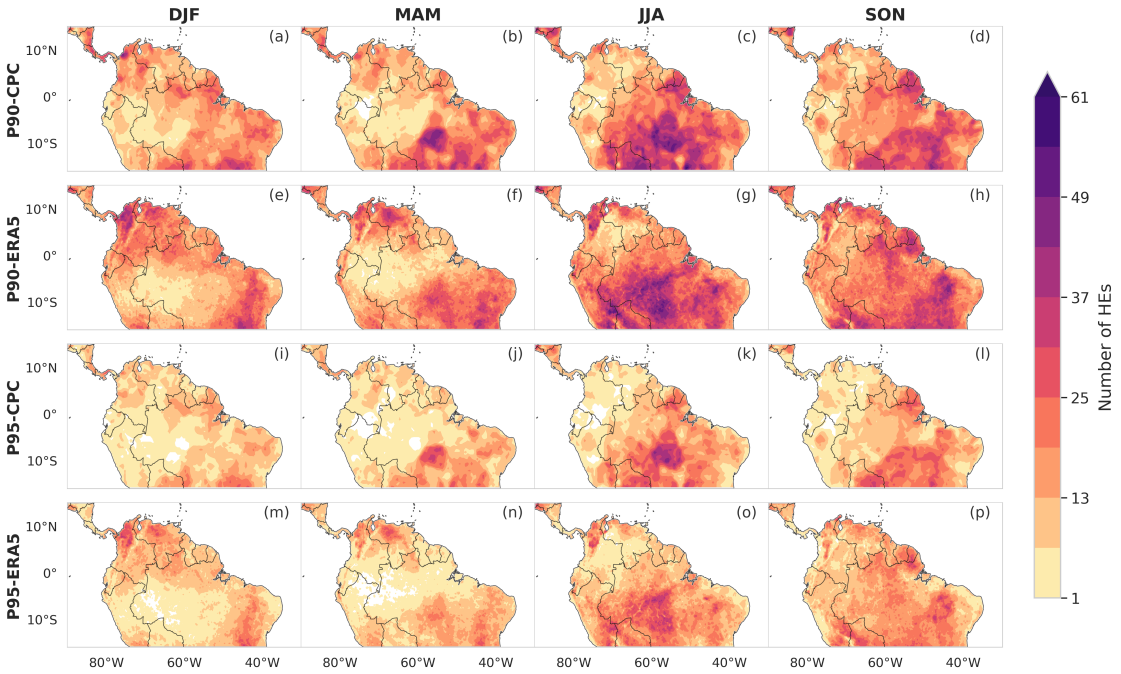

Figure 3.2: Seasonal count of Hot Events (number of HEs) based on CPC and ERA5 datasets over tropical South America during the 1981–2024 period. Events were identified using the 90th (P90) and 95th (P95) percentile thresholds. White areas indicate regions where no HEs were recorded in these datasets.

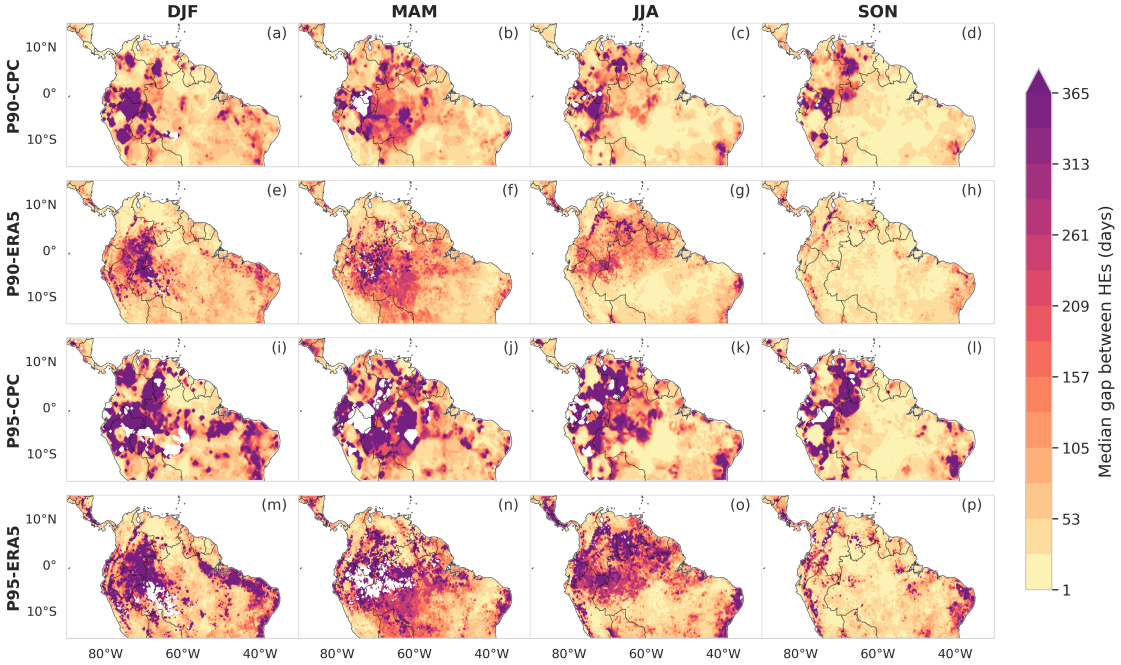

Figure 3.3: Seasonal median gap (days) between Hot Events (HEs) based on CPC and ERA5 datasets over tropical South America during the 1981–2024 period. The panel shows the median time gap between events identified using the 90th (P90) and 95th (P95) percentile thresholds. White areas indicate regions where no HEs were recorded in these datasets.

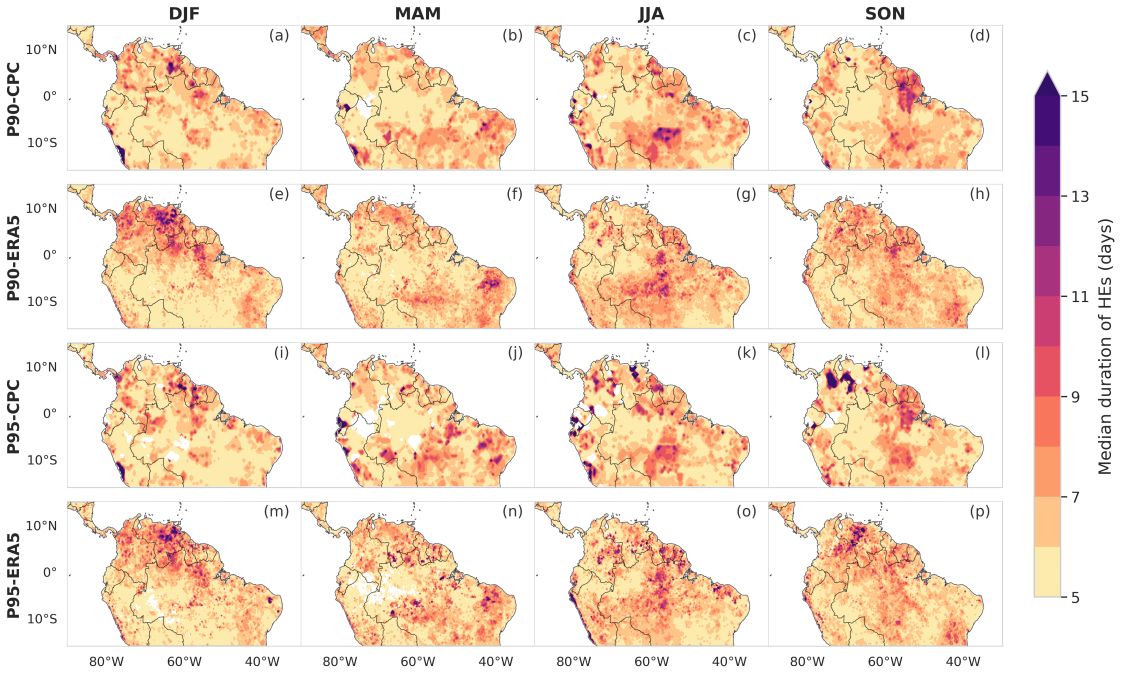

Figure 3.4: Seasonal median duration (days) of Hot Events (HEs) based on CPC and ERA5 datasets over tropical South America during the 1981–2024 period. Events were identified using the 90th (P90) and 95th (P95) percentile thresholds. White areas indicate regions where no HEs were recorded in these datasets.

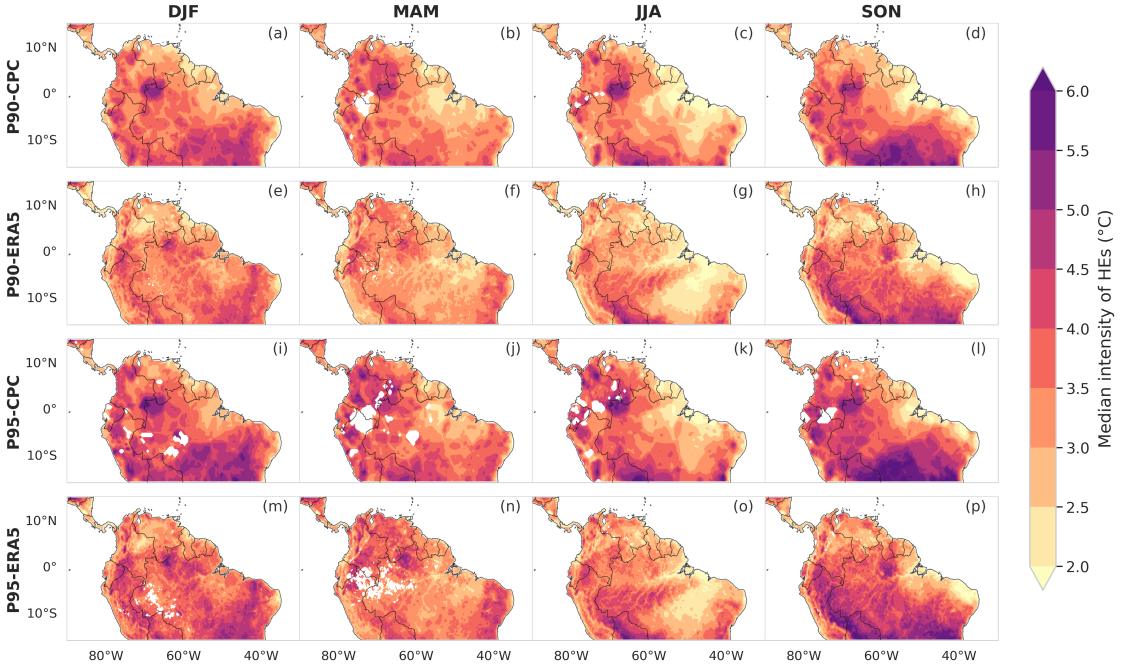

Figure 3.5: Seasonal median intensity (°C) of Hot Events (HEs) based on CPC and ERA5 datasets over tropical South America during the 1981–2024 period. Events were identified using the 90th (P90) and 95th (P95) percentile thresholds. White areas indicate regions where no HEs were recorded in these datasets.

due to the more stringent temperature threshold used in their definition; however, they retain a similar geographical distribution of the most intense events with respect to those defined by P90. A similar analysis is derived from the P99 (not shown).

Trends in hot events

Da Silva et al. (2019), Feron et al. (2019), Rusticucci & Zazulie (2021), de Araújo et al. (2022), and Monteiro Dos Santos et al. (2024b) have evidenced an increase in the frequency of HEs in various regions of South America. To determine if HEs are becoming more frequent and to assess changes in their characteristics over TSA, the evaluated metrics were compared between the periods 1981–2002 and 2003–2024. Figure 3.6 shows a substantial increase in both the frequency and duration of HEs during the 2003–2024 period compared to 1981–2002, across much of TSA. Events defined using the P90 threshold show the largest increases over Brazil, the Guianas, and central Bolivia, with more than 100 events and 1000 days compared to the 1981–2002 period (Figures 3.6a, 3.6e, 3.6b and 3.6f). ERA5 also shows these increases in the northern Andes, northern Venezuela, and southern Peru. The increase in HEs in northern regions of South America is consistent with Feron et al. (2019). Although these same regions exhibit increases for events defined by the P95 threshold (Figures 3.6i, 3.6m, 3.6j and 3.6n), the magnitude of the changes is smaller than for P90. CPC and ERA5 present increases in the median duration of HEs, with values between 2 and 4 days across broad portions of TSA, especially in central and northern TSA and eastern Brazil, for both analyzed percentiles (Figures 3.6c, 3.6g, 3.6k and 3.6o). Increases in the median intensity of HEs are observed over the western and southern portions of TSA, being more pronounced for events defined by the P95 threshold (Figure 3.6l and 3.6p). In contrast, in the rest of TSA, both datasets show a decrease in the median intensity of HEs during 2003–2024 compared to 1981–2002. The statistical significance of the differences between the 1981–2002 and 2003–2024 periods was assessed using the nonparametric Wilcoxon test, indicating statistically significant changes ($p < 0.05$) across most of TSA in the number of days associated with HEs (Figures 3.6b, 3.6f, 3.6j and 3.6n).

To complement this analysis, HE trends were calculated. The corresponding results are presented in Figure A.1. Trends show significant increases in HEs across much of TSA according to ERA5, compared to the smaller area identified by CPC. Both datasets show increases of 1 to 2 events/decade in southeastern Peru, Bolivia, and northern/central Brazil, with CPC showing greater increases in central Brazil and Bolivia. On the other hand, ERA5 shows a significant increase in the northern Andes and Venezuela. The increased event frequency is accompanied with more days associated with HEs, following similar spatial patterns. Both datasets indicate substantial increases (8-12 days/decade) in central Brazil and the southern part of the study region. CPC shows > 12 days/decade increases in the Guianas, while ERA5 shows the most pronounced increases in the northern Andes and Venezuela. These same areas exhibit increased median duration of HEs (1-2 days/decade) according to both datasets. For P95, frequency increases (0.5–1 event/decade) occur over smaller areas than for P90, mainly in the southern region and central Brazil, with CPC also showing increases in the Guianas and ERA5 in the northern Andes. These areas also show more days (4–8 days/decade) and longer duration (1–2 days/decade). No significant trends in median intensity are observed in P90 and P95, although both datasets show increases in parts of Brazil, western and southern Colombia, Bolivia and eastern Peru.

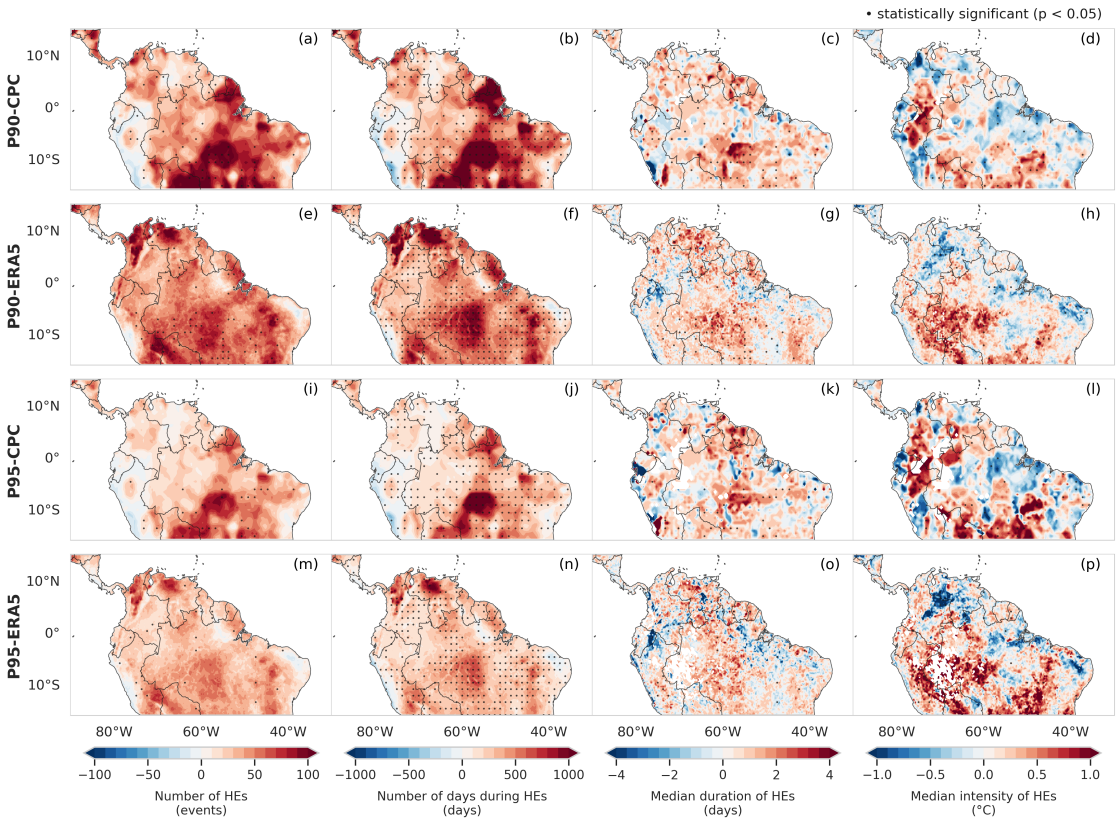

Figure 3.6: Changes in the characteristics of Hot Events (HEs) between 1981–2002 and 2003–2024 over tropical South America, based on CPC and ERA5 datasets using the 90th (P90) and 95th (P95) percentile thresholds. Dots denote statistically significant differences based on the Wilcoxon test ($p < 0.05$).

3.3.2 Dry events

This section analyzes the main characteristics of DEs. TSA exhibits events throughout the study area and in all seasons (Figure 3.7a-h). The highest event frequencies during DJF and MAM occur mainly in the northern region and eastern Brazil. During JJA, events occur in southern TSA and western Peru, while SON shows a higher frequency in eastern Brazil. In particular, for the SON period, ERA5 data (Figure 3.7h) indicates a lower number of DEs compared to CHIRPS (Figure 3.7d). Event frequency decreases in SPI6 compared to SPI3, but some regions still show more than 21 events in JJA and SON (Figures 3.7k, 3.7l, 3.7o and 3.7p). In DJF, these events are more frequent in the eastern part of the study area. During MAM, both CHIRPS (Figure 3.7j) and ERA5 (Figure 3.7n) show a concentration of DEs in northern and central Venezuela. CHIRPS also highlights Colombia, while ERA5 indicates a notable occurrence in eastern Brazil. JJA records the highest number of events in southeastern TSA (Figures 3.7k and 3.7o), while SON shows a higher concentration in western Peru and eastern Brazil (Figures 3.7 and 3.7). The SPI12 shows similar results (not shown).

The SPI3 shows a higher frequency of DEs over most of TSA, with the median gap between events of approximately 1 to 17 months (Figure 3.8a-h). However, small areas show longer gaps, with more than 25 months between DEs. While SPI6 also shows regions where DEs are frequent

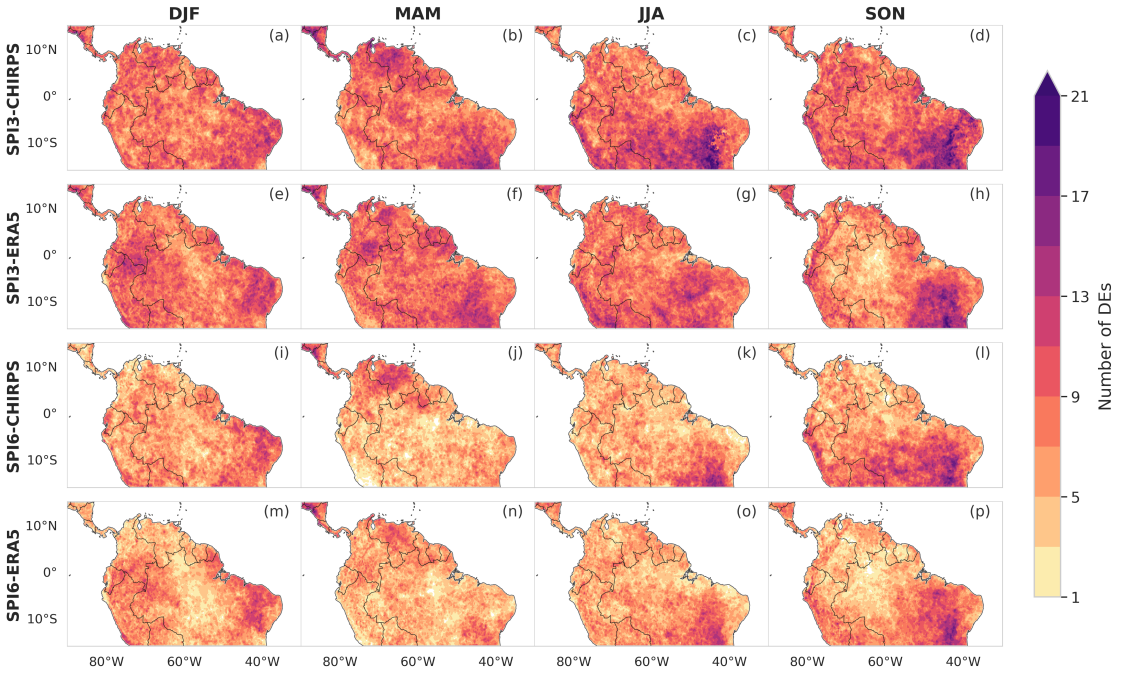

Figure 3.7: Seasonal count of Dry Events (DEs) based on CHIRPS v2 and ERA5 datasets over tropical South America during the 1981–2024 period. DEs were identified using SPI3 and SPI6.

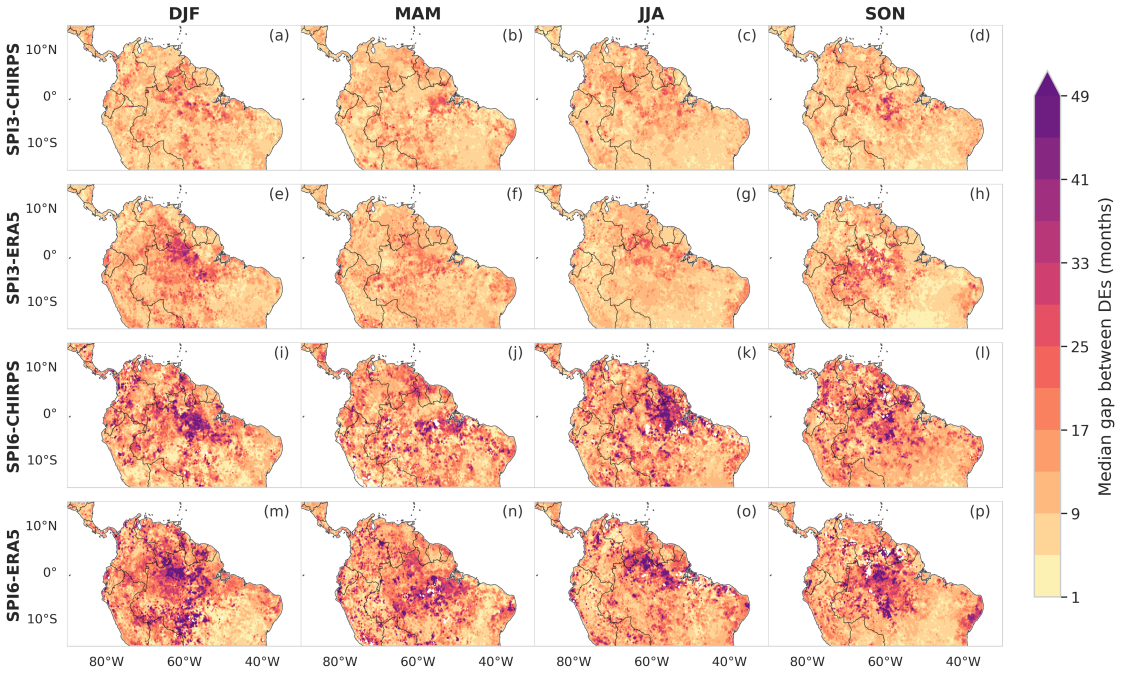

Figure 3.8: Seasonal median gap (months) between Dry Events (DEs) based on CHIRPS v2 and ERA5 datasets over tropical South America during the 1981–2024 period. The panel shows the median time gap between events identified using SPI3 and SPI6.

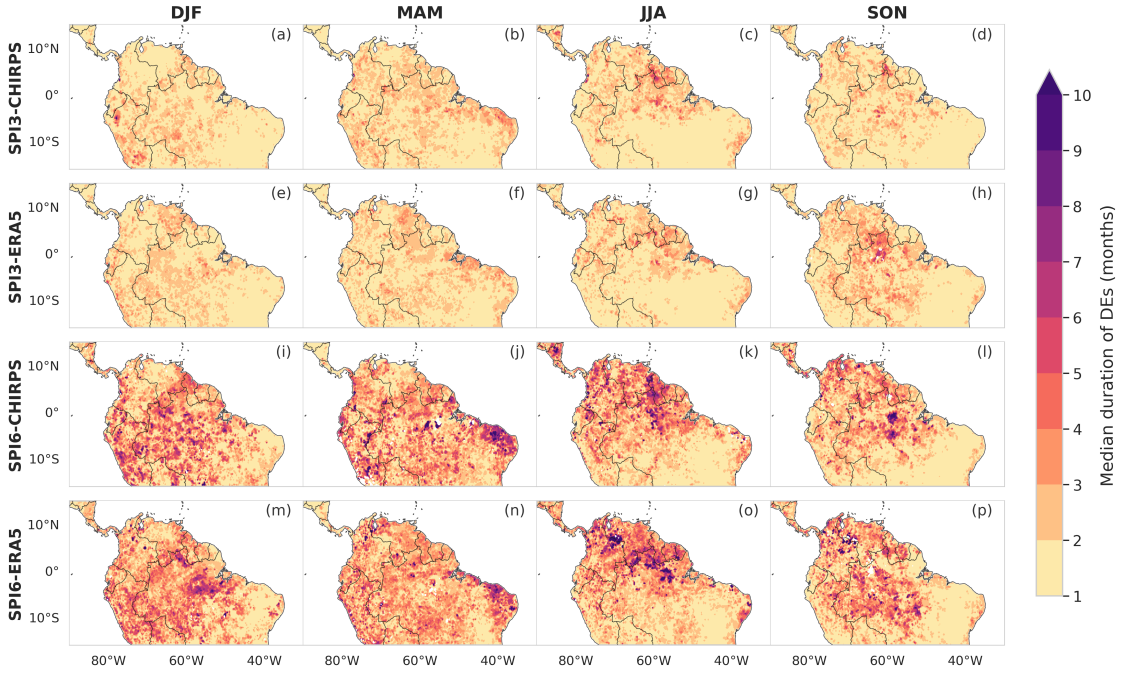

Figure 3.9: Seasonal median duration (months) of Dry Events (DEs) based on CHIRPS v2 and ERA5 datasets over tropical South America during the 1981–2024 period. DEs were identified using SPI3 and SPI6.

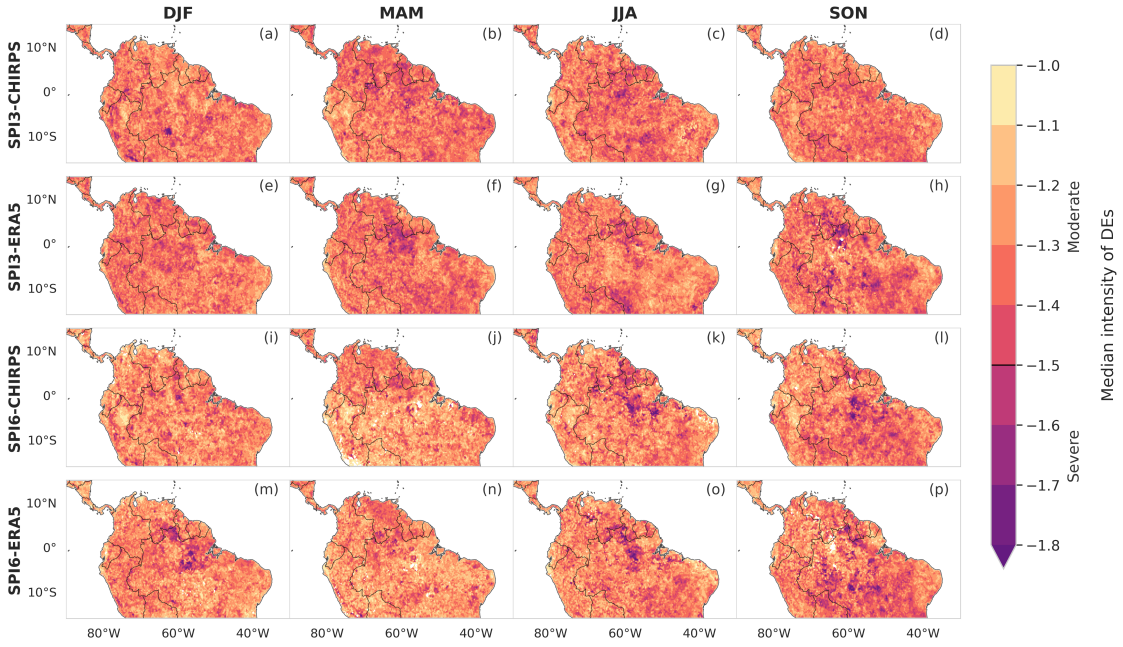

Figure 3.10: Seasonal median SPI intensity of Dry Events (DEs) based on CHIRPS v2 and ERA5 datasets over tropical South America during the 1981–2024 period. DEs were identified using SPI3 and SPI6. The drought category (McKee et al., 1993) is shown: Moderate ($-1.5 \leq \text{SPI} < -1.0$) and Severe ($-2.0 \leq \text{SPI} < -1.5$).

(Figure 3.7i-p), with gaps from 1 to 17 months, it shows a greater extent of areas where such events are less frequent than SPI3, particularly in some regions of the Amazon Basin where gaps exceed 49 months. Moreover, both datasets tend to highlight the same areas with longer gaps. Similar patterns are found when considering the SPI12, although with smaller values (not shown).

Both datasets show a very similar median duration of DEs. For SPI3, most of the study region has durations between 1 and 4 months in all seasons (Figure 3.9a-h). The shortest durations occur in the southern part of the region during JJA, in eastern Brazil during DJF, MAM, and SON, and in northern South America during DJF. For SPI6 (Figure 3.9i-p), CHIRPS and ERA5 indicate that DEs generally last longer than the events detected using SPI3. However, for DJF, JJA, and SON, the median duration in eastern Brazil remains between 1 and 2 months. Although eastern Brazil has a high number of DEs (Figure 3.7), they tend to be short-lived (Figure 3.9). DEs have median SPI3 and SPI6 intensities between -1.0 and -1.5 in most of TSA during all seasons (Figure 3.10). These values correspond to moderate drought intensity according to the categories proposed by McKee et al. (1993). However, in some localized areas, median intensities range between -1.5 and -2.0, indicating severe drought conditions. Similar patterns in DEs median duration are found when considering the SPI12 (not shown).

Trends in dry events

ERA5 and CHIRPS exhibit very similar spatial patterns in both the number of events and the number of months, for SPI3 and SPI6. According to ERA5, the largest increases are observed across most of Brazil and western TSA, with 10 to 20 more events compared to the 1981–2002 period (Figures 3.11e and 3.11m). Meanwhile, a decrease in the number of DEs is observed in northeastern TSA. CHIRPS shows smaller areas with increases in the number of DEs (Figures 3.11a and 3.11i) and months during DEs (Figures 3.11b and 3.11j), particularly in central and western Brazil, as well as in parts of northern South America. In contrast, the rest of the region exhibits a decrease.

For DEs defined by SPI3, ERA5 shows an increase in the median duration of approximately 0.5 to 1 month in western TSA and eastern Brazil during 2003–2024, compared to 1981–2002 (Figure 3.11g). CHIRPS shows increases that are more spatially dispersed across TSA, with the longest durations concentrated over the Guianas (Figure 3.11c). Duration changes are more pronounced for SPI6 than for SPI3. Whereas ERA5 indicates the most substantial increases in western TSA (Figure 3.11o), CHIRPS locates them in northern South America (Figure 3.11k). Both databases indicate drier conditions in Bolivia, northern South America, and central Brazil for both SPI3 and SPI6 during 2003-2024 compared to 1981-2002. Additionally, ERA5 shows drier conditions over much of Peru during the latter period (Figure 3.11p). Based on the nonparametric Wilcoxon test, statistically significant differences in the number of months during DEs are identified for both datasets, mainly over northern and eastern TSA, as well as central and eastern Brazil.

SPI3 trends show no significant increases in the number of DEs (Figure A.2), except in central Brazil where ERA5 indicates increases of $\sim$0.3 events/decade. ERA5 shows larger areas with more months of events in central Brazil (northern Cerrado), Bolivia, eastern Peru, and the Orinoco basin, and a decrease in the Guianas. CHIRPS shows increases in parts of central Brazil but decreases in northern and southern Peru, opposite to ERA5. Duration patterns are similar, with ERA5 showing the largest increase ($\sim$0.5 days/decade) in central Brazil and the Orinoco basin. For median intensity, ERA5 shows a decrease in SPI3 in regions with more days and longer duration, while

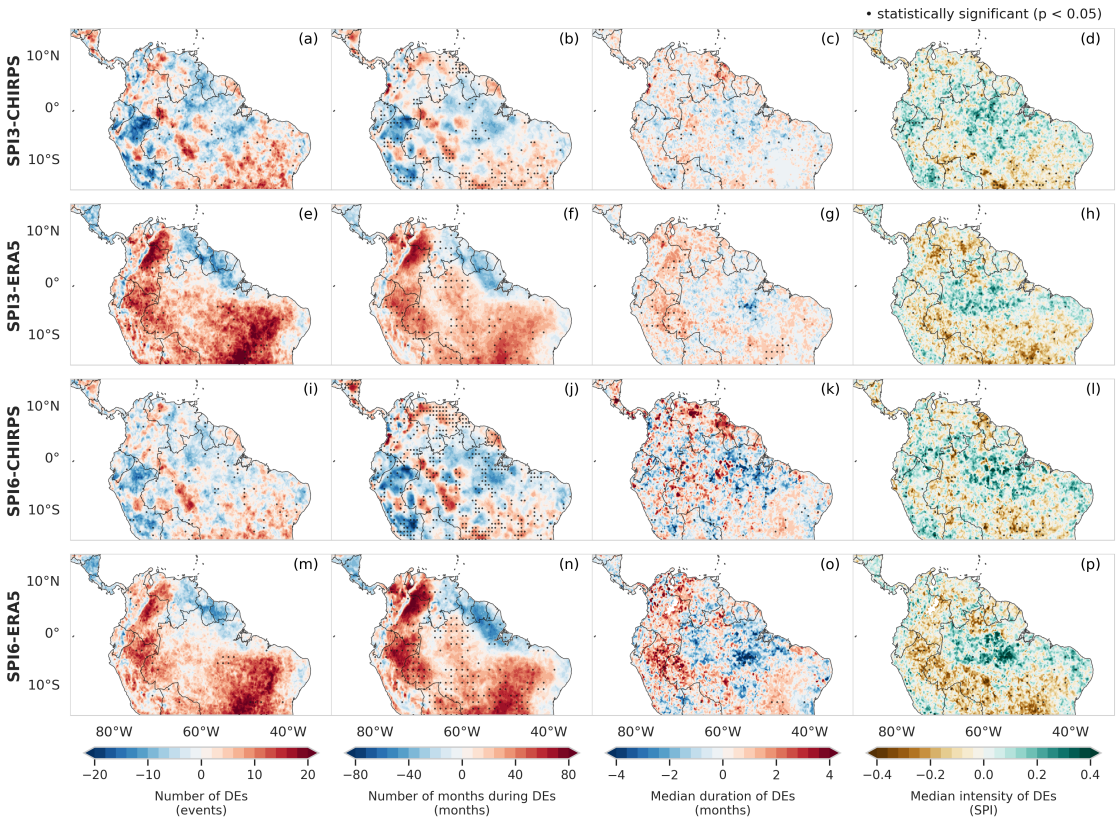

Figure 3.11: Changes in the characteristics of Dry Events (DEs) between 1981–2002 and 2003–2024 over tropical South America, based on CHIRPS v2 and ERA5 datasets using SPI3 and SPI6 indices. Dots denote statistically significant differences based on the Wilcoxon test ($p < 0.05$).

CHIRPS shows a decrease in central Brazil and an increase in northern and southwestern Peru. A decrease in SPI is associated with greater drought severity. For SPI6, CHIRPS shows no relevant trends, while ERA5 shows increases in months, duration, and drought severity in central Brazil and the Orinoco basin, but over smaller areas than for SPI3.

3.3.3 Compound dry and hot events

In this section, we focus on CDHEs, defined by the concurrent occurrence of dry conditions (identified from SPI3) and hot events exceeding the 90th and 95th percentiles (Figure 3.12). We do not focus on other SPI thresholds since the analysis using SPI6 resulted in very similar spatial patterns (not shown). CDHEs present a lower frequency compared to the individual occurrence of HEs (Figure 3.2) and DEs (Figure 3.7). However, CDHEs show similar spatial patterns to HEs in terms of the areas with the highest number of events in each season. During DJF and MAM, CDHEs are concentrated in northern South America, and in eastern and central Brazil. In JJA, events are more common in central and southern Brazilian Amazon, as well as in the northern Andes and Venezuela, according to ERA5 (Figures 3.12g and 3.12o). In SON, the highest number of CDHEs is observed in eastern and southern TSA, although ERA5 shows a wider distribution of events throughout TSA (Figures 3.12h and 3.12p). CHIRPS-CPC exhibits a lower number of CDHEs than ERA5. Furthermore, using the P95 instead of the P90 results in a smaller number

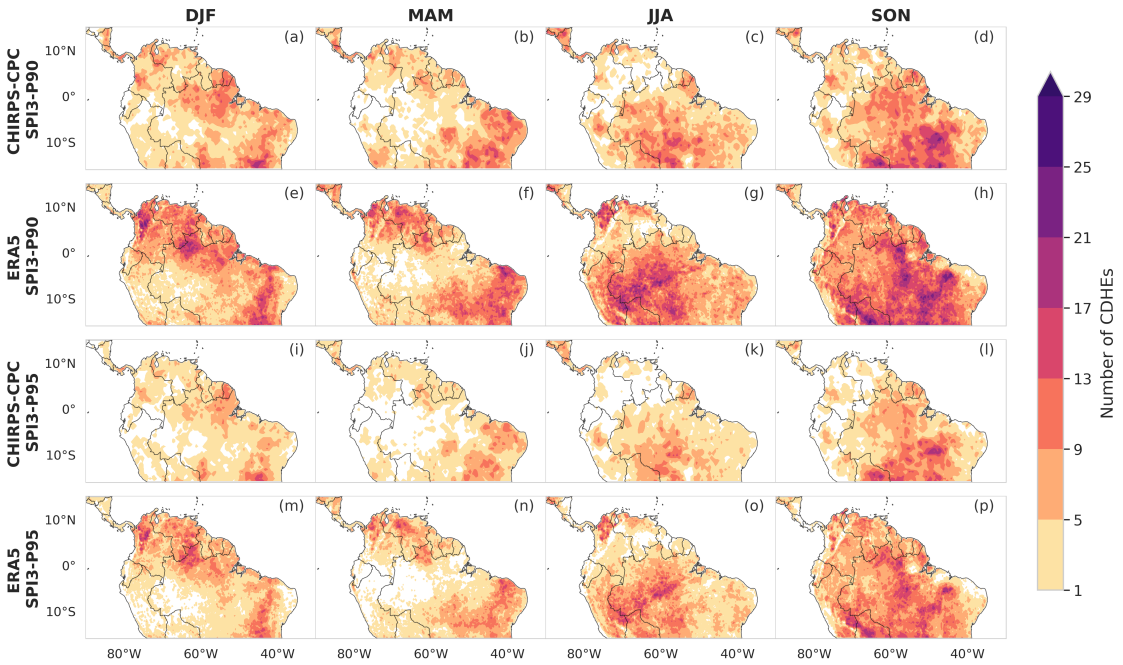

Figure 3.12: Seasonal count of Compound Dry and Hot Events (CDHEs) based on CHIRPSv2-CPC and ERA5 datasets over tropical South America during the 1981–2024 period. CDHEs were identified by the concurrent occurrence of SPI3-P90 and SPI3-P95 events. White areas indicate regions where no CDHEs were recorded in these datasets.

of CDHEs and a smaller area of occurrence throughout TSA due to the higher stringency of the selection criterion for HEs (Figure 3.2i-1p). Despite this decrease, ERA5 still suggests a substantial number of CDHEs.

The median time between CDHEs defined with SPI3-P90 and SPI3-P95 show similar patterns in both datasets for each combination (Figure 3.13). However, ERA5 exhibits more frequent events in the northern part of South America. Areas with shorter event intervals (1–33 days) correspond to regions where the highest number of events occurs (Figure 3.12). Similar to HEs (Figure 3.3), the extent of areas with short inter-event intervals is greater during SON in ERA5 (Figures 3.13h and 3.13p), suggesting a higher frequency of CDHEs in much of TSA, as shown in Figure 3.12.

Although less frequent (Figure 3.12) compared to HEs (Figure 3.2), CDHEs have a higher median duration in most of TSA (Figure 3.14). For SPI3-P90 and SPI3-P95, the longest durations in DJF are concentrated in northern South America, especially in the Guianas, according to CHIRPS-CPC. In MAM, the most prolonged durations are located in southern and eastern TSA, while ERA5 also highlights longer durations in Colombia and Venezuela. During JJA, both databases show the longest durations in northeastern Brazil. However, CHIRPS-CPC also shows it in western Peru, while ERA5 highlights the northern Amazon region in Colombia. In SON, both databases show the highest durations in central, eastern, and northern Brazil. CHIRPS-CPC also identifies important durations in the Guianas, and ERA5 shows important values in eastern Colombia and most of Venezuela.

A comparison between the median temperature intensity of CDHEs and that of HEs shows

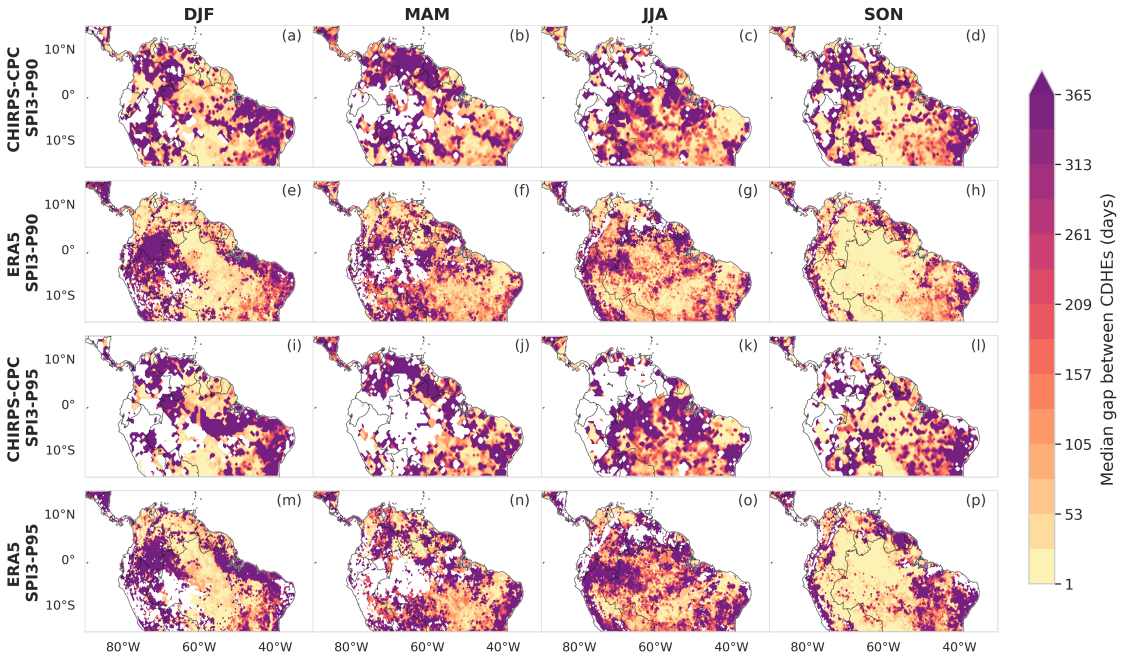

Figure 3.13: Seasonal median gap (days) between Compound Dry and Hot Events (CDHEs) based on CHIRPSv2/CPC and ERA5 datasets over tropical South America during the 1981–2024 period. The panel shows the median number of days between CDHEs, identified by the concurrent occurrence of SPI3-P90 and SPI3-P95 events. White areas indicate regions where no CDHEs were recorded in these datasets.

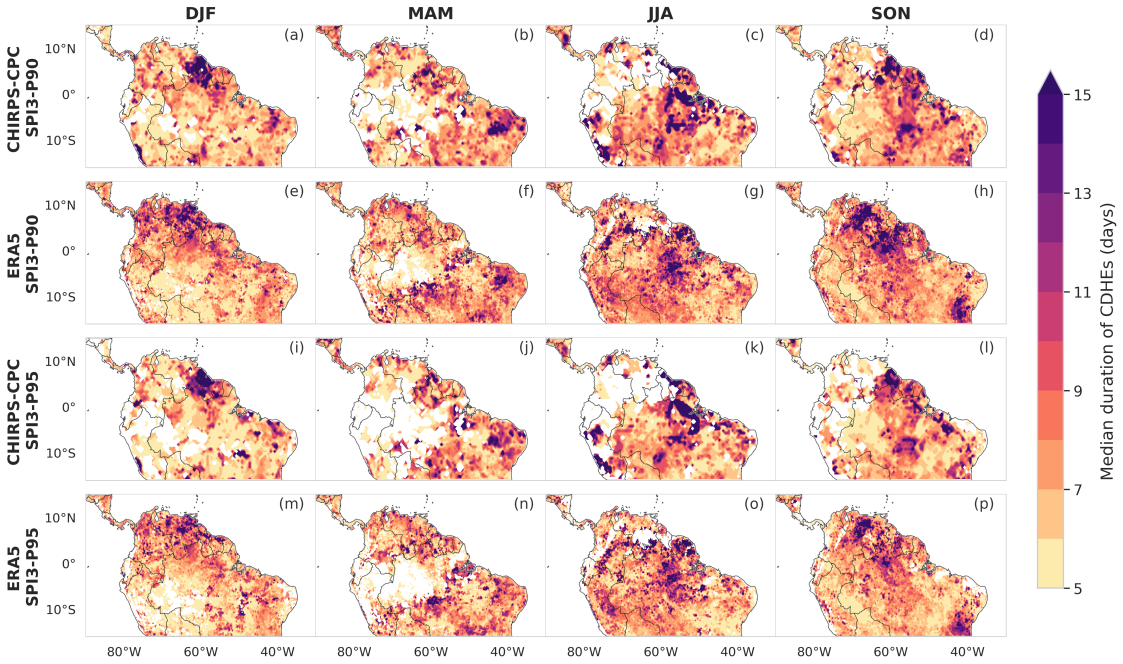

Figure 3.14: Seasonal median duration (days) of Compound Dry and Hot Events (CDHEs) based on CHIRPSv2/CPC and ERA5 datasets over tropical South America during the 1981–2024 period. CDHEs were identified by the concurrent occurrence of SPI3-P90 and SPI3-P95 events. White areas indicate regions where no CDHEs were recorded in these datasets.

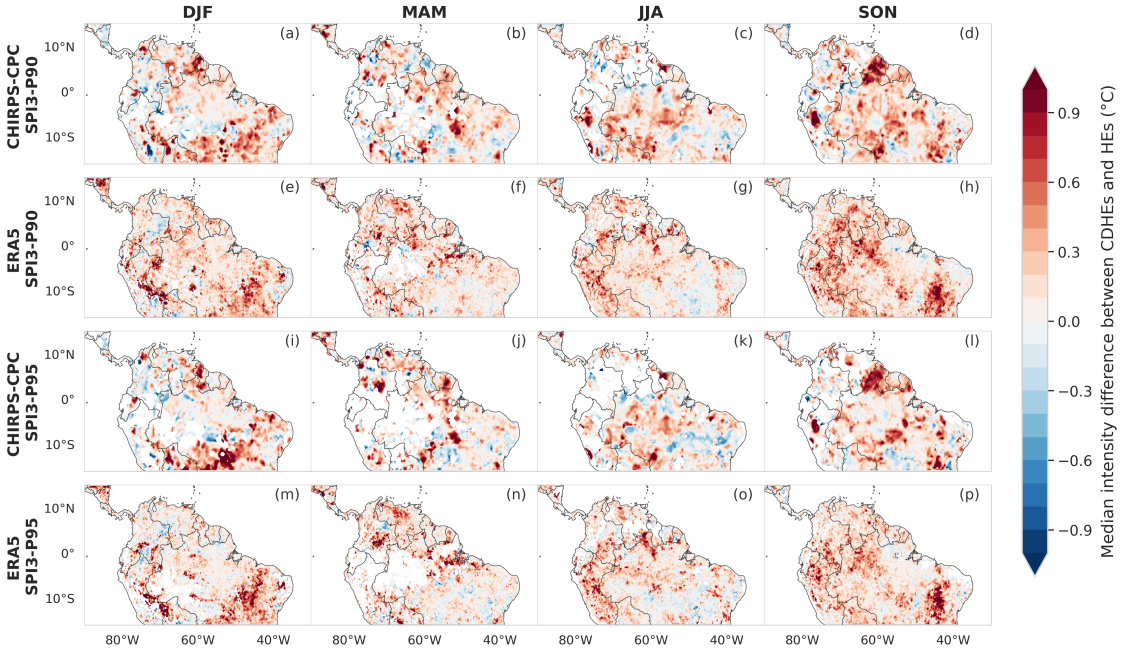

Figure 3.15: Difference in Seasonal median intensity (°C) between Compound Dry and Hot Events (CDHEs) and Hot Events (HEs) based on CPC and ERA5 datasets over tropical South America. White areas indicate regions where no CDHEs were recorded in these datasets.

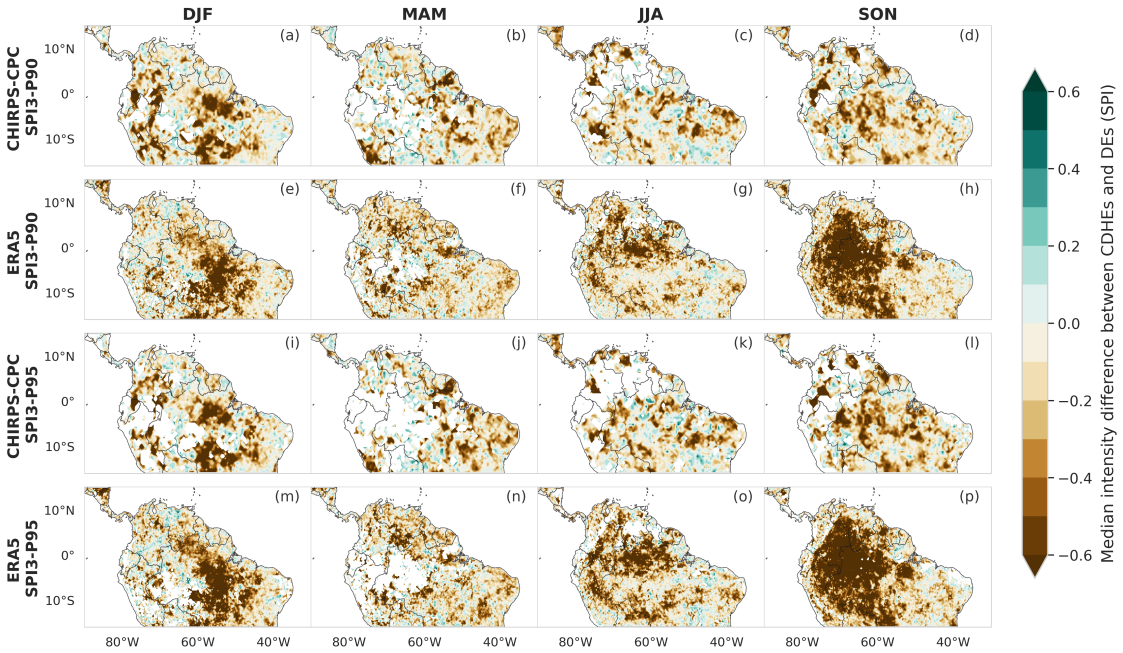

Figure 3.16: Difference in seasonal median SPI3 intensity between Compound Dry and Hot Events (CDHEs) and Dry Events (DEs) based on CHIRPS v2 and ERA5 datasets over tropical South America. White areas indicate regions where no CDHEs were recorded in these datasets.

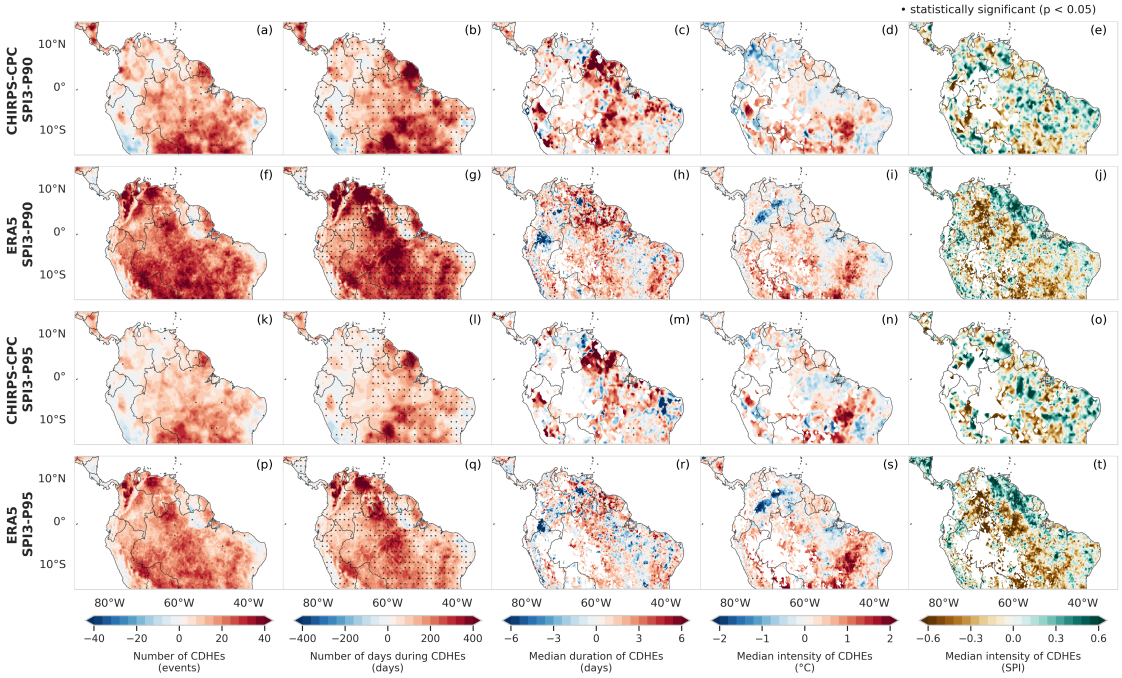

Figure 3.17: Changes in the characteristics of Compound Dry and Hot Events (CDHEs) (SPI3/P90 and SPI3/P95) between 1981–2002 and 2003–2024 over tropical South America, based on CPC/CHIRPSv2 and ERA5 datasets. Dots denote statistically significant differences based on the Wilcoxon test ($p < 0.05$).

that CDHEs exhibit higher intensities across much of TSA for both the 90th and 95th percentile thresholds (Figure 3.15). However, in certain regions of Brazil, Peru, and northern South America, particularly for events identified using CHIRPS-CPC, the median intensity is lower than that observed for HEs. We also analyzed the median intensity of CDHEs relative to the intensity of DEs, based on SPI3 values (Figure 3.16). The most pronounced differences are observed during DJF, when both datasets indicate drier conditions during CDHEs in central Brazil and in some regions of Peru and southern Colombia, particularly in CHIRPS-CPC. In these areas, SPI differences reach values below –0.6, indicating greater drought intensity during CDHEs. Similar values are observed in northern and eastern TSA during JJA, and across much of eastern TSA during SON, according to ERA5 data. In contrast, CHIRPS-CPC shows a more spatially dispersed pattern of regions experiencing the driest conditions during CDHEs in the remaining seasons.

Trends in compound dry and hot events

Figure 3.17 shows a substantial increase in the number of events and the number of days associated with CDHEs in most of TSA during 2003-2024, compared to 1981-2002. This increase is more marked in the SPI3-P90 of ERA5. For both combinations (SPI3-P90 and SPI3-P95), ERA5 exhibits the largest increases in northern South America, central and eastern Brazil, Bolivia, and eastern Peru, with a number of CDHEs greater than 40 and a number of days with CDHEs greater than 300. Both databases show the longest durations in the same regions, with the highest values in northeastern TSA and some areas of Colombia, Brazil, and Peru. Regarding the median intensity of temperature for CDHEs, both datasets show an increase over Brazil, Peru, and some

regions in northern South America, with eastern Brazil exhibiting the most pronounced increases. In contrast, the Orinoco basin shows a decrease in this intensity, particularly in the ERA5 data. On the other hand, drought intensity has increased in parts of western and central TSA, with a broader spatial extent in ERA5. This shift toward drier conditions is also evident in the trend analysis, although it is not statistically significant (Figure A.2). The Guianas region shows a decrease in SPI values during the 2003–2024 period compared to 1981–2002, more markedly in ERA5 and to a lesser extent in CPC/CHIRPS, indicating a lower drought intensity in this area during the most recent period. We also analyzed the characteristics of CDHEs using SPI6-P90 and SPI6-P95 (Figure A.3), finding very similar patterns to those observed with combinations of SPI3-P90 and SPI3-P95. As with HEs, CDHEs exhibit statistically significant changes ($p < 0.05$) only in the number of associated days across most of TSA (Figures 3.17b, 3.17g, 3.17i and 3.17q).

To complement this analysis, we examine the trend of CDHEs characteristics; however, unlike for individual events (HEs and DEs), no significant trends are observed (not shown).

Dominant conditions for compound dry and hot events

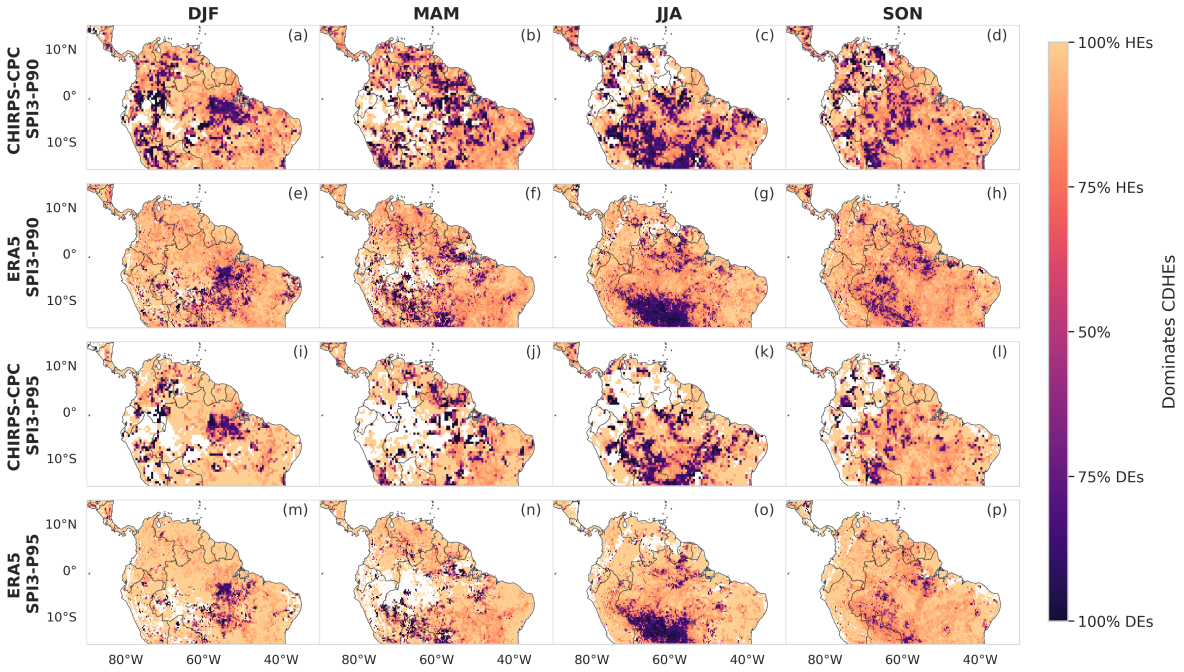

Figure 3.18: Dominant seasonal factor of Compound Dry and Hot Events (CDHEs) (SPI3-P90 and SPI3-P95) based on CHIRPSv2/CPC and ERA5 datasets over tropical South America.

Since CDHEs result from the combination between extreme hot and dry conditions, we evaluated the percentage of CDHEs that are temperature-dominated and drought-dominated. A large part of the TSA shows a marked dominance of hot conditions in more than 75 % of the CDHEs, according to SPI3-P90 and SPI3-P95 (Figure 3.18). However, CHIRPS-CPC exhibits greater extensions, especially for the SPI3-P90, where the totality of the CDHEs are dominated by dry conditions, particularly during JJA. In the same season, ERA5 shows a large region in south-central TSA where 100 % of the CDHEs are drought-dominated (Figure 3.18g and 3.18o). A similar pattern is

observed for SPI6-P90 and SPI6-P95 (not shown).

3.3.4 Hot, dry, and compound events in the TSA regions with the largest changes

Since 1981, the Northern Andes, Orinoco, Brazilian Amazon, and Northern Cerrado regions (Figure 3.1) have been affected by the occurrence of HEs, with a substantial increase in the frequency and number of days under these conditions since the late 1990s (Figures 3.19 and A.4), particularly for P90 (Figure 3.19). In 2024, the northern Andes region (ERA5) and the Orinoco region (ERA5 and CPC) present more than 190 days with hot conditions according to P90. HEs defined by the 90th percentile tend to be longer median duration; however, in 2023, the Orinoco and Brazilian Amazon regions record higher median durations for 95th percentile events, exceeding 18 days. The median HE intensity shows values between 1.5 °C and 3 °C for all regions except the northern Cerrado, which exhibits an increase between 2 °C and 4 °C for P95 (Figure A.4d). In the northern Andes, CPC shows higher HE intensities than ERA5. The median gaps of days between HEs decrease across all regions and for all percentiles, consistent with the observed increase in HE frequency.

The DEs present a higher frequency over these regions, using SPI3 (1–3 events/year) compared to SPI6 (1–2 events/year) (Figures 3.20 and A.5). However, the number of months with DEs and the median duration of DEs are higher in SPI6 (Figure A.5). The northern Cerrado exhibits the highest frequency of DEs among the four regions (Figures 3.19 and A.5), both in SPI3 and SPI6. Unlike the HEs, the DEs do not show a clear trend of increase or decrease throughout the study period in any of the regions. Differences are observed between the CHIRPS and ERA5 databases in the identification of DEs. For example, Panisset et al. (2018) identified an event of large extent and severity in the Amazon basin in 2010, detected by CHIRPS but not recorded by ERA5. The median intensity of events using SPI3 and SPI6 varies between moderate ($-1.5 \leq \text{SPI} < -1.0$) and severe ($-2.0 \leq \text{SPI} < -1.5$) dry conditions. The median time (months) between DEs does not show a definite trend, which is consistent with what was observed for the number of DEs. However, the intervals between DEs are shorter in SPI3, which is consistent with its higher frequency.

In addition, we analyzed CDHEs in these four regions based on various combinations, including SPI3-P90/P95 (Figures 3.21 and A.6) and SPI6-P90/P95 (Figures A.7 and A.8). For all combinations, we find a substantial frequency of CDHEs across all combinations since 2000, especially in the northern Cerrado and the Brazilian Amazon. All regions, with the exception of the northern Cerrado, show a marked increase in CDHEs toward the end of the 1981–2024 period. Since 2010, all regions show an increase in the median duration of CDHEs, with a more pronounced increase in the northern Andes according to ERA5 data. The CDHEs exhibit temperature intensities between 2 °C and 3 °C in most regions, except in the northern Cerrado, where intensities have fluctuated between 2 °C and 5 °C since 2000. Meanwhile, CDHEs show SPI values between -1.0 and -2.0 in all regions, indicating moderate to severe drought conditions. Finally, a notable decrease in the time between CDHEs is observed in the Brazilian Amazon and the northern Cerrado, consistent with the increasing number of CDHEs in these regions.

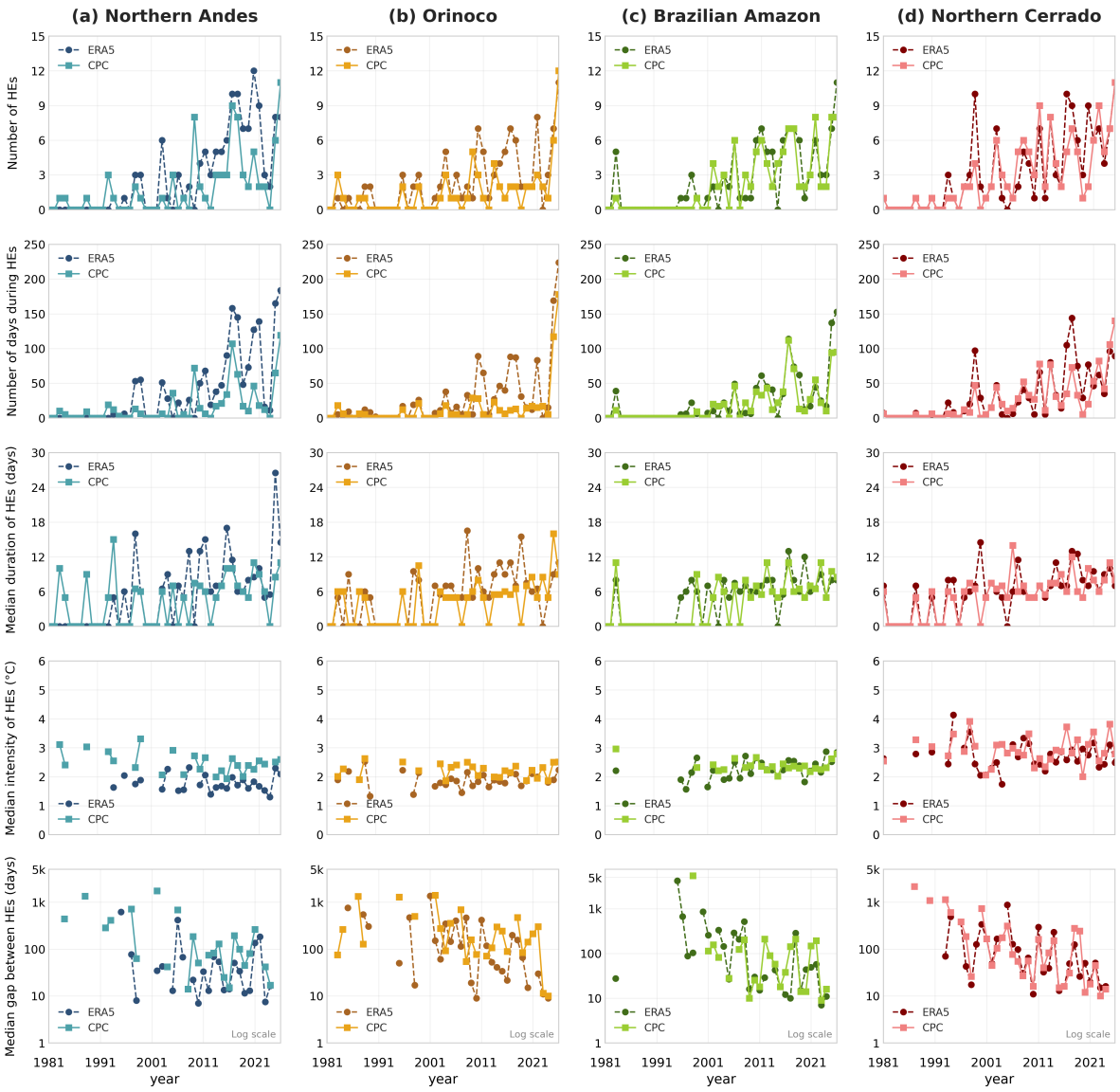

Figure 3.19: Temporal Evolution of Hot Events (HEs) based on CPC and ERA5 datasets in a) northern Andes, b) Orinoco, c) Brazilian Amazon, and d) northern Cerrado during 1981–2024. The panel shows the HEs identified using the 90th (P90) percentile threshold.

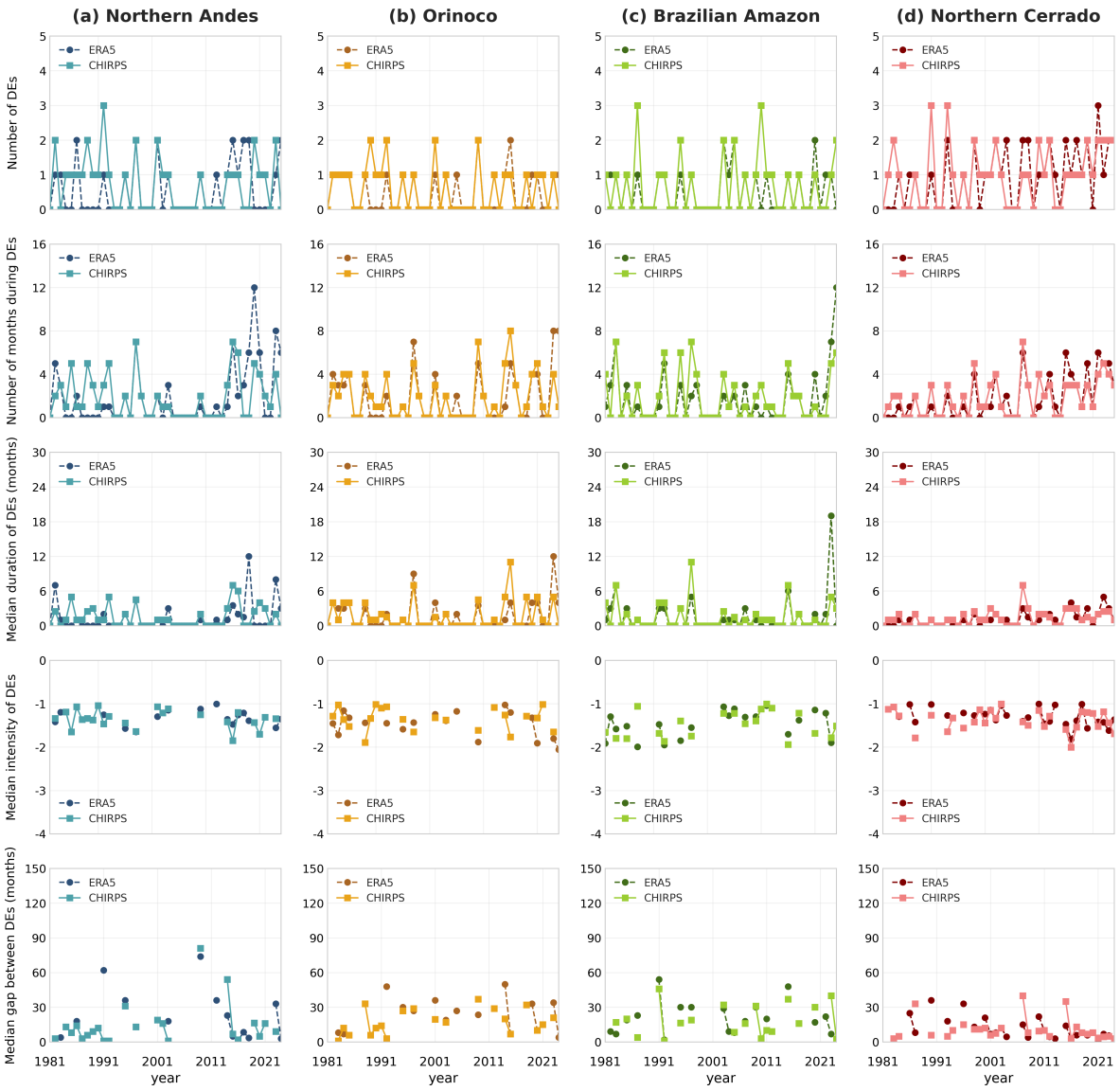

Figure 3.20: Temporal Evolution of Dry Events (DEs) based on CHIRPS v2 and ERA5 datasets in a) northern Andes, b) Orinoco, c) Brazilian Amazon, and d) northern Cerrado during 1981–2024. The panel shows the DEs identified using SPI3.

Figure 3.21: Temporal Evolution of Compound Dry and Hot Events (CDHEs) based on CHIRPSv2/CPC and ERA5 datasets in a) northern Andes, b) Orinoco, c) Brazilian Amazon, and d) northern Cerrado during 1981–2024. The panel shows the events identified using SPI3-P90.

3.4 Summary and discussion

Although recent years have seen a rise in research on CDHEs in the region, most studies have primarily focused on southern South America. For this reason, this chapter proposes to analyze the occurrence of CDHEs during the period 1981-2024 in TSA, which includes the NWS, NSA, and SAM regions, as defined by the IPCC. To this end, the characteristics of HEs, DEs, and CDHEs were examined using different databases and indices. In terms of spatial distribution, we identified a seasonal pattern in the occurrence of HEs defined by the 90th and 95th percentiles (Figure 3.2). These events were more frequent during DEF and MAM in northern South America, southern Peru, and eastern and central Brazil. During JJA, HEs were mainly concentrated in central and southern Amazonia, while in SON the highest number of events was recorded in the eastern and southern parts of TSA.

Our results indicated substantial increases in the number of HEs, their duration, and consequently the number of days associated with these events at both the 90th and 95th percentiles across much of TSA when comparing the periods 2003–2024 and 1981–2002 (Figure 3.6). Some regions of Brazil, Peru, and the northern part of the study region exhibited statistically significant increases in these characteristics (Figure A.1). For the median intensity during HEs, some regions of western and southern TSA showed significant increases during 2003-2024 with respect to 1981-2002, especially in the HEs defined by the P95. However, for this characteristic, very few regions showed a statistically significant trend. These findings are consistent with those reported by Brogno et al. (2025), who found that HEs are becoming more intense, frequent, and of longer duration over most land areas.

The seasonal analysis of DEs showed a higher frequency of events defined using SPI3, mainly associated with meteorological droughts, compared to SPI6, related to agricultural and ecological droughts (Figure 3.7). However, droughts identified with SPI6 exhibited longer median durations than those detected with SPI3 (Figure 3.9). Regarding DE median intensity, we found that much of TSA presented SPI3/SPI6 values corresponding to moderate drought conditions (Figure 3.10). However, some localized regions showed severe drought conditions, according to the categories proposed by McKee et al. (1993).

The results showed notable differences between the databases analyzed when evaluating changes in the DEs between the periods 2003-2024 and 1981-2002 (Figure 3.11). In particular, ERA5 evidenced substantial increases in the frequency and number of days associated with DEs over much of TSA, while CHIRPS showed more limited increases in spatial extent. These differences were also detected in the trend analysis (Figure A.2), where ERA5 showed significant increases in the occurrence and duration of DEs, especially in central Brazil, eastern Peru, and the Orinoco River basin, in contrast to CHIRPS, which did not show significant trends. This may be associated with differences in the accuracy of precipitation estimates between ERA5 and CHIRPS (e.g., Jahn et al., 2025).

Several studies have evaluated the performance of these products in the region. For precipitation, CHIRPSv2 shows high correlation with station observations in Venezuela and northeastern Brazil, although it tends to overestimate low values and underestimate higher ones (Paredes Trejo et al., 2016; Paredes-Trejo et al., 2017). In Colombia, it has demonstrated the best performance compared to other satellite-based products at different temporal scales, both at the national level and in the Magdalena River basin (Baez-Villanueva et al., 2018; Valencia et al., 2023), although

it underestimates precipitation during the wettest months in the Brazilian Amazon (Cavalcante et al., 2020). For maximum temperature, CHIRTS shows good agreement with station data across South America, particularly in representing hot days, outperforming ERA5 (Verdin et al., 2020), while CPC shows good agreement with both maximum and minimum temperatures in central South America (Marengo et al., 2025). However, it is important to note that gridded and reanalysis products represent spatial averages, whereas station data correspond to point measurements, which introduces representativeness differences (Montiel et al., 2026). In addition, limitations have been documented in reproducing precipitation at the daily scale and in detecting extreme events, as well as uncertainties associated with sensor type, estimation algorithms, temporal scale, and topographic complexity (Sun et al., 2018; Arregocés et al., 2024; Montiel et al., 2026).

The CDHEs exhibited an occurrence pattern in TSA similar to that of HEs; however, because they require the simultaneous concurrence of hot extremes and drought conditions, CDHEs occurred less frequently than HEs (Figures 3.2 and 3.12). On the other hand, when comparing the duration (days) of both types of events, it was observed that CDHEs had a longer median duration than HEs (Figures 3.4 and 3.14). This result is consistent with that reported by Shi et al. (2021), who found that the duration of heatwaves tends to increase when they occur simultaneously with drought conditions, in contrast to individual events.

Multiple studies have reported an increase in the frequency of simultaneous CDHEs events in different regions of the world (e.g., Mukherjee & Mishra, 2021; Xu & Luo, 2019; Yu & Zhai, 2020). Mukherjee et al. (2022) reported an annual increase in the number of CDHEs after 2000 compared to the last two decades of the 20th century. Furthermore, the total monthly number of CDHEs days showed significant positive and negative correlations with the interannual variability of several natural modes of climate variability in certain IPCC Fifth Assessment Report (AR5) climate regions. In contrast, anthropogenic warming exhibited a significant positive correlation across all the 26 climate regions defined by the IPCC AR5 during the period 1982–2016.

This increase was also observed in much of TSA when comparing the number of CDHEs between the periods 2003-2024 and 1981-2002 (Figure 3.17). Nevertheless, a more detailed analysis is required, as different mechanisms can lead to the occurrence of CDHEs (Collazo et al., 2023). These mechanisms include climate variability modes such as ENSO (Collazo et al., 2023; Feng & Hao, 2021), large-scale atmospheric circulation patterns (Seneviratne et al., 2012), and the influence of climate change (Chiang et al., 2022; Li et al., 2025; Pan et al., 2023). In addition, we observed that the intensities of both temperature and drought tend to be higher during CDHEs compared to individual events, which is consistent with findings reported by Shi et al. (2021), Costa et al. (2022), and Arias et al. (2025b). An analysis of these intensities showed that temperature is generally the dominant factor during CDHEs throughout most of TSA. However, this proportion may vary depending on the season and the database used (Figure 3.18).

The northern Andes, Orinoco, Brazilian Amazon, and northern Cerrado regions exhibit the largest changes in all types of events during the 1981-2024 period, according to the databases used. All these regions showed important increases in the number and days associated with HEs since the late 1990s (Figures 3.19 and A.4). In the Brazilian Amazon, hot extremes are more frequent and of greater intensity, according to observations (Costa et al., 2022). Some studies suggest that climate change and deforestation are two important factors driving these trends (Costa et al., 2022).

Among the regions analyzed, the northern Cerrado registered the highest frequency of DEs

during the period 1981-2024 (Figures 3.20 and A.5). In this biome, droughts are more frequent and severe, which has contributed to a decrease in agricultural productivity (Tomasella et al., 2023; Vieira et al., 2023). In addition, recent DEs in the Cerrado have been associated with increased soil degradation (Tomasella et al., 2023), as well as a higher frequency and broader extent of fires (da Silva Arruda et al., 2024; Silva et al., 2024). Regarding the intensity of DEs, we observe that all regions have experienced drought conditions ranging from moderate to severe. In the case of the northern Andes, these findings are consistent with those reported by Arregocés et al. (2025b).

We found that although a substantial frequency of CDHEs has been observed since 2000, all regions except for the northern Cerrado region presented the highest number of events and days under compound conditions by the end of the study period (Figures 3.21 and A.6). For the Brazilian Amazon, Ferreira et al. (2025) identified that some of the hottest and driest years in the Amazon region were 1983, 1998, 2010, 2015, 2016, 2023, and 2024. These years showed pronounced peaks in the mean number of CDHEs, with 2023 and 2024 ranking the highest values in the period analyzed. This pattern is consistent with what we observed in our study for this region (Figure 3.21). Studies by Espinoza et al. (2024), Marengo et al. (2024), and Yang et al. (2025) indicated that the Amazon experienced extreme droughts between 2023 and 2024, noting that increased temperatures during the winter and spring austral of 2023 exacerbated drought conditions in this region (Marengo et al., 2024). In addition, Espinoza et al. (2024) found that the Amazon basin experienced record temperature values during August, September, and October 2023, representing the highest air temperature anomaly since 1980. For the Orinoco, the study by Arias et al. (2025b) analyzed CDHEs in this region, observing various events between 2009 and 2020 which contributed to the increase in the area burned in the region.

Chapter 4

Assessing the performance of CMIP6/HighResMIP models in simulating hot, dry, and compound dry and hot events in Tropical South America (1983–2014)

4.1 Introduction

General circulation models (GCMs) are essential tools for assessing changes in climate and weather extremes under past and future conditions. However, accurately representing the climatic characteristics of South America remains a challenge for these models. Although these models capture the main features of precipitation and temperature in the region, studies such as Sierra et al. (2015) and Rivera & Arnould (2020) have reported biases in the simulated precipitation magnitudes. The latest generation of models included in the Coupled Model Intercomparison Project Phase 6 (CMIP6) shows improved performance in simulating seasonal precipitation compared to previous phases 3 and 5 (CMIP3 and CMIP5, respectively) (Arias et al., 2021b; Ortega et al., 2021). However, the persistent double Intertropical Convergence Zone (ITCZ) bias continues to affect the representation of precipitation over tropical South America (TSA) (Ortega et al., 2021). Almazroui et al. (2021) evaluated the performance of a large ensemble of CMIP6 models over South America. While these models reproduce the main regional features, their ability to capture the spatiotemporal distribution of temperature and precipitation at subregional scales, particularly in areas of high latitude and altitude, remains limited. Wang et al. (2021a) also found that, although the models exhibit important correlations over South America, they show larger standard deviations near the equator. Bazzanela et al. (2024) observed that model performance varies across study regions, likely due to the continent's climatic diversity. Complementarily, Arias et al. (2025a) reported that CMIP6 models adequately reproduce the wetter and drier regions of the continent, as well as seasonal precipitation patterns. However, the ensemble mean exhibits a double ITCZ bias during DJF and MAM, along with an overestimation of precipitation in the northern and southern regions of the continent, and an underestimation in northeastern Brazil and the western side of the Andes over Ecuador, Peru and Bolivia (Arias et al., 2025a).

Kim et al. (2020) evaluates CMIP6 models using the indices defined by the Expert Team on Climate Change Detection and Indices (ETCCDI). The study found that the CMIP6 models accurately capture the observed climatological patterns of extreme temperature indices. However, reduced hot biases are observed in the mid-latitude regions of South America and Asia. Although CMIP6 models are similar to CMIP5 models in their ability to represent extreme precipitation events, the newer generation shows improved performance in reproducing the intensity of such events (Kim et al., 2020). Avila-Diaz et al. (2023) also evaluated these ETCCDI indices using HighResMIP models and found no strong relationship between increased resolution and improved model performance.

Some studies have evaluated the performance of CMIP6 models in simulating hot extremes, dry, and compound dry and hot events (CDHEs). For example, Cook et al. (2020) found that both CMIP5 and CMIP6 models show similarities in the responses to drought. They also point out that there are similar uncertainties in both sets of models, associated with difficulties in these models in representing aspects such as vegetation and precipitation. Moreover, the variability in drought responses in CMIP6 model projections depends on the region, season, drought type, and drought metric considered (Cook et al., 2020; Jha et al., 2023). Ridder et al. (2021) emphasized that extreme temperatures are generally simulated more accurately than precipitation in climate models. In South America, Collazo et al. (2022) analyzed trends in extreme temperature indices in South America using 33 CMIP6 models. Their results indicated that minimum temperature trends are slightly better simulated than maximum temperature trends. However, no single model outperformed the others, and all exhibited limitations in representing trends, particularly for cold days (Collazo et al., 2022). Therefore, evaluating how well models capture the likelihood of such events is essential before assessing future projections.

Most CMIP6 models are able to reasonably simulate the four types of compound events involving temperature and precipitation (hot/dry, hot/wet, cold/dry, and cold/wet) when compared with observations (Wu et al., 2021b). However, differences are observed in certain specific regions. In addition, these models show poor performance in low latitudes and tropical regions (Wu et al., 2021b). For CDHEs, Collazo et al. (2023) evaluated the ability of CMIP6 models to simulate these events in South America, showing that the ensemble median of the CMIP6 models performs more accurately than the individual models. The individual models showed poor results in simulating the duration of heatwaves, although they better represent their intensity (Collazo et al., 2023).

After characterizing hot (HEs), dry (DEs), CDHEs based on observational data (Chapter 3), this chapter assesses the ability of CMIP6/HighResMIP models to reproduce these characteristics in TSA during the period 1983–2014. Subsection 4.3.1 presents the model evaluation for maximum temperature and precipitation, Subsection 4.3.2 presents the evaluation for HEs, Subsection 4.3.3 discusses the performance for DEs, and Subsection 4.3.4 examines the model simulation of CDHEs. Finally, Section 4.4 summarizes the main findings.

4.2 Data and methodology

4.2.1 CMIP6/HighResMIP simulations

This study uses simulations from 22 CMIP6 models and 6 HighResMIP models, based on the historical and hist-1950 experiments, respectively, considering the first model realization (r1i1p1f1)

(Table 4.1). We analyze historical simulations of daily temperature and monthly precipitation from CMIP6/HighResMIP models, which are publicly available through the Earth System Grid Federation (`https://esgf-node.llnl.gov/projects/cmip6/`). These simulations incorporate observed forcings during the period 1980–2014, including solar variability, volcanic activity, and anthropogenic influences such as greenhouse gas emissions and aerosols. A detailed description of the CMIP6 simulations is provided by Eyring et al. (2016).

HighResMIP corresponds to an intercomparison project of high-resolution global simulations. HighResMIP aims to evaluate the benefits of high-resolution models. The high-resolution experiments target a grid spacing of approximately 25–50 km in the atmosphere, which is significantly higher than the typical CMIP5 resolution (∼150 km). In addition, they have a longer simulation period (1950–2014) than the DECK AMIPII, which covers 1979–2014 (Haarsma et al., 2016). Haarsma et al. (2016) provides a detailed description of the HighResMIP simulations.

Table 4.1: CMIP6 and HighResMIP models used in this study for the historical experiment.

Model	**Type**	**Institution**	**Resolution Atmosphere (lat × lon)**	**Reference**
ACCESS-CM2	CMIP6	Commonwealth Scientific and Industrial Research Organisation (CSIRO) and Australian Research Council Centre of Excellence for Climate System Science (ARCCSS)	1.2° × 1.8°	Bi et al. (2020)
ACCESS-ESM1-5	CMIP6	Commonwealth Scientific and Industrial Research Organisation (CSIRO)	1.2° × 1.8°	Ziehn et al. (2020)
CMCC-ESM2	CMIP6	Euro-Mediterranean Centre on Climate Change (CMCC)	0.9° × 1.2°	Lovato et al. (2022)
CanESM5	CMIP6	Canadian Centre for Climate Modelling and Analysis (CCCma)	2.8° × 2.8°	Swart et al. (2019)
EC-Earth3	CMIP6	Earth Consortium (EC)	0.7° × 0.7°	Döscher et al. (2022)
EC-Earth3-Veg	CMIP6	Earth Consortium (EC)	0.7° × 0.7°	Döscher et al. (2022)
EC-Earth3-Veg-LR	CMIP6	Earth Consortium (EC)	1.1° × 1.1°	Döscher et al. (2022)
FGOALS-g3	CMIP6	Chinese Academy of Sciences (CAS)	2.0° × 2.0°	Li et al. (2020)

Table 4.1 – *Continuation*

Model	**Type**	**Institution**	**Resolution Atmosphere (lat × lon)**	**Reference**
GFDL-ESM4	CMIP6	National Oceanic and Atmospheric Administration, Geophysical Fluid Dynamics Laboratory (NOAA-GFDL)	1.0° × 1.2°	Dunne et al. (2020)
INM-CM4-8	CMIP6	Institute for Numerical Mathematics (INM)	1.5° × 2.0°	Volodin et al. (2018)
INM-CM5-0	CMIP6	Institute for Numerical Mathematics (INM)	1.5° × 2.0°	Volodin et al. (2018)
IPSL-CM6A-LR	CMIP6	Institut Pierre-Simon Laplace (IPSL)	1.3° × 2.5°	Boucher et al. (2020)
KACE-1-0-G	CMIP6	National Institute of Meteorological Sciences, Korea Meteorological Administration (NIMS-KMA)	1.2° × 1.8°	Lee et al. (2020a)
KIOST-ESM	CMIP6	Korea Institute of Ocean Science and Technology (KIOST)	1.9° × 1.9°	Pak et al. (2021)
MIROC6	CMIP6	Consortium JAMSTEC, AORI, NIES, R-CCS (MIROC)	1.4° × 1.4°	Tatebe et al. (2019)
MPI-ESM1-2-HR	CMIP6	Max Planck Institute for Meteorology (MPI)	0.9° × 0.9°	Mauritsen et al. (2019)
MPI-ESM1-2-LR	CMIP6	Max Planck Institute for Meteorology (MPI)	1.9° × 1.9°	Mauritsen et al. (2019)
MRI-ESM2-0	CMIP6	Meteorological Research Institute (MRI)	1.1° × 1.1°	Yukimoto et al. (2019)
NESM3	CMIP6	Nanjing University of Information Science and Technology (NUIST)	1.9° × 1.9°	Cao et al. (2018)
NorESM2-LM	CMIP6	Norwegian Climate Centre (NCC)	1.9° × 2.5°	Seland et al. (2020)
NorESM2-MM	CMIP6	Norwegian Climate Centre (NCC)	0.9° × 1.2°	Seland et al. (2020)
TaiESM1	CMIP6	Research Center for Environmental Changes, Academia Sinica (AS-RCEC)	0.9° × 1.2°	Lee et al. (2020b)
HadGEM3-GC31-HH	HighResMIP	Met Office Hadley Centre	0.23° × 0.35°	Roberts et al. (2019)
HadGEM3-GC31-HM	HighResMIP	Met Office Hadley Centre	0.23° × 0.35°	Roberts et al. (2019)

Table 4.1 – *Continuation*

Model	Type	Institution	Resolution Atmosphere (lat × lon)	Reference
HadGEM3-GC31-LL	HighResMIP	Met Office Hadley Centre	1.25° × 1.87°	Roberts et al. (2019)
HadGEM3-GC31-MM	HighResMIP	Met Office Hadley Centre	0.55° × 0.83°	Roberts et al. (2019)
MPI-ESM1-2-HR	HighResMIP	Max Planck Institute for Meteorology (MPI)	0.93° × 0.93°	Gutjahr et al. (2019)
MPI-ESM1-2-XR	HighResMIP	Max Planck Institute for Meteorology (MPI)	0.46° × 0.46°	Gutjahr et al. (2019)

4.2.2 Gridded data

The CMIP6/HighResMIP models were evaluated using daily maximum temperature data from the CHIRTS dataset developed by the Climate Hazards Center (Verdin et al., 2020). This dataset has a spatial resolution of 0.05° and provides data from 1983 to 2016. It combines three components: a high-resolution climatology (0.05° × 0.05°), interpolated in situ temperature anomaly fields, and remotely sensed infrared land surface emission anomalies from satellite observations, to support the monitoring and assessment of temperature extremes (Verdin et al., 2020).

For monthly precipitation, the models were evaluated using the CHIRPS v2 dataset, which is described in Chapter 3. This dataset combines climatological information from the Climate Hazards Center, 0.25° resolution satellite imagery, and in situ station records to generate a gridded rainfall product useful for seasonal drought monitoring and trend analysis (Funk et al., 2015). In addition, the latest CHIRPS version (v3) was considered for comparison. This new version incorporates four times more observational data sources than CHIRPS v2, significantly improving the spatial and temporal accuracy of precipitation estimates (Climate Hazards Center, 2025).

4.2.3 Model evaluation

To evaluate the performance of the CMIP6/HighResMIP models, we used Taylor diagrams (Taylor, 2001), a widely used tool in climate model assessment studies over South America (e.g., Arias et al., 2025a; Bazzanela et al., 2024; Collazo et al., 2023; Negron-Juarez et al., 2024; Ortega et al., 2021). These diagrams summarize the degree of statistical similarity between the reference data (CHIRTS for maximum temperature and CHIRPS for precipitation) and the simulations of each model, using three metrics (Taylor, 2001). The spatial correlation coefficient quantifies the similarity between the observed and simulated spatial patterns, with values closer to 1 indicating a strong spatial agreement. The root mean square error (RMSE) is defined as the square root of the mean of the squared differences between observed and simulated data; lower RMSE values (i.e., closer to 0) denote a better fit. Finally, the normalized standard deviation evaluates the model's ability to reproduce the spatial variability of the data, expressed as the ratio between the simulated and observed standard deviations. Values close to 1 suggest that the model adequately represents the spatial dispersion of the data.

The evaluation was performed considering a single combination of events: HEs defined from the 90th percentile (P90), DEs identified using the SPI3, and their combination (CDHEs identified from SPI3 and P90; SPI3-P90). The statistics used in the Taylor diagrams were calculated using the original resolution of each model. Additionally, for the multi-model median ensemble, all models were interpolated to a common $1^\circ \times 1^\circ$ grid using the conservative technique (Remapcon), suitable for conservative variables such as precipitation (Omay et al., 2024).

To classify the models according to their performance in simulating the characteristics of HEs, DEs, and CDHEs, we used the Taylor Skill Score (TS). This metric, derived from Taylor diagrams, evaluates model performance based on the Pearson correlation coefficient and the standard deviation with respect to the reference dataset for each spatial field (Arias et al., 2025a). The TS was computed following equation 4.1, as proposed by Hirota & Takayabu (2013):

$$TS = \frac{(1+R)^4}{4 \cdot \left(\frac{\sigma_m}{\sigma_o} + \frac{\sigma_o}{\sigma_m}\right)^2} \tag{4.1}$$

where R represents the correlation coefficient between the model and reference spatial fields, and σ_o and σ_m denote the standard deviations of the reference and simulated fields, respectively Arias et al. (2025a).

4.3 Results

4.3.1 Performance of CMIP6/HighResMIP models in the simulation of maximum temperature and precipitation

Although the main objective of this study is not the direct evaluation of maximum temperature and precipitation, we conducted a preliminary analysis of these variables in order to examine how the models represent them, given that they are the basis for calculating the extreme indices used in this work.

The Taylor diagrams show correlations above 0.6 for all seasons in most individual models, ERA5, CPC, and the ensemble median, relative to the reference dataset (CHIRTS), suggesting that they are able to reproduce, to some extent, the spatial pattern of maximum temperature over the TSA (Figure 4.1a-d). Most of the analyzed datasets exhibit standard deviations greater than 1, indicating an overestimation of variability compared with CHIRTS, with the bias being smaller in June-July-August (JJA). CPC shows the highest correlations across all seasons, with values close to 0.95, as well as the lowest root mean square error (RMSE) relative to the reference. According to the TS (Figure B.1), CPC and ERA5 exhibit the highest values, exceeding 0.76. In JJA, the multimodel ensemble performs better than the individual models. Overall, all HighResMIP models record good TS values. Most CMIP6 models also stand out for exhibiting moderate to good TS values, with IPSL-CM6A-LR showing TS values above 0.7 for all seasons. KIOST-ESM and MIROC6 display the poorest performance for maximum temperature. During JJA, the highest skill is observed across most of the analyzed datasets.

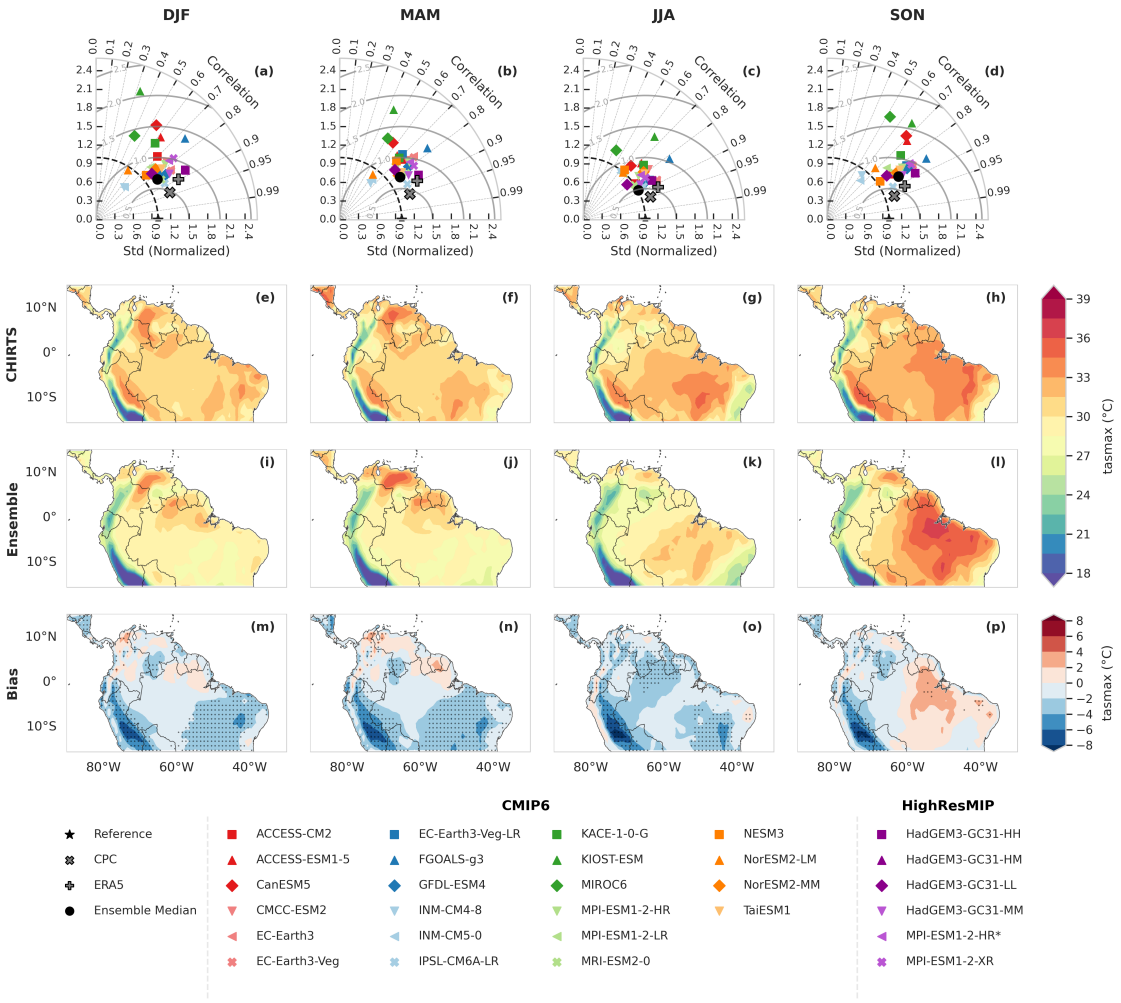

Figure 4.1: Seasonal evaluation of daily maximum temperature over tropical South America. (a–d) Taylor diagrams. (e–h) Seasonal climatology for CHIRTS (reference). (i–l) Multimodel seasonal median. (m–p) Multimodel seasonal median biases. Dots indicate where at least 80 % of the CMIP6/HighResMIP models agree on the sign of the multimodel median bias. All spatial fields (e–p) are shown at a common resolution of 1° × 1°.

The ensemble median shows a maximum temperature field similar to that of CHIRTS (Figure 4.1e-l). Nevertheless, the bias maps (Figure 4.1m–p) show that the ensemble underestimates the maximum temperature over most of the TSA during December-January-February (DJF), March-April-May (MAM), and JJA, with high agreement over Peru, eastern and central Brazil, and some northern regions of the TSA. In September-October-November (SON), the ensemble overestimates temperature in northeastern Brazil, but only a small part of this region shows agreement among models.

Regarding precipitation, the CMIP6/HighResMIP models show a range of correlations between 0.3 and 0.8 with respect to the reference database (CHIRPS v2), during DJF and MAM (Figure 4.2a-d). The FGOALS-g3 and NESM3 models have correlations close to zero in DJF and MAM, respectively. For JJA and SON, most models cluster around correlation values between moderate (0.6) and strong (0.8), with better correlations in JJA. Most models have standard deviations

greater than 1, suggesting an overestimation of variability with respect to CHIRPS v2. In JJA, the models have a lower RMSE, in contrast to the other seasons. The multimodel ensemble exhibits strong correlations in all seasons, with the best performance observed in JJA, showing a correlation of 0.9, the smallest difference from the reference standard deviation, and the lowest RMSE. ERA5 and CHIRPS v3 also show strong correlations and standard deviations close to the reference across all seasons; however, during DJF, MAM, and JJA, some individual models outperform them, and in JJA, the ensemble median shows superior performance.

Based on the TS (Figure B.2), NorESM2-MM (CMIP6) demonstrates the best performance, with TS values in DJF and MAM exceeding those of ERA5, CHIRPS v3, and the ensemble. In contrast, FGOALS-s2 (CMIP6) shows the poorest performance across all seasons. As observed in the Taylor diagram, the ensemble median attains the highest skill in JJA, with a TS value of 0.77.

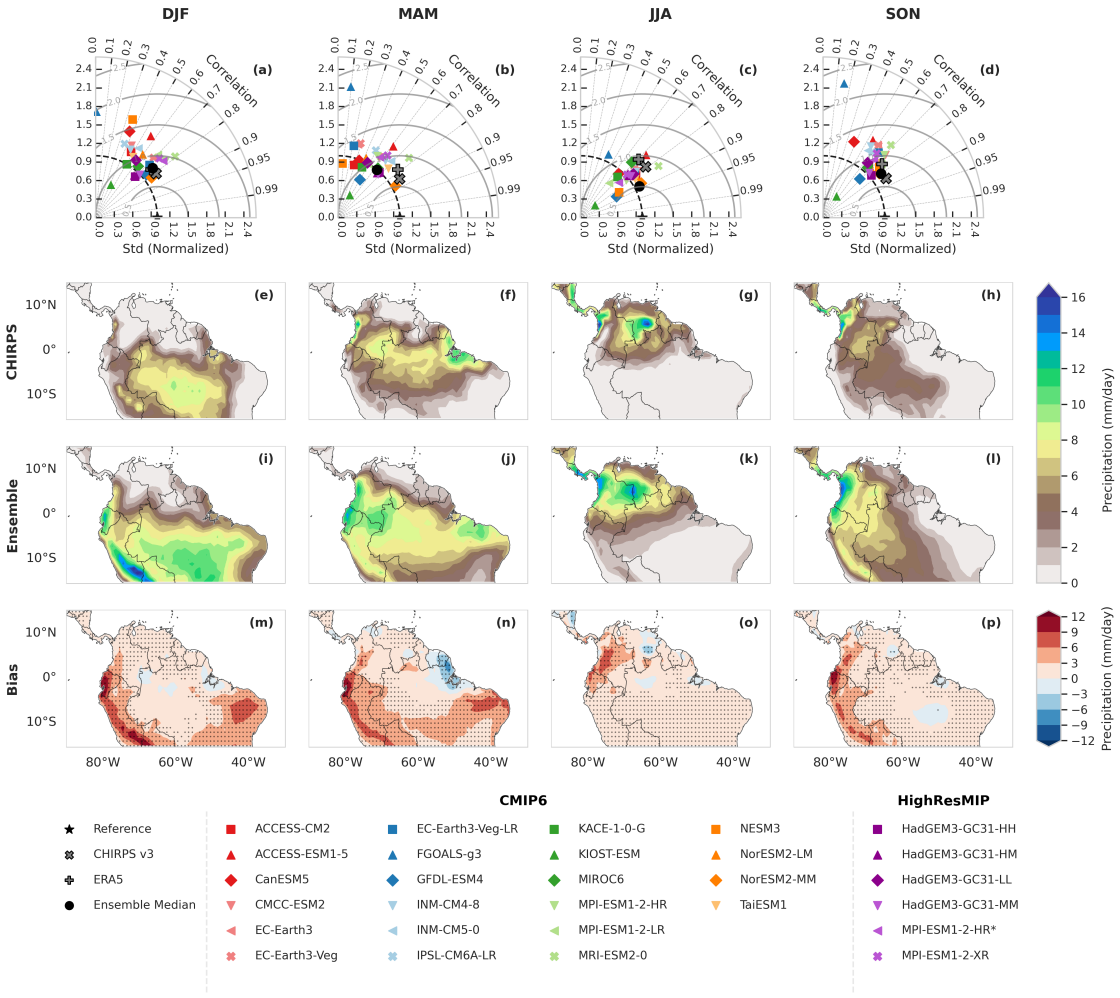

Figure 4.2: Seasonal evaluation of daily precipitation over tropical South America. (a–d) Taylor diagrams. (e–h) Seasonal climatology for CHIRPS v2 (reference). (i–l) Multimodel seasonal median. (m–p) Multimodel seasonal median biases. Dots indicate where at least 80 % of the CMIP6/HighResMIP models agree on the sign of the multimodel median bias. All spatial fields (e–p) are shown at a common resolution of 1° × 1°.

Similar to maximum temperature, most of the analyzed datasets exhibit their best performance for precipitation during JJA (Figure B.2).

When comparing the ensemble median precipitation rate field with CHIRPS v2 (Figure 4.2e-l), it is observed that, although the ensemble reproduces the seasonal pattern, it tends to spatially expand areas with higher precipitation (mm/day). The bias maps indicate an overestimation across much of the TSA (Figure 4.2m-p), with the largest differences located over the tropical Andes in all seasons, where there is also a high degree of agreement between models.

4.3.2 Performance of CMIP6/HighResMIP models in the simulation of hot events

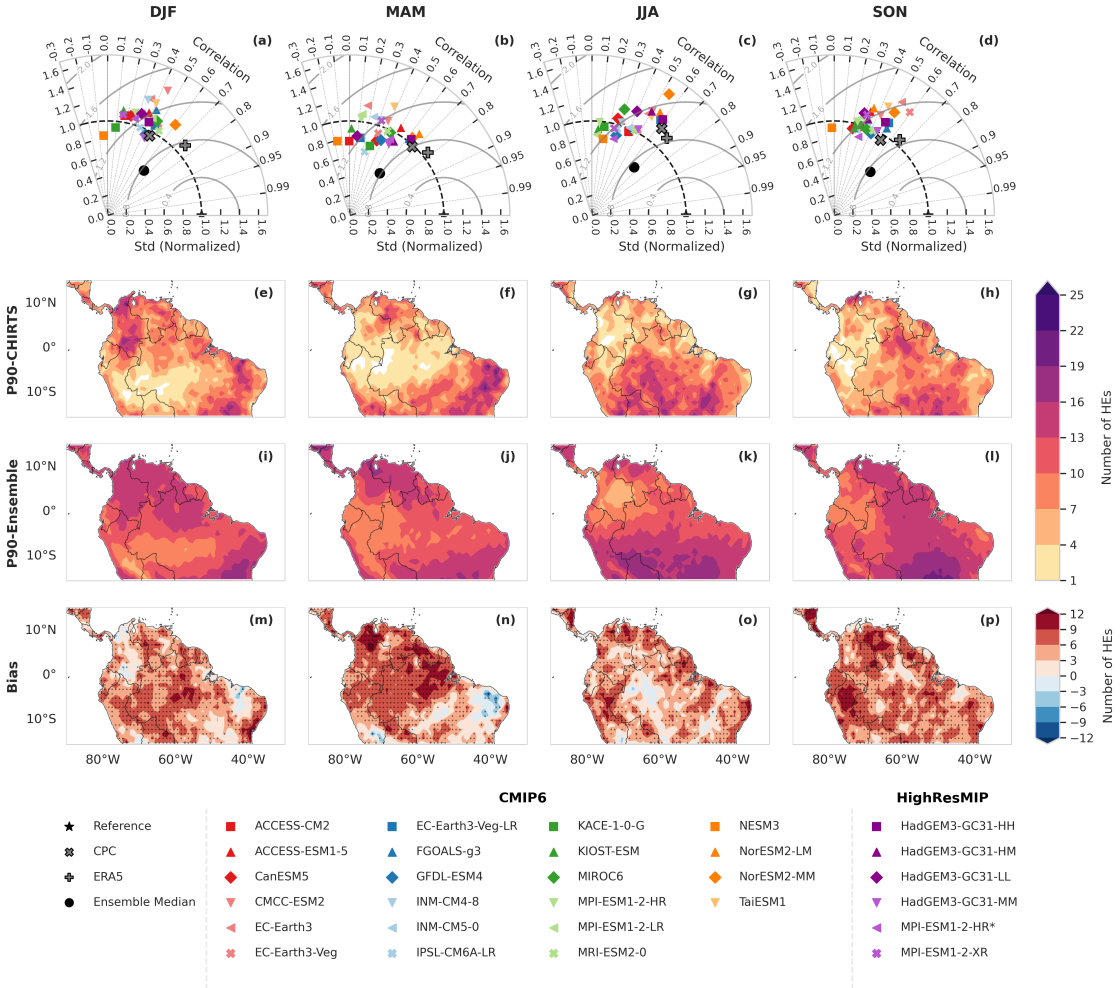

Figure 4.3: Seasonal evaluation of count of Hot Events (number of HEs) over tropical South America. (a–d) Taylor diagrams. (e–h) Seasonal climatology for CHIRTS (reference). (i–l) Multimodel seasonal median. (m–p) Multimodel seasonal median biases. Dots indicate where at least 80 % of the CMIP6/HighResMIP models agree on the sign of the multimodel median bias. All spatial fields (e–p) are shown at a common resolution of 1° × 1°.

Figure 4.3a–b shows how CMIP6/HighResMIP models simulate the number of HEs over TSA. Most models show weak to moderate correlations (0.1 – 0.6) relative to CHIRTS, while NESM3 stands out by exhibiting negative correlations during DJF, MAM, and SON. In contrast, the multimodel ensemble attains higher correlations than most individual models, with values close to 0.65 in all seasons. Regarding the standard deviation, most models exhibit greater variability during DJF, JJA, and SON, whereas the ensemble median underestimates variability compared to CHIRTS in all seasons. Regarding RMSE, the ensemble median also stands out by achieving the lowest values compared to the individual models. Both ERA5 and CPC perform considerably better than the models, except in DJF, where differences in correlation and RMSE are observed between the two datasets, with ERA5 showing the best performance. In the TS analysis (Figure B.3), the ERA5 reanalysis shows the best performance in the count of HEs, particularly during DJF and MAM. CPC presents moderate performance in MAM and JJA, while the ensemble median shows its best performance in JJA.

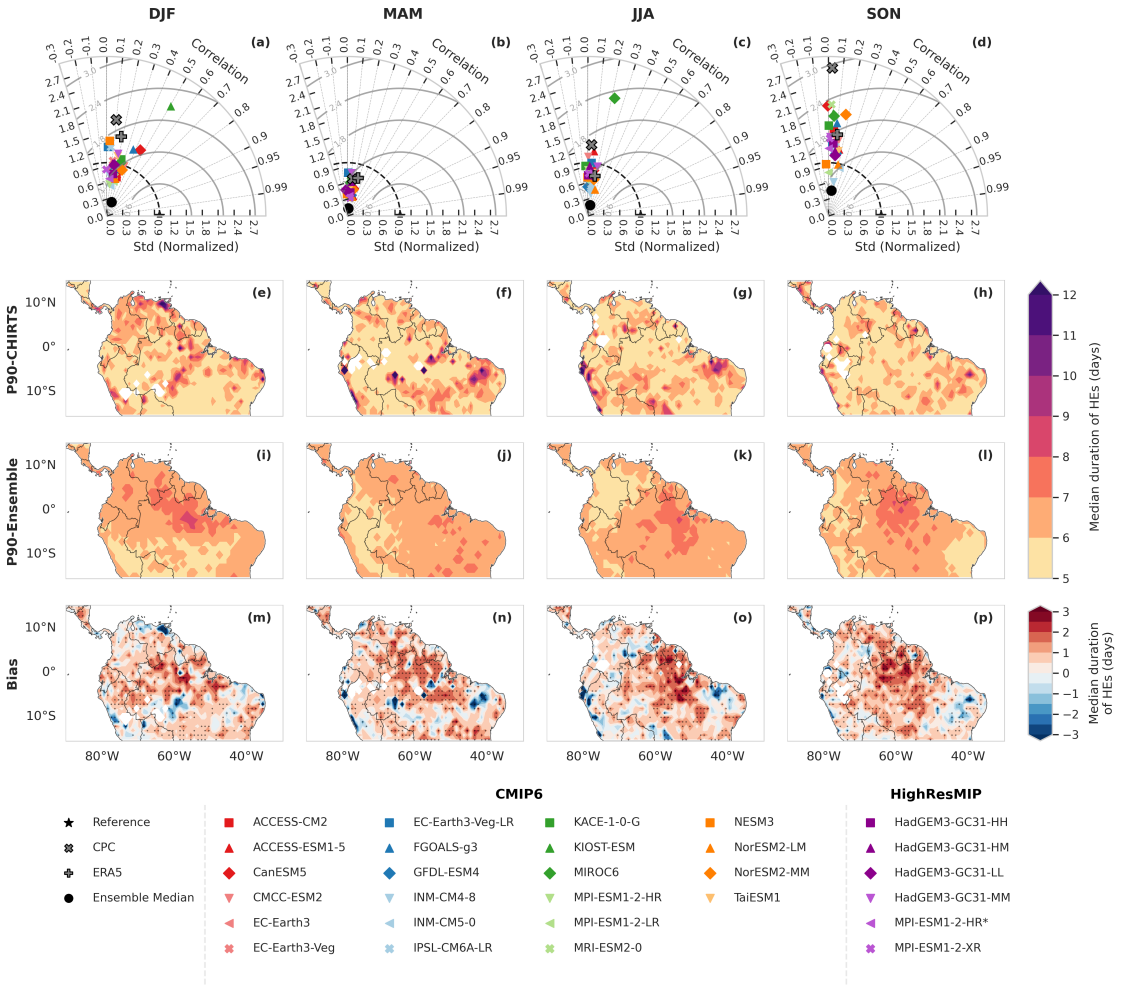

Figure 4.4: Seasonal evaluation of median duration of Hot Events (HEs) over tropical South America. (a–d) Taylor diagrams. (e–h) Seasonal climatology for CHIRTS (reference). (i–l) Multimodel seasonal median. (m–p) Multimodel seasonal median biases. Dots indicate where at least 80 % of the CMIP6/HighResMIP models agree on the sign of the multimodel median bias. All spatial fields (e–p) are shown at a common resolution of 1° × 1°.

When compared with the individual models, the ensemble outperforms them in three out of the four seasons, highlighting the value of model combination for improving simulation representation. Although most individual models show poor performance according to the TS, NorESM2-MM stands out in DJF, and HadGEM3-GC31HH (HighResMIP), FGOALS-s2, NorESM2-LM, and NorESM2-MM perform better than the ensemble in MAM. By contrast, NESM3 shows the poorest performance in the four seasons (Figure B.3).

The ensemble median (Figure 4.3i–j) tends to reproduce the occurrence pattern of HEs observed in CHIRTS (Figure 4.3e–h), showing the areas with higher occurrences in northern and eastern TSA during DJF and MAM, in central and southern Amazonia during JJA, and in eastern and southern TSA during SON. However, the areas of higher occurrence are more widespread in the ensemble compared to the more localized regions shown by the reference dataset. When analyzing the bias (Figure 4.3m–p), the ensemble median overestimates the number of events across much of TSA.

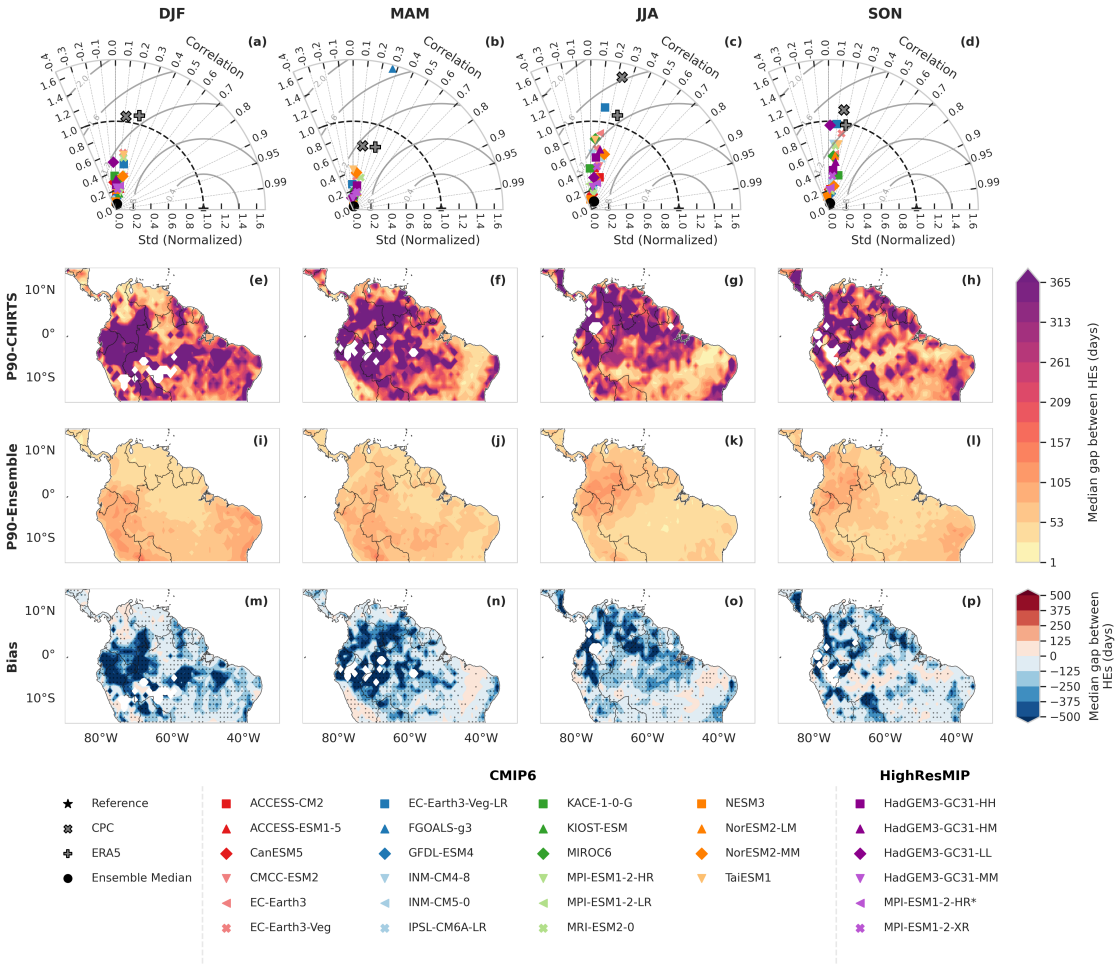

Figure 4.5: Seasonal evaluation of median gap between Hot Events (HEs) over tropical South America. (a–d) Taylor diagrams. (e–h) Seasonal climatology for CHIRTS (reference). (i–l) Multimodel seasonal median. (m–p) Multimodel seasonal median biases. Dots indicate where at least 80 % of the CMIP6/HighResMIP models agree on the sign of the multimodel median bias. All spatial fields (e–p) are shown at a common resolution of 1° × 1°.

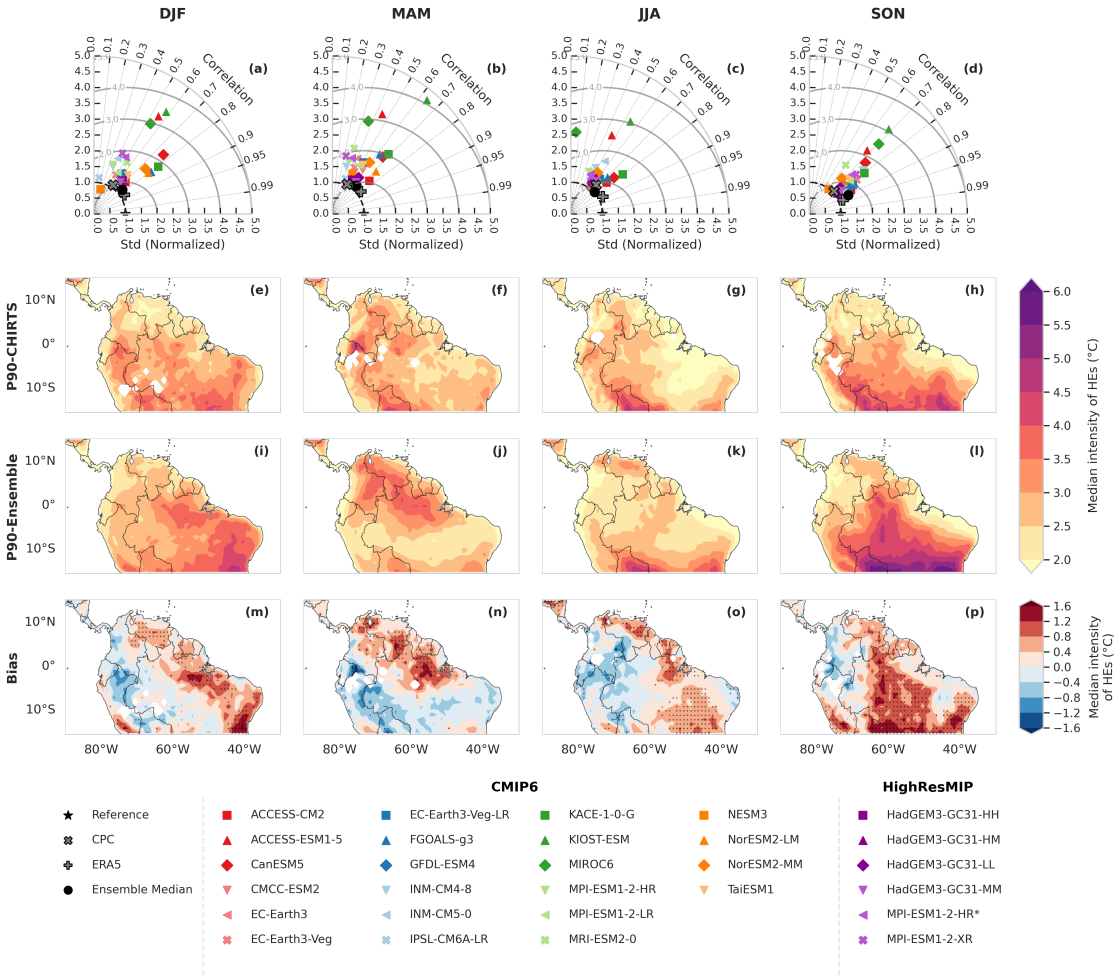

Figure 4.6: Seasonal evaluation of median intensity of Hot Events (HEs) over tropical South America. (a–d) Taylor diagrams. (e–h) Seasonal climatology for CHIRTS (reference). (i–l) Multimodel seasonal median. (m–p) Multimodel seasonal median biases. Dots indicate where at least 80 % of the CMIP6/HighResMIP models agree on the sign of the multimodel median bias. All spatial fields (e–p) are shown at a common resolution of 1° × 1°.

In addition, a high level of agreement is observed among CMIP6/HighResMIP models, suggesting that these biases are common across models. On the other hand, underestimations are identified in northern and southern Colombia, as well as in northeastern Brazil during DJF, in southern Peru and eastern Brazil during MAM (also with high agreement), and in northwestern Brazil during JJA (Figure 4.3m–p).

Regarding the duration of HEs (Figure 4.4), the CMIP6/HighResMIP models, CPC and ERA5, show weak correlations in all seasons, with values concentrated between 0.0 and 0.4. During MAM and JJA, the standard deviations are generally below 1, suggesting that these databases tend to underestimate variability compared to CHIRTS. In SON, most CMIP6/HighResMIP models, as well as CPC and ERA5, exhibit higher variability. The ensemble median shows a very low correlation, close to 0.1 in all seasons, and also underestimates the spatial variability in each of them, indicating a limited ability to reproduce the spatial pattern of HEs duration observed in CHIRTS. Although the TS is calculated for this characteristic, the highest ranks correspond to some individual models

with values of 0.1 and 0.2, indicating very limited performance among the models, ERA5, and CPC (Figure B.4). The ensemble ranks last in MAM with a TS of 0.01. Figure 4.4i-l shows that the ensemble's low score is due to its inability to adequately reproduce the duration pattern of HEs observed in CHIRTS. The bias analysis shows that the ensemble tends to overestimate the duration of HEs in much of TSA, while underestimating it in specific areas, such as western Peru. In both cases, there is a high degree of agreement among the models.

Similar to what is observed for duration, datasets present limitations in reproducing the spatial pattern of the median gap between HEs (Figure 4.5). All of them exhibit weak correlations (between 0.0 and 0.4) and an underestimation of variability compared to CHIRTS, except during JJA, when CPC, ERA5, and EC-Earth3-Veg-LR (CMIP6) show higher variability (Figure 4.5a–d). The ensemble median records the lowest performance compared to the individual models, ranking last according to the TS in all seasons. Although ERA5 and CPC achieve the highest TS values among the datasets analyzed, these remain between 0.1 and 0.2, indicating that performance is low across all datasets (Figure B.5). The poor ability of the models to represent the median gap between HEs is associated with their simulation of a greater number of events and longer durations across much of TSA compared to CHIRTS. As a result, the median gap between events in the ensemble is shorter, ranging from 53 to 157 days, while CHIRTS has medians greater than 365 days in regions of western and northern TSA (Figure 4.5e–l). This difference is reflected in the bias maps (Figure 4.5m–p), where the ensemble median underestimates the gap between events, with differences exceeding –500 days in some areas of western and northern TSA. In addition, a high degree of agreement is observed among the models.

Most of the databases analyzed show correlations above 0.6, indicating that they tend to reproduce the spatial pattern of median HE intensity observed in CHIRTS (Figure 4.6a–d). The strongest correlations occur during SON, ranging from 0.6 to 0.9. Across all seasons, an overestimation of variability is observed relative to CHIRTS; however, ERA5 and the ensemble median stand out by displaying standard deviations close to the reference and a lower RMSE. The TS ranks ERA5 first in all seasons (between 0.6 and 0.8), followed by the ensemble median (between 0.4 and 0.7) (Figure B.6). During MAM, the ACCESS-CM2 model also stands out, outperforming the ensemble. Overall, the highest TS values are obtained during SON, with three HadGEM3-GC31 models from HighResMIP and the ACCESS-CM2 model from CMIP6 showing values above 0.6 (Figure B.6). When analyzing the spatial field of temperature intensity from the ensemble median, a pattern similar to CHIRTS is observed (Figure 4.6e–l). However, the magnitude of intensity is overestimated over southern Peru and eastern TSA during DJF and JJA, over northern TSA in MAM, and over Venezuela, the Guianas, and central and southern TSA in SON (Figure 4.6m–p). These overestimations exhibit a high degree of agreement among the models, indicating that this is a common bias. In the rest of the region, the models underestimate the intensity relative to CHIRTS.

4.3.3 Performance of CMIP6/HighResMIP models in the simulation of Dry events

Figure 4.7 shows how the models reproduce the spatial pattern of the number of DEs compared to CHIRPS v2. Individual models and ERA5 exhibit weak, and in some cases even negative, correlations (Figure 4.7a–d). Nevertheless, they tend to capture the amplitude of spatial variability, with standard deviations close to 1, although some models exceed this during SON. The ensemble median also displays weak correlations in most seasons, except in JJA, where it reaches values near

0.5. However, the ensemble underestimates variability across all seasons relative to CHIRPS v2. CHIRPS v3 exhibits variability closer to the reference but shows correlations between 0.5 and 0.6 in all seasons. The TS shows very limited performance, with low values in CMIP6/HighResMIP, ERA5 and CHIRPS v3 (Figure B.7). The ensemble median, in particular, records TS values below 0.1, ranking among the lowest during DJF and MAM.

Although the ensemble median reproduces the highest number of events in the regions where CHIRPS v2 also records the greatest frequency, it simulates a broader spatial extent (Figure 4.7e–l). In addition, the ensemble exhibits a more homogeneous pattern, whereas CHIRPS v2 shows greater spatial variability.

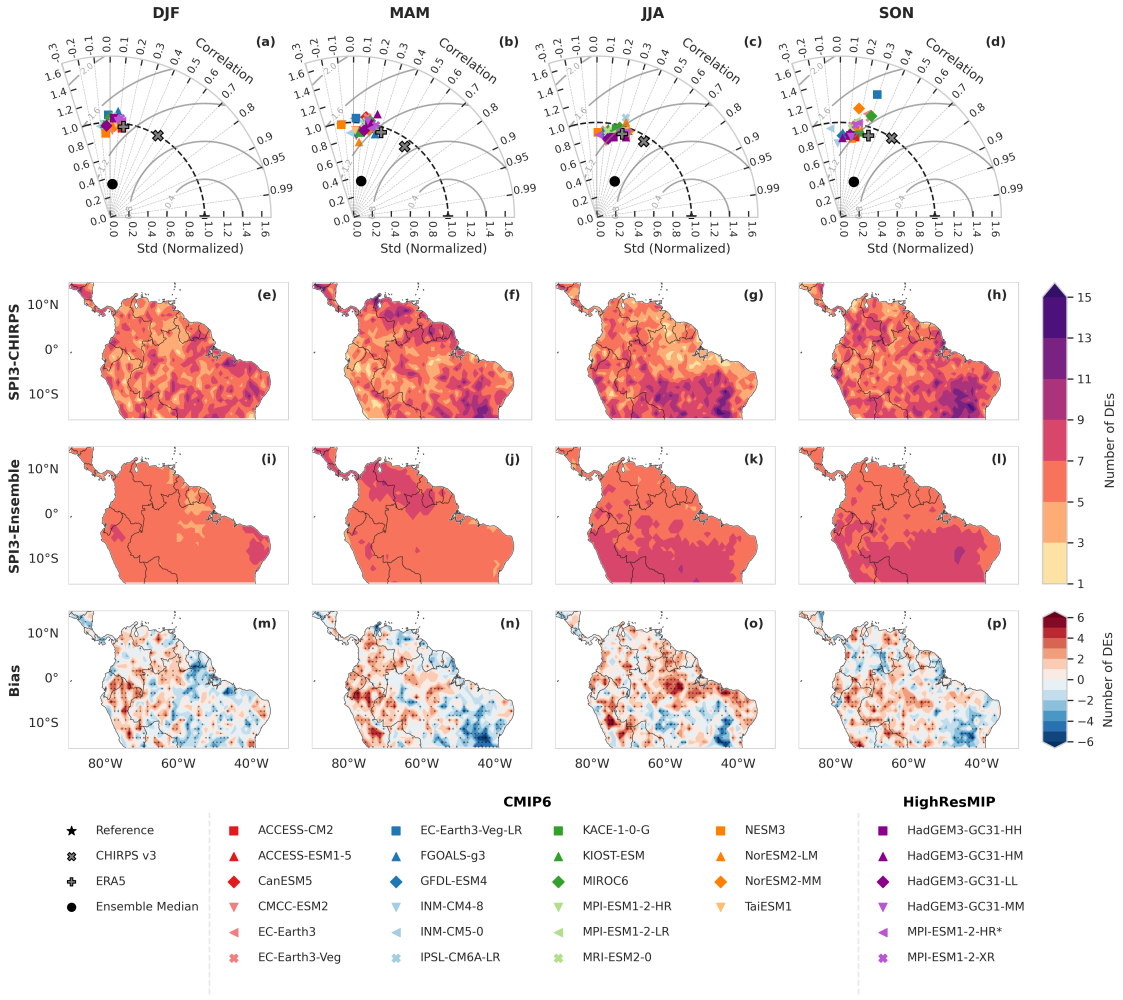

Figure 4.7: Seasonal evaluation of count of Dry Events (number of DEs) over tropical South America. (a–d) Taylor diagrams. (e–h) Seasonal climatology for CHIRPS v2 (reference). (i–l) Multimodel seasonal median. (m–p) Multimodel seasonal median biases. Dots indicate where at least 80 % of the CMIP6/HighResMIP models agree on the sign of the multimodel median bias. All spatial fields (e–p) are shown at a common resolution of 1° × 1°.

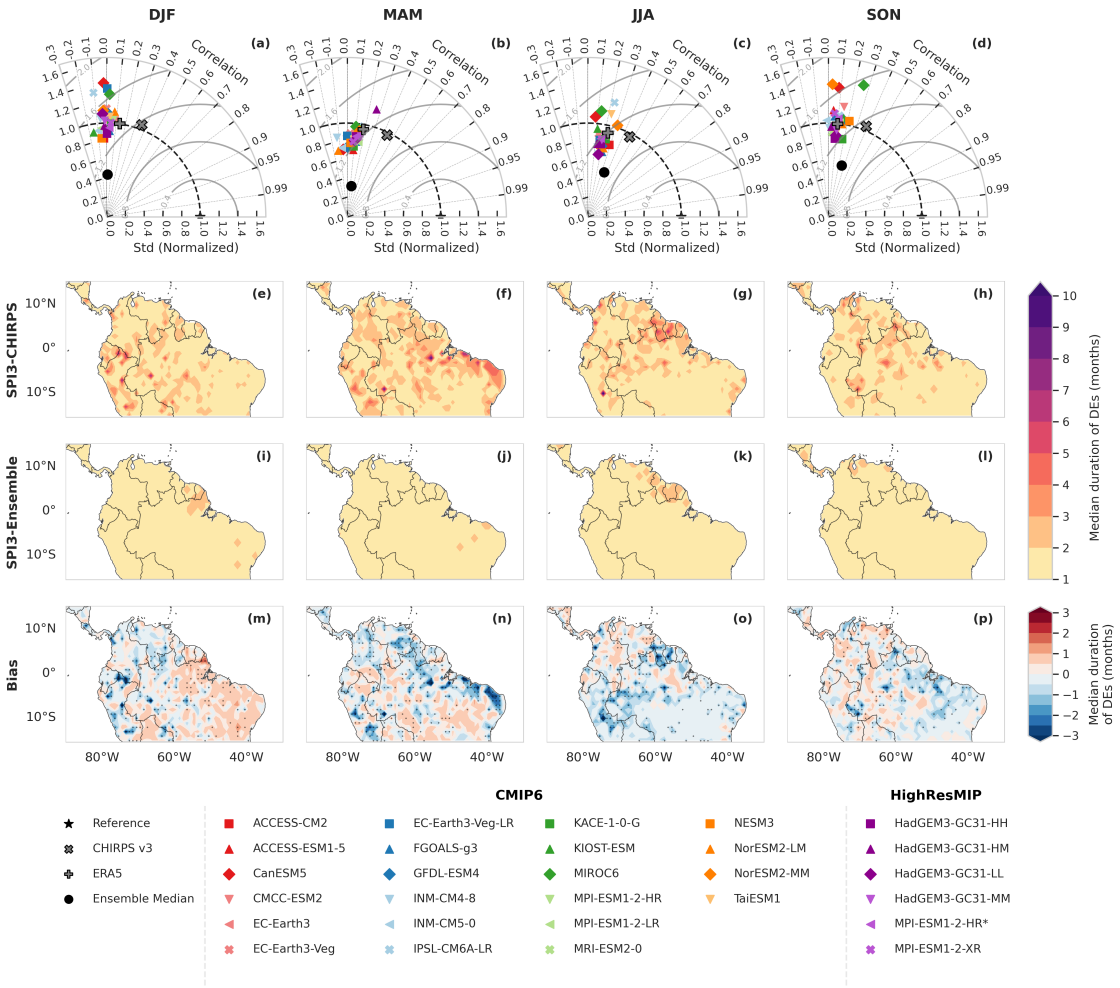

Figure 4.8: Seasonal evaluation of median duration of Dry Events (DEs) over tropical South America. (a–d) Taylor diagrams. (e–h) Seasonal climatology for CHIRPS v2 (reference). (i–l) Multimodel seasonal median. (m–p) Multimodel seasonal median biases. Dots indicate where at least 80 % of the CMIP6/HighResMIP models agree on the sign of the multimodel median bias. All spatial fields (e–p) are shown at a common resolution of 1° × 1°.

The bias analysis shows that the models tend to overestimate the number of DEs in western TSA and northeastern Brazil during DJF, MAM, and SON, while in JJA the largest overestimations are concentrated in western and northern TSA (Figure 4.7m–p). In contrast, the rest of the region shows an underestimation of the number of events, which is most pronounced in southeastern Brazil.

The CMIP6/HighResMIP models and ERA5 present limitations in reproducing the spatial pattern of the median duration of DEs compared to CHIRPS v2, with weak correlations close to zero and even negative during DJF and MAM (Figure 4.8a–d). The multimodel ensemble does not provide improvements over the individual models in these seasons, ranking among the lowest in the TS. In JJA and SON, the ensemble achieves higher correlations than the individual models and ERA5; however, they remain weak (0.3 – 0.4) and underestimate variability relative to CHIRPS v2 across all seasons. CHIRPS v3, in turn, exhibits standard deviations close to the reference in all seasons, although its correlations remain between 0.3 and 0.5. Overall, although a performance

ranking is obtained (Figure B.8), all evaluated datasets show low skill for this characteristic.

The ensemble shows a median duration of 1 to 3 months over TSA, while CHIRPS v2 exhibits longer durations in some areas, exceeding 5 months (Figure 4.8e–l). The bias of the ensemble median presents an overestimation of duration in Bolivia and eastern Brazil during DJF, in southern and central TSA during MAM, in the north during JJA, and in the west during SON (Figure 4.8m-p). Across the rest of the region, the ensemble tends to underestimate duration compared to CHIRPS v2.

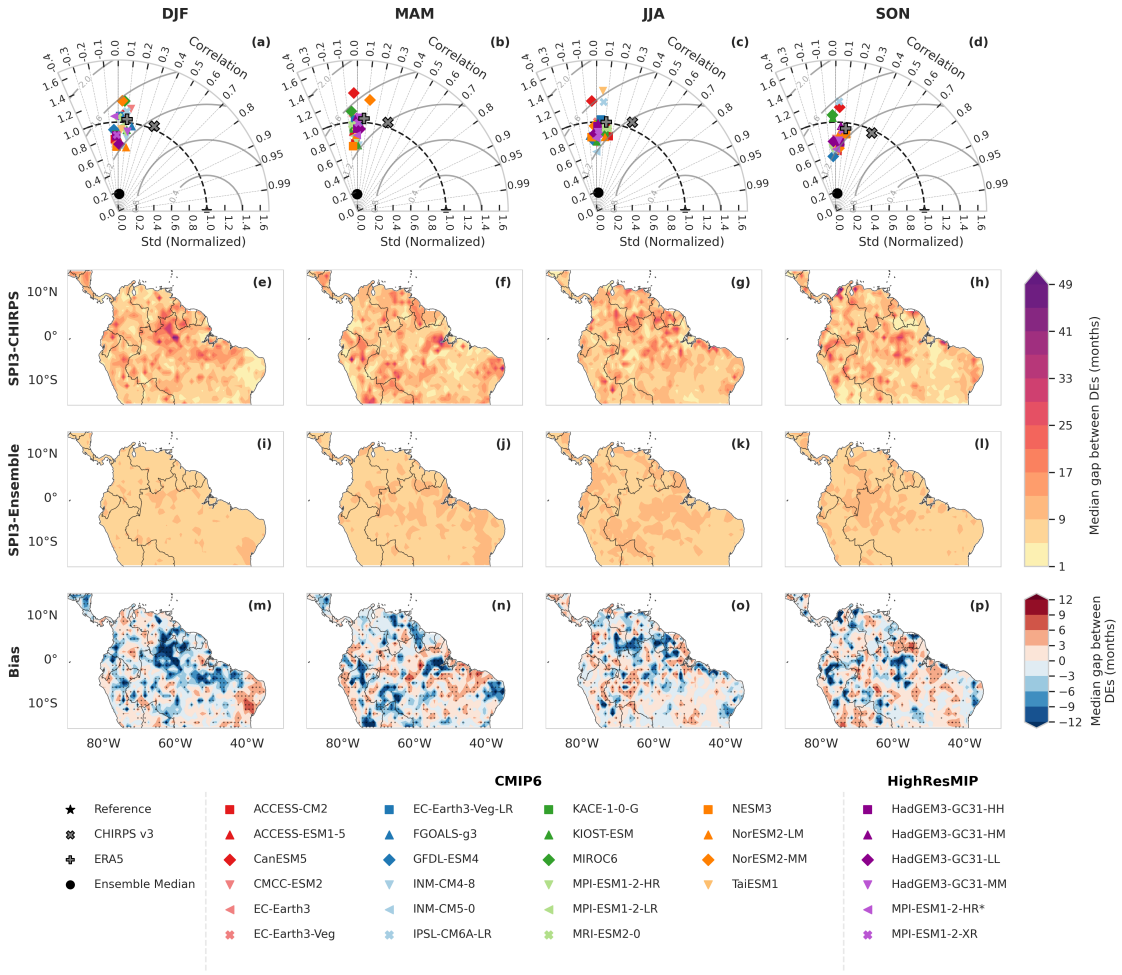

Figure 4.9: Seasonal evaluation of median gap between Dry Events (DEs) over tropical South America. (a–d) Taylor diagrams. (e–h) Seasonal climatology for CHIRPS v2 (reference). (i–l) Multimodel seasonal median. (m–p) Multimodel seasonal median biases. Dots indicate where at least 80 % of the CMIP6/HighResMIP models agree on the sign of the multimodel median bias. All spatial fields (e–p) are shown at a common resolution of 1° × 1°.

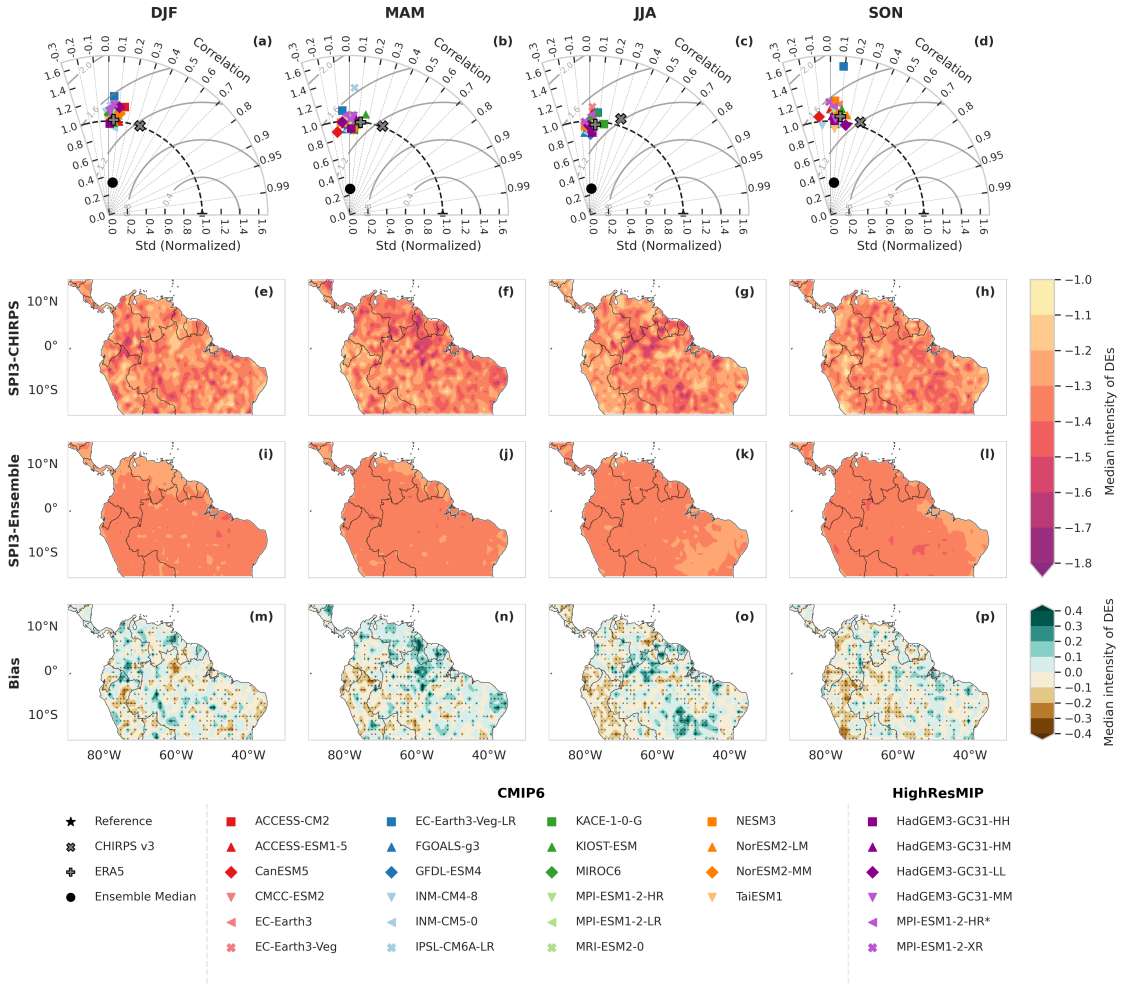

Figure 4.10: Seasonal evaluation of median intensity of Dry Events (DEs) over tropical South America. (a–d) Taylor diagrams. (e–h) Seasonal climatology for CHIRPS v2 (reference). (i–l) Multimodel seasonal median. (m–p) Multimodel seasonal median biases. Dots indicate where at least 80 % of the CMIP6/HighResMIP models agree on the sign of the multimodel median bias. All spatial fields (e–p) are shown at a common resolution of 1° × 1°.

The poor performance of the models in simulating DEs frequency and median duration is also reflected in the median gap between events, with correlations ranging from –0.2 to 0.2 (Figure 4.9a–d). Most models, as well as the ensemble, underestimate variability with respect to CHIRPS v2 across all seasons, with this underestimation being more pronounced in the multimodel ensemble. ERA5 and CHIRPS v3 show standard deviations close to the reference, but their correlations remain weak. However, correlations are slightly higher in CHIRPS v3 (∼0.4) compared to ERA5 (∼0.1). Consequently, the TS indicates low performance, with values below 0.25 (Figure B.9). Similar to what is observed for the other DEs characteristics, the ensemble shows more homogeneous distributions, with a median gap between events in TSA ranging from 5 to 13 months (Figure 4.9i–l). In contrast, CHIRPS v2 shows a more heterogeneous distribution, with values ranging from 9 to 33 months in some regions (Figure 4.9e–h). The bias analysis indicates that the models mainly underestimate the gap between events in the north of the TSA, the Amazon, and Peru, while the most pronounced overestimations are concentrated in eastern Brazil and the tropical Andes (Figure

4.9m–p).

Unlike HEs, where some CMIP6/HighResMIP models show good performance in representing intensity (Figure 4.6a–d), for DEs the models exhibit clear limitations in reproducing the drought severity pattern observed in CHIRPS v2 (Figure 4.10a–d). The individual models, the ensemble median, and ERA5 cluster around correlation values between –0.2 and 0.2, while CHIRPS v3 reaches slightly higher values, between 0.3 and 0.4. ERA5 and CHIRPS v3 maintain standard deviations close to the reference across all seasons, in contrast to the ensemble median, which tends to underestimate them. During DJF and SON, most models overestimate variability, whereas in MAM and JJA some overestimate and others underestimate it. All datasets show high RMSE relative to the reference, confirming their limitations in representing drought severity. This is reflected in the TS, where none of the datasets stand out, with performance values below 0.2 (Figure B.10).

The ensemble median exhibits a more homogeneous distribution of drought severity across all seasons compared to CHIRPS v2. While CHIRPS v2 records median intensity values below –1.8 in some TSA regions, associated with severe droughts ($-2.0 \leq \text{SPI} < -1.5$), the model ensemble tends to show moderate droughts ($-1.5 \leq \text{SPI} < -1.0$) over much of the region (Figure 4.10e–l). The bias maps exhibit an underestimation of intensity by the ensemble relative to CHIRPS v2, although overestimations appear in certain areas (Figure 4.10m–p). In both cases, there is a high degree of agreement among the models in specific regions.

4.3.4 Performance of CMIP6/HighResMIP models in the simulation of compound dry and hot events

Figure 4.11 shows the performance of the datasets in simulating the number of CDHEs over TSA. The CMIP6/HighResMIP models display correlations ranging from –0.2 to 0.5, with NESM3 standing out for its negative value (–0.3) in MAM (Figure 4.11a–d). Overall, most models exhibit standard deviations higher than the reference (CHIRPSv2/CHIRTS), along with high RMSE. The ensemble median does not outperform the individual models, recording correlations between 0.3 and 0.4 and underestimating the variability of CDHEs counts compared to the reference. ERA5 shows the best performance in DJF and MAM, with correlations above 0.6 and standard deviations close to 1. The TS highlights the overall limitations across datasets, with the exception of ERA5, which reaches a value of 0.48 in MAM (Figure B.11).

When comparing the ensemble median with CHIRPSv2/CHIRTS (Figure 4.11e–l), several limitations become evident. One of them is its tendency to suggest CDHEs across the entire TSA, whereas CHIRPSv2/CHIRTS, depending on the season, show regions without events: the south in DJF, the central area in MAM, the north in JJA, and the west in SON. The ensemble not only overestimates the spatial extent of events but also their frequency compared to the reference datasets. This is reflected in the bias maps (Figure 4.11m–p), which show overestimations exceeding 2 events across much of TSA during DJF and MAM, in the north during JJA, and in the west and central areas during SON, with model agreement. An exception occurs in MAM, when the ensemble shows fewer events in eastern Brazil, with differences ranging from 4 to 8 events relative to the reference datasets.

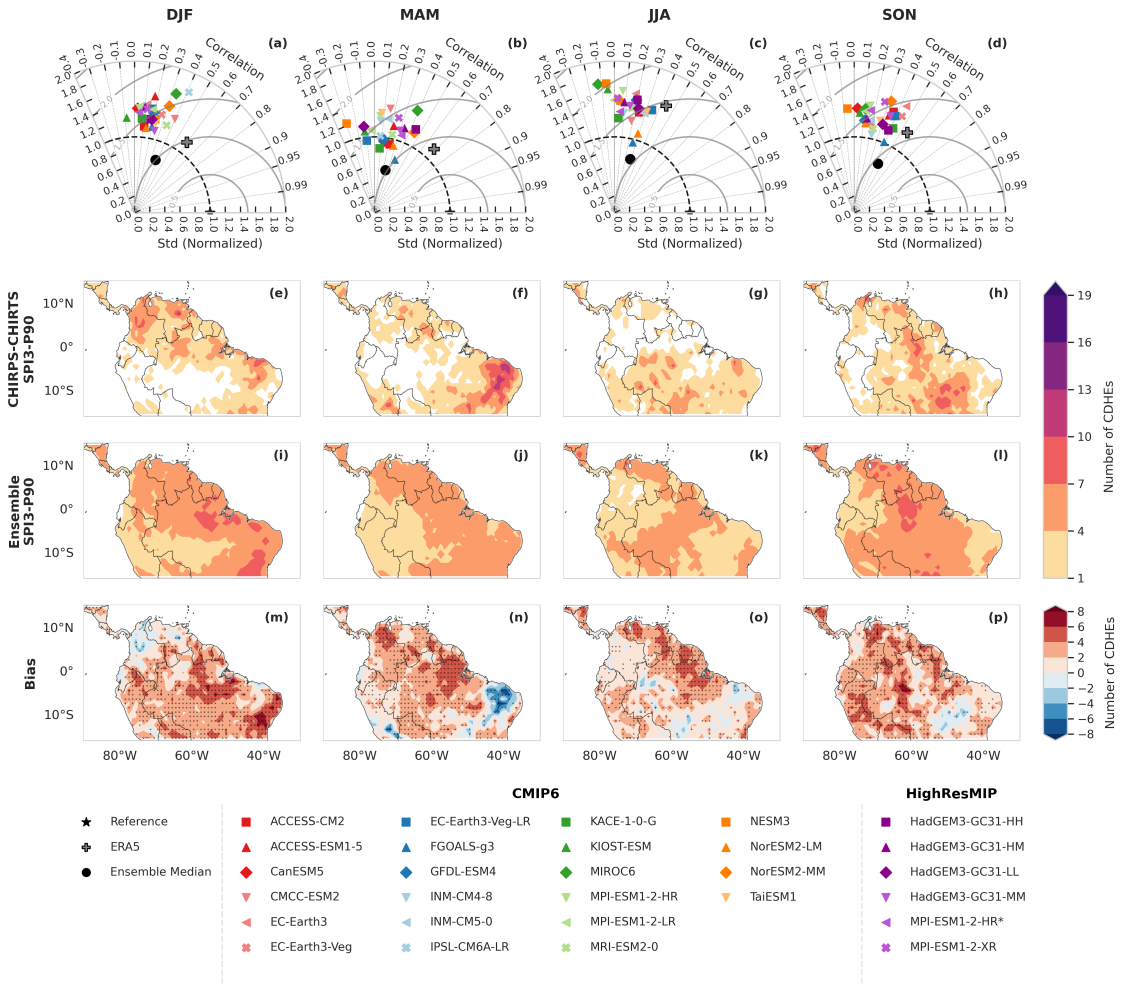

Figure 4.11: Seasonal evaluation of count of Compound Dry and Hot Events (number of CDHEs) over tropical South America. (a–d) Taylor diagrams. (e–h) Seasonal climatology for CHIRPS v2/CHIRTS (reference). (i–l) Multimodel seasonal median. (m–p) Multimodel seasonal median biases. Dots indicate where at least 80 % of the CMIP6/HighResMIP models agree on the sign of the multimodel median bias. All spatial fields (e–p) are shown at a common resolution of 1° × 1°.

For the median duration of CDHEs, ERA5, the ensemble median, and most individual models show correlations close to 0.0, except in DJF, when ACCESS-ESM1-5, CanESM5, and KIOST-ESM reach values between 0.3 and 0.4 (Figure 4.11a–d). Regarding the standard deviation, during DJF and MAM some CMIP6/HighResMIP models and ERA5 record values close to 1. However, in MAM and JJA, the largest overestimations are observed, along with the highest RMSE in most individual models. The ensemble median, in turn, underestimates the variability of median duration in all seasons. These limitations are reflected in the TS values, which do not exceed 0.2 (Figure B.12).

The ensemble median shows the longest CDHEs durations in northern and eastern TSA during DJF, in the east during MAM, and in central TSA during the remaining seasons, with values ranging from 8 to 11 days (Figure 4.12i–l). CHIRPSv2/CHIRTS agree in identifying the same regions as those with the longest durations, although in some cases the reference reaches values above 15 days, such as in central Brazil during MAM (Figure 4.12e–h). It is noteworthy that in DJF and

MAM, when the reference does not report durations (white areas over TSA) due to the absence of events, the ensemble suggests the shortest durations, as observed in southern TSA in DJF and in the west in MAM. The bias (Figure 4.12m–p), calculated only for regions where both datasets present values, indicates that the ensemble tends to overestimate duration across much of TSA, with a high level of agreement among models. However, substantial underestimations are found in central Brazil during DJF, in northern Peru and eastern Brazil during JJA, and in northern and eastern TSA during SON.

Similar to HEs and DEs, the models show limitations in reproducing the spatial pattern of the time between CDHEs, with low correlations and an underestimation of variability relative to the reference (Figure 4.13a–d).

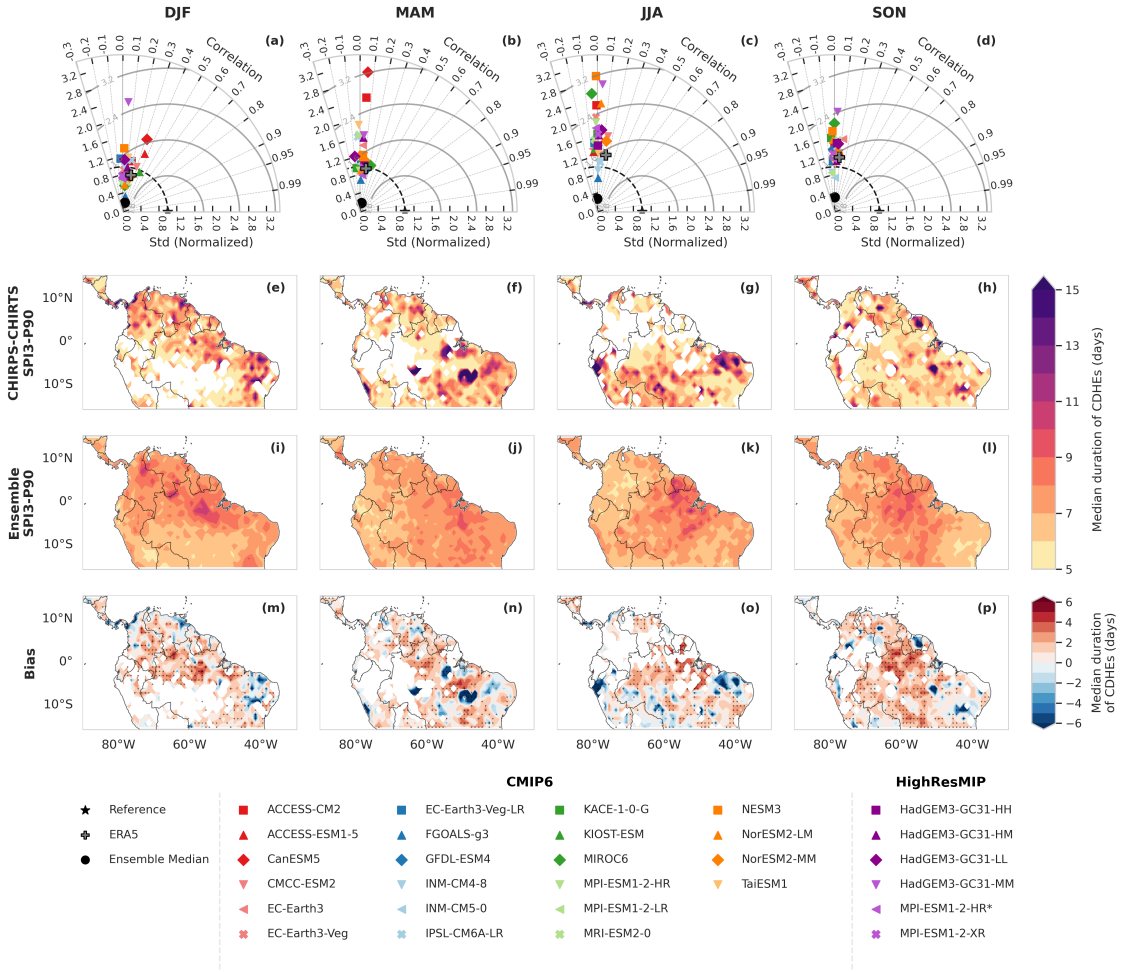

Figure 4.12: Seasonal evaluation of median duration of Compound Dry and Hot Events (CDHEs) over tropical South America. (a–d) Taylor diagrams. (e–h) Seasonal climatology for CHIRPS v2/CHIRTS (reference). (i–l) Multimodel seasonal median. (m–p) Multimodel seasonal median biases. Dots indicate where at least 80 % of the CMIP6/HighResMIP models agree on the sign of the multimodel median bias. All spatial fields (e–p) are shown at a common resolution of 1° × 1°.

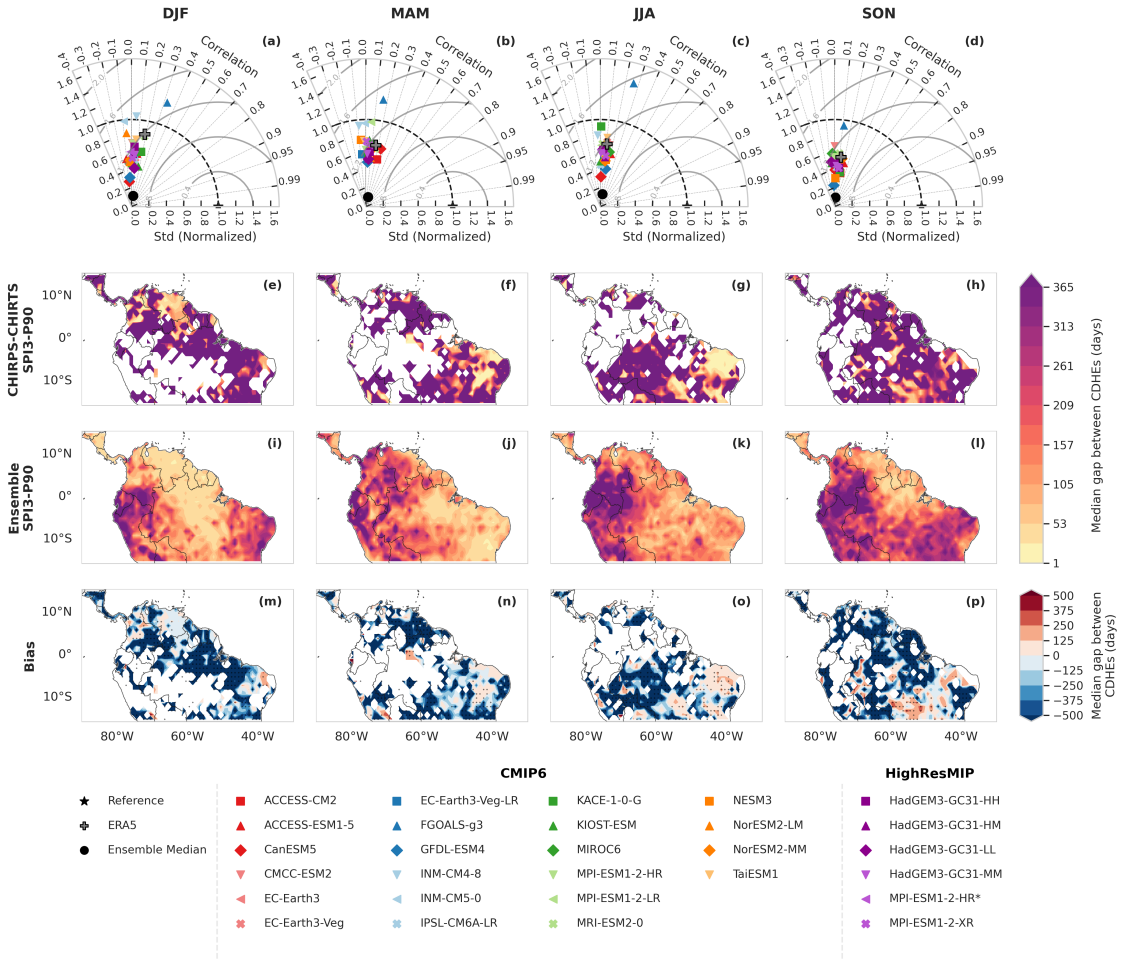

Figure 4.13: Seasonal evaluation of median gap between Compound Dry and Hot Events (CDHEs) over tropical South America. (a–d) Taylor diagrams. (e–h) Seasonal climatology for CHIRPS v2/CHIRTS (reference). (i–l) Multimodel seasonal median. (m–p) Multimodel seasonal median biases. Dots indicate where at least 80 % of the CMIP6/HighResMIP models agree on the sign of the multimodel median bias. All spatial fields (e–p) are shown at a common resolution of 1° × 1°.

ERA5 also performs poorly in this metric. While CHIRPSv2/CHIRTS reports median gap between events exceeding one year (365 days) across much of the TSA, the ensemble median shows values ranging from 3 to 105 days in eastern and northern TSA, and greater than 313 days in the west (Figure 4.13e–l). This underestimation across much of the region shows high agreement among models (Figure 4.13m–p). A shorter gap between events in the ensemble is linked to the overestimation of event frequency, as well as to the longer durations simulated by the ensemble compared to the reference, as previously discussed. These limitations are reflected in the TS, with values below 0.1 in most models and in the ensemble, the latter showing the lowest value and ranking last in all seasons (Figure B.13).

The Taylor diagram for SPI intensity during CDHEs (Figure 4.14a–d) is very similar to that observed for DEs (Figure 4.10a-b), where all datasets exhibit low performance. This indicates that the models struggle to capture drought intensity both in individual events (DEs) and in combined events (CDHEs). Although the ensemble for CDHEs shows a more diverse spatial distribution of

intensities over TSA (Figure 4.14i–l), in contrast to the more homogeneous pattern observed for DEs, it presents limitations in reproducing the CHIRPSv2 pattern (Figure 4.14e–h). In particular, biases are identified, with underestimation in northern TSA during DJF and MAM, and overestimation across much of the region throughout all seasons (Figure 4.14m–p). The ranking, according to the TS, indicates poor performance across all datasets, with values below 0.2 (Figure B.14).

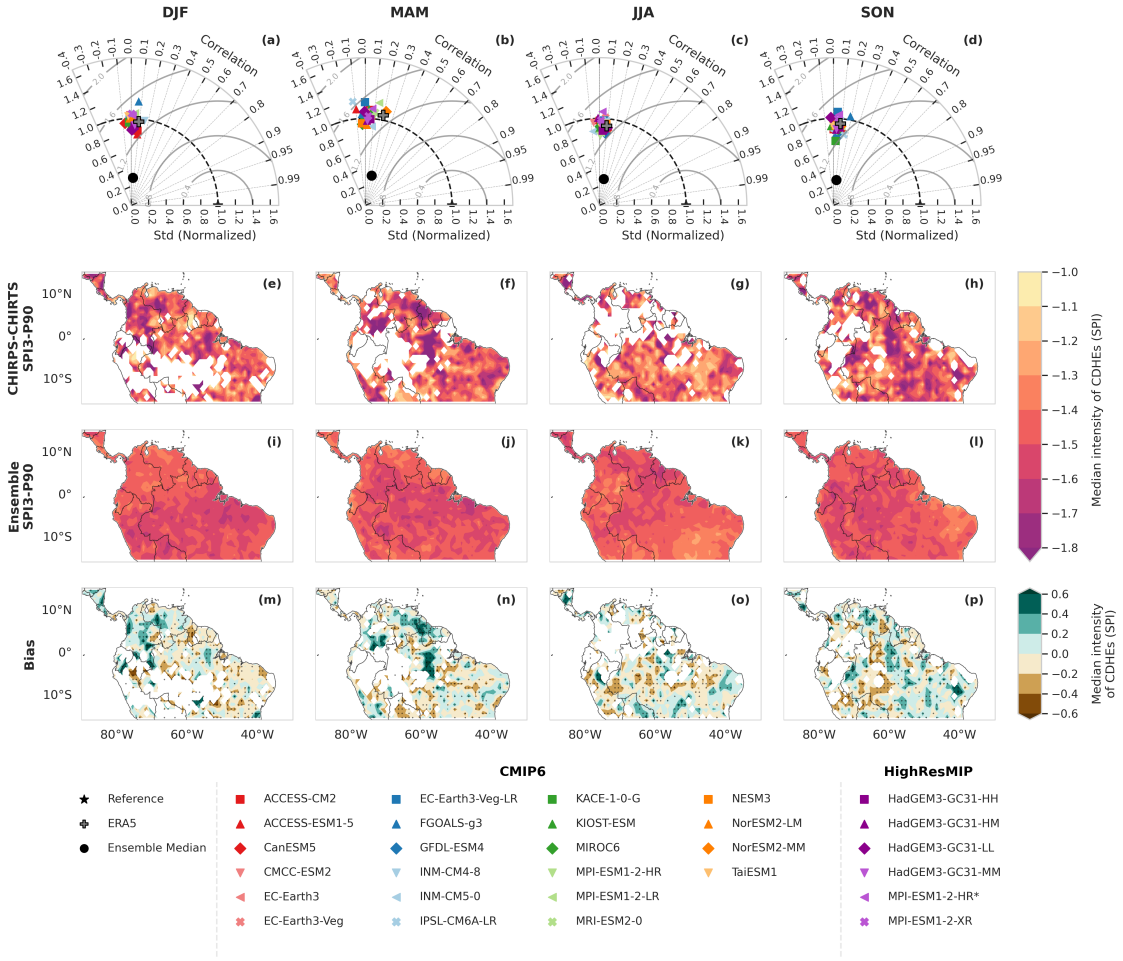

Figure 4.14: Seasonal evaluation of median intensity (SPI) of Compound Dry and Hot Events (CDHEs) over tropical South America. (a–d) Taylor diagrams. (e–h) Seasonal climatology for CHIRPS v2 (reference). (i–l) Multimodel seasonal median. (m–p) Multimodel seasonal median biases. Dots indicate where at least 80 % of the CMIP6/HighResMIP models agree on the sign of the multimodel median bias. All spatial fields (e–p) are shown at a common resolution of 1° × 1°.

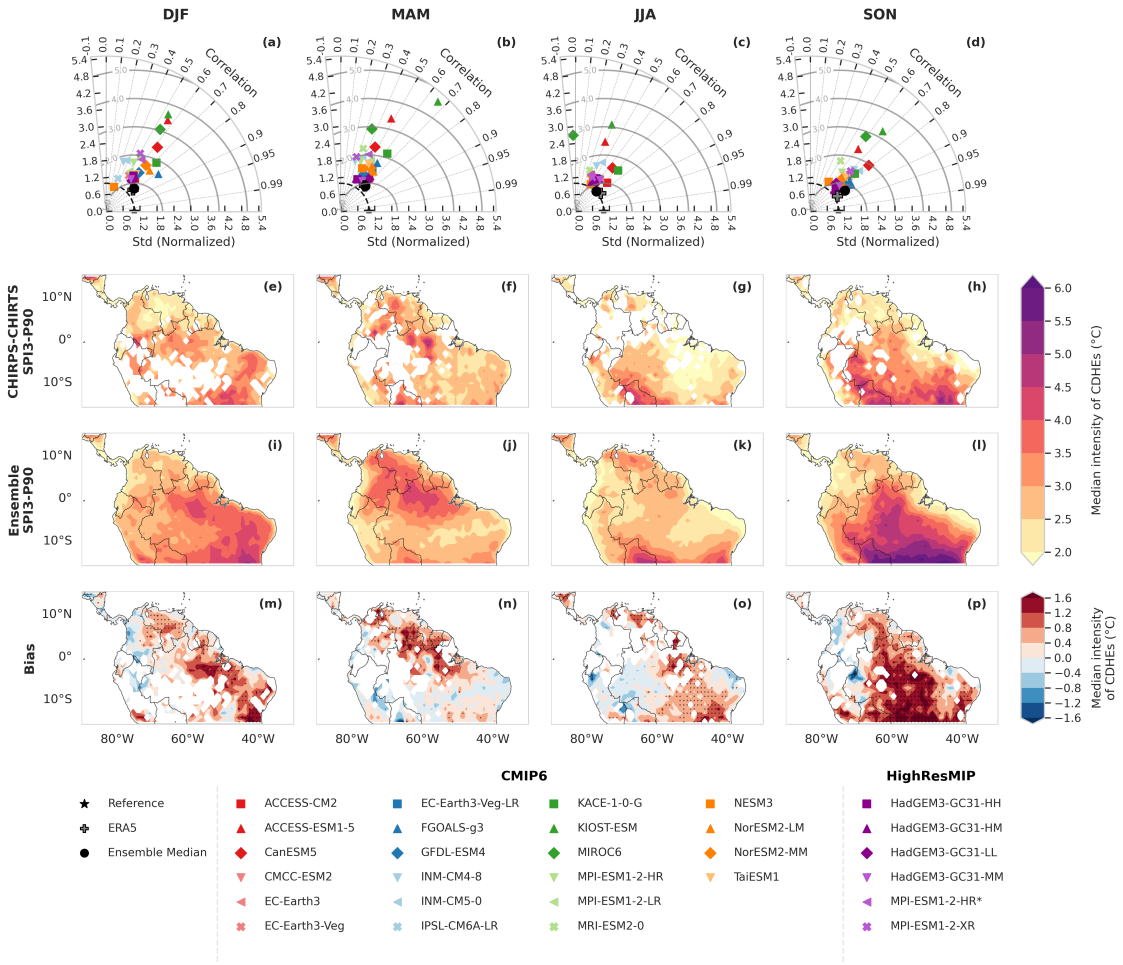

Figure 4.15: Seasonal evaluation of median intensity (°C) of Compound Dry and Hot Events (CDHEs) over tropical South America. (a–d) Taylor diagrams. (e–h) Seasonal climatology for CHIRTS (reference). (i–l) Multimodel seasonal median. (m–p) Multimodel seasonal median biases. Dots indicate where at least 80 % of the CMIP6/HighResMIP models agree on the sign of the multimodel median bias. All spatial fields (e–p) are shown at a common resolution of 1° × 1°.

Similar to what is observed for the intensity of HEs (Figure 4.6a–d), the CMIP6/HighResMIP models show better performance in simulating maximum temperature intensity during CDHEs (Figure 4.15a–d), with correlations ranging from moderate (0.4) to strong (0.8). In all seasons, individual models display standard deviations greater than 1, suggesting higher variability compared to the reference. Both ERA5 and the ensemble stand out by exhibiting strong correlations across all seasons, along with standard deviation values close to 1. The TS analysis indicates that most datasets achieve their best performance in SON, the season in which the highest skill is also observed for HE intensity. In the other seasons, most models show TS values below 0.4 (Figure B.15).

The ensemble median (Figure 4.15i–l) exhibits a spatial pattern of intensities similar to that observed for HEs (Figure 4.6i–l), with higher values in eastern TSA during DJF, in the north during MAM, in the south during JJA, and in the south and central regions during SON. However, the ensemble shows greater intensities during CDHEs, which is consistent with the findings reported

in Chapter 3 based on observational datasets and the ERA5 reanalysis. When compared with the reference, overestimations greater than 1.6 °C are identified, spatially coinciding with the regions where positive biases in HE intensity were also detected (Figure 4.15m–p).

4.4 Summary and discussion

This chapter addresses the evaluation of a set of CMIP6 (22) and HighResMIP (6) models in simulating the characteristics of event count, duration, gap between events, and intensity of HEs, DEs, and their combination (CDHEs) in TSA during the period 1983–2014. Results allow us to establish the extent to which models reproduce the main characteristics of these extreme events, which is essential for future research on impact assessment, risk management, and the design of adaptation and mitigation strategies in the region under climate change scenarios.

First, we evaluated the models' ability to represent maximum temperature (Figure 4.1) and precipitation (Figure 4.2) in TSA, as these are the variables required to estimate the indices. Results suggest a better performance in simulating maximum temperature across all seasons compared to precipitation. For both variables, the highest skill was found during JJA, which is consistent with the findings of Bazzanela et al. (2024) and Arias et al. (2025a) for precipitation. Similarly, the HighResMIP models and the ensemble median showed the highest skill in simulating temperature across all seasons, in contrast to most CMIP6 models. Based on the TS, NorESM2-MM (CMIP6) achieved the best performance in simulating precipitation throughout all seasons, surpassing the ensemble median, ERA5, and CHIRPS v3. This model also stood out as one of the best in representing the seasonal precipitation pattern over South America, according to Arias et al. (2025a). Regarding temperature, IPSL-CM6A-LR (CMIP6) exhibited the highest skill across all four seasons, followed by the six evaluated HighResMIP models and the ensemble median. IPSL-CM6A-LR has also demonstrated good performance in simulating mean temperature in other studies for specific regions of South America (e.g., Dias & Reboita, 2021; Reboita et al., 2024).

Subsequently, we evaluated the ability of the models to represent the characteristics of HEs, DEs, and CDHEs in TSA in the historical period, considering the number of events, median duration, median gap between events, and median intensity. The results showed that the individual models and the ensemble median had limitations in adequately reproducing the characteristics of these extreme events observed in the reference databases, particularly the number, duration, and gap between events. The number of HEs is slightly well represented in some individual models and for some seasons. In contrast, the ensemble median and individual models better represented the intensity of maximum temperature associated with HEs and CDHEs, especially during SON. Although the ensemble median outperformed the individual models in this characteristic, it had limitations in the rest, achieving inferior performance in some cases.

These results are partly consistent with those reported by Collazo et al. (2023), who found that for HEs, individual CMIP6 models provided a very poor representation of heatwave duration, while intensity was better captured. Hirsch et al. (2021) conducted the first systematic global assessment of heatwaves using the CMIP6 model ensemble, analyzing their ability to reproduce observed historical characteristics. They found that during the period 1950–2014, both the CMIP5 and CMIP6 ensembles overestimated heatwave frequency in the Amazon region, while underestimating it across the rest of the TSA. In addition, CMIP6 models tend to overestimate heatwave duration in the Amazon, with a bias of approximately six days. Complementarily, Wu et al. (2021b) noted that

although most CMIP6 models are able to simulate the four types of compound temperature and precipitation extremes (hot/dry, hot/wet, cold/dry, and cold/wet), their performance is poor in tropical regions.

For DEs, Papalexiou et al. (2021) evaluated how well the CMIP6 models reproduce historical characteristics of droughts, such as their duration and severity. Their analysis showed that the variability of drought statistics is greater in the tropics compared to other latitudes, indicating that climate models still require improvements to adequately capture these patterns in the tropical region.

Among the limitations encountered, the models overestimate the number of events and median duration and underestimate the gap between events for HEs and CDHEs compared to the reference over much of the TSA, with some regions exhibiting high agreement between models (more than 80 %). The models, in turn, exhibited a more spatially homogeneous distribution of DEs characteristics compared to CHIRPS, overestimating them in some regions while underestimating them in others. Furthermore, whereas the CMIP6/HighResMIP models indicated the occurrence of CDHEs across the entire TSA region, the reference datasets (CHIRTS/CHIRPSv2) showed a more distinct seasonal pattern. In the latter, some subregions did not record CDHEs during specific seasons, in contrast to the more pervasive signal suggested by the models. This study did not delve into the causes of model biases, which constitute a fundamental aspect that should be addressed in future research. Therefore, it is necessary to advance in the study of the climatic processes that explain these limitations in representing the characteristics of extreme events and their combination. This evaluation constitutes a necessary step toward identifying the most suitable CMIP6 and HighResMIP models for studies in the TSA, which are essential for assessing the impacts of climate change in a highly vulnerable region (Castellanos et al., 2022; Cavazos et al., 2024).

In this chapter, we also evaluated the performance of observational databases such as CPC (maximum temperature), CHIRPS v3 (precipitation), and ERA5 reanalysis (precipitation and maximum temperature) in representing the spatial distribution of individual and compound extreme events characteristics. While these databases outperformed the CMIP6/HighResMIP models and the ensemble median for some characteristics, they generally performed poorly. The exception was temperature intensity in HEs and CDHEs, where, like the models, they performed better.

The comparison among the different datasets (CPC, ERA5, CHIRPSv3, and CMIP6/HighResMIP) revealed substantial differences. Although the models were able to simulate maximum temperature and, to a lesser extent, precipitation, they showed limitations in reproducing the count, duration, and gap between events associated with HEs, DEs, and CDHEs. This limitation was not exclusive to the models but was also present in the observational datasets and in the ERA5 reanalysis. An example of this is the difference between CHIRPSv2 and CHIRPSv3, which did not consistently reproduce the same patterns of extremes, highlighting that representation challenges extended even to observational datasets with respect to CHIRTS/CHIRPS references.

Chapter 5

Projected changes in the characteristics of hot, dry, and compound dry-hot events under different climate change scenarios

5.1 Introduction

Climate change projections indicate that mean annual temperature in South America will increase toward the end of the 21st century, particularly under the highest emission scenario (SSP5-8.5) (Bustos Usta et al., 2022). The region is highly vulnerable to the effects of climate change due to the projected temperature increase, regardless of the scenario considered, with greater impacts in countries such as Colombia, Brazil, Venezuela, Guyana, Suriname, French Guiana, Peru, Bolivia, and Paraguay (Bustos Usta et al., 2022). Moreover, Latin America is one of the most urbanized regions in the world (DESA, 2019), experiencing increased human exposure to extreme temperatures as a result of the interaction between climate change and urbanization (Kephart et al., 2022). The results of Gasparrini et al. (2017) suggest that climate change generates a substantial increase in mortality associated with extreme hot and cold events, with a stronger impact in tropical regions. However, the impacts tend to be lower under scenarios that assume mitigation strategies, which highlights the importance of implementing effective climate policies (Gasparrini et al., 2017).

Several studies have documented a projected increase in the occurrence and intensity of hot extremes (HEs) in Latin America. Ramarao et al. (2024) analyzed projected changes in heatwaves across the region and found that these events will increase in frequency, duration, and intensity toward mid-century under the RCP2.6 and RCP8.5 scenarios, with the latter showing the most pronounced increases. Furthermore, their results indicate that population exposure to heatwave days in Central and South America could be 3 to 10 times greater by the mid-21st century. Feron et al. (2019) reported that under the RCP8.5 scenario, half or more of the days in a year could be extremely hot in the region by mid-century, with the largest increases projected in tropical zones. Consistently, De Luca & Donat (2023) found an increase in the frequency, duration, and intensity of HEs toward the end of the 21st century, with the greatest increases under the SSP5-8.5 scenario, particularly over northern South America. Similarly, Collazo et al. (2023) reported that the highest heatwave frequencies occur in Tropical South America (TSA) under SSP2-4.5 and in central South America under SSP5-8.5, with longer durations projected in TSA primarily under SSP5-8.5. This

increase in extreme temperatures can have cascading effects, exacerbating other events such as droughts or wildfires (AghaKouchak et al., 2020).

For dry events (DEs), an increase in the frequency, duration, and spatial extent of droughts is projected across most regions of the world during the 21st century (Wang et al., 2021a). The greatest increase in drought duration was observed in northeastern South America, central Africa, and northern Oceania, where the duration of these events doubled (Wang et al., 2021a). Additionally, flash drought occurrence is expected to increase under all climate change scenarios globally, with the greatest increases under the highest radiative forcing scenario (Christian et al., 2023).

Given that South America is a particularly vulnerable region to droughts, Silverman & Engström (2025) assessed the relative vulnerability of countries in the region considering exposure, sensitivity, adaptive capacity, and overall vulnerability level. Their results indicate that Ecuador, due to its high population density and limited water resources, exhibits the highest vulnerability, followed by Colombia and Uruguay. The analysis suggests that both geographic and economic factors influence the different vulnerability levels among countries. Merz & Zachariah (2025) show a discouraging outlook regarding drought development across much of South America, particularly under the high-emission scenario. Similarly, Wainwright et al. (2022) project an increase in the number of dry days and the duration of drought periods for South America, particularly during the dry season, with an estimated increase of 5 to 10 days in the mean duration of dry periods in the northeastern region. Penalba & Rivera (2013) assessed the impact of climate change on droughts in southern South America under moderate and high emission scenarios, finding higher drought frequency in both the near-term and long-term, with shorter duration but higher severity across much of the region.

For the Amazon, models project increases in the frequency and geographic extent of meteorological droughts in the eastern region under the RCP8.5 scenario (Duffy et al., 2015). Specifically, CMIP5 models estimate that the area affected by moderate and severe meteorological droughts in the Amazon will nearly double and triple, respectively, by 2100 (Duffy et al., 2015). CMIP6 models show greater agreement that much of the Amazon basin will experience decreased precipitation in the future, particularly in the eastern and southern regions during the 21st century (Parsons, 2020). Furthermore, models suggest that the recent particularly hot and severe droughts will become increasingly frequent due to rising global temperatures (Parsons, 2020).

Although HEs and DEs have been the subject of numerous studies, several authors have highlighted the growing importance of compound dry and hot events (CDHEs). According to the Intergovernmental Panel on Climate Change (IPCC), there is high confidence that CDHEs have increased in frequency at the global scale during the last century as a result of human influence (Seneviratne et al., 2021). Likewise, high confidence remains that the probability of occurrence of these events will continue to increase in most land regions as global mean temperature rises (Seneviratne et al., 2021). Based on climate projections, hot/dry and hot/wet compound events are expected to increase in frequency over the coming decades, while cold/dry and cold/wet events are projected to become less frequent (Wu et al., 2021b).

The spatial extent of CDHEs globally shows an increasing trend during the 2015–2100 period, with more pronounced increases under the high-emission scenario (SSP5-8.5) compared to the low-emission scenario (SSP2-4.5) (Li et al., 2025). CMIP6 models projections indicate substantial increases across South America, Central America, southern North America, Africa, Europe,

western Asia, and Australia, although the magnitude of the increase varies among the different indices used for their identification (Hosseinzadehtalaei et al., 2024). Additionally, the probability of individual DEs is projected to increase over approximately 50 % of the land surface, which will expand areas prone to CDHEs due to the widespread increase in HEs probability (Tabari & Willems, 2023). Overall, the increase in CDHEs probability is significant at the global scale, with the greatest increases projected for regions such as South America (Chiang et al., 2022; Tabari & Willems, 2023).

CDHEs can cause considerable damage and pose significant challenges to socioeconomic systems, often exceeding their response capacities (Tabari & Willems, 2023). Globally, by the end of the 21st century, an additional 700 to 1,700 million people are projected to be exposed to amplified compound events, with countries characterized by weak governance facing approximately twice the associated risk compared to those with strong governance (Tabari & Willems, 2023). Consistently, the frequency and magnitude of CDHEs are expected to increase toward the end of the 21st century compared to the mid-century period (2050s) (De Luca & Donat, 2023; Meng et al., 2022; Yin et al., 2023; Zhang et al., 2022a). Similarly, population exposure to CDHEs is projected to rise substantially in response to the higher levels of global warming anticipated under the SSP3-7.0 and SSP5-8.5 scenarios (Zhang et al., 2022a).

Considering the importance of analyzing 21st-century projections of HEs, DEs, and their combination (CDHEs) in a highly vulnerable region such as TSA, this chapter examines their main characteristics under four emission scenarios (SSP1-2.6, SSP2-4.5, SSP3-7.0, and SSP5-8.5) from CMIP6, as well as under the HighresFuture scenario from the HighResMIP experiment, for the near-term (2021–2040) and long-term (2081–2100). First, Subsection 5.3.1 analyzes the projected changes in HEs. Subsequently, Subsection 5.3.3 presents the corresponding results for DEs, while Subsection 5.3.5 examines CDHEs. Finally, Section 5.4 summarizes the conclusions and discusses the most relevant findings.

5.2 Data and methodology

5.2.1 CMIP6/HighResMIP simulations

To assess projected changes in the main characteristics of HEs, DEs, and their combination (CDHEs) over TSA, projections for the 21st century from the CMIP6 and HighResMIP model ensembles were analyzed (Table 5.1). For the CMIP6 models, projections corresponding to the Shared Socioeconomic Pathways (SSPs) for the period 2015–2100 were considered, while the HighResMIP simulations were based on the HighresFuture scenario, covering the period 2015–2050.

Table 5.1: Projections from CMIP6 and HighResMIP models used in this study under different greenhouse gas (GHG) emission scenarios. The number of models used was 17 for SSP1-2.6, 21 for SSP2-4.5 and SSP5-8.5, 19 for SSP3-7.0, and 5 for HighresFuture. SSP: Shared Socioeconomic Pathway, CMIP6. Differences in the number of models with respect to chapter 4 are due to data availability per scenario.

Model	**Type**	**Experiment**
ACCESS-CM2	CMIP6	SSP245, SSP370
ACCESS-ESM1-5	CMIP6	SSP126, SSP245, SSP370, SSP585

Table 5.1 - Continuation

Model	Type	Experiment
CMCC-ESM2	CMIP6	SSP126, SSP245, SSP370, SSP585
CanESM5	CMIP6	SSP126, SSP245, SSP370, SSP585
EC-Earth3	CMIP6	SSP245, SSP585
EC-Earth3-Veg	CMIP6	SSP370, SSP585
EC-Earth3-Veg-LR	CMIP6	SSP126, SSP245, SSP370, SSP585
FGOALS-g3	CMIP6	SSP245, SSP370, SSP585
GFDL-ESM4	CMIP6	SSP126, SSP245, SSP370, SSP585
INM-CM4-8	CMIP6	SSP126, SSP245, SSP370, SSP585
INM-CM5-0	CMIP6	SSP126, SSP245, SSP370, SSP585
IPSL-CM6A-LR	CMIP6	SSP126, SSP245, SSP370, SSP585
KACE-1-0-G	CMIP6	SSP126, SSP245, SSP370, SSP585
KIOST-ESM	CMIP6	SSP126, SSP245, SSP585
MIROC6	CMIP6	SSP126, SSP245, SSP370, SSP585
MPI-ESM1-2-HR	CMIP6	SSP126, SSP245, SSP370, SSP585
MPI-ESM1-2-LR	CMIP6	SSP126, SSP245, SSP370, SSP585
MRI-ESM2-0	CMIP6	SSP126, SSP245, SSP370, SSP585
NESM3	CMIP6	SSP245, SSP585
NorESM2-LM	CMIP6	SSP126, SSP245, SSP370, SSP585
NorESM2-MM	CMIP6	SSP126, SSP245, SSP370, SSP585
TaiESM1	CMIP6	SSP126, SSP245, SSP370, SSP585
HadGEM3-GC31-HH	HighResMIP	highres-future
HadGEM3-GC31-HM	HighResMIP	—
HadGEM3-GC31-LL	HighResMIP	highres-future
HadGEM3-GC31-MM	HighResMIP	highres-future
MPI-ESM1-2-HR	HighResMIP	highres-future
MPI-ESM1-2-XR	HighResMIP	highres-future

Shared Socioeconomic Pathways

For the CMIP6 models, projections based on four greenhouse gas emission SSPs, were considered:

SSP1-1.6: This scenario depicts a world moving toward more sustainable and inclusive development, with greater international cooperation and improved management of common goods. Investments in education, health, and environmental technologies reduce inequality and enhance resource efficiency. Economic growth focuses on human well-being and the use of renewable energy, posing fewer challenges for climate change mitigation and adaptation (O'Neill et al., 2017).

SSP2-4.5: This scenario describes a world that maintains historical social, economic, and technological trends. Economic and social development proceed unevenly, with overall political stability and imperfect global markets. Institutions make slow progress toward the Sustainable Development Goals (SDGs). Environmental degradation persists, with limited improvements, thus leaving moderate challenges for climate change mitigation and adaptation (O'Neill et al., 2017).

SSP3-7.0: This scenario portrays a world where the resurgence of nationalism and regional conflicts limits international cooperation and institutional development. Policies focus on security

and self-sufficiency, reducing investment in education and technology. Economic development is slow, with high inequality and environmental degradation. Dependence on fossil fuels and weak global cooperation create major challenges for climate change mitigation and adaptation (O'Neill et al., 2017).

SSP5-8.5: This scenario envisions a world in which economic success fosters confidence in markets, innovation, and social participation as pathways to sustainable development. Global integration and substantial investment in health, education, and institutions strengthen human and social capital, promoting rapid economic growth based on intensive use of fossil fuels and natural resources, leading to a radiative forcing level of 8.5 W/m^2 by 2100. Confidence in technology and risk management reduces environmental concerns, thereby creating high challenges for mitigation but low challenges for adaptation to climate change (O'Neill et al., 2017).

HighresFuture scenario

The HighresFuture (highres-future) scenario, developed within the HighResMIP models, corresponds to a high-emission pathway similar to SSP5-8.5 (Haarsma et al., 2016). This configuration leads to the highest radiative forcing among the CMIP6 scenarios (O'Neill et al., 2017).

5.2.2 Events identification

Extreme events under climate change projections were calculated following the methodology described in Chapter 3. In this chapter, projected changes were analyzed only for the combination of HEs with the P90 threshold (i.e. those events for which maximum daily temperature exceeds the 90th percentile), and DEs with the SPI3 (i.e. Standardized Precipitation Index of 3 months), following Collazo et al. (2023). For projected HEs, the same reference period as for historical data (1981–2010) was used (Collazo et al., 2023). In the case of DEs, different approaches exist to assess future droughts using standardized drought indices (Wang et al., 2021b). Two methodologies were applied in this study. The first involved fitting the projected precipitation to the probability distribution of the historical period (e.g., Ridder et al., 2022). For this fitting, the entire period 1981–2014 was considered, since no reference period was defined in the historical analysis, in order to have a broader temporal basis for parameter estimation. The second methodology, exploratory in nature, consisted of fitting the projected precipitation to its own probability distribution (e.g., Collazo et al., 2023; Wang et al., 2021b) (see supplementary material C). Finally, CDHEs were identified when HEs occurred during DEs (Collazo et al., 2023).

5.2.3 Projected changes and temporal evolution of HEs, DEs, and CDHEs

For the analysis of projections throughout the 21st century, future changes in the characteristics of HEs, DEs, and CDHEs were estimated from the CMIP6 and HighResMIP simulations. The analysis was based on two periods suggested by the IPCC: near-term (2021–2040) and long-term (2081–2100). In the case of HighResMIP ensemble projections, only the near-term period was considered, since projections for this project are only available until 2050. For both analysis periods, 1991–2010 was defined as the reference period. All models were interpolated to a common $1^\circ \times 1^\circ$ grid resolution using the conservative remapping technique (Remapcon) (Omay et al., 2024).

To examine in detail the differences among the five emission scenarios, annual event characteristics during the 1983–2100 period were analyzed for the four regions selected in subsection 3.3.4 (see Figure 3.1), considering each model individually and at its original resolution.

5.3 Results

5.3.1 Projected changes of hot events

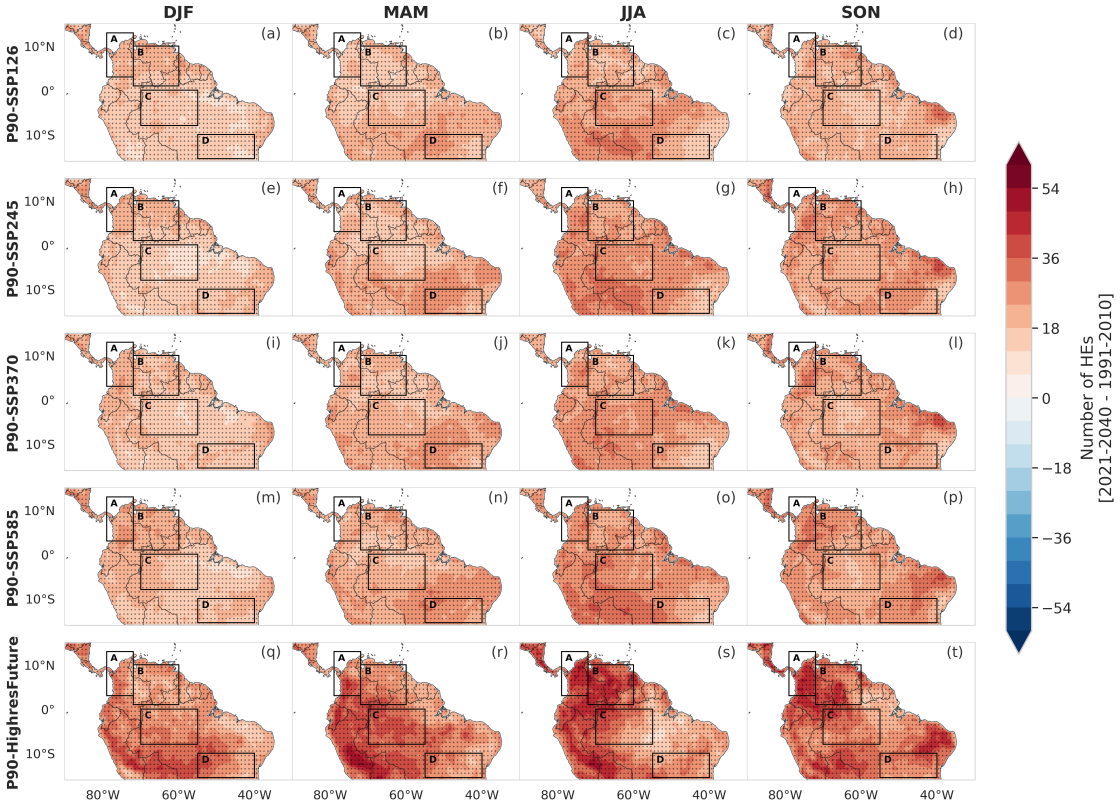

Figure 5.1: Projected changes in the seasonal number of Hot Events (HEs) for the near-term period (2021–2040) based on the ensemble median under different emission scenarios: SSP1-2.6 (a–d), SSP2-4.5 (e–h), SSP3-7.0 (i–l), and SSP5-8.5 (m–p) from CMIP6, and HighresFuture (HighresFuture) (q–t) from HighResMIP. Dots indicate grid points where at least 80 % of the CMIP6 or HighResMIP models agree on the sign of the projected change. Black rectangles highlight the four subregions: (A) northern Andes, (B) Orinoco, (C) Brazilian Amazon, and (D) northern Cerrado. All spatial fields are shown at a common resolution of 1° × 1°.

Climate change scenarios for the near-term period (2021–2040) project an increase in the number of HEs across TSA, with the most pronounced increase under HighresFuture (Figure 5.1). Across all scenarios, models show high agreement on the type of change for TSA. The SSPs show similar spatial patterns in the distribution of higher occurrences, with increases ranging from 12 to 36 events relative to the reference period (1991–2010). The HighresFuture scenario exhibits increases exceeding 42 events over Peru and southern TSA during December-January-February (DJF); over the western region during March-April-May (MAM) and June-July-August (JJA), including the Brazilian Amazon (region C) during MAM; over northern TSA, including the northern Andes (region A) and the Orinoco (region B), during JJA and September-October-November (SON); and over eastern Brazil during SON. For the long-term period (2081–2100) (Figure 5.2), the number of events increases under the SSP1-2.6 and SSP2-4.5 scenarios, showing larger magnitudes than those projected for the near-term period. The increase is greater (> 42 events) under SSP2-4.5,

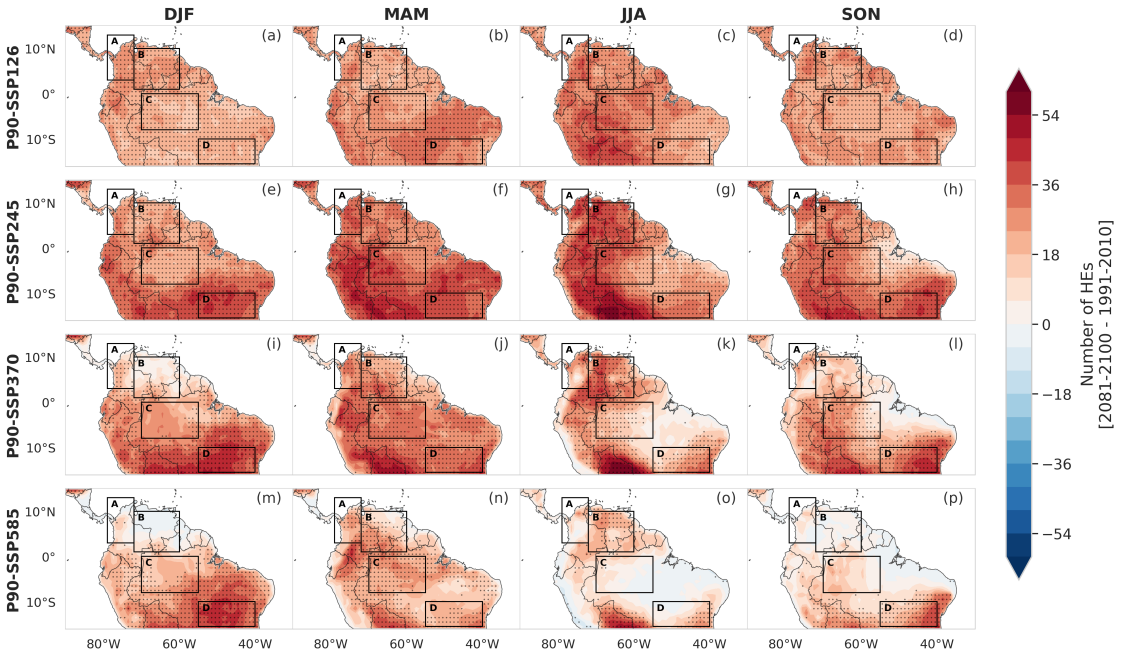

Figure 5.2: Projected changes in the seasonal number of Hot Events (HEs) for the long-term period (2081–2100) based on the ensemble median under different emission scenarios: SSP1-2.6 (a–d), SSP2-4.5 (e–h), SSP3-7.0 (i–l), and SSP5-8.5 (m–p) from CMIP6. Dots indicate grid points where at least 80 % of the CMIP6 models agree on the sign of the projected change. Black rectangles highlight the four regions: (A) northern Andes, (B) Orinoco, (C) Brazilian Amazon, and (D) northern Cerrado. All spatial fields are shown at a common resolution of 1° × 1°.

particularly over the southern and western regions of TSA. Models exhibit high agreement on the sign of change in both scenarios. Similarly, SSP3-7.0 and SSP5-8.5 also show substantial increases in the southern and western regions of TSA, with consistent inter-model agreement. However, a decrease in the number of events is projected for northern TSA during DJF and for regions of Brazil and western TSA during JJA and SON, relative to the historical period (1991–2010). These decreases show low agreement among CMIP6 models regarding the sign of change.

For the near-term period, the SSPs suggest median durations 0 to 2 days longer compared to the historical period (Figure 5.3), with some regions showing durations 2 to 4 days longer, which cover a larger area over central Brazil under the SSP5-8.5 scenario during JJA. For this characteristic, very few regions exhibit inter-model agreement on the sign of change. HighresFuture suggests longer durations for this period, with the highest values (exceeding 6 days) concentrated over northern TSA during DJF and SON, over central Brazil during MAM, and over much of Brazil, Peru, and the central northern Andes (region A) during JJA. There is agreement among the HighResMIP models on the increase in duration for TSA.

The SSP1-2.6 and SSP2-4.5 scenarios suggest durations 0 to 15 days longer for the long-term (Figure 5.4), with the longest durations observed over northeastern Brazil during JJA under SSP2-4.5. Few regions show agreement among models under the SSP1-2.6 scenario. In contrast, the SSP3-7.0 and SSP5-8.5 scenarios show the largest changes (exceeding 50 days), covering a greater area under the higher-emission scenario (SSP5-8.5). Regions showing the largest changes include

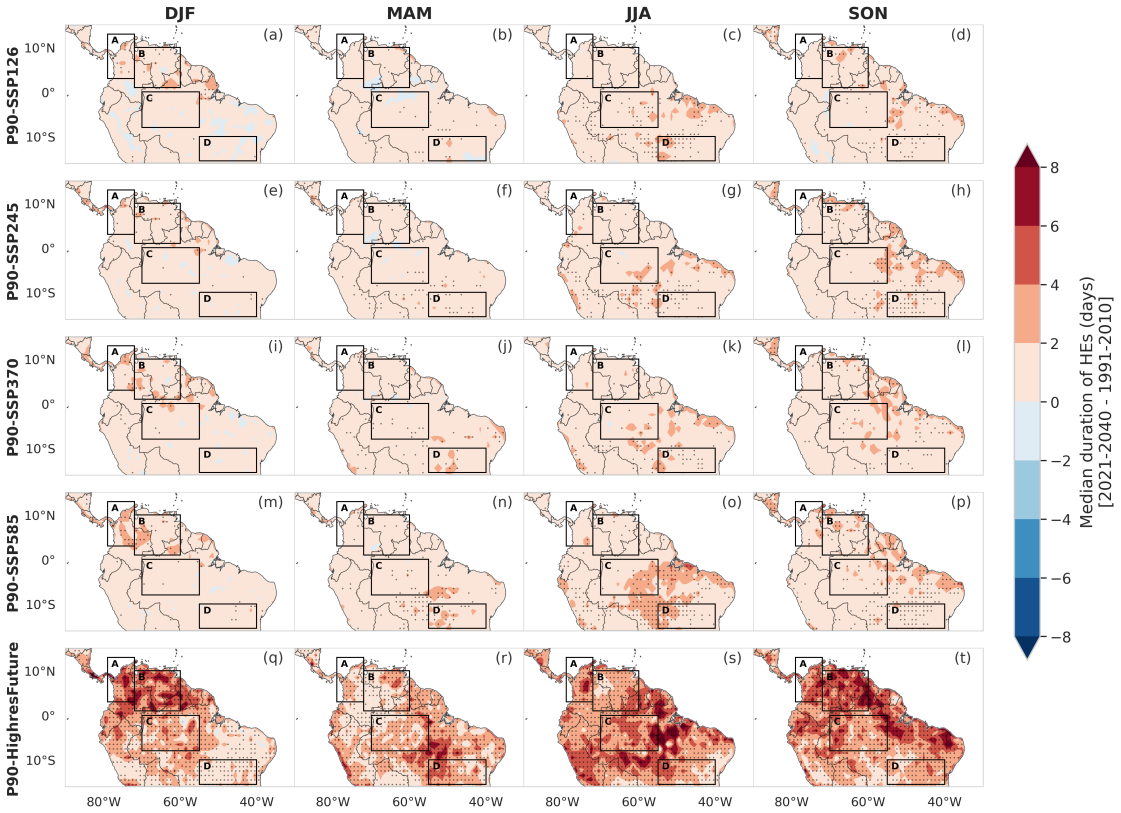

Figure 5.3: Projected changes in the seasonal median duration (days) of Hot Events (HEs) for the near-term period (2021–2040) based on the ensemble median under different emission scenarios: SSP1-2.6 (a–d), SSP2-4.5 (e–h), SSP3-7.0 (i–l), and SSP5-8.5 (m–p) from CMIP6, and HighresFuture (HighresFuture) (q–t) from HighResMIP. Dots indicate grid points where at least 80 % of the CMIP6 or HighResMIP models agree on the sign of the projected change. Black rectangles highlight the four regions: (A) northern Andes, (B) Orinoco, (C) Brazilian Amazon, and (D) northern Cerrado. All spatial fields are shown at a common resolution of 1° × 1°.

northern TSA during DJF and SON, eastern Brazil and western TSA during MAM, and much of TSA during JJA, with a high level of inter-model consensus on the direction of change. Notably, the regions showing the largest increases in median duration of HEs under SSP3-7.0 and SSP5-8.5 coincide with those where fewer events occur (Figure 5.2), suggesting that although events become less frequent under these scenarios, they last longer.

In both periods (Figures 5.5 and 5.6), the scenarios show a decrease in the median gap between HEs by more than 90 days relative to the historical period, consistent with the projected increase in the number and duration of events. The largest differences are found in the western of TSA, particularly over Colombia during SON in all scenarios, and also during JJA in the HighresFuture scenario for the short term (Figure 5.5s). Overall, the models show a high level of agreement in TSA.

In terms of median temperature intensity during HEs, the scenarios show increases of approximately 0.2 °C over much of TSA for the near-term compared to 1991–2010 (Figure 5.7). During JJA and SON, southern TSA exhibits values exceeding 0.4 °C, with inter-model agreement on the sign of change in some areas. All SSPs scenarios exhibit regions with decreases in intensity, such

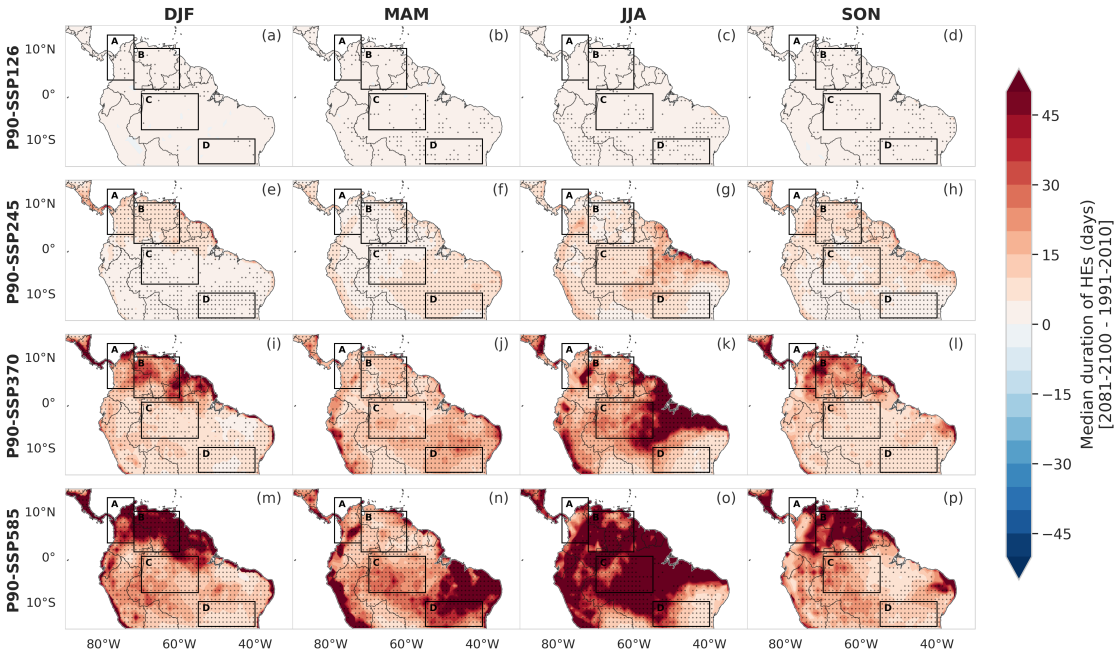

Figure 5.4: Projected changes in the seasonal median duration (days) of Hot Events (HEs) for the long-term period (2081–2100) based on the ensemble median under different emission scenarios: SSP1-2.6 (a–d), SSP2-4.5 (e–h), SSP3-7.0 (i–l), and SSP5-8.5 (m–p) from CMIP6. Dots indicate grid points where at least 80 % of the CMIP6 models agree on the sign of the projected change. Black rectangles highlight the four regions: (A) northern Andes, (B) Orinoco, (C) Brazilian Amazon, and (D) northern Cerrado. All spatial fields are shown at a common resolution of 1° × 1°.

as eastern Brazil during DJF and central TSA during MAM. Overall, very few regions show inter-model agreement on the type of change. The HighresFuture scenario projects the largest increases in median intensity for the near-term period, with values exceeding 0.4 °C across TSA. Models show high agreement on the sign of change across the region. Nevertheless, this scenario suggests a decrease in intensity magnitude over northeastern Brazil, also with inter-model agreement. Increases in median intensity of HEs are greater toward the end of the century (2081–2100) (Figure 5.8), with SSP3-7.0 and SSP5-8.5 standing out as projecting the largest increases, particularly over central TSA, including the Brazilian Amazon (region C) during JJA under SSP5-8.5, with differences exceeding 2.8 °C relative to the historical period.

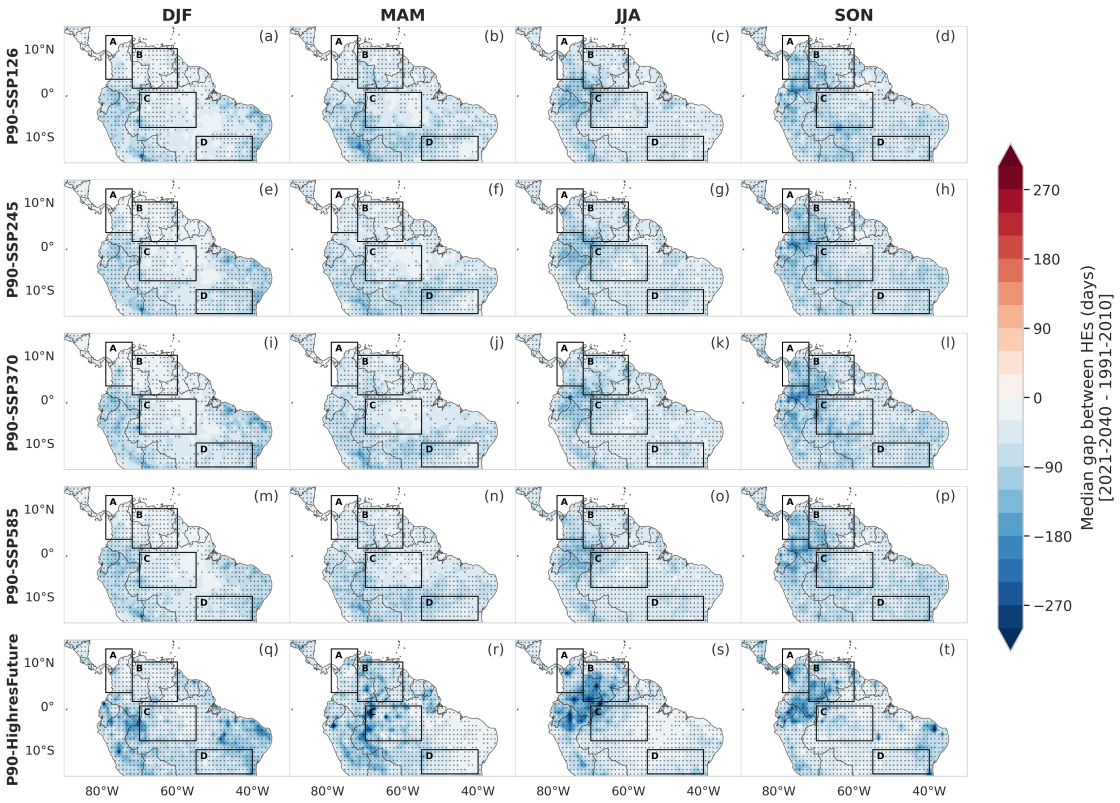

Figure 5.5: Projected changes in the seasonal median gap (days) between Hot Events (HEs) for the near-term period (2021–2040) based on the ensemble median under different emission scenarios: SSP1-2.6 (a–d), SSP2-4.5 (e–h), SSP3-7.0 (i–l), and SSP5-8.5 (m–p) from CMIP6, and HighresFuture (HighresFuture) (q–t) from HighResMIP. Dots indicate grid points where at least 80 % of the CMIP6 or HighResMIP models agree on the sign of the projected change. Black rectangles highlight the four regions: (A) northern Andes, (B) Orinoco, (C) Brazilian Amazon, and (D) northern Cerrado. All spatial fields are shown at a common resolution of 1° × 1°.

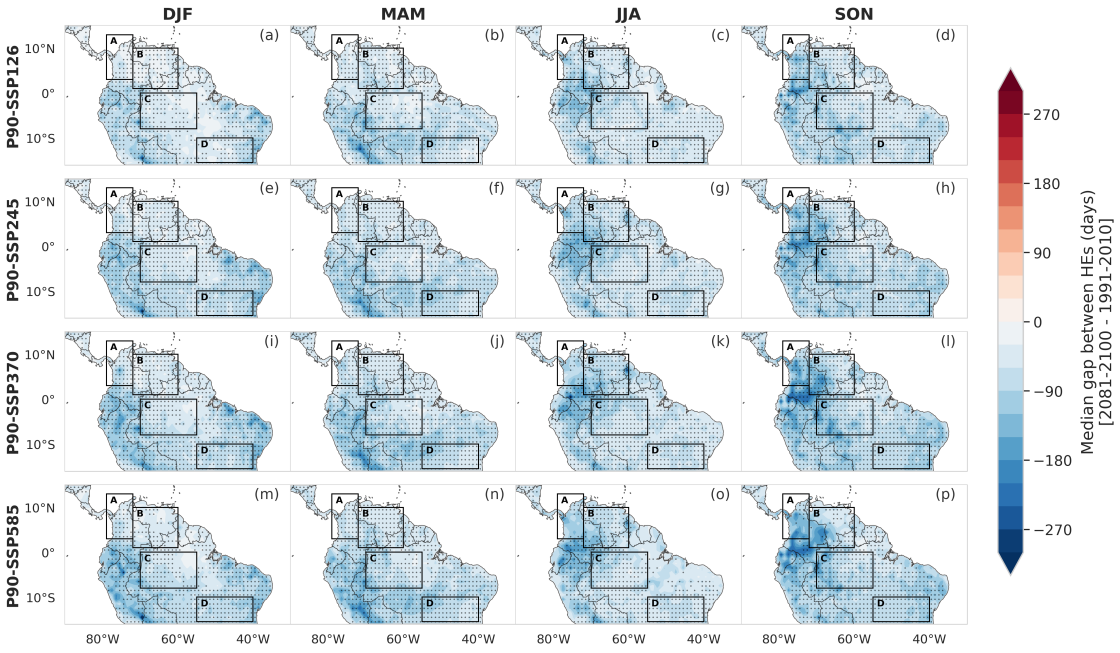

Figure 5.6: Projected changes in the seasonal median gap (days) between Hot Events (HEs) for the long-term period (2081–2100) based on the ensemble median under different emission scenarios: SSP1-2.6 (a–d), SSP2-4.5 (e–h), SSP3-7.0 (i–l), and SSP5-8.5 (m–p) from CMIP6. Dots indicate grid points where at least 80 % of the CMIP6 models agree on the sign of the projected change. Black rectangles highlight the four regions: (A) northern Andes, (B) Orinoco, (C) Brazilian Amazon, and (D) northern Cerrado. All spatial fields are shown at a common resolution of $1^\circ \times 1^\circ$.

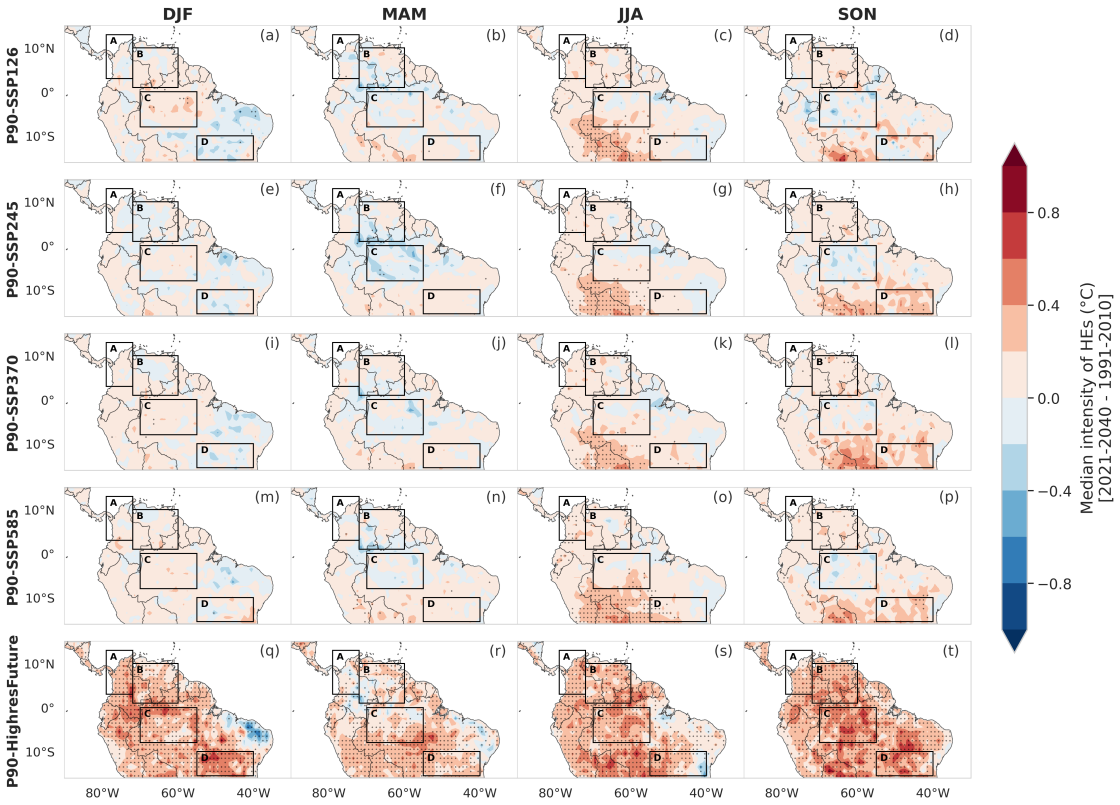

Figure 5.7: Projected changes in the seasonal median intensity (°C) of Hot Events (HEs) for the near-term period (2021–2040) based on the ensemble median under different emission scenarios: SSP1-2.6 (a–d), SSP2-4.5 (e–h), SSP3-7.0 (i–l), and SSP5-8.5 (m–p) from CMIP6, and HighresFuture (HighresFuture) (q–t) from HighResMIP. Dots indicate grid points where at least 80 % of the CMIP6 or HighResMIP models agree on the sign of the projected change. Black rectangles highlight the four regions: (A) northern Andes, (B) Orinoco, (C) Brazilian Amazon, and (D) northern Cerrado. All spatial fields are shown at a common resolution of 1° × 1°.

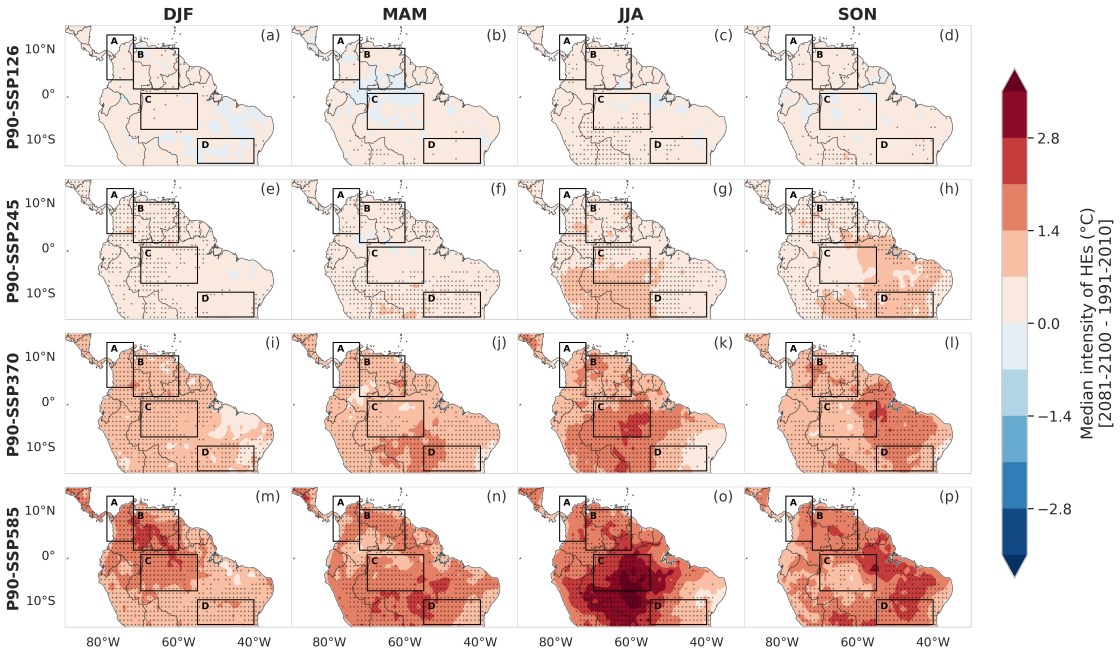

Figure 5.8: Projected changes in the seasonal median intensity (°C) of Hot Events (HEs) for the long-term period (2081–2100) based on the ensemble median under different emission scenarios: SSP1-2.6 (a–d), SSP2-4.5 (e–h), SSP3-7.0 (i–l), and SSP5-8.5 (m–p) from CMIP6. Dots indicate grid points where at least 80 % of the CMIP6 models agree on the sign of the projected change. Black rectangles highlight the four regions: (A) northern Andes, (B) Orinoco, (C) Brazilian Amazon, and (D) northern Cerrado. All spatial fields are shown at a common resolution of 1° × 1°.

5.3.2 Trends in the characteristics of HEs in the TSA regions under climate change scenarios

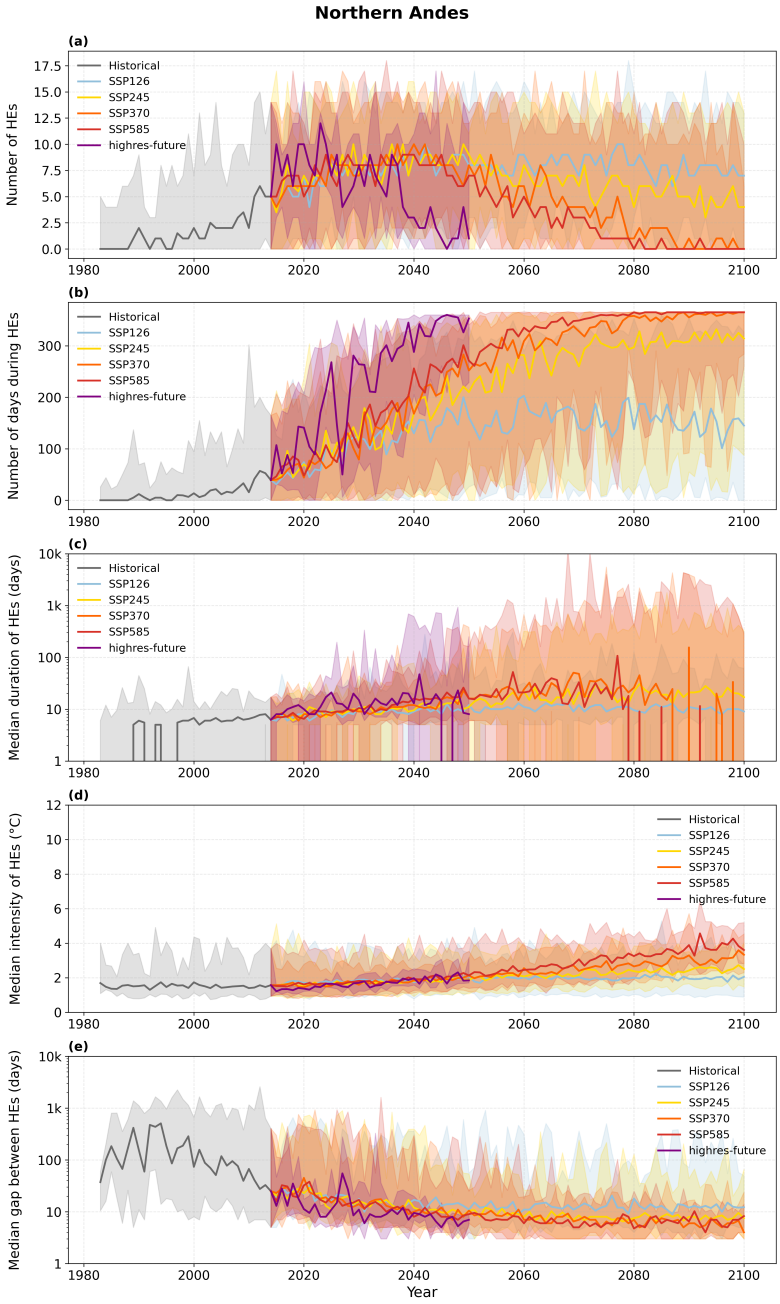

Figure 5.9: Time series of hot events (HEs) characteristics for the northern Andes region, based on the ensemble median. The 1983–2014 series corresponds to the multimodel median of the historical simulations (gray line). For the 2015–2100 period (2015–2050 for the HighresFuture scenario), the ensemble median for each of the scenarios considered are shown: SSP1-2.6 (blue line), SSP2-4.5 (yellow line), SSP3-7.0 (orange line), SSP5-8.5 (red line), and HighresFuture (purple line). The shaded areas indicate the spread associated with the historical simulation or each scenario, calculated from the minimum and maximum values of the multimodel ensemble.

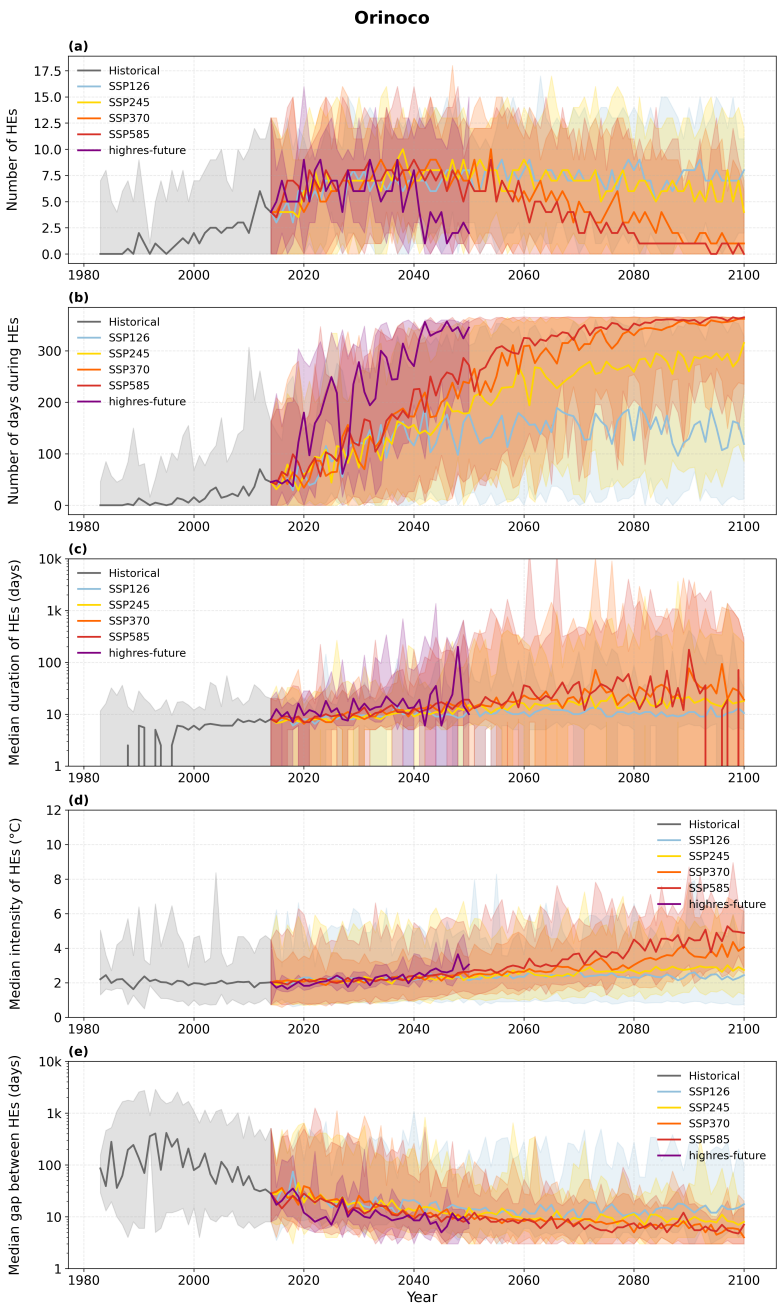

Figure 5.10: Time series of hot events (HEs) characteristics for the Orinoco region based on the ensemble median. The 1983–2014 series corresponds to the multimodel median of the historical simulations (gray line). For the 2015–2100 period (2015–2050 for the HighresFuture scenario), the ensemble median for each of the scenarios considered are shown: SSP1-2.6 (blue line), SSP2-4.5 (yellow line), SSP3-7.0 (orange line), SSP5-8.5 (red line), and HighresFuture (purple line). The shaded areas indicate the spread associated with the historical simulation or each scenario, calculated from the minimum and maximum values of the multimodel ensemble.

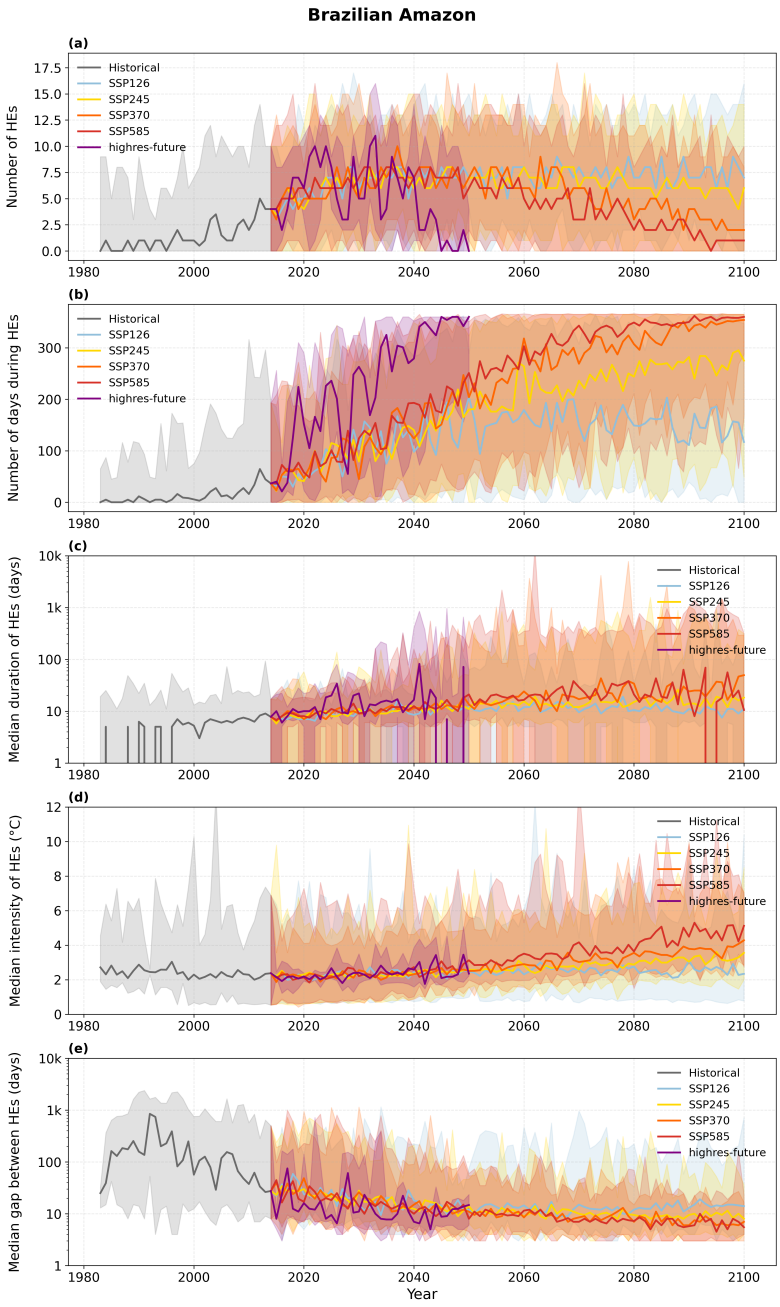

Figure 5.11: Time series of hot events (HEs) characteristics for the Brazilian Amazon region based on the ensemble median. The 1983–2014 series corresponds to the multimodel median of the historical simulations (gray line). For the 2015–2100 period (2015–2050 for the HighresFuture scenario), the ensemble median for each of the scenarios considered are shown: SSP1-2.6 (blue line), SSP2-4.5 (yellow line), SSP3-7.0 (orange line), SSP5-8.5 (red line), and HighresFuture (purple line). The shaded areas indicate the spread associated with the historical simulation or each scenario, calculated from the minimum and maximum values of the multimodel ensemble.

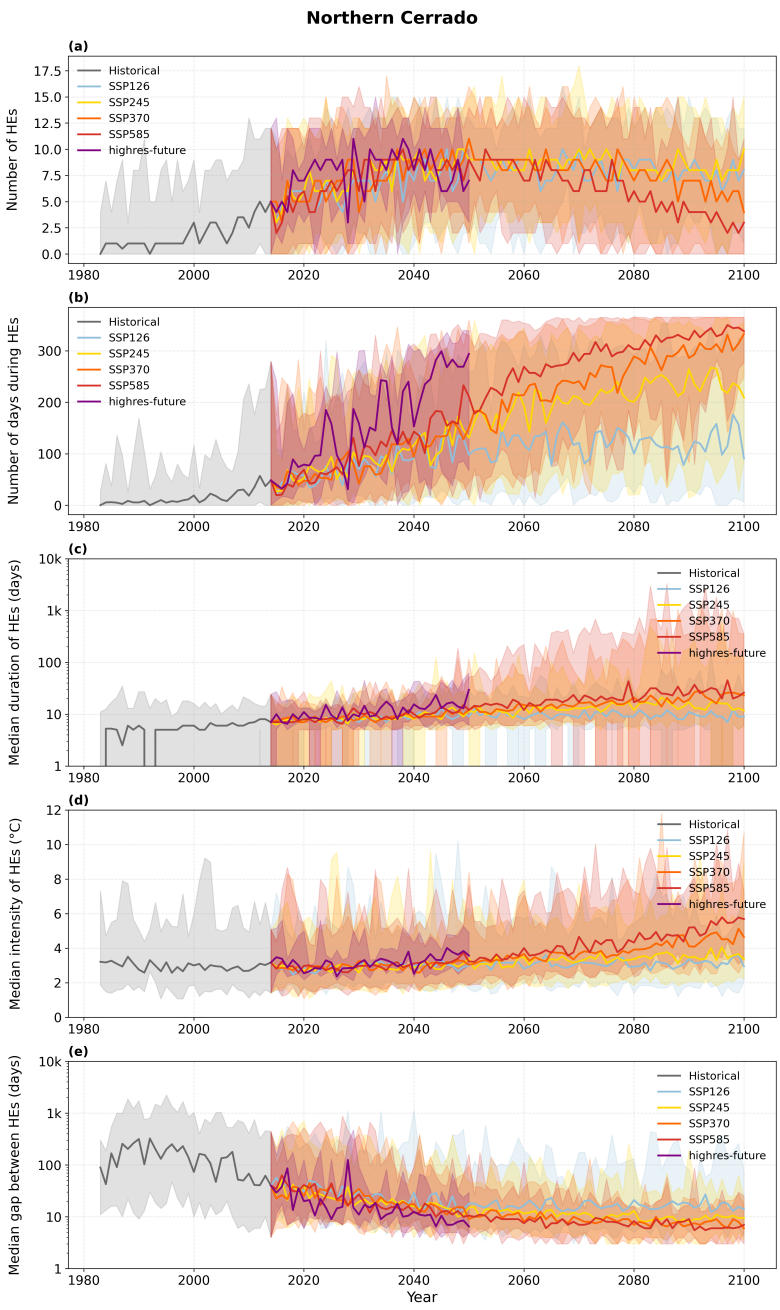

Figure 5.12: Time series of hot events (HEs) characteristics for the northern Cerrado region based on the ensemble median. The 1983–2014 series corresponds to the multimodel median of the historical simulations (gray line). For the 2015–2100 period (2015–2050 for the HighresFuture scenario), the ensemble median for each of the scenarios considered are shown: SSP1-2.6 (blue line), SSP2-4.5 (yellow line), SSP3-7.0 (orange line), SSP5-8.5 (red line), and HighresFuture (purple line). The shaded areas indicate the spread associated with the historical simulation or each scenario, calculated from the minimum and maximum values of the multimodel ensemble.

Building on the analysis of the regions that exhibited the greatest changes detected in subsection 3.3.4, the temporal evolution and trends of the different HEs characteristics in each region were evaluated. The analysis was conducted for the historical period (1983–2014) using the multi-model median of the historical simulations. For the future period (2015–2100), simulations under the SSP scenarios were considered while the HighresFuture scenario was analyzed for the period 2015–2050.

For the historical period, all four regions (Figures 5.9a, 5.10a, 5.11a, and 5.12a) show an increase in the number of HEs since 2000, with up to five HEs per year observed in all regions by the end of the historical period. The scenarios considered in this study tend to follow the upward trend in the number of events at the beginning of the projection period. After 2050, SSP3-7.0 and SSP5-8.5 show a decrease in the number of events, with this decrease being more pronounced in the Brazilian Amazon, Orinoco, and northern Andes regions. This decrease is also evident in the HighresFuture scenario from ∼2030 onward across all regions, except for the northern Cerrado. Trend analysis shows a statistically significant decrease in the number of HEs in most regions under SSP3-7.0 and SSP5-8.5. The largest significant negative trends are found under SSP5-8.5, with values of −1.21 events/decade in the northern Andes and −1.05 events/decade in the Orinoco region. Under SSP3-7.0 and SSP2-4.5, the strongest significant trends are also observed in the northern Andes, with values of −1.11 events/decade and −0.44 events/decade, respectively (Table C.1). In contrast, SSP1-2.6 shows significant positive trends in the northern Cerrado (0.25 events/decade) and in the Orinoco region (0.14 events/decade). The HighresFuture scenario indicates the strongest significant negative trends across all regions compared to the SSPs, except in the northern Cerrado where no trend is projected.

The ensemble median shows an increase in the number of days associated with HEs since 2000. This positive trend in the number of days persists across all regions and under all SSPs considered (Figures 5.9b, 5.10b, 5.11b, and 5.12b). By the end of the century, a greater number of days is projected under SSP3-7.0 and SSP5-8.5. The Orinoco, Brazilian Amazon, and northern Andes regions suggest years during 2081–2100 in which all days are associated with HEs. The HighresFuture scenario shows the largest increases in the near-term and mid-term compared to the SSPs, reaching values of up to 365 days by 2050 across all regions, except in the northern Cerrado, where values close to 300 days are observed for that year. All regions exhibit positive and statistically significant trends under the scenarios analyzed (Table C.1). Under the SSPs, positive trends increase with rising emissions, with the highest values observed under SSP5-8.5 for the Brazilian Amazon (40.28 days/decade) and the northern Cerrado (40.20 days/decade). For this characteristic, HighresFuture suggests more pronounced positive trends, doubling the number of days projected under SSP5-8.5 in most regions (Table C.1).

All regions show a slight increase in median duration of HEs during the historical period (Figures 5.9c, 5.10c, 5.11c, and 5.12c). In the projections, this trend persists, with more pronounced increases under the SSP3-7.0 and SSP5-8.5 scenarios. HighresFuture exhibits longer durations than those observed under the SSP scenarios for the 2015–2050 period. In the projections, durations range from approximately 10 to 100 days. However, models display considerable spread, reaching values on the order of 1,000 days in some cases. This reflects the high uncertainty among models. The regions show statistically significant trends in most climate change scenarios, with the largest increases occurring in the SSP3-7.0 scenario. Under this scenario, the Brazilian Amazon, northern Andes, and Orinoco regions show increases of 2.32, 2.14, and 2.95 days/decade, respectively (Table C.1). In contrast, SSP5-8.5 shows no significant trend for the northern Andes.

Although the median ensemble shows no trend in median intensity of HEs (°C) during the historical period (Figures 5.9d, 5.10d, 5.11d, and 5.12d), climate change scenarios do show an increase in temperature intensity, with statistically significant trends across all regions and under all scenarios (Table C.1). Intensities increase consistently with the emission level of each SSP, reaching the highest values by the end of the century under the SSP5-8.5 scenario, with increases of close to 6 °C across all regions, followed by SSP3-7.0. The gap between events shows a decrease in the number of days since the historical period (Figures 5.9e, 5.10e, 5.11e, and 5.12e), a trend that is maintained in all scenarios considered. Towards the end of the century, the shortest intervals between events are projected under SSP3-7.0 and SSP5-8.5, with negative and statistically significant trends in all regions (Table C.1). The largest negative trends are recorded in the northern Cerrado region in all scenarios (Table C.1). The HighresFuture scenario exhibits the most negative and statistically significant trends compared to the SSP scenarios in 3 of the 4 regions.

5.3.3 Projected changes of dry events

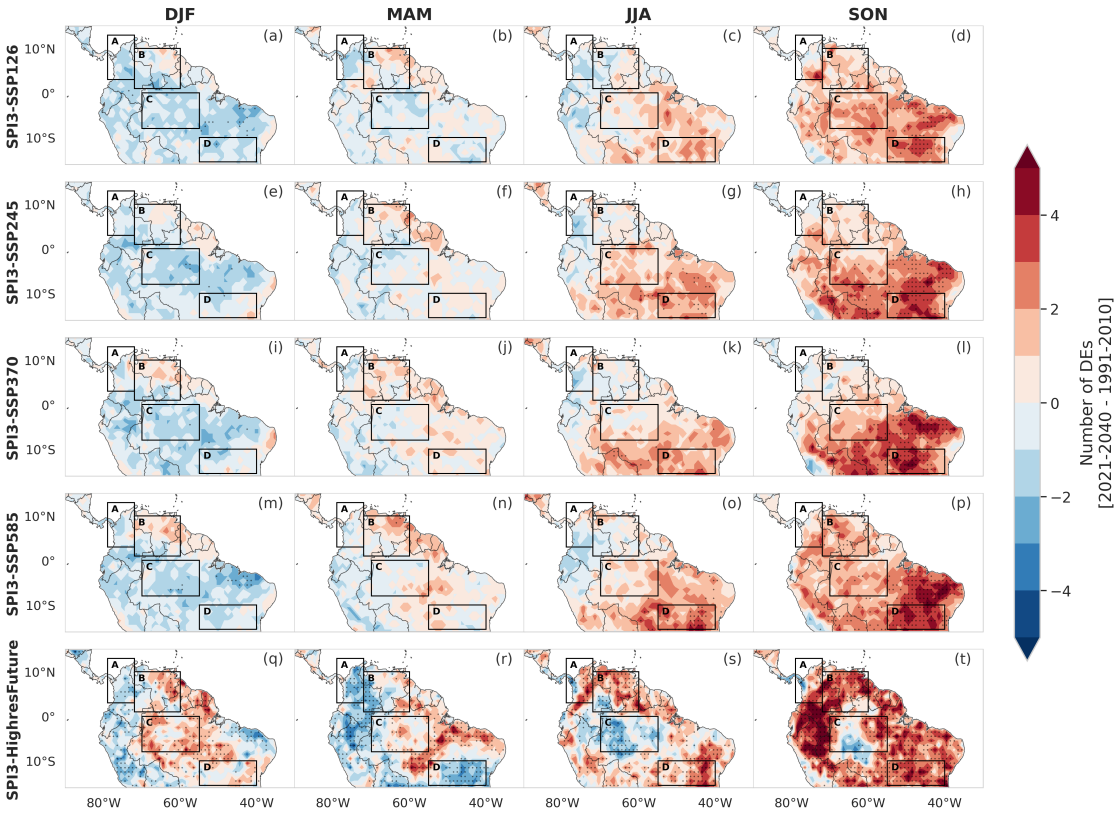

Figure 5.13: Projected changes in the seasonal count of Dry Events (DEs) for the near-term period (2021–2040) based on the ensemble median under different emission scenarios: SSP1-2.6 (a–d), SSP2-4.5 (e–h), SSP3-7.0 (i–l), and SSP5-8.5 (m–p) from CMIP6, and HighresFuture (HighresFuture) (q–t) from HighResMIP. Dots indicate grid points where at least 80 % of the CMIP6 or HighResMIP models agree on the sign of the projected change. Black rectangles highlight the four subregions: (A) northern Andes, (B) Orinoco, (C) Brazilian Amazon, and (D) northern Cerrado. All spatial fields are shown at a common resolution of 1° × 1°.

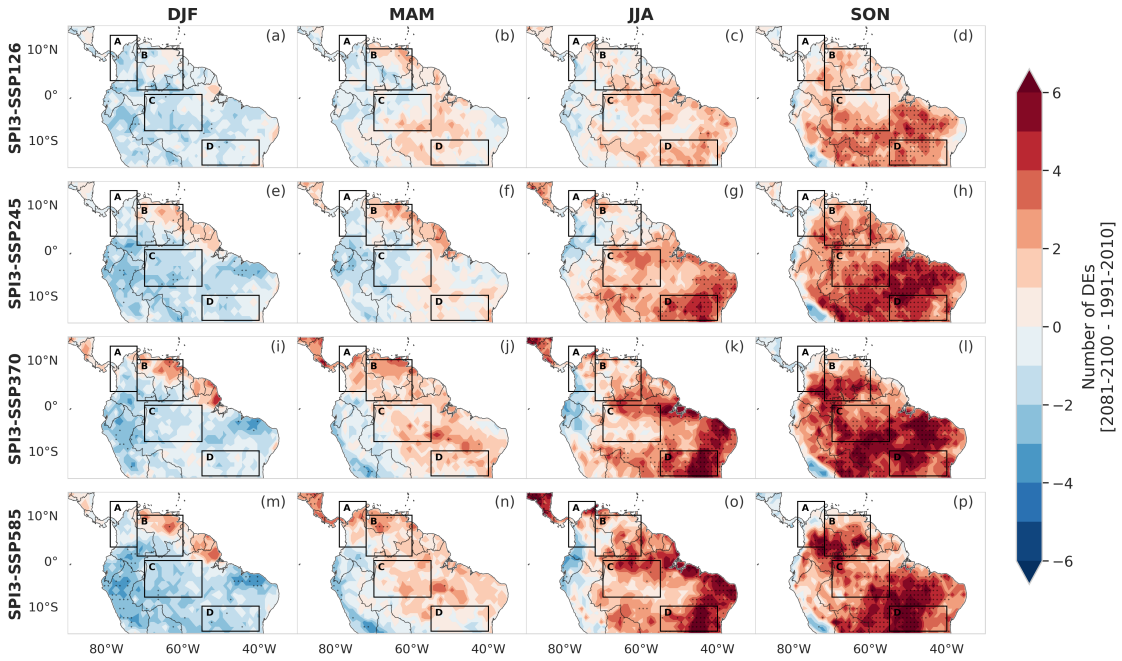

Figure 5.14: Projected changes in the seasonal count of Dry Events (DEs) for the long-term period (2081–2100) based on the ensemble median under different emission scenarios: SSP1-2.6 (a–d), SSP2-4.5 (e–h), SSP3-7.0 (i–l), and SSP5-8.5 (m–p) from CMIP6. Dots indicate grid points where at least 80 % of the CMIP6 models agree on the sign of the projected change. Black rectangles highlight the four regions: (A) northern Andes, (B) Orinoco, (C) Brazilian Amazon, and (D) northern Cerrado. All spatial fields are shown at a common resolution of 1° × 1°.

Between 2021 and 2040, models project an increase in the occurrence of DEs over much of TSA during JJA and SON in all SSP scenarios (Figure 5.13). The largest increases are observed in eastern Brazil and southern TSA, including the Cerrado region (D), with more than three additional events compared to the historical period. During DJF and MAM, an increase of 1 to 2 events is projected over the northern Orinoco basin. Very few regions show agreement between models in the sign of change. The HighresFuture scenario shows a different pattern from that of the SSPs. The largest increases occur in northern and central TSA during DJF, in eastern TSA during MAM, in the north and south during JJA, and in much of TSA during SON. The latter season shows the most pronounced increases, especially in the west of the region. In contrast, during JJA and SON, the Brazilian Amazon region shows a decrease in the number of DEs.

For the long-term period (Figure 5.14), the SSP scenarios show a similar spatial pattern to that observed in the near-term (Figure 5.13). However, the number of events projected for this period exceeds both the historical values and those estimated for the near-term. The SSP1-2.6 scenario shows the smallest increases compared to the other SSPs. Under SSP2-4.5, SSP3-7.0, and SSP5-8.5, increases exceeding 5 events are observed during JJA in the northern Andes (region A) and eastern and central TSA, and in central Brazil, Bolivia, and southern Colombia and Venezuela during SON, with high inter-model agreement on the sign of change. During DJF, as in the near-term period, a decrease in the number of DEs is observed relative to the historical period over much of TSA; however, there is no inter-model consensus on the sign of change for this region.

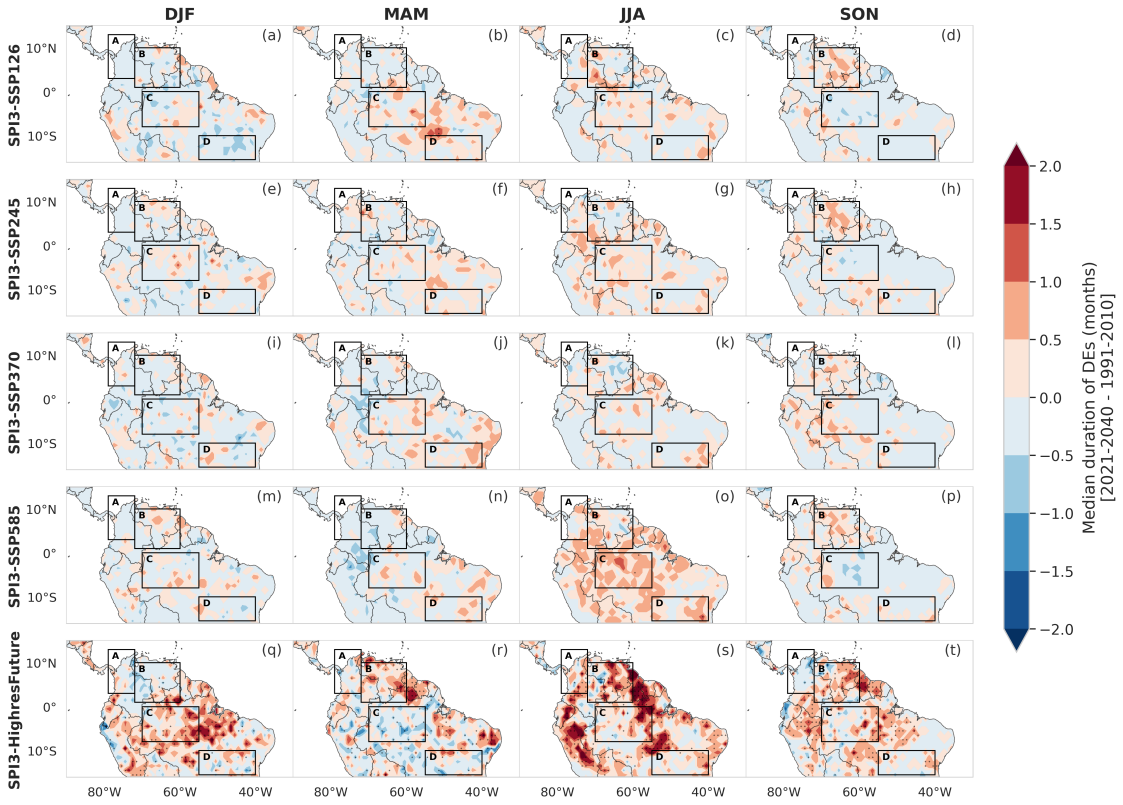

Figure 5.15: Projected changes in the seasonal median duration (months) of Dry Events (DEs) for the near-term period (2021–2040) based on the ensemble median under different emission scenarios: SSP1-2.6 (a–d), SSP2-4.5 (e–h), SSP3-7.0 (i–l), and SSP5-8.5 (m–p) from CMIP6, and HighresFuture (HighresFuture) (q–t) from HighResMIP. Dots indicate grid points where at least 80 % of the CMIP6 or HighResMIP models agree on the sign of the projected change. Black rectangles highlight the four subregions: (A) northern Andes, (B) Orinoco, (C) Brazilian Amazon, and (D) northern Cerrado. All spatial fields are shown at a common resolution of 1° × 1°.

The SSPs show an increase in median duration of DEs between 1 to 2 months over small regions of TSA (Figure 5.15). However, SSP5-8.5 suggests a greater spatial extent of this increase, particularly over the Brazilian Amazon (region C). The HighresFuture scenario continues to show the largest changes, as well as a greater spatial extent compared to the SSPs. The longest durations are observed in northern Brazil during DJF, northern TSA during MAM, and eastern and western TSA during SON and JJA, with the largest increases occurring during this last season, with durations exceeding 2 months. By the end of the century (Figure 5.16), longer durations covering larger areas are observed as emissions increase. The longest durations over TSA occur during JJA under the SSP3-7.0 and SSP5-8.5 scenarios, with median durations exceeding 2 months over the Orinoco (region B). For this characteristic, very few regions show inter-model agreement on the type of change compared to the historical period.

For both periods considered (Figures 5.17 and 5.18), the SSPs suggest a decrease in the gap (months) between DEs over much of TSA, except for some western regions that show an increase in the number of months during all seasons. The largest decreases are observed during DJF and MAM, with greater reductions in the long-term period (2081–2100) and under the SSP3-7.0 and

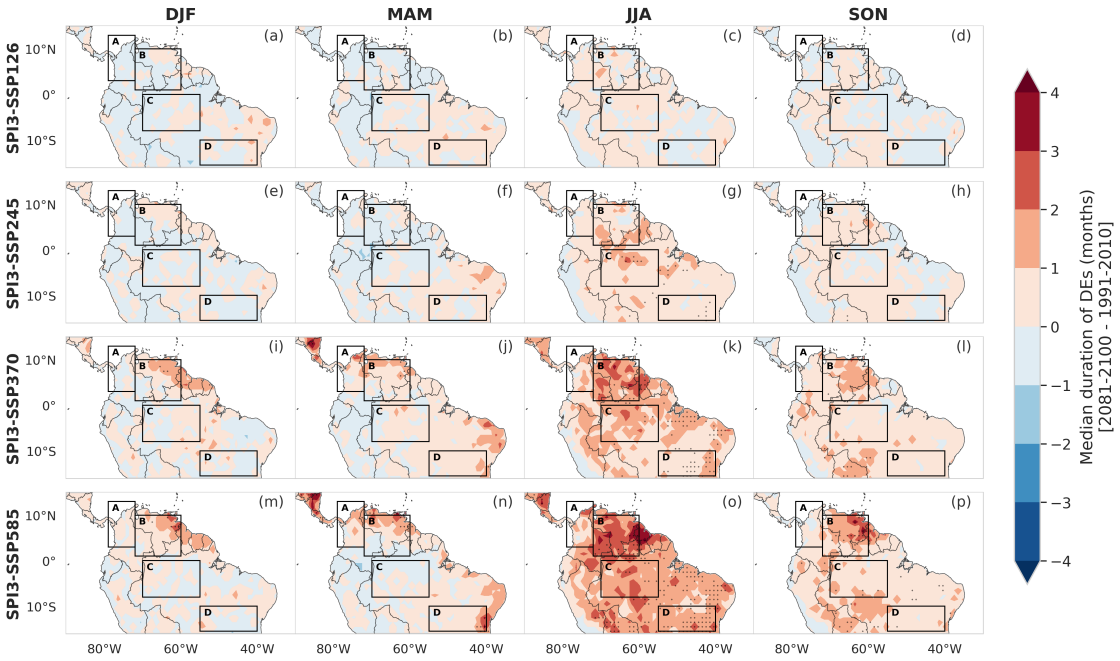

Figure 5.16: Projected changes in the seasonal median duration (months) of Dry Events (DEs) for the long-term period (2081–2100) based on the ensemble median under different emission scenarios: SSP1-2.6 (a–d), SSP2-4.5 (e–h), SSP3-7.0 (i–l), and SSP5-8.5 (m–p) from CMIP6. Dots indicate grid points where at least 80 % of the CMIP6 models agree on the sign of the projected change. Black rectangles highlight the four regions: (A) northern Andes, (B) Orinoco, (C) Brazilian Amazon, and (D) northern Cerrado. All spatial fields are shown at a common resolution of 1° × 1°.

SSP5-8.5 scenarios, with values below -8 months. For the near-term period, HighresFuture shows the largest reductions in the gap between events over northern and central TSA across all seasons. This scenario also shows an increase in the number of months between DEs over the southwestern portions of the northern Andes (region A) and the Orinoco (region B) during MAM. High agreement among the HighResMIP models on the type of change is observed over much of TSA.

The SSPs exhibit increased drought severity (negative values) over several regions of TSA for the near-term period (Figure 5.19), which reach greater spatial extent during JJA and SON. Changes in severity below -0.1 relative to the historical period are observed. The HighresFuture scenario exhibits the greatest drought severity for the near-term period, with values below -0.3 over central TSA and the Brazilian Amazon (region C) during DJF, over northern TSA during MAM, and over eastern and central TSA during the remaining seasons. Unlike the SSPs, projected changes under the HighresFuture scenario show high inter-model agreement. Changes toward more severe drought conditions intensify toward the end of the century (Figure 5.20), with the greatest severity observed under SSP3-7.0 and SSP5-8.5, especially during JJA and SON. Differences of -0.4 are observed particularly over the Orinoco (region B) and Brazilian Amazon (region C), where models show high agreement. Northern TSA also shows more severe droughts, with models agreeing on the sign of change.

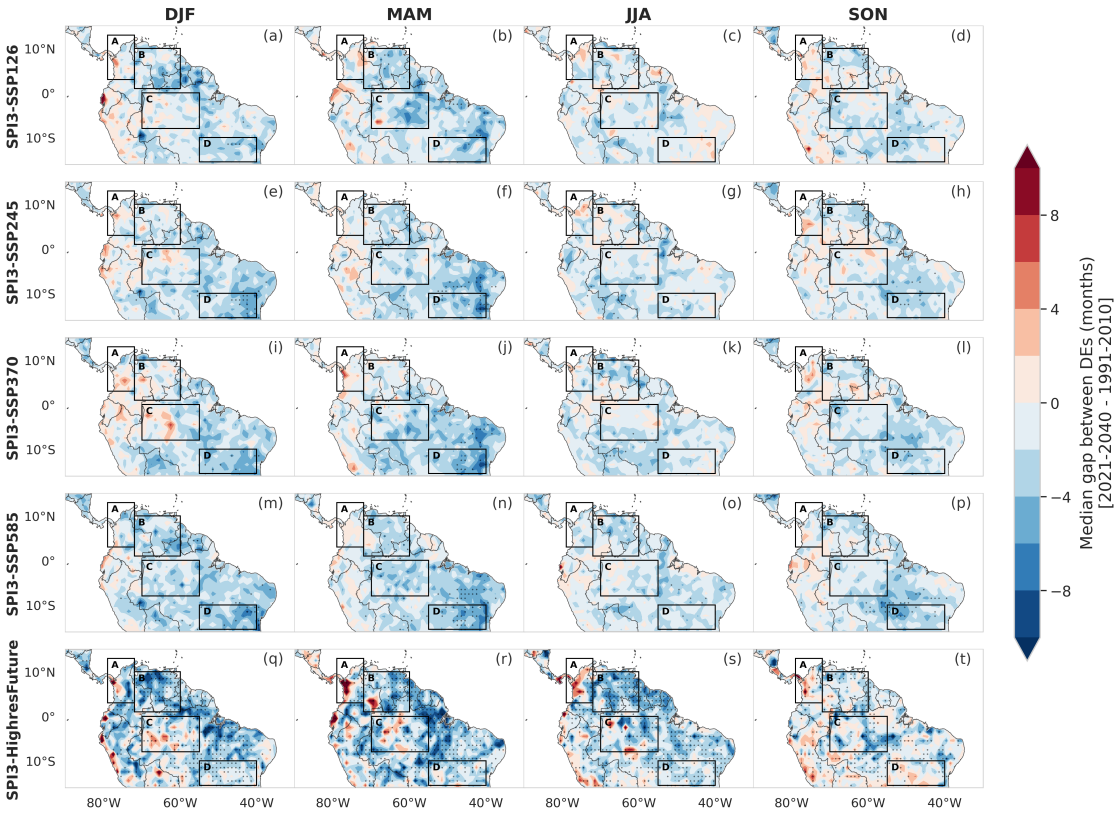

Figure 5.17: Projected changes in the seasonal median gap (months) between Dry Events (DEs) for the near-term period (2021–2040) based on the ensemble median under different emission scenarios: SSP1-2.6 (a–d), SSP2-4.5 (e–h), SSP3-7.0 (i–l), and SSP5-8.5 (m–p) from CMIP6, and HighresFuture (HighresFuture) (q–t) from HighResMIP. Dots indicate grid points where at least 80 % of the CMIP6 or HighResMIP models agree on the sign of the projected change. Black rectangles highlight the four subregions: (A) northern Andes, (B) Orinoco, (C) Brazilian Amazon, and (D) northern Cerrado. All spatial fields are shown at a common resolution of 1° × 1°.

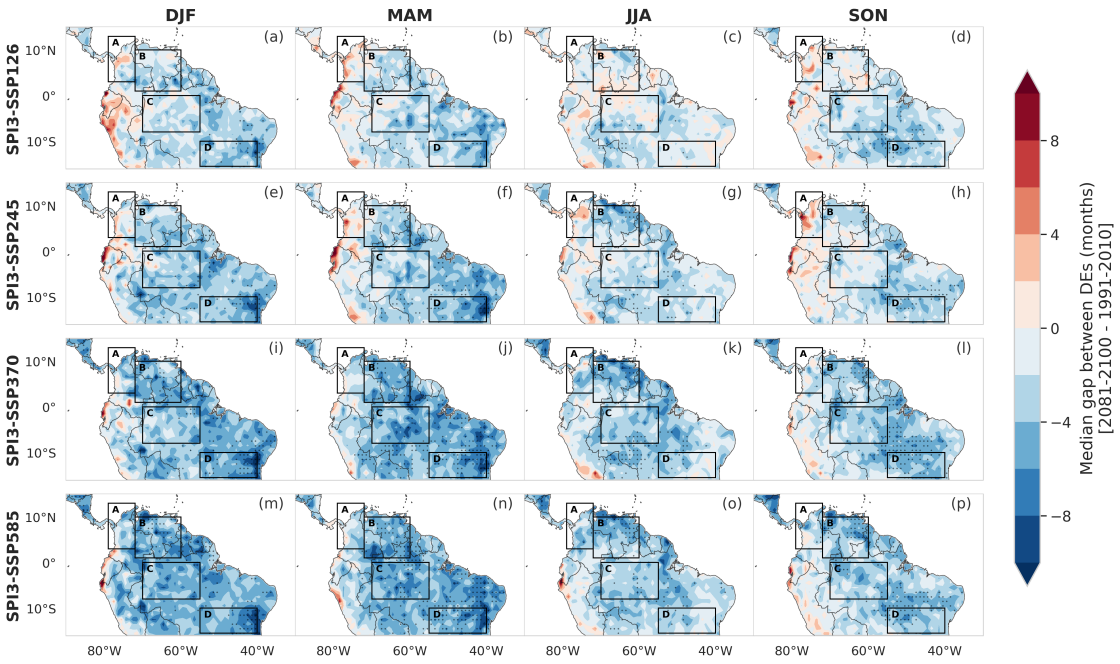

Figure 5.18: Projected changes in the seasonal median gap (months) between Dry Events (DEs) for the long-term period (2081–2100) based on the ensemble median under different emission scenarios: SSP1-2.6 (a–d), SSP2-4.5 (e–h), SSP3-7.0 (i–l), and SSP5-8.5 (m–p) from CMIP6. Dots indicate grid points where at least 80 % of the CMIP6 models agree on the sign of the projected change. Black rectangles highlight the four regions: (A) northern Andes, (B) Orinoco, (C) Brazilian Amazon, and (D) northern Cerrado. All spatial fields are shown at a common resolution of 1° × 1°.

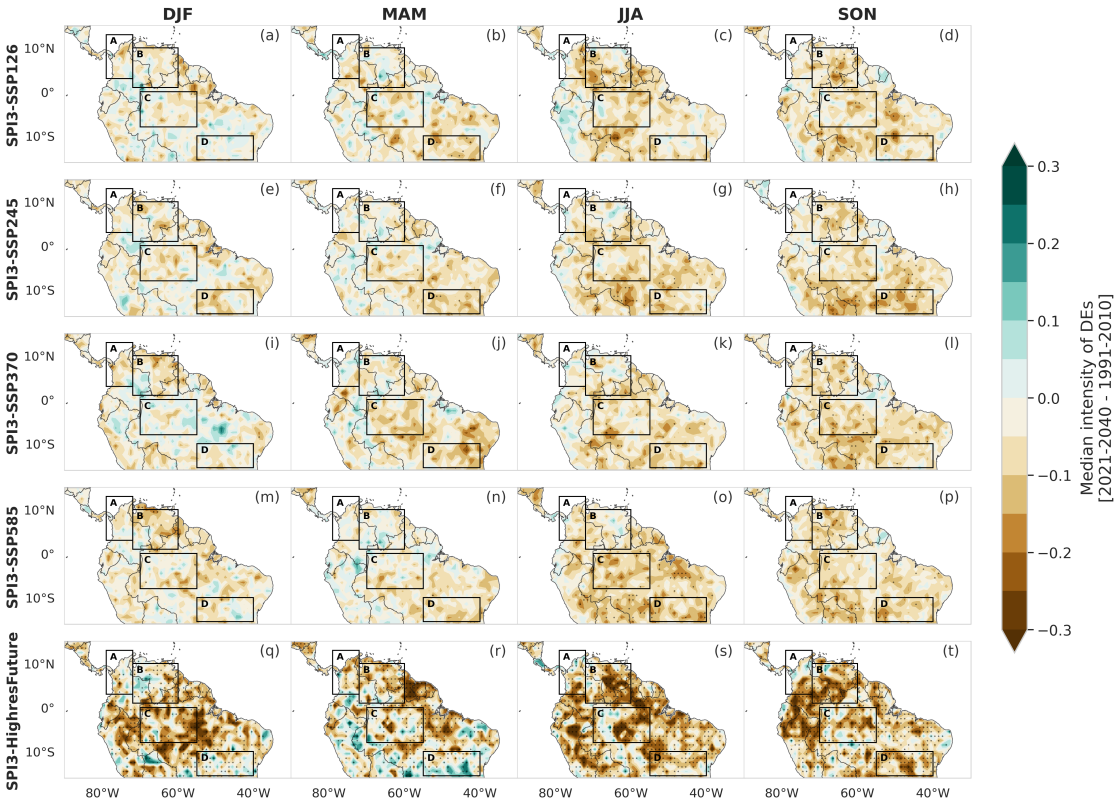

Figure 5.19: Projected changes in the seasonal median intensity (SPI) of Dry Events (DEs) for the near-term period (2021–2040) based on the ensemble median under different emission scenarios: SSP1-2.6 (a–d), SSP2-4.5 (e–h), SSP3-7.0 (i–l), and SSP5-8.5 (m–p) from CMIP6, and HighresFuture (HighresFuture) (q–t) from HighResMIP. Dots indicate grid points where at least 80 % of the CMIP6 or HighResMIP models agree on the sign of the projected change. Black rectangles highlight the four regions: (A) northern Andes, (B) Orinoco, (C) Brazilian Amazon, and (D) northern Cerrado. All spatial fields are shown at a common resolution of 1° × 1°.

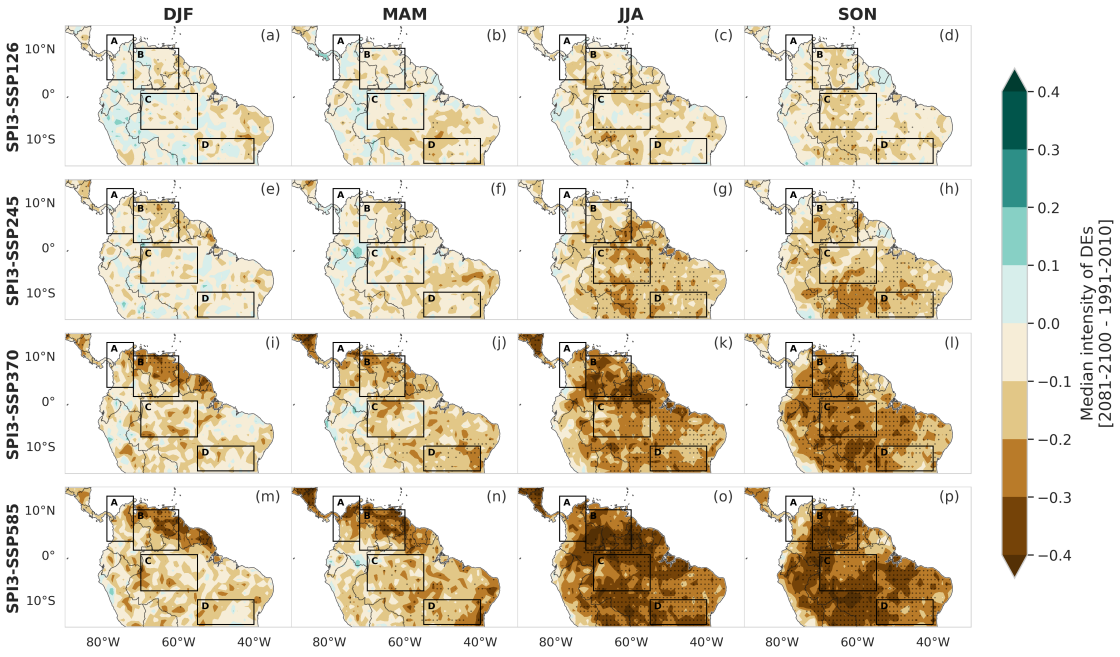

Figure 5.20: Projected changes in the seasonal median intensity (SPI) of Dry Events (DEs) for the long-term period (2081–2100) based on the ensemble median under different emission scenarios: SSP1-2.6 (a–d), SSP2-4.5 (e–h), SSP3-7.0 (i–l), and SSP5-8.5 (m–p) from CMIP6. Dots indicate grid points where at least 80 % of the CMIP6 models agree on the sign of the projected change. Black rectangles highlight the four regions: (A) northern Andes, (B) Orinoco, (C) Brazilian Amazon, and (D) northern Cerrado. All spatial fields are shown at a common resolution of 1° × 1°.

In this work, a second methodology was explored for calculating DEs, which consists of fitting the SPI using parameters from the projection period itself (Collazo et al., 2023; Wang et al., 2021b). Under this approach, the characteristics exhibit a different spatial pattern of projected changes in both their distribution and sign (Figure C.1 to Figure C.8), compared to the results obtained when fitting the SPI with parameters from the historical period (Figure 5.13 to Figure 5.20). In general, changes are more pronounced when using the first methodology for both the near-term and long-term periods.

5.3.4 Trends in the characteristics of DEs in the TSA regions under climate change scenarios

The ensemble median exhibits a maximum of 1 event/year across all regions for the historical period, with some years showing no events (Figures 5.21a, 5.22a, 5.23a, and 5.24a). For the projections, regions exhibit between 1 and 2 events/year, with higher frequency observed in the northern Cerrado region throughout the projection period. Unlike what was observed for HEs, there is no increasing or decreasing trend in the number of DEs across the projected scenarios. Consequently, when analyzing trends for all scenarios, all regions exhibit a trend of 0.0 events/decade, which is statistically significant in some cases (Table C.3).

Although no trend is observed in the number of DEs per decade, an increase in the number of months associated with these events is observed (Figures 5.21b, 5.22b, 5.23b, and 5.24b). This increase is more pronounced in the higher-emission scenarios (SSP3-7.0 and SSP5-8.5). In the near-term and mid-term period (2015–2050), the HighresFuture scenario shows the highest number of months associated with DEs. This increase is linked to a slight rise in median duration, as shown across all regions (Figures 5.21c, 5.22c, 5.23c, and 5.24c). For both the number of months and the median duration, the SSP1-2.6 scenario exhibits no trends in any of the analyzed regions (Table C.3). In the northern Andes and northern Cerrado regions, the SSP2-4.5 scenario also shows no trend in either of these two characteristics. The strongest trends are found in HighresFuture across all regions, and are statistically significant in most cases (Table C.3).

The median ensemble of drought severity shows no trends during the historical period in any of the analyzed regions (Figures 5.21d, 5.22d, 5.23d, and 5.24d). However, for the projected period, the scenarios indicate a trend toward more severe drought conditions ($-2.0 \leq \text{SPI} < -1.5$), with the most intense conditions occurring in the HighresFuture scenario in the near-term and mid-term, and in SSP5-8.5 in the long term. Most scenarios exhibit negative and statistically significant trends across all four regions, with the strongest trend found in the HighresFuture scenario in the Brazilian Amazon (-0.08 SPI/decade) and in both the HighresFuture and SSP5-8.5 scenarios in the Orinoco region, where values reach -0.05 SPI/decade (Table C.3). The median gap between events shows a negative trend, which becomes more pronounced under SSP5-8.5 toward the end of the century (Figures 5.21e, 5.22e, 5.23e, and 5.24e). This behavior is associated with the occurrence of longer-lasting events. All regions exhibit negative and statistically significant trends in most scenarios (Table C.3), with the exception of SSP1-2.6 and HighresFuture, which show no significant trends in any region, and the SSP2-4.5 scenario in the northern Andes region.

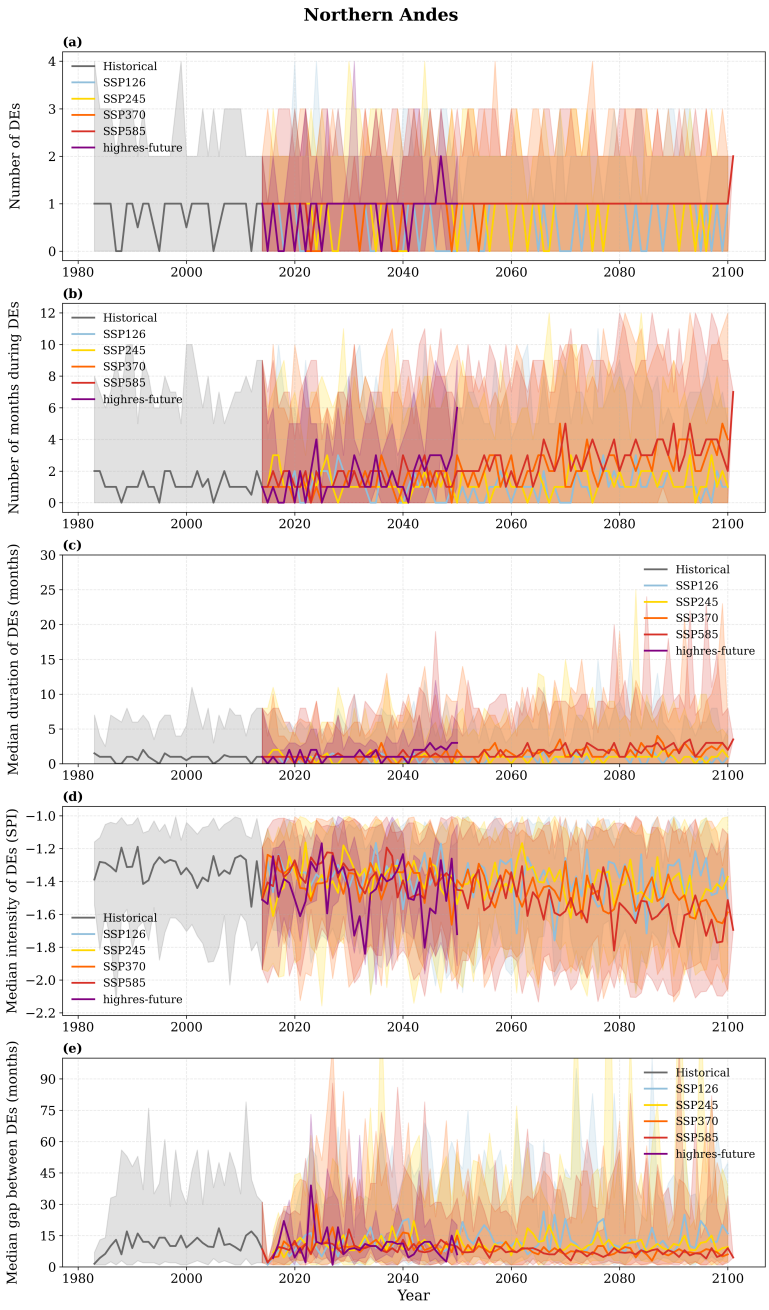

Figure 5.21: Time series of dry events (DEs) characteristics for the northern Andes region based on the ensemble median. The 1983–2014 series corresponds to the multimodel median of the historical simulations (gray line). For the 2015–2100 period (2015–2050 for the HighresFuture scenario), the ensemble median for each of the scenarios considered are shown: SSP1-2.6 (blue line), SSP2-4.5 (yellow line), SSP3-7.0 (orange line), SSP5-8.5 (red line), and HighresFuture (purple line). The shaded areas indicate the spread associated with the historical simulation or each scenario, calculated from the minimum and maximum values of the multimodel ensemble.

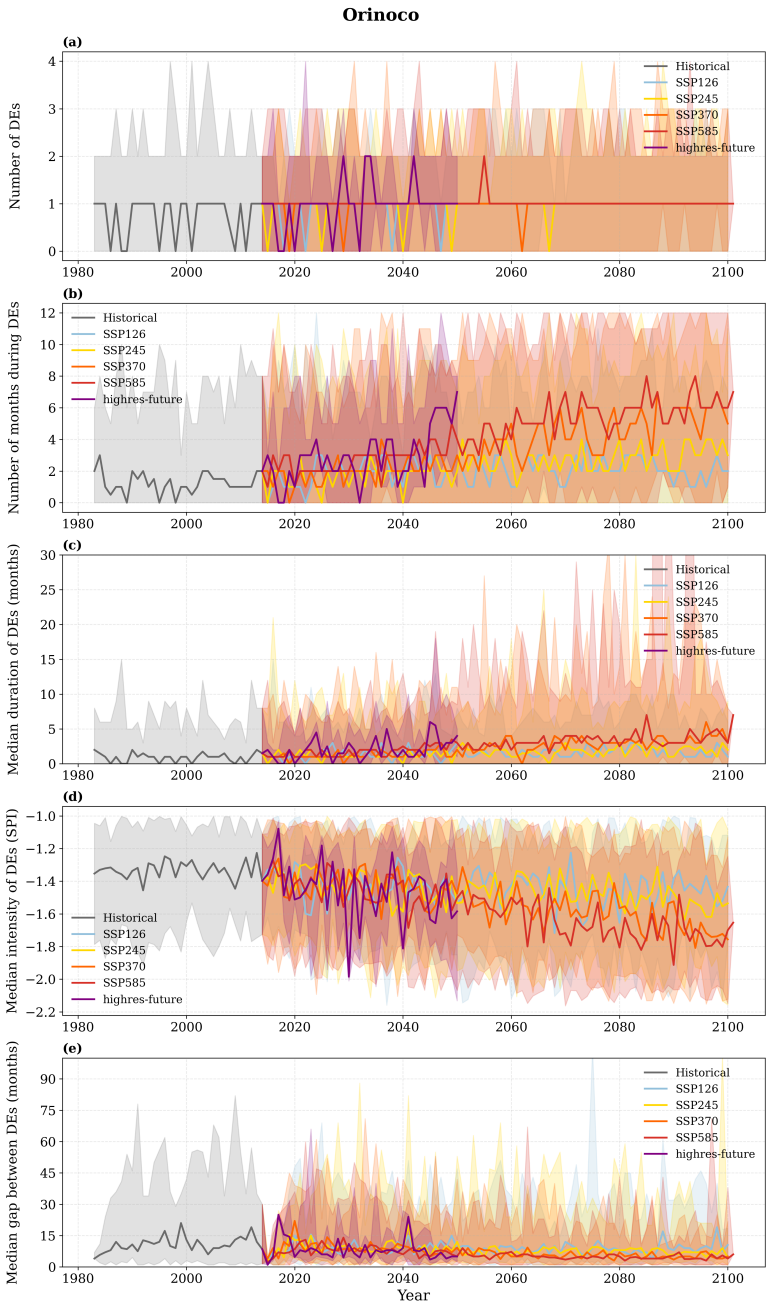

Figure 5.22: Time series of dry events (DEs) characteristics for the Orinoco region based on the ensemble median. The 1983–2014 series corresponds to the multimodel median of the historical simulations (gray line). For the 2015–2100 period (2015–2050 for the HighresFuture scenario), the ensemble median for each of the scenarios considered are shown: SSP1-2.6 (blue line), SSP2-4.5 (yellow line), SSP3-7.0 (orange line), SSP5-8.5 (red line), and HighresFuture (purple line). The shaded areas indicate the spread associated with the historical simulation or each scenario, calculated from the minimum and maximum values of the multimodel ensemble.

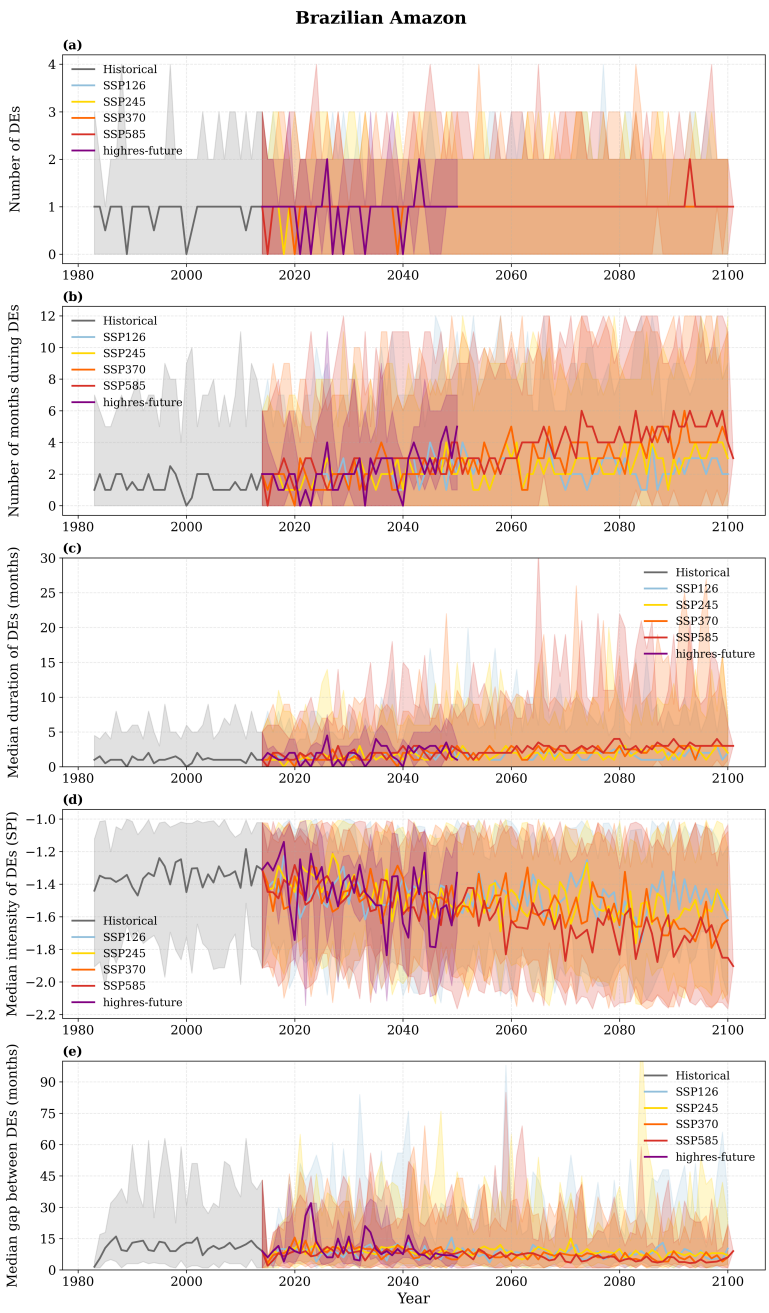

Figure 5.23: Time series of dry events (DEs) characteristics for the Brazilian Amazon region based on the ensemble median. The 1983–2014 series corresponds to the multimodel median of the historical simulations (gray line). For the 2015–2100 period (2015–2050 for the HighresFuture scenario), the ensemble median for each of the scenarios considered are shown: SSP1-2.6 (blue line), SSP2-4.5 (yellow line), SSP3-7.0 (orange line), SSP5-8.5 (red line), and HighresFuture (purple line). The shaded areas indicate the spread associated with the historical simulation or each scenario, calculated from the minimum and maximum values of the multimodel ensemble.

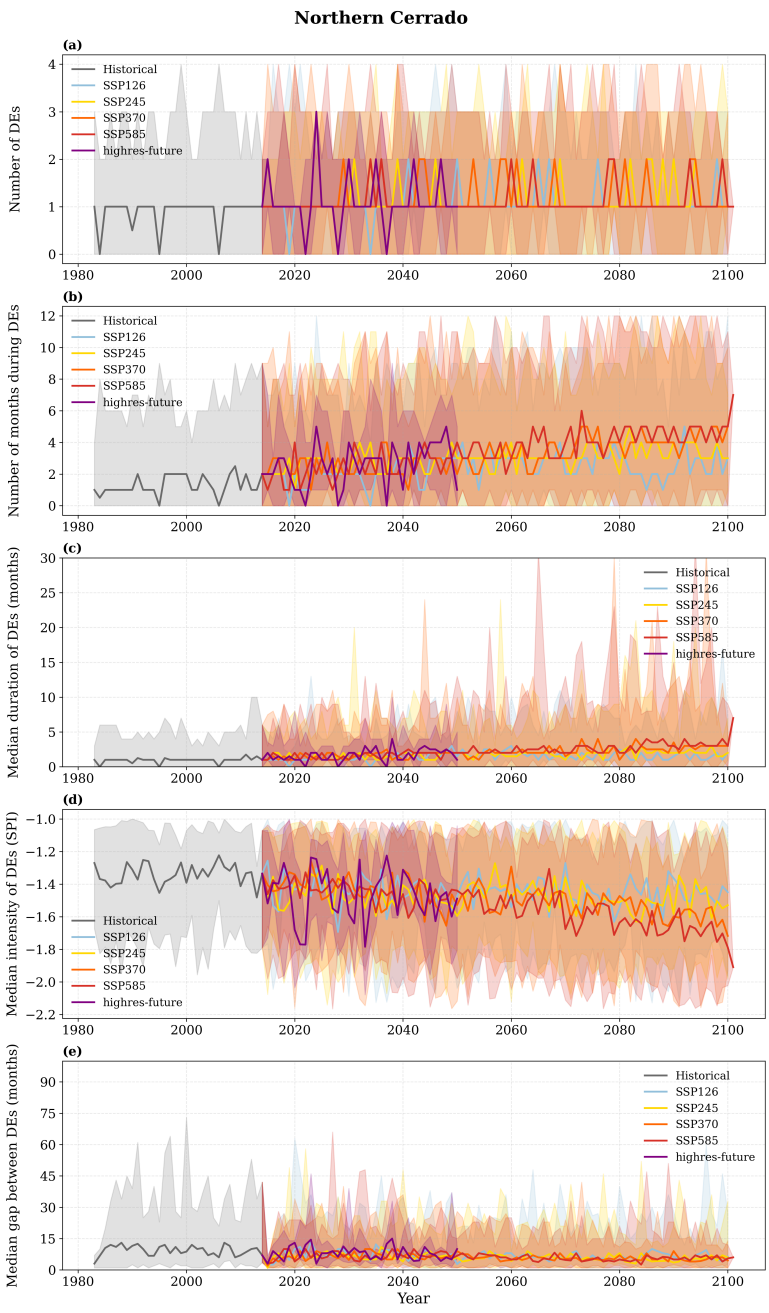

Figure 5.24: Time series of dry events (DEs) characteristics for the northern Cerrado region based on the ensemble median. The 1983–2014 series corresponds to the multimodel median of the historical simulations (gray line). For the 2015–2100 period (2015–2050 for the HighresFuture scenario), the ensemble median for each of the scenarios considered are shown: SSP1-2.6 (blue line), SSP2-4.5 (yellow line), SSP3-7.0 (orange line), SSP5-8.5 (red line), and HighresFuture (purple line). The shaded areas indicate the spread associated with the historical simulation or each scenario, calculated from the minimum and maximum values of the multimodel ensemble.

5.3.5 Projected changes of compound dry and hot events

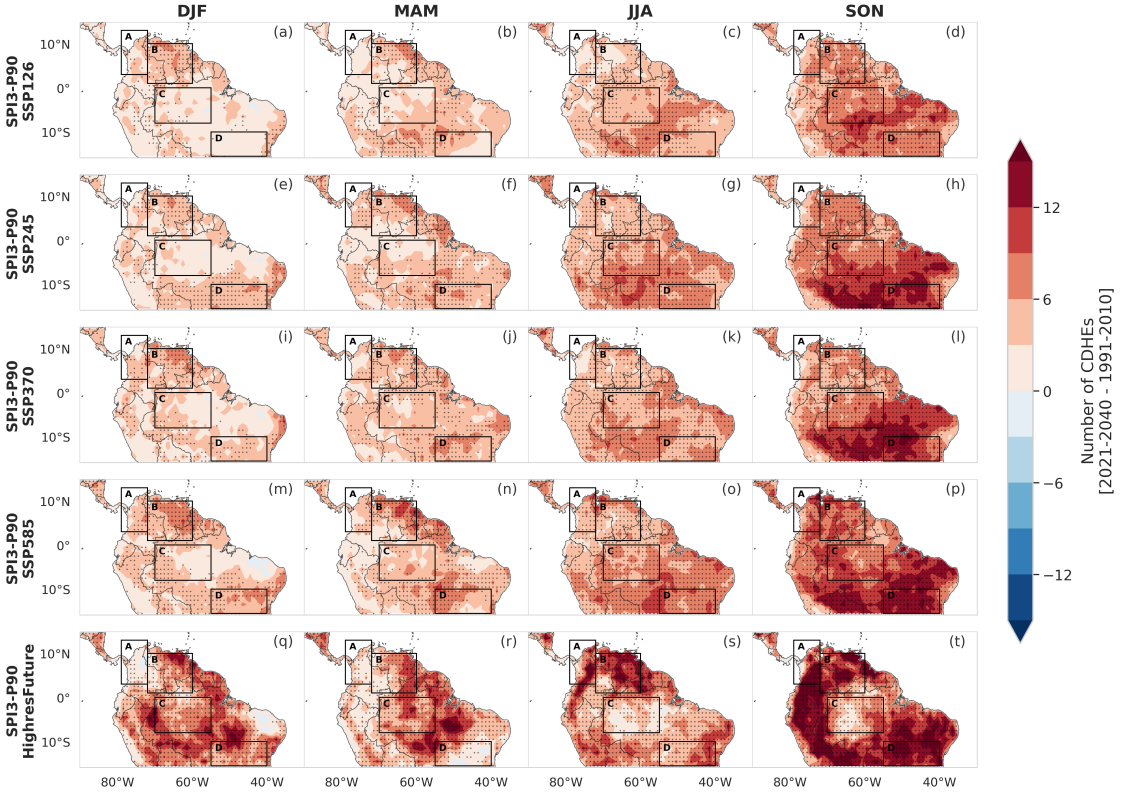

Figure 5.25: Projected changes in the seasonal count of Compound Dry and Hot Events (CDHEs) for the near-term period (2021–2040) based on the ensemble median under different emission scenarios: SSP1-2.6 (a–d), SSP2-4.5 (e–h), SSP3-7.0 (i–l), and SSP5-8.5 (m–p) from CMIP6, and HighresFuture (HighresFuture) (q–t) from HighResMIP. Dots indicate grid points where at least 80 % of the CMIP6 or HighResMIP models agree on the sign of the projected change. Black rectangles highlight the four subregions: (A) northern Andes, (B) Orinoco, (C) Brazilian Amazon, and (D) northern Cerrado. All spatial fields are shown at a common resolution of 1° × 1°.

Near-term projections indicate an increase in the occurrence of CDHEs in TSA under the different SSP scenarios (Figure 5.25). This increase is more pronounced in the southern part of the region during SON, particularly in the northern Cerrado (region D). In all scenarios except SSP1-2.6, southern TSA shows increases that exceed historical values by more than 12 events. SSP5-8.5 also shows an increase in northern TSA, with the strongest changes occurring during SON. The models show agreement on the type of change in some regions during DJF and MAM, and over a larger area of agreement during JJA and SON. The HighresFuture scenario shows the largest changes compared to the SSP scenarios, with the highest values found in DJF and MAM over northern and central TSA, in JJA over northern TSA, especially in the Orinoco (region B), and in SON over most of TSA except the Brazilian Amazon region. The HighResMIP models show agreement on the sign of change across much of TSA in all seasons. The number of CDHEs increases by the end of the century (2081-2100) (Figure 5.26), particularly over southern and central TSA during SON in SSP2-4.5 and SSP3-7.0, with values exceeding 16 events compared to historical values. SSP5-8.5 shows a similar spatial pattern, but to a lesser extent. In JJA, substantial increases are also

observed over the northern Cerrado (region D) and over much of Bolívar in all scenarios, except SSP1-2.6. The models show agreement in few regions of TSA during DJF across all SSPs.

For the period 2021–2040 (Figure 5.27), the SSP scenarios show similar patterns in the median duration of events, with higher values in northern TSA during DJF (between 2 and 10 days longer than in the historical period) in all scenarios, and in central TSA during JJA under SSP5-8.5. For this characteristic, only a few regions show model agreement on the type of change. The Highres-Future scenario suggests longer durations over northern TSA during DJF and SON, eastern TSA during MAM, and much of Brazil (including the Brazilian Amazon (region C)), the Guianas, and Peru during JJA, with increases of more than 12 days. The HighResMIP models show agreement on the type of change under this scenario. In the long-term projection (2081–2100) (Figure 5.28), the median duration of CDHEs is longer compared to the near-term period. In the most optimistic scenario (SSP1-2.6), increases of close to 10 days are observed compared to the historical median duration (1991-2010). As radiative forcing increases across the different SSPs, the durations become longer. In particular, SSP3-7.0 and SSP5-8.5 show increases of more than 60 days in northern and central TSA during DJF and SON, in eastern Brazil during MAM, and over a large area of TSA during JJA, compared to the reference period. These areas are more extensive under the SSP5-8.5 scenario.

Both analyzed periods show a decrease in the number of days between CDHEs over TSA (Figures 5.29 and 5.30), associated with the increase in both the number and duration of events. The largest differences are observed over Ecuador and southern Colombia during JJA, and over western and southern TSA during SON. The models show agreement on the sign of change in eastern Brazil during DJF, as well as in southern TSA and some central regions during SON. The HighresFuture scenario suggests the largest changes compared to the SSP scenarios for the 2021–2040 period, consistent with the more pronounced differences observed in the previous characteristics. In this scenario, the HighResMIP models show high agreement over much of TSA.

The intensity of temperature associated with CDHEs increases over much of TSA, with larger increases projected for the long-term period. In the near-term period (Figure 5.31), the greatest increases occur in southern TSA during JJA across all SSP scenarios. Notably, decreases in temperature intensity relative to the historical period are observed in regions such as eastern Brazil during SON and in northern Peru and southern Colombia during MAM. The HighresFuture scenario continues to show the largest changes compared with the SSP scenarios, with increases exceeding 1.0 °C over central TSA during all seasons. Only under the HighresFuture scenario do the models show agreement on the sign of change for 2021–2040. For the long-term period (Figure 5.32), the largest changes are projected under SSP3-7.0 and SSP5-8.5, particularly during JJA in SSP5-8.5, with intensities exceeding 5 °C. In these two scenarios, the models show broader regions of agreement on the sign of change.

The ensemble median shows more heterogeneous patterns in the sign of change of drought severity across the two analyzed periods. In the near-term (Figure 5.33), more severe conditions are observed in some regions of western and northern TSA, as well as in some areas of central and northern Brazil in all scenarios, compared to the historical period. In the rest of the region, SSPs suggest less severe drought conditions and even wetter conditions (positive values). In the HighresFuture scenario, this pattern persists but with larger differences relative to the historical period. Over much of TSA, the HighResMIP models show agreement on the sign of change. For the long-term period (Figure 5.34), although some regions exhibit drier conditions relative to the

reference period, the spatial extent of these areas is larger during JJA and SON under SSP3-7.0 and SSP5-8.5. The strongest severities are found southwest of the Orinoco region in JJA under these two scenarios. The CMIP6 models show no agreement on the sign of change in any region, in either the near-term or long-term period, under any of the SSP scenarios.

CDHEs were also analyzed using the results obtained from the second methodology applied to the calculation of DEs (Figure C.9 to Figure C.18). The largest contrasts in spatial patterns and in the sign of change are found for the number of events, which is lower than the number of events derived from the first methodology (i.e. using the historical reference period). Drought severity also shows notable differences when using the second method, with positive changes over TSA that indicate less severe SPI conditions and even wetter conditions.

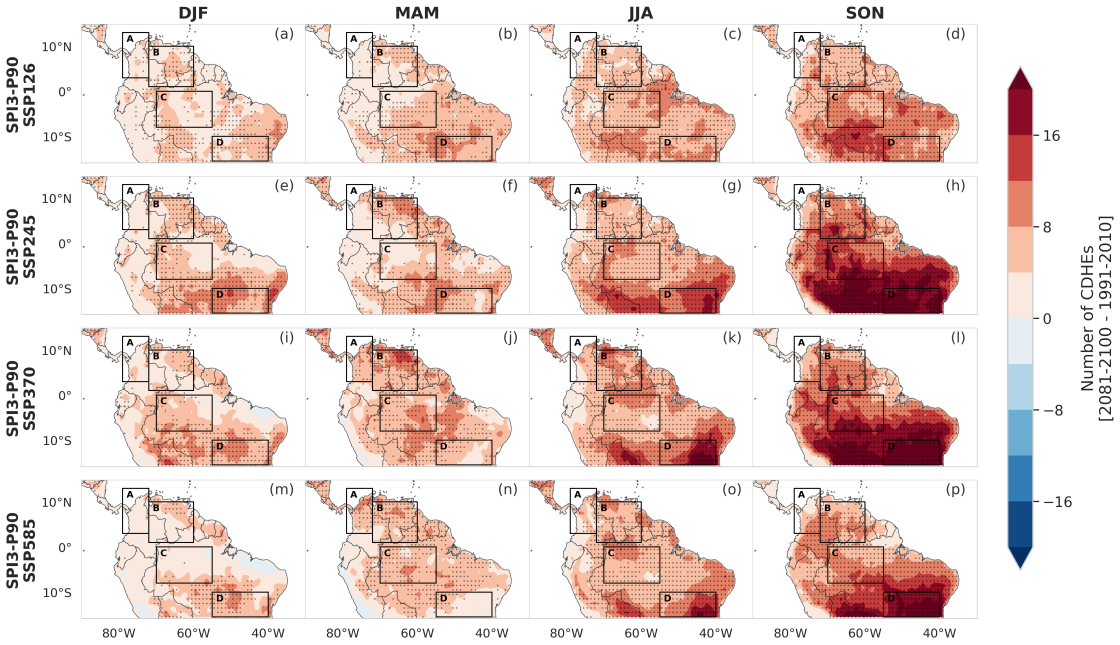

Figure 5.26: Projected changes in the seasonal count of Compound Dry and Hot Events (CDHEs) for the long-term period (2081–2100) based on the ensemble median under different emission scenarios: SSP1-2.6 (a–d), SSP2-4.5 (e–h), SSP3-7.0 (i–l), and SSP5-8.5 (m–p) from CMIP6. Dots indicate grid points where at least 80 % of the CMIP6 models agree on the sign of the projected change. Black rectangles highlight the four regions: (A) northern Andes, (B) Orinoco, (C) Brazilian Amazon, and (D) northern Cerrado. All spatial fields are shown at a common resolution of 1° × 1°.

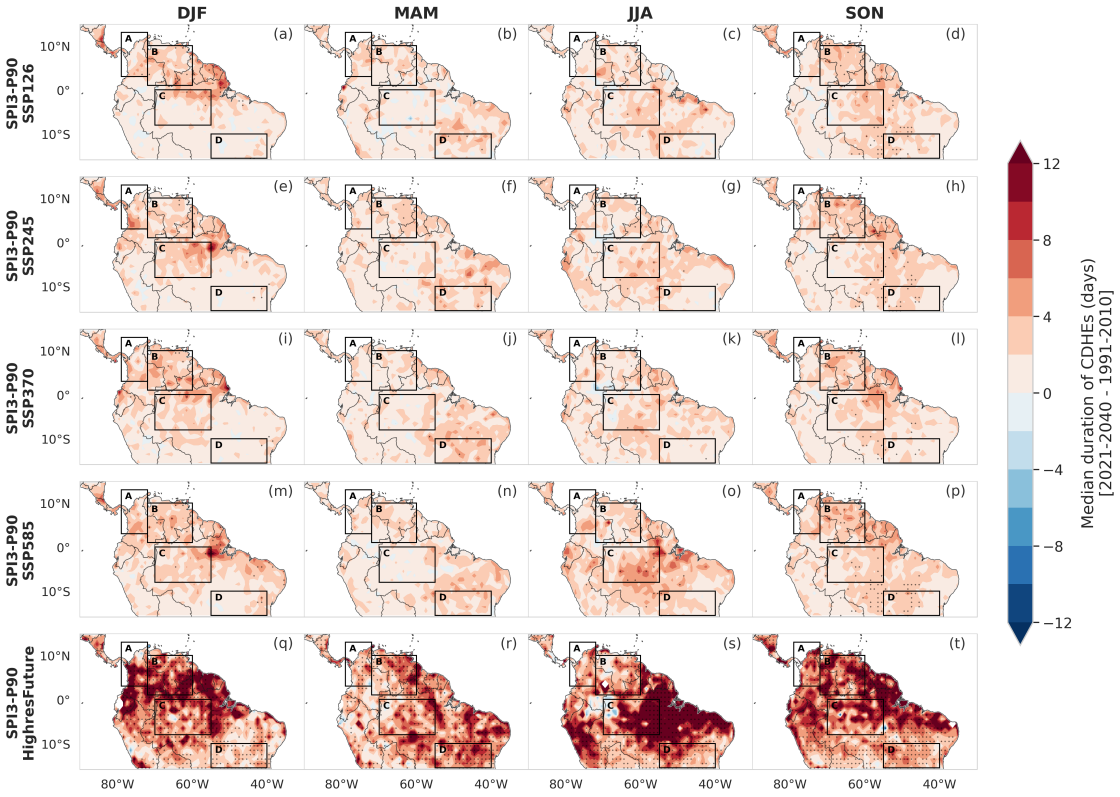

Figure 5.27: Projected changes in the seasonal median duration (days) of Compound Dry and Hot Events (CDHEs) for the near-term period (2021–2040) based on the ensemble median under different emission scenarios: SSP1-2.6 (a–d), SSP2-4.5 (e–h), SSP3-7.0 (i–l), and SSP5-8.5 (m–p) from CMIP6, and HighresFuture (HighresFuture) (q–t) from HighResMIP. Dots indicate grid points where at least 80 % of the CMIP6 or HighResMIP models agree on the sign of the projected change. Black rectangles highlight the four regions: (A) northern Andes, (B) Orinoco, (C) Brazilian Amazon, and (D) northern Cerrado. All spatial fields are shown at a common resolution of 1° × 1°.

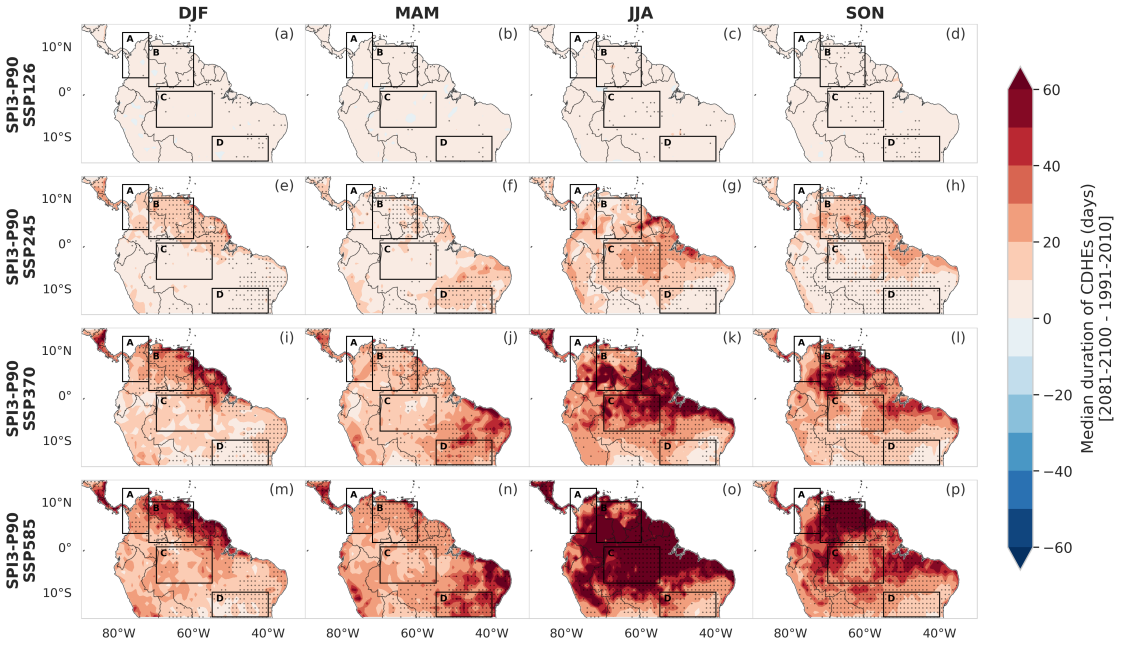

Figure 5.28: Projected changes in the seasonal median duration (days) of Compound Dry and Hot Events (CDHEs) for the long-term period (2081–2100) based on the ensemble median under different emission scenarios: SSP1-2.6 (a–d), SSP2-4.5 (e–h), SSP3-7.0 (i–l), and SSP5-8.5 (m–p) from CMIP6. Dots indicate grid points where at least 80 % of the CMIP6 models agree on the sign of the projected change. Black rectangles highlight the four regions: (A) northern Andes, (B) Orinoco, (C) Brazilian Amazon, and (D) northern Cerrado. All spatial fields are shown at a common resolution of $1^\circ \times 1^\circ$.

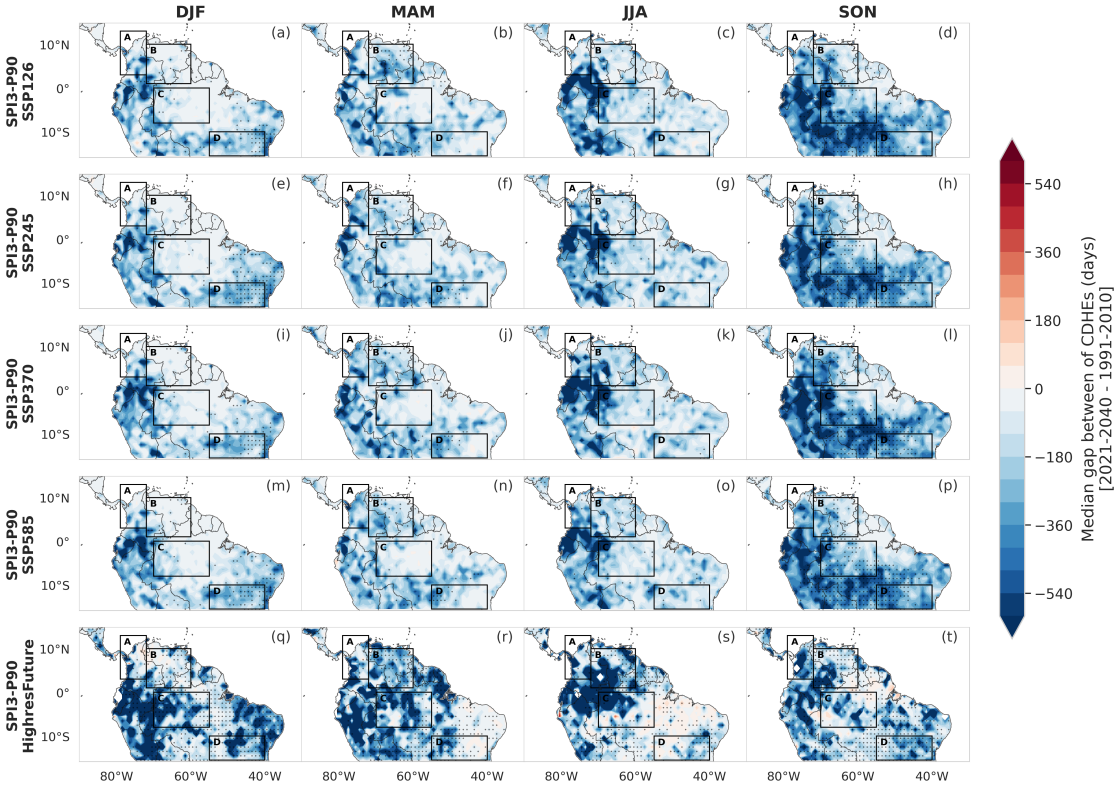

Figure 5.29: Projected changes in the seasonal median gap (days) between Compound Dry and Hot Events (CDHEs) for the near-term period (2021–2040) based on the ensemble median under different emission scenarios: SSP1-2.6 (a–d), SSP2-4.5 (e–h), SSP3-7.0 (i–l), and SSP5-8.5 (m–p) from CMIP6, and HighresFuture (HighresFuture) (q–t) from HighResMIP. Dots indicate grid points where at least 80 % of the CMIP6 or HighResMIP models agree on the sign of the projected change. Black rectangles highlight the four regions: (A) northern Andes, (B) Orinoco, (C) Brazilian Amazon, and (D) northern Cerrado. All spatial fields are shown at a common resolution of 1° × 1°.

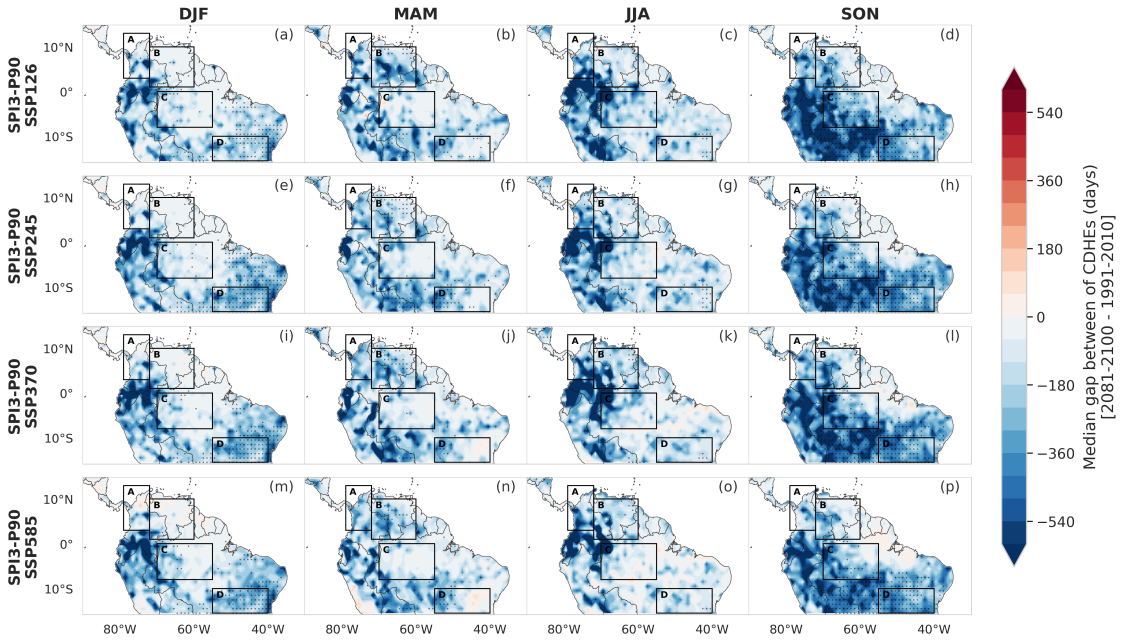

Figure 5.30: Projected changes in the seasonal median gap (days) between Compound Dry and Hot Events (CDHEs) for the long-term period (2081–2100) based on the ensemble median under different emission scenarios: SSP1-2.6 (a–d), SSP2-4.5 (e–h), SSP3-7.0 (i–l), and SSP5-8.5 (m–p) from CMIP6. Dots indicate grid points where at least 80 % of the CMIP6 models agree on the sign of the projected change. Black rectangles highlight the four regions: (A) northern Andes, (B) Orinoco, (C) Brazilian Amazon, and (D) northern Cerrado. All spatial fields are shown at a common resolution of $1^\circ \times 1^\circ$.

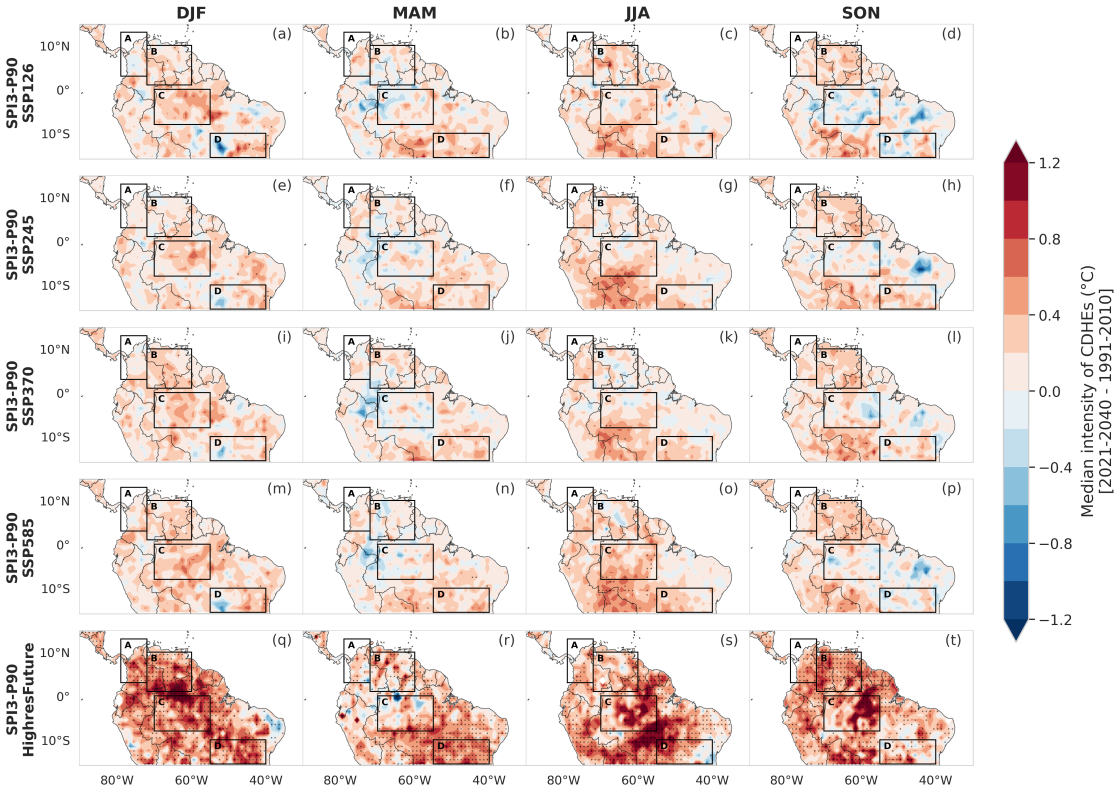

Figure 5.31: Projected changes in the seasonal median intensity (°C) of Compound Dry and Hot Events (CDHEs) for the near-term period (2021–2040) based on the ensemble median under different emission scenarios: SSP1-2.6 (a–d), SSP2-4.5 (e–h), SSP3-7.0 (i–l), and SSP5-8.5 (m–p) from CMIP6, and HighresFuture (HighresFuture) (q–t) from HighResMIP. Dots indicate grid points where at least 80 % of the CMIP6 or HighResMIP models agree on the sign of the projected change. Black rectangles highlight the four regions: (A) northern Andes, (B) Orinoco, (C) Brazilian Amazon, and (D) northern Cerrado. All spatial fields are shown at a common resolution of 1° × 1°.

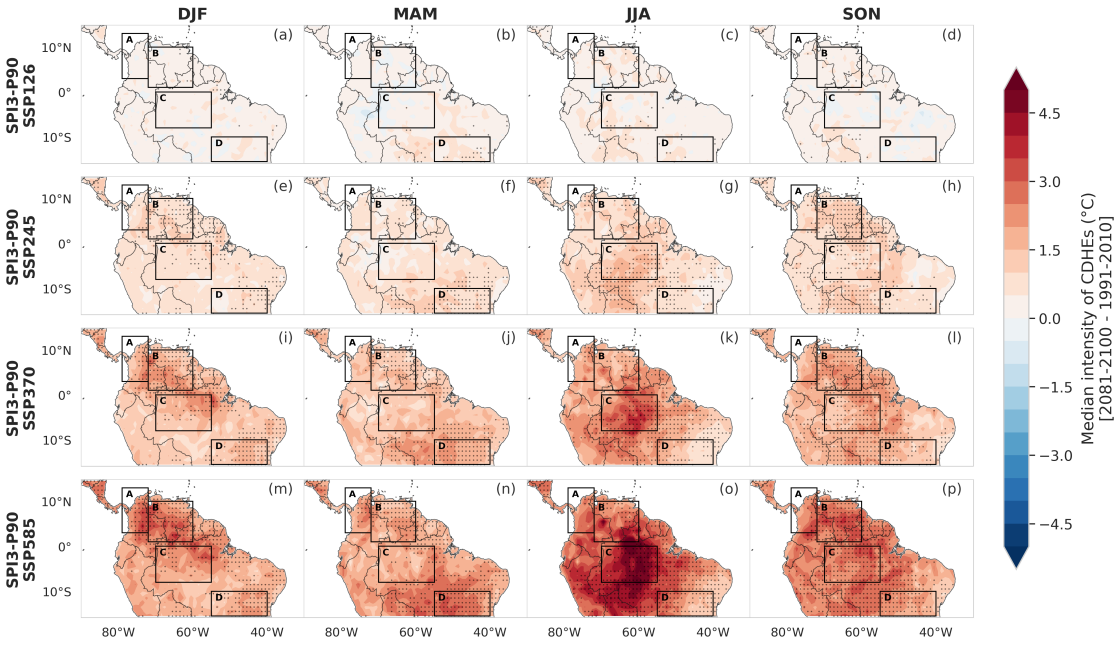

Figure 5.32: Projected changes in the seasonal median intensity (°C) of Compound Dry and Hot Events (CDHEs) for the long-term period (2081–2100) based on the ensemble median under different emission scenarios: SSP1-2.6 (a–d), SSP2-4.5 (e–h), SSP3-7.0 (i–l), and SSP5-8.5 (m–p) from CMIP6. Dots indicate grid points where at least 80 % of the CMIP6 models agree on the sign of the projected change. Black rectangles highlight the four regions: (A) northern Andes, (B) Orinoco, (C) Brazilian Amazon, and (D) northern Cerrado. All spatial fields are shown at a common resolution of 1° × 1°.

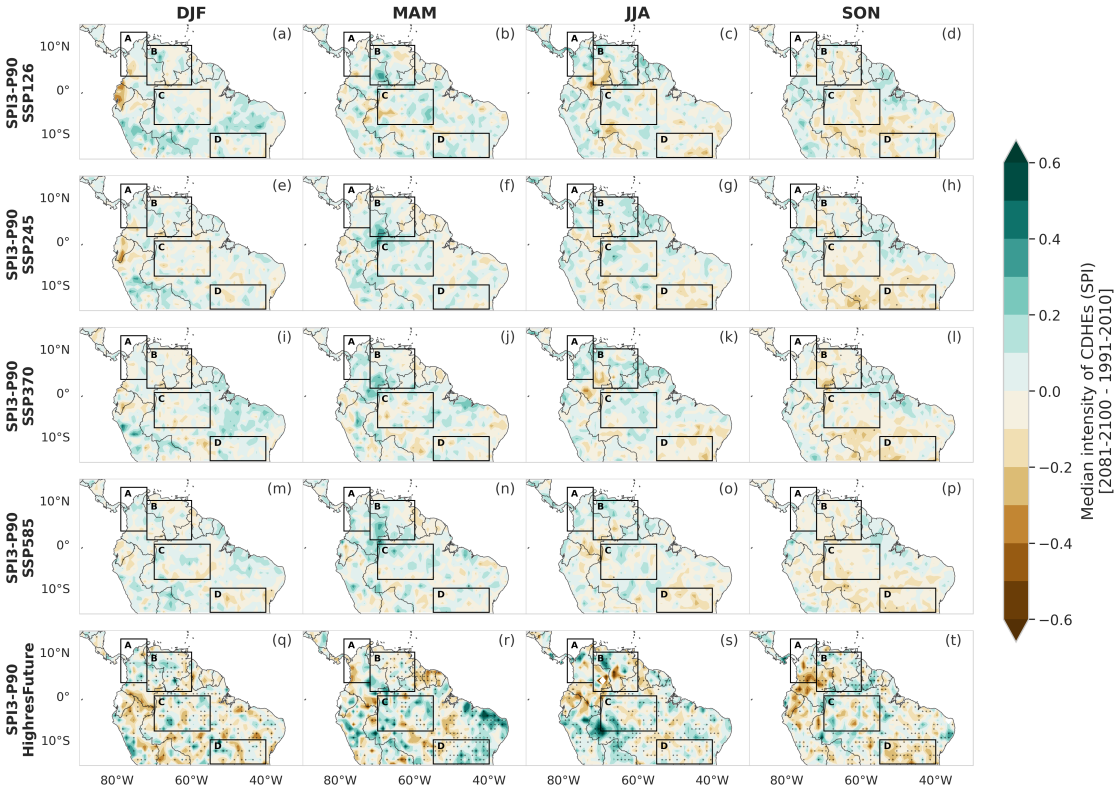

Figure 5.33: Projected changes in the seasonal median intensity (SPI) of Compound Dry and Hot Events (CDHEs) for the near-term period (2021–2040) based on the ensemble median under different emission scenarios: SSP1-2.6 (a–d), SSP2-4.5 (e–h), SSP3-7.0 (i–l), and SSP5-8.5 (m–p) from CMIP6, and HighresFuture (HighresFuture) (q–t) from HighResMIP. Dots indicate grid points where at least 80 % of the CMIP6 or HighResMIP models agree on the sign of the projected change. Black rectangles highlight the four regions: (A) northern Andes, (B) Orinoco, (C) Brazilian Amazon, and (D) northern Cerrado. All spatial fields are shown at a common resolution of 1° × 1°.

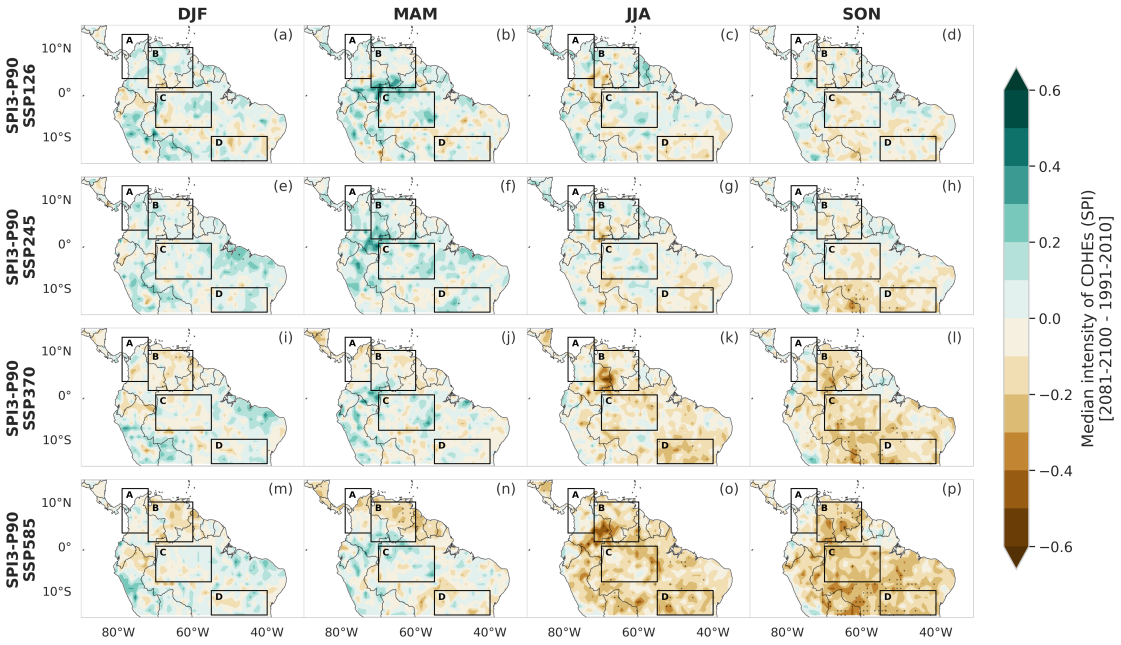

Figure 5.34: Projected changes in the seasonal median intensity (SPI) of Compound Dry and Hot Events (CDHEs) for the long-term period (2081–2100) based on the ensemble median under different emission scenarios: SSP1-2.6 (a–d), SSP2-4.5 (e–h), SSP3-7.0 (i–l), and SSP5-8.5 (m–p) from CMIP6. Dots indicate grid points where at least 80 % of the CMIP6 models agree on the sign of the projected change. Black rectangles highlight the four regions: (A) northern Andes, (B) Orinoco, (C) Brazilian Amazon, and (D) northern Cerrado. All spatial fields are shown at a common resolution of 1° × 1°.

5.3.6 Trends in the characteristics of CDHEs in the TSA regions under climate change scenarios

For the historical period, the ensemble median shows the occurrence of CDHEs since 2000 across all four regions (Figures 5.35a, 5.36a, 5.37a, and 5.38a), with a frequency of 1–2 events/year, although some years exhibit no events. In the projected scenarios, the annual event frequency increases relative to the historical period, reaching 1–3 events/year in most regions, except in the northern Cerrado, where higher frequencies are observed (3–4 events/year). None of the regions exhibit a significant temporal trend in event frequency under any scenario, with slopes equal to 0.0, some of which are statistically significant (Table C.5).

Although the ensemble median does not exhibit a trend in the number of CDHEs, substantial increases are observed in both the number of days (Figures 5.35b, 5.36b, 5.37b, and 5.38b) and the median duration (Figures 5.35c, 5.36c, 5.37c, and 5.38c) of these events across all regions, with larger increases projected toward the end of the century under SSP3-7.0 and SSP5-8.5. The trends are statistically significant under all scenarios, except for the northern Andes region, which shows no significant trend for either characteristic under SSP1-2.6 (Table C.5). The strongest trends occur under the HighresFuture and SSP5-8.5 scenarios in all regions.

The intensity of temperature during CDHEs, based on the ensemble median, does not show a clear trend during the historical period in any of the four regions (Figures 5.35d, 5.36d, 5.37d, and 5.38d). However, beginning in 2020, the projected scenarios exhibit an increasing trend in intensity, which is more pronounced in the short term under the HighresFuture scenario and in the long term under SSP5-8.5. The northern Andes exhibit lower model dispersion and lower intensities compared to the other regions. Trend analysis indicates statistically significant increases in temperature intensity across all regions and SSPs (Table C.5), except in the northern Cerrado under SSP1-2.6. The strongest trends occur in the Brazilian Amazon region under SSP5-8.5 and HighresFuture, with increases of 0.53 °C/decade and 0.72 °C/decade, respectively.

Although the ensemble median shows no trends in drought severity during CDHEs in the historical period, the projected scenarios suggest a negative trend toward more severe drought conditions, which is more pronounced under SSP5-8.5 (Figures 5.35e, 5.36e, 5.37e, and 5.38e). Under this scenario, SPI values between -1.6 and -1.8 are projected across most regions by the end of the century. Trend analysis shows negative and statistically significant values in all regions, although not consistently across all scenarios (Table C.5). The Orinoco region tends to exhibit more pronounced negative trends compared to the other regions, with the strongest trend under the HighresFuture scenario (-0.06 SPI/decade).

Finally, the ensemble median shows a negative trend in the median gap between events during the historical period beginning in 2000, consistent with the increased frequency of CDHEs observed across all regions since that year (Figures 5.35f, 5.36f, 5.37f, and 5.38f). However, for the projected period, the ensemble median indicates an increase in the number of days between events under most scenarios and regions, with more pronounced increases under SSP3-7.0, SSP5-8.5, and HighresFuture. This increase is statistically significant across all scenarios for the Orinoco region (Table C.5). The northern Andes exhibit the largest increases across all scenarios compared to the other regions. In contrast, the northern Cerrado region shows negative trends under the HighresFuture and SSP2-4.5 scenarios, with the latter being statistically significant (Table C.5).

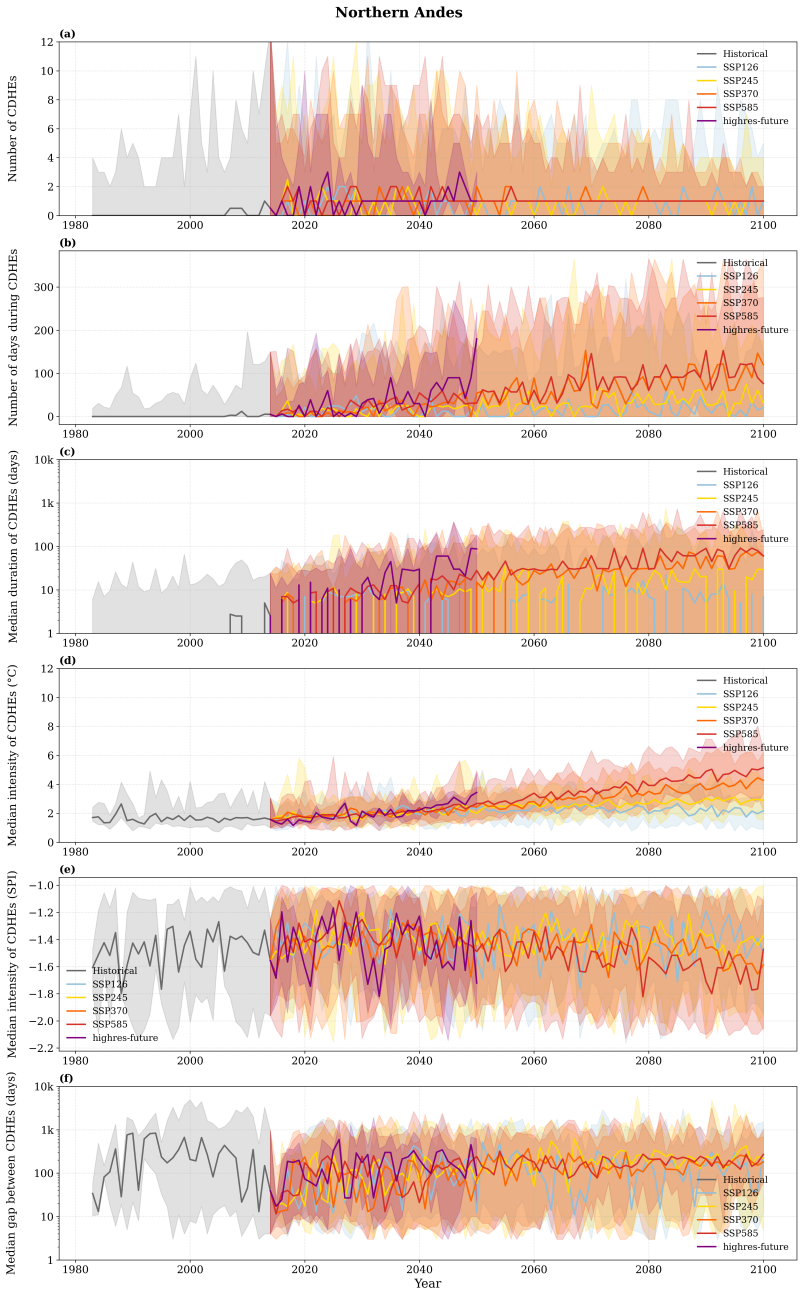

Figure 5.35: Time series of compound dry and hot events (CDHEs) characteristics for the northern Andes region based on the ensemble median. The 1983–2014 series corresponds to the multimodel median of the historical simulations (gray line). For the 2015–2100 period (2015–2050 for the HighresFuture scenario), the multimodel medians for each of the scenarios considered are shown: SSP1-2.6 (blue line), SSP2-4.5 (yellow line), SSP3-7.0 (orange line), SSP5-8.5 (red line), and HighresFuture (purple line). The shaded areas indicate the spread associated with the historical simulation or each scenario, calculated from the minimum and maximum values of the multimodel ensemble.

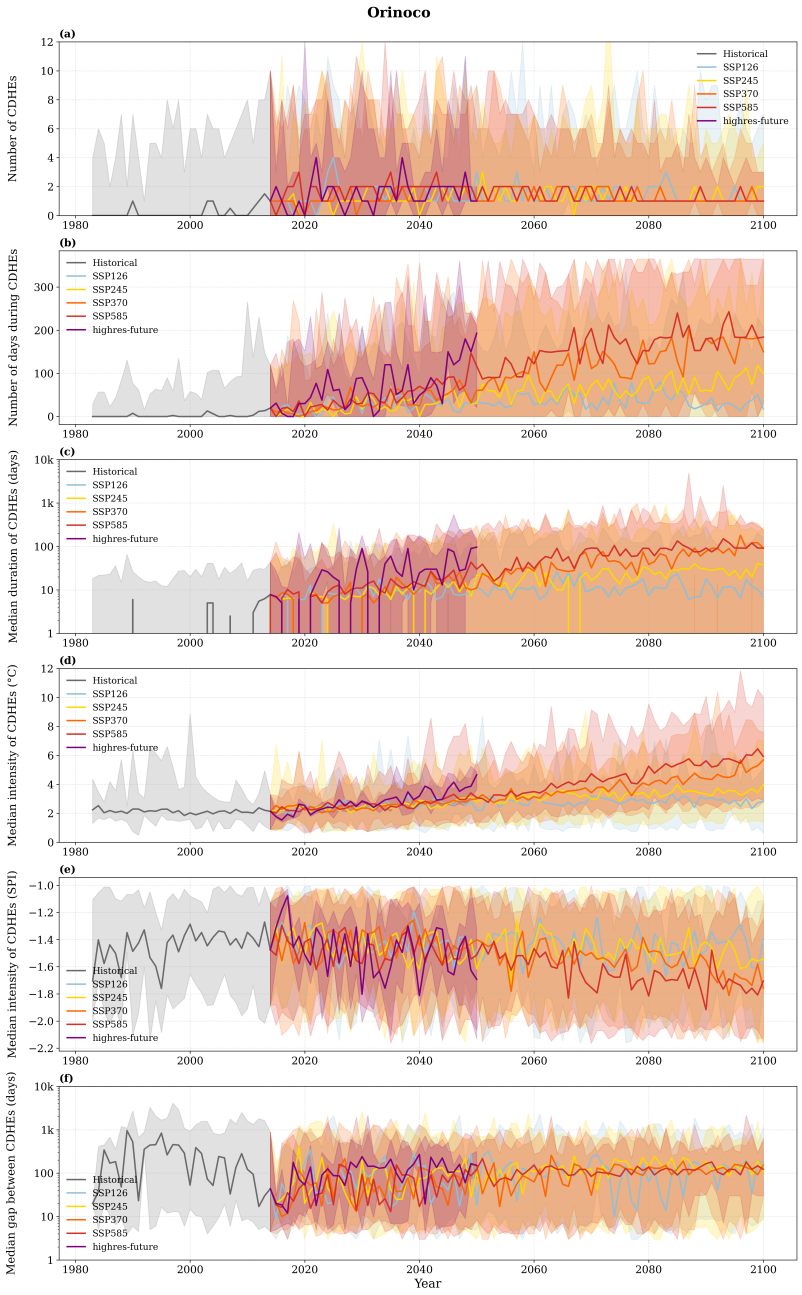

Figure 5.36: Time series of compound dry and hot events (CDHEs) characteristics for the Orinoco region based on the ensemble median. The 1983–2014 series corresponds to the multimodel median of the historical simulations (gray line). For the 2015–2100 period (2015–2050 for the HighresFuture scenario), the multimodel medians for each of the scenarios considered are shown: SSP1-2.6 (blue line), SSP2-4.5 (yellow line), SSP3-7.0 (orange line), SSP5-8.5 (red line), and HighresFuture (purple line). The shaded areas indicate the spread associated with the historical simulation or each scenario, calculated from the minimum and maximum values of the multimodel ensemble.

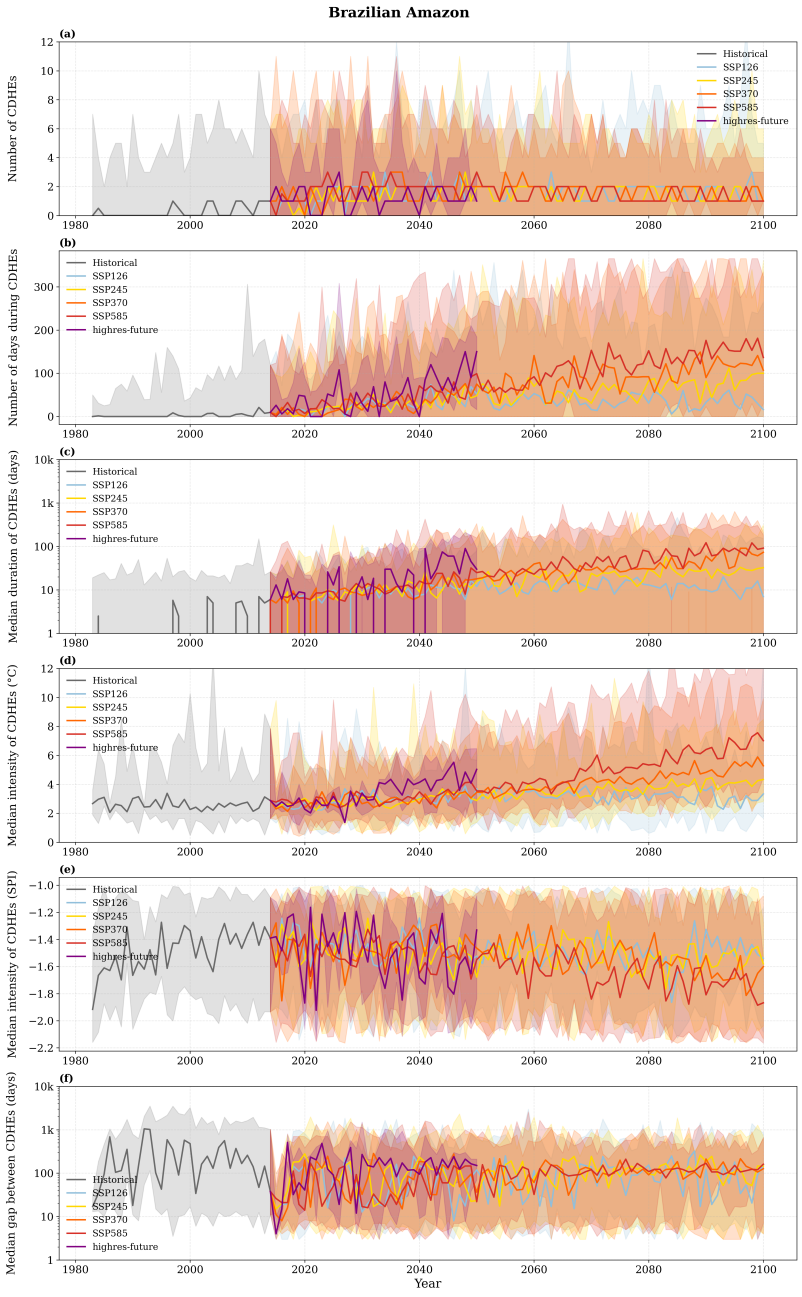

Figure 5.37: Time series of compound dry and hot events (CDHEs) characteristics for the Brazilian Amazon region based on the ensemble median. The 1983–2014 series corresponds to the multimodel median of the historical simulations (gray line). For the 2015–2100 period (2015–2050 for the HighresFuture scenario), the multimodel medians for each of the scenarios considered are shown: SSP1-2.6 (blue line), SSP2-4.5 (yellow line), SSP3-7.0 (orange line), SSP5-8.5 (red line), and HighresFuture (purple line). The shaded areas indicate the spread associated with the historical simulation or each scenario, calculated from the minimum and maximum values of the multimodel ensemble.

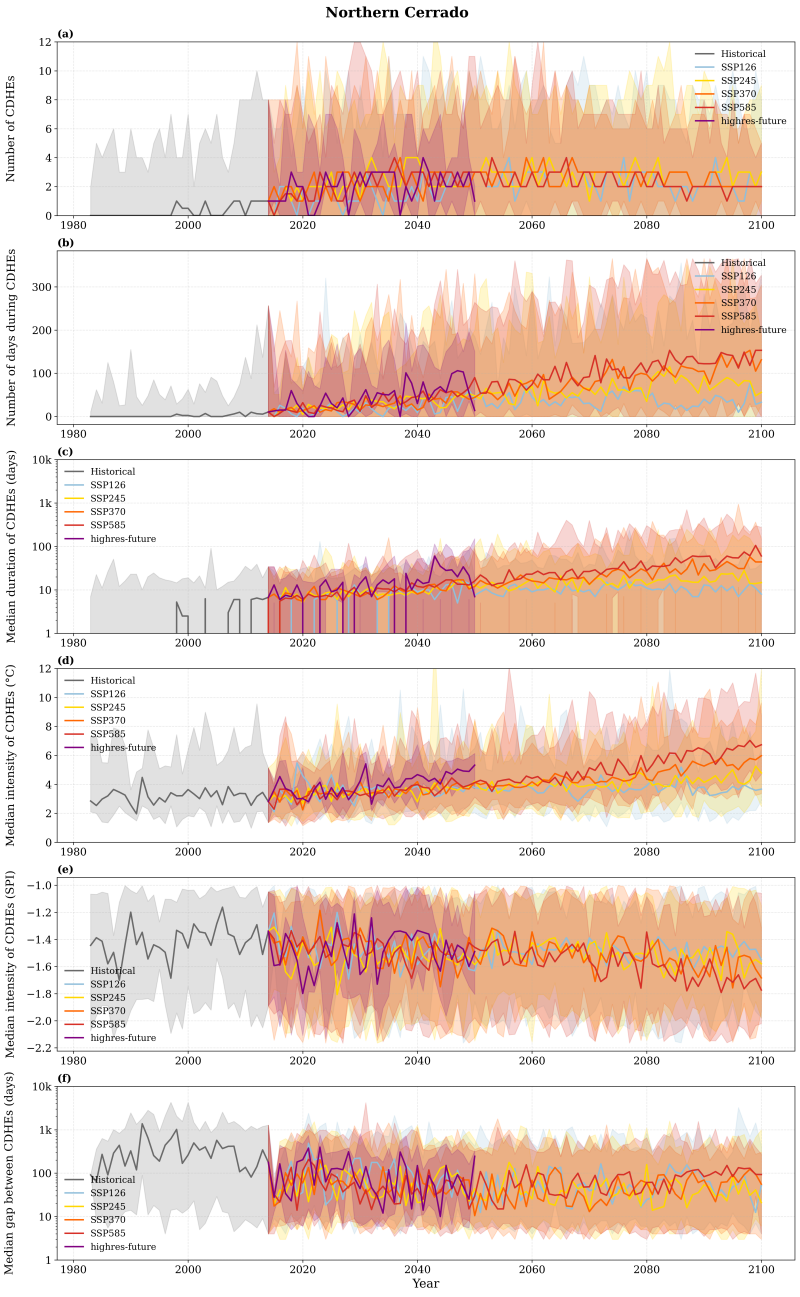

Figure 5.38: Time series of compound dry and hot events (CDHEs) characteristics for the northern Cerrado region based on the ensemble median. The 1983–2014 series corresponds to the multimodel median of the historical simulations (gray line). For the 2015–2100 period (2015–2050 for the HighresFuture scenario), the multimodel medians for each of the scenarios considered are shown: SSP1-2.6 (blue line), SSP2-4.5 (yellow line), SSP3-7.0 (orange line), SSP5-8.5 (red line), and HighresFuture (purple line). The shaded areas indicate the spread associated with the historical simulation or each scenario, calculated from the minimum and maximum values of the multimodel ensemble.

5.4 Summary and discussion

This chapter focused on the potential future changes in the characteristics of HEs, DEs, and CDHEs in the TSA. To this end, projections from a set of CMIP6 and HighResMIP models under different emission scenarios were used. These projections were estimated for the near-term (2021–2040) and the long-term (2081–2100). To provide a general view of the main characteristics, four CMIP6 emission scenarios (SSP1-2.6, SSP2-4.5, SSP3-7.0, SSP5-8.5) from 22 models were used, as well as the HighresFuture scenario from 5 HighResMIP models.

An increase in the frequency, duration, and intensity of HEs over TSA is projected for the 21st century. In the near-term, the increase in the number of HEs is more pronounced under the HighresFuture scenario, while in the long-term, SSP2-4.5 shows the largest increase in HEs frequency. SSP3-7.0 and SSP5-8.5 exhibit the greatest increases in duration and intensity of HEs, particularly in the southern and western regions of the TSA. The CMIP6 models showed strong agreement on the sign of change for HEs frequency in both time horizons, although agreement for median duration and intensity is observed only in some regions. A decrease in the number of HEs is projected in northern TSA during DJF and in regions of Brazil and western TSA during JJA and SON by the end of the century under high-emission scenarios, compared to the 1991–2010 period. This decrease is associated with increases in median duration of HEs over these areas.

The projected increase in the frequency, duration, and intensity of HEs is consistent with previous studies for South America (e.g., Collazo et al., 2023; De Luca & Donat, 2023; Feron et al., 2019; Ramarao et al., 2024. The increase in HEs aligns with projections suggesting a rise in annual mean temperature in South America toward the end of the 21st century, particularly under the highest-emission scenario (Bustos Usta et al., 2022). The contrast between emission scenarios is notable. Adopting low-emission pathways could reduce heatwave exposure in South America by up to 50 % (Ramarao et al., 2024), underscoring the importance of mitigation policies.

In contrast to HEs, DEs exhibited heterogeneous spatial patterns and showed no agreement among CMIP6 models regarding the sign of change for all analyzed characteristics across much of the TSA, reflecting high uncertainty in the projections. This pattern is consistent with the findings of De Luca & Donat (2023), who reported that global-scale drought projections under SSP5-8.5 show signals of both drier and wetter conditions depending on the region. However, they identified a significant increase in drought occurrence based on the SPI for Central and South America, consistent with the increases projected in this study. The largest increases in the number of DEs are projected in eastern Brazil and southern TSA during JJA and SON, with greater changes in the long-term under SSP2-4.5, SSP3-7.0, and SSP5-8.5.

Median duration and severity of DEs increase toward the end of the century, with greater magnitude and spatial extent of severity under SSP3-7.0 and SSP5-8.5 during JJA and SON, where greater agreement among CMIP6 models was observed regarding the sign of change over TSA. These results are consistent with the findings of De Luca & Donat (2023), the global trend of increasing drought frequency, duration, and spatial extent during the 21st century reported by Wang et al. (2021a), and regional projections of increases in mean and maximum DEs duration in South America described by Wainwright et al. (2022).

For CDHEs, our results project an increase in the occurrence, duration, and intensity of these events over TSA, with greater increases in the long-term and under higher-emission scenarios, con-

sistent with the findings of Seneviratne et al. (2021), Wu et al. (2021b), Zhang et al. (2022a), Meng et al. (2022), De Luca & Donat (2023), Yin et al. (2023), and Li et al. (2025). In the long-term, the largest frequencies are projected mainly in southern TSA during JJA and SON under the SSP2-4.5 and SSP3-7.0 scenarios. Under SSP5-8.5, the spatial extent of higher frequencies is smaller, associated with greater event duration. The CMIP6 models showed strong agreement on the sign of change.

The increases in CDHEs are dominated by the increase in HEs, as they occur despite reductions in DEs frequency in some regions, particularly during DJF and MAM. This pattern is consistent with the global-scale findings of Ridder et al. (2022), who reported that increases in CDHEs are driven primarily by increasing heatwaves frequency, even in regions where drought frequency is decreasing. The projected increase in the frequency of CDHEs in the TSA is consistent with the reported by Tabari & Willems (2023), who attribute this increase to the increased probability of individual hot and dry events, as well as to stronger coupling between temperature and soil moisture due to the amplification of land-atmosphere feedbacks and changes in common forcings such as large-scale atmospheric circulation patterns. These conditions are met in regions such as South America (Tabari & Willems, 2023).

For the near-term, the HighresFuture scenario projects the largest changes in all characteristics of the analyzed events compared to the SSPs, even with respect to SSP5-8.5, which has similar radiative forcing. These projected changes showed strong agreement on the sign of change among the five models considered. This is consistent with Müller et al. (2025), who evaluated the intensification of extreme events in the Bajos Submeridionales Basin, Argentina, finding that projected changes indicate consistent regional warming whose magnitude increases with the severity of the forcing scenario, with high-resolution projections yielding the strongest warming signal. The differences between CMIP6 and HighResMIP are partly attributable to the experimental design of each framework. HighResMIP enables the isolation of resolution effects through shorter simulations; however, it presents notable limitations, including a reduced simulation period (1950–2050), a smaller number of ensemble members owing to the computational cost of higher-resolution configurations, and a limited spin-up period in coupled models, which does not necessarily guarantee the absence of model drift (Roberts et al., 2020).

The methodology used to calculate DEs from the SPI has a considerable influence on the projected changes. When comparing DEs obtained by fitting the projected precipitation to the historical distribution (e.g., Ridder et al., 2022) with those derived from fitting using parameters estimated from the projection period itself (e.g., Collazo et al., 2023; Wang et al., 2021b), substantial differences were found in the sign of the change and the spatial distribution of the DEs, which are subsequently reflected in the CDHEs patterns. The first methodology produces more pronounced changes in both periods, highlighting the sensitivity of the projections to the parameter-estimation period.

DEs projections also show sensitivity to the choice of index used (De Luca & Donat, 2023; Hosseinzadehtalaei et al., 2024; Zeng et al., 2022). Droughts can be quantified exclusively from precipitation, as was done in this work and in previous research (e.g., Collazo et al., 2023; Ridder et al., 2022), or through the combination of precipitation and evapotranspiration, incorporating in the latter case the effect of temperature increase (for instance using the Standardized Precipitation and Evapotranspiration Index, SPEI) (Vicente-Serrano et al., 2010). The methodological choice considerably influences the projected changes in DEs, substantially altering the magnitude

and even the signal of the projected changes in CDHEs (Hosseinzadehtalaei et al., 2024), as observed in this study. It has been documented that defining CDHEs based on precipitation results in projected changes of smaller magnitude compared to definitions based on soil moisture (Tabari & Willems, 2023) and evapotranspiration (Wang et al., 2021a). These methodological differences have substantial implications for adaptation and mitigation strategies, as different definitions may require differentiated investments in infrastructure and land-use planning to prepare for such events (Hosseinzadehtalaei et al., 2024).

In this chapter, we also analyzed the temporal evolution of different characteristics of HEs, DEs, and CDHEs for the four regions that showed the greatest changes in the observational analysis (subsection 3.3.4). The northern Andes, Orinoco, Brazilian Amazon, and northern Cerrado regions project an increase in the frequency, duration, and intensity of HEs, with these increases being greater by the end of the century. However, under the SSP3-7.0 and SSP5-8.5 scenarios, a statistically significant reduction in the number of events is observed across all regions, although this reduction is less pronounced in northern Cerrado compared to the other regions. This negative trend is associated with an increase in the median duration of these events. These findings are consistent with those reported by (Collazo et al., 2023), who found that heat waves in TSA will have longer duration toward the end of the century under SSP5-8.5.

Unlike HEs, DEs do not show a trend toward an increase in the number of events per year according to the scenarios considered. However, under the higher emission scenarios (SSP3-7.0 and SSP5-8.5), an increase in the number of months associated with these events is expected, which is related to an increase in the median duration across all analyzed regions. Long-term projections indicate more severe drought conditions under the SSP5-8.5 scenario, with statistically significant trends in all four regions. It should be noted that the absence of an increasing trend in annual events does not imply that there is not a greater number of events compared to the historical period, as observed in Figures 5.13 and 5.14 for particular seasons.

Regional studies support these projections of increasing drought conditions. For the Amazon region, Duffy et al. (2015) project increases in the frequency and spatial extent of meteorological droughts in eastern Amazonia, while Rodrigues et al. (2020) anticipate an increase in the frequency, duration, and intensity of meteorological and hydrological droughts in the Cerrado, with the latter expected to be of greater magnitude. Regarding the Orinoco basin, Correa et al. (2024) suggest a trend toward drier conditions throughout the 21st century, attributed to the weakening and reduction of the Orinoco low-level jet. Additionally, Arregocés et al. (2025a) project precipitation decreases of 10 % to 17 % under SSP1-2.6 and 13 % to 20 % under SSP5-8.5 during the dry months for northern Colombia and Venezuela, particularly in the coastal lowlands. These areas are likely to face severe drought conditions by the middle and end of the 21st century (Arregocés et al., 2025a).

CDHEs do not show an increasing trend in the number of events per year in the regions considered. However, Figures 5.25 and 5.26 indicate an increase in their frequency during the TSA compared to the historical period, more pronounced toward the end of the century. The trend analysis shows an increase in the number of hot and dry days, as well as in the median duration and temperature intensity, along with greater severity of dry conditions projected toward the end of the century, particularly under the higher emissions scenario in the four regions. An increase in these characteristics for these regions is consistent with the findings of Parsons (2020), Ridder et al. (2022), Collazo et al. (2023), and Alves et al. (2024). The Orinoco shows the largest significant trends in number of days, duration, and severity of drought in all scenarios, while the Brazilian

Amazon projects the largest temperature intensity trends in all scenarios.

Chapter 6

General conclusions and future research

South America is a region highly vulnerable to extreme hydrometeorological events, due to the limited socioeconomic development of many of its countries and the low adaptive capacity of human systems (Castellanos et al., 2022; Cavazos et al., 2024). In particular, hot extremes and droughts have gained increasing interest in the scientific community because of their negative impacts on natural and socioeconomic systems, which tend to be more severe when both extremes occur simultaneously (AghaKouchak et al., 2020; Seneviratne et al., 2021; Zhao et al., 2023). However, for South America, most research has focused on these events individually, underestimating the effects that arise when they occur in combination. This research addresses this gap by characterizing the occurrence of hot events (HEs), dry events (DEs), and compound dry and hot events (CDHEs) based on the analysis of observations, as well as historical simulations and projections from a set of CMIP6/HighResMIP models for Tropical South America (TSA) that includes the Northwestern South America (NWS), Northern South America (NSA), and South American Monsoon (SAM) climate regions, as defined in the Sixth Assessment Report (AR6) of the Intergovernmental Panel on Climate Change (IPCC) (Iturbide et al., 2020).

For the observational period, we identified a seasonal pattern in the occurrence of HEs, with higher frequency in northern South America from December to May, and in the Amazon during June–July–August. Meteorological droughts were more frequent, whereas agricultural and ecological droughts exhibited longer durations. CDHEs occurred less frequently than HEs but had greater duration, and their frequency increased across much of TSA in recent decades, when comparing 2003–2024 with 1981–2002. The mechanisms driving the increase in CDHEs range from climate variability modes, such as El Niño-Southern Oscillation (ENSO) (Collazo et al., 2023; Feng & Hao, 2021), to large-scale atmospheric circulation patterns (Seneviratne et al., 2012), as well as effects associated with climate change (Chiang et al., 2022; Li et al., 2025; Pan et al., 2023; Seneviratne et al., 2021). We also found that temperature is generally the dominant factor during CDHEs across most of the TSA. However, this contribution may vary depending on the season and dataset used.

General Circulation Models (GCMs) constitute the primary and most comprehensive tool for simulating climate processes and projecting future climate conditions. Although previous studies have focused on evaluating models included in the sixth phase of the Coupled Model Intercomparison Project (CMIP6) and the High Resolution Model Intercomparison Project (HighResMIP) in

representing temperature and precipitation extreme indices over South America (e.g., Avila-Diaz et al., 2023; Collazo et al., 2022; Cook et al., 2020; Jha et al., 2023; Kim et al., 2020; Lagos-Zuniga et al., 2024; Ridder et al., 2021), fewer studies have addressed the analysis of compound extremes (e.g., Collazo et al., 2023; Wu et al., 2021b). The results showed that both individual models and the ensemble median inadequately reproduced the characteristics of extreme events observed in the reference datasets, particularly the number, duration, and inter-event gaps. While the ensemble median outperformed most individual models in capturing maximum temperature intensity associated with HEs and CDHEs, it underperformed in other metrics. Key limitations identified were the overestimation of event number and duration, along with the underestimation of the gap between events, for both HEs and CDHEs throughout most of the TSA, with high agreement between models (> 80 %) observed in particular regions. Additionally, models exhibited a more spatially homogeneous distribution of DEs characteristics compared to CHIRPS, overestimating them in some areas while underestimating them in others. This study did not delve into the underlying causes of these model biases, which remains an essential topic for future research.

For the projections, all scenarios indicate an increase in the frequency, duration, and intensity of HEs and CDHEs, particularly in the long term and under higher-emission pathways. The projected increases in CDHEs are primarily driven by increases in HEs, even though the frequency of DEs decreases in some areas, especially during December–January–February and March–April–May. For the characteristics of HEs and CDHEs, models show high agreement on the sign of projected change over much of the TSA, mainly in the long term and under high-emission scenarios. In contrast, DEs exhibit a heterogeneous spatial pattern in the type of change, with very few regions showing high agreement between models. These results reflect the high uncertainty in projected drought changes over much of the TSA, consistent with what is reported in the IPCC AR6 (Arias et al., 2021a).

The northern Andes, Orinoco, Brazilian Amazon, and northern Cerrado regions showed substantial changes in the occurrence of individual and CDHEs during the observational period. For this reason, we focused on analyzing the temporal evolution of the characteristics of these events using historical simulations from CMIP6/HighResMIP models, as well as under different climate change scenarios. Our results indicate that all regions will experience an increase in the number of hot and dry days, longer duration and intensity of temperature, and more severe droughts by the end of the century, especially under the high emissions scenario. The Orinoco region exhibits the greatest significant trends in temperature intensities, drought severity, and number of days/months, both for individual and compound events for the projected period 2015-2100, followed by the Brazilian Amazon region.

Regarding drought identification, the Standardized Precipitation Index (SPI) was used, which is widely used to determine and quantify drought severity because it requires only precipitation data (e.g., Cerpa Reyes et al., 2022; de Brito et al., 2021; Oñate-Valdivieso et al., 2020; Penalba & Rivera, 2016; Teodoro et al., 2015). However, this simplicity constitutes one of its main limitations, since the SPI does not incorporate other variables influencing droughts, such as evapotranspiration and temperature (Vicente-Serrano et al., 2010). Consequently, the SPI overlooks critical land surface and soil conditions that play an important role in drought development (Hosseinzadehtalaei et al., 2024). Additionally, the SPI does not allow the assessment of the role of temperature increase, nor the consideration of the influence of its variability or the occurrence of HEs, factors that could intensify drought conditions under future scenarios (Vicente-Serrano et al., 2010). As an alternative, the Standardized Precipitation Evapotranspiration Index (SPEI), proposed by Vicente-

Serrano et al. (2010), integrates precipitation and temperature information, which makes it possible to capture more precisely the combined effects of both variables. Therefore, future analyses using the SPEI could complement and expand the results obtained in this work, particularly to reduce uncertainties in projecting drought changes and their characteristics. As observed in this study, drought patterns differ substantially depending on the reference period selected for distribution fitting and the drought index employed, as suggested by several studies (e.g., De Luca & Donat, 2023; Hosseinzadehtalaei et al., 2024; Zeng et al., 2022).

The combination of different temperature extremes and drought types during the observational period was explored. Although some similar patterns were identified among different characteristics, notable variations in event duration and intensity were observed in some cases. However, the evaluation of models and climate projections was limited to events defined by the 90th percentile (P90) of maximum temperature and the three-month accumulated SPI index (SPI3), which primarily characterize meteorological droughts. As future work, it is essential to extend this analysis to more severe temperature extremes (P95 and P99) and evaluate their relationship with other drought types (e.g., agricultural-ecological, and hydrological). This analysis will allow us to determine whether droughts with longer temporal scales show more pronounced trends in their interaction with temperature, providing a more comprehensive understanding of climate change impacts across different sectors and temporal scales.

Finally, this work contributed to the understanding of hot-dry events and their combination in TSA through the analysis of four key characteristics. The results show that projected changes are more severe under higher emission scenarios, which is consistent with existing scientific literature that projects increases in heatwaves and droughts, extreme heat mortality, and negative impacts on natural systems under these scenarios. The evidence highlights the urgency of a transition toward low-carbon energy sources, particularly critical for South America, a region already highly vulnerable to extreme events whose intensification will continue according to projections. Limiting emissions can substantially reduce the intensity and frequency of these events, protecting natural and social systems. The choice of emission pathways transcends the technical realm; it constitutes a matter of climate justice with profound implications for present and future generations.

References

Afroz, M., Chen, G., & Anandhi, A. (2023). Drought-and heatwave-associated compound extremes: A review of hotspots, variables, parameters, drivers, impacts, and analysis frameworks. *Frontiers in Earth Science*, 10, 914437.

AghaKouchak, A., Chiang, F., Huning, L. S., Love, C. A., Mallakpour, I., Mazdiyasni, O., Moftakhari, H., Papalexiou, S. M., Ragno, E., & Sadegh, M. (2020). Climate extremes and compound hazards in a warming world. *Annual review of earth and planetary sciences*, 48(1), 519–548.

Alizadeh, M. R., Adamowski, J., Nikoo, M. R., AghaKouchak, A., Dennison, P., & Sadegh, M. (2020). A century of observations reveals increasing likelihood of continental-scale compound dry-hot extremes. *Science advances*, 6(39), eaaz4571.

Almazroui, M., Ashfaq, M., Islam, M. N., Rashid, I. U., Kamil, S., Abid, M. A., O'Brien, E., Ismail, M., Reboita, M. S., Sörensson, A. A., et al. (2021). Assessment of cmip6 performance and projected temperature and precipitation changes over south america. *Earth Systems and Environment*, 5(2), 155–183.

Alves, L. M., Firpo, M. Â. F., Bettolli, M. L., Hasson, S. u., Guerron, O. V. C., Añazco, A. A., & Llopart, M. P. (2024). Projected changes in the frequency of compound hot and dry events over tropical brazil in cordex-core simulations. *Climate Dynamics*, 62(11), 10203–10216.

Arias, P., Bellouin, N., Coppola, E., Jones, R., Krinner, G., Marotzke, J., Naik, V., Palmer, M., Plattner, G.-K., Rogelj, J., et al. (2021a). Climate change 2021: the physical science basis. contribution of working group i to the sixth assessment report of the intergovernmental panel on climate change; technical summary. *Cambridge University Press, Cambridge, United Kingdom and New York, NY, USA*, (pp. 3–32).

Arias, P. A., Correa, I. C., Fita, L., Martínez, J. A., Alvarez-Garreton, C., Alves, L. M., Boisier, J. P., Campozano, L., Espinoza, J.-C., Junquas, C., et al. (2025a). How well cmip6 models simulate key boundary conditions affecting south american climate? insights for regional modeling efforts. *Climate Dynamics*, 63(5), 231.

Arias, P. A., Fernández-Berrío, A., Bedoya-Pineda, V., Acevedo-Ortiz, M. Y., & Martínez, J. A. (2025b). Compound dry and hot extremes and their implications for fire activity over the orinoco river basin in northern south america. *Climate Dynamics*, 63(4), 175.

Arias, P. A., Ortega, G., Villegas, L. D., & Martínez, J. A. (2021b). Colombian climatology in cmip5/cmip6 models: Persistent biases and improvements. *Revista Facultad de Ingeniería Universidad de Antioquia*, (100), 75–96.

Arias, P. A., Rivera, J. A., Sörensson, A. A., Zachariah, M., Barnes, C., Philip, S., Kew, S., Vautard, R., Koren, G., Pinto, I., et al. (2024). Interplay between climate change and climate variability: the 2022 drought in central south america. *Climatic Change*, 177(1), 6.

Arregocés, H. A., Estrada, E., & Moscote, C. D. (2025a). Drought projections in the northernmost region of south america under different climate change scenarios. *Earth*, 6(4), 122.

Arregocés, H. A., Gómez, D., & Castellanos, M. L. (2024). Annual and monthly precipitation

trends: An indicator of climate change in the caribbean region of colombia. *Case Studies in Chemical and Environmental Engineering*, 10, 100834.

Arregocés, H. A., Rojano, R., & Castellanos, M. L. (2025b). Trends and variability of drought in northern south america between 1982 and 2022. *Earth Systems and Environment*, (pp. 1–16).

Avila-Diaz, A., Benezoli, V., Justino, F., Torres, R., & Wilson, A. (2020). Assessing current and future trends of climate extremes across brazil based on reanalyses and earth system model projections. *Climate Dynamics*, 55(5), 1403–1426.

Avila-Diaz, A., Torres, R. R., Zuluaga, C. F., Cerón, W. L., Oliveira, L., Benezoli, V., Rivera, I. A., Marengo, J. A., Wilson, A. B., & Medeiros, F. (2023). Current and future climate extremes over latin america and caribbean: assessing earth system models from high resolution model intercomparison project (highresmip). *Earth Systems and Environment*, 7(1), 99–130.

Baez-Villanueva, O. M., Zambrano-Bigiarini, M., Ribbe, L., Nauditt, A., Giraldo-Osorio, J. D., & Thinh, N. X. (2018). Temporal and spatial evaluation of satellite rainfall estimates over different regions in latin-america. *Atmospheric Research*, 213, 34–50.

Bazzanela, A. C., Dereczynski, C., Luiz-Silva, W., & Regoto, P. (2024). Performance of cmip6 models over south america. *Climate Dynamics*, 62(2), 1501–1516.

Bi, D., Dix, M., Marsland, S., O'farrell, S., Sullivan, A., Bodman, R., Law, R., Harman, I., Srbinovsky, J., Rashid, H. A., et al. (2020). Configuration and spin-up of access-cm2, the new generation australian community climate and earth system simulator coupled model. *Journal of Southern Hemisphere Earth Systems Science*, 70(1), 225–251.

Boucher, O., Servonnat, J., Albright, A. L., Aumont, O., Balkanski, Y., Bastrikov, V., Bekki, S., Bonnet, R., Bony, S., Bopp, L., et al. (2020). Presentation and evaluation of the ipsl-cm6a-lr climate model. *Journal of Advances in Modeling Earth Systems*, 12(7), e2019MS002010.

Boulton, C. A., Lenton, T. M., & Boers, N. (2022). Pronounced loss of amazon rainforest resilience since the early 2000s. *Nature Climate Change*, 12(3), 271–278.

Brogno, L., Barbano, F., Leo, L., & Di Sabatino, S. (2025). Review on heatwaves: a risk perspective. *Environmental Research Letters*, 20(6), 063004.

Bustos Usta, D. F., Teymouri, M., & Chatterjee, U. (2022). Projections of temperature changes over south america during the twenty-first century using cmip6 models. *GeoJournal*, 87(Suppl 4), 739–763.

Cao, J., Wang, B., Yang, Y.-M., Ma, L., Li, J., Sun, B., Bao, Y., He, J., Zhou, X., & Wu, L. (2018). The nuist earth system model (nesm) version 3: description and preliminary evaluation. *Geoscientific Model Development*, 11(7), 2975–2993.

Castellanos, E. J., Lemos, M. F., Astigarraga, L., Chacón, N., Cuvi, N., Huggel, C., Miranda, L., Moncassim Vale, M., Pierre Ometto, J., Peri, P. L., et al. (2022). Central and south america.

Cavalcante, R. B. L., da Silva Ferreira, D. B., Pontes, P. R. M., Tedeschi, R. G., da Costa, C. P. W., & de Souza, E. B. (2020). Evaluation of extreme rainfall indices from chirps precipitation estimates over the brazilian amazonia. *Atmospheric Research*, 238, 104879.

Cavazos, T., Bettolli, M. L., Campbell, D., Sánchez Rodríguez, R. A., Mycoo, M., Arias, P. A., Rivera, J., Reboita, M. S., Gulizia, C., Hidalgo, H. G., et al. (2024). Challenges for climate change adaptation in latin america and the caribbean region. *Frontiers in Climate*, 6, 1392033.

Cerón, W. L., Kayano, M. T., Andreoli, R. V., Avila-Diaz, A., Ayes, I., Freitas, E. D., Martins, J. A., & Souza, R. A. (2021). Recent intensification of extreme precipitation events in the la plata basin in southern south america (1981–2018). *Atmospheric Research*, 249, 105299.

Cerpa Reyes, L. J., Ávila Rangel, H., & Herazo, L. C. S. (2022). Adjustment of the standardized precipitation index (spi) for the evaluation of drought in the arroyo pechelín basin, colombia, under zero monthly precipitation conditions. *Atmosphere*, 13(2), 236.

Chiang, F., Greve, P., Mazdiyasni, O., Wada, Y., & AghaKouchak, A. (2022). Intensified likelihood

of concurrent warm and dry months attributed to anthropogenic climate change. *Water Resources Research*, 58(6), e2021WR030411.

Christian, J. I., Martin, E. R., Basara, J. B., Furtado, J. C., Otkin, J. A., Lowman, L. E., Hunt, E. D., Mishra, V., & Xiao, X. (2023). Global projections of flash drought show increased risk in a warming climate. *Communications Earth & Environment*, 4(1), 165.

Climate Hazards Center (2025). CHIRPS3: Climate Hazards Center Infrared Precipitation with Stations version 3. Data Repository.

Collazo, S., Barrucand, M., & Rusticucci, M. (2022). Evaluation of cmip6 models in the representation of observed extreme temperature indices trends in south america. *Climatic Change*, 172(1), 21.

Collazo, S., Barrucand, M., & Rusticucci, M. (2023). Hot and dry compound events in south america: present climate and future projections, and their association with the pacific ocean. *Natural Hazards*, 119(1), 299–323.

Collazo, S., Suli, S., Zaninelli, P. G., García-Herrera, R., Barriopedro, D., & Garrido-Perez, J. M. (2024). Influence of large-scale circulation and local feedbacks on extreme summer heat in argentina in 2022/23. *Communications Earth & Environment*, 5(1), 231.

Cook, B. I., Mankin, J. S., Marvel, K., Williams, A. P., Smerdon, J. E., & Anchukaitis, K. J. (2020). Twenty-first century drought projections in the cmip6 forcing scenarios. *Earth's Future*, 8(6), e2019EF001461.

Correa, I. C., Arias, P. A., Vieira, S. C., & Martínez, J. A. (2024). A drier orinoco basin during the twenty-first century: the role of the orinoco low-level jet. *Climate Dynamics*, 62(3), 2369–2398.

Costa, D. F., Gomes, H. B., Silva, M. C. L., & Zhou, L. (2022). The most extreme heat waves in amazonia happened under extreme dryness. *Climate Dynamics*, 59(1), 281–295.

Costa, M. C., Marengo, J. A., Alves, L. M., & Cunha, A. P. (2024). Multiscale analysis of drought, heatwaves, and compound events in the brazilian pantanal in 2019–2021. *Theoretical and Applied Climatology*, 155(1), 661–677.

Da Silva, P. E., Santos e Silva, C. M., Spyrides, M. H. C., & Andrade, L. d. M. B. (2019). Precipitation and air temperature extremes in the amazon and northeast brazil. *International Journal of Climatology*, 39(2), 579–595.

da Silva Arruda, V. L., Alencar, A. A. C., de Carvalho Júnior, O. A., de Figueiredo Ribeiro, F., de Arruda, F. V., Conciani, D. E., da Silva, W. V., & Shimbo, J. Z. (2024). Assessing four decades of fire behavior dynamics in the cerrado biome (1985 to 2022). *Fire Ecology*, 20(1), 64.

de Araújo, G. R. G., Frassoni, A., Sapucci, L. F., Bitencourt, D., & de Brito Neto, F. A. (2022). Climatology of heatwaves in south america identified through era5 reanalysis data. *International Journal of Climatology*, 42(16), 9430–9448.

de Brito, C. S., da Silva, R. M., Santos, C. A. G., Neto, R. M. B., & Coelho, V. H. R. (2021). Monitoring meteorological drought in a semiarid region using two long-term satellite-estimated rainfall datasets: A case study of the piranhas river basin, northeastern brazil. *Atmospheric Research*, 250, 105380.

De Luca, P. & Donat, M. G. (2023). Projected changes in hot, dry, and compound hot-dry extremes over global land regions. *Geophysical Research Letters*, 50(13), e2022GL102493.

DESA, U. (2019). United nations, department of economic and social affairs, population division. 2018. world urbanization prospects: The 2018 revision. *Online Edition*.

Dias, C. G. & Reboita, M. S. (2021). Assessment of cmip6 simulations over tropical south america. *Revista Brasileira de Geografia Física*, 14(3), 1282–1295.

Döscher, R., Acosta, M., Alessandri, A., Anthoni, P., Arsouze, T., Bergman, T., Bernardello, R.,

Boussetta, S., Caron, L.-P., Carver, G., Castrillo, M., Catalano, F., Cvijanovic, I., Davini, P., Dekker, E., Doblas-Reyes, F. J., Docquier, D., Echevarria, P., Fladrich, U., Fuentes-Franco, R., Gröger, M., v. Hardenberg, J., Hieronymus, J., Karami, M. P., Keskinen, J.-P., Koenigk, T., Makkonen, R., Massonnet, F., Ménégoz, M., Miller, P. A., Moreno-Chamarro, E., Nieradzik, L., van Noije, T., Nolan, P., O'Donnell, D., Ollinaho, P., van den Oord, G., Ortega, P., Prims, O. T., Ramos, A., Reerink, T., Rousset, C., Ruprich-Robert, Y., Le Sager, P., Schmith, T., Schrödner, R., Serva, F., Sicardi, V., Sloth Madsen, M., Smith, B., Tian, T., Tourigny, E., Uotila, P., Vancoppenolle, M., Wang, S., Wårlind, D., Willén, U., Wyser, K., Yang, S., Yepes-Arbós, X., & Zhang, Q. (2022). The ec-earth3 earth system model for the coupled model intercomparison project 6. *Geoscientific Model Development*, 15(7), 2973–3020.

Duffy, P. B., Brando, P., Asner, G. P., & Field, C. B. (2015). Projections of future meteorological drought and wet periods in the amazon. *Proceedings of the National Academy of Sciences*, 112(43), 13172–13177.

Dunne, J. P., Horowitz, L., Adcroft, A., Ginoux, P., Held, I., John, J., Krasting, J. P., Malyshev, S., Naik, V., Paulot, F., et al. (2020). The gfdl earth system model version 4.1 (gfdl-esm 4.1): Overall coupled model description and simulation characteristics. *Journal of Advances in Modeling Earth Systems*, 12(11), e2019MS002015.

Espinoza, J.-C., Jimenez, J. C., Marengo, J. A., Schongart, J., Ronchail, J., Lavado-Casimiro, W., & Ribeiro, J. V. M. (2024). The new record of drought and warmth in the amazon in 2023 related to regional and global climatic features. *Scientific Reports*, 14(1), 8107.

Eyring, V., Bony, S., Meehl, G. A., Senior, C. A., Stevens, B., Stouffer, R. J., & Taylor, K. E. (2016). Overview of the coupled model intercomparison project phase 6 (cmip6) experimental design and organization. *Geoscientific Model Development*, 9(5), 1937–1958.

Feng, S. & Hao, Z. (2021). Quantitative contribution of enso to precipitation-temperature dependence and associated compound dry and hot events. *Atmospheric Research*, 260, 105695.

Feng, S., Hao, Z., Wu, X., Zhang, X., & Hao, F. (2021). A multi-index evaluation of changes in compound dry and hot events of global maize areas. *Journal of Hydrology*, 602, 126728.

Feron, S., Cordero, R., Damiani, A., Llanillo, P., Jorquera, J., Sepulveda, E., Asencio, V., Laroze, D., Labbe, F., Carrasco, J., et al. (2019). Observations and projections of heat waves in south america. *Scientific reports*, 9(1), 8173.

Feron, S., Cordero, R. R., Damiani, A., MacDonell, S., Pizarro, J., Goubanova, K., Valenzuela, R., Wang, C., Rester, L., & Beaulieu, A. (2024). South america is becoming warmer, drier, and more flammable. *Communications Earth & Environment*, 5(1), 501.

Ferreira, V., Buras, A., Zscheischler, J., Mahecha, M. D., & Rammig, A. (2025). Evaluating the 2023-2024 record dry-hot conditions in the amazon in the context of historical compound extremes. *Environmental Research Letters*.

Funk, C., Peterson, P., Landsfeld, M., Pedreros, D., Verdin, J., Shukla, S., Husak, G., Rowland, J., Harrison, L., Hoell, A., et al. (2015). The climate hazards infrared precipitation with stations—a new environmental record for monitoring extremes. *Scientific data*, 2(1), 1–21.

Garcia, B. N., Libonati, R., & Nunes, A. M. (2018). Extreme drought events over the amazon basin: The perspective from the reconstruction of south american hydroclimate. *Water*, 10(11), 1594.

Gasparrini, A., Guo, Y., Sera, F., Vicedo-Cabrera, A. M., Huber, V., Tong, S., Coelho, M. d. S. Z. S., Saldiva, P. H. N., Lavigne, E., Correa, P. M., et al. (2017). Projections of temperature-related excess mortality under climate change scenarios. *The Lancet Planetary Health*, 1(9), e360–e367.

Geirinhas, J., Russo, A., Libonati, R., Miralles, D., Ramos, A., Gimeno, L., & Trigo, R. (2023). Combined large-scale tropical and subtropical forcing on the severe 2019–2022 drought in

south america. *npj Climate and Atmospheric Science*, 6(1), 185.

Geirinhas, J. L., Russo, A., Libonati, R., Sousa, P. M., Miralles, D. G., & Trigo, R. M. (2021). Recent increasing frequency of compound summer drought and heatwaves in southeast brazil. *Environmental Research Letters*, 16(3), 034036.

Ghanbari, M., Arabi, M., Georgescu, M., & Broadbent, A. M. (2023). The role of climate change and urban development on compound dry-hot extremes across us cities. *Nature communications*, 14(1), 3509.

Gutjahr, O., Putrasahan, D., Lohmann, K., Jungclaus, J. H., von Storch, J.-S., Brüggemann, N., Haak, H., & Stössel, A. (2019). Max planck institute earth system model (mpi-esm1. 2) for the high-resolution model intercomparison project (highresmip). *Geoscientific Model Development*, 12(7), 3241–3281.

Haarsma, R. J., Roberts, M. J., Vidale, P. L., Senior, C. A., Bellucci, A., Bao, Q., Chang, P., Corti, S., Fučkar, N. S., Guemas, V., et al. (2016). High resolution model intercomparison project (highresmip v1. 0) for cmip6. *Geoscientific Model Development*, 9(11), 4185–4208.

Hao, Z., Hao, F., Singh, V. P., & Zhang, X. (2018a). Changes in the severity of compound drought and hot extremes over global land areas. *Environmental Research Letters*, 13(12), 124022.

Hao, Z., Hao, F., Singh, V. P., & Zhang, X. (2018b). Quantifying the relationship between compound dry and hot events and el niño–southern oscillation (enso) at the global scale. *Journal of Hydrology*, 567, 332–338.

Hao, Z., Hao, F., Xia, Y., Feng, S., Sun, C., Zhang, X., Fu, Y., Hao, Y., Zhang, Y., & Meng, Y. (2022). Compound droughts and hot extremes: Characteristics, drivers, changes, and impacts. *Earth-Science Reviews*, 235, 104241.

Hayes, M., Svoboda, M., Wall, N., & Widhalm, M. (2011). The lincoln declaration on drought indices: universal meteorological drought index recommended. *Bulletin of the American Meteorological Society*, 92(4), 485–488.

Hersbach, H., Bell, B., Berrisford, P., Biavati, G., Horányi, A., Muñoz Sabater, J., Nicolas, J., Peubey, C., Radu, R., Rozum, I., et al. (2023). Era5 hourly data on single levels from 1940 to present. *Copernicus climate change service (c3s) climate data store (cds)*, 10.

Hirota, N. & Takayabu, Y. N. (2013). Reproducibility of precipitation distribution over the tropical oceans in cmip5 multi-climate models compared to cmip3. *Climate Dynamics*, 41(11), 2909–2920.

Hirsch, A. L., Ridder, N. N., Perkins-Kirkpatrick, S. E., & Ukkola, A. (2021). Cmip6 multi-model evaluation of present-day heatwave attributes. *Geophysical Research Letters*, 48(22), e2021GL095161.

Hosseinzadehtalaei, P., Termonia, P., & Tabari, H. (2024). Projected changes in compound hot-dry events depend on the dry indicator considered. *Communications Earth & Environment*, 5(1), 220.

Iturbide, M., Gutiérrez, J. M., Alves, L. M., Bedia, J., Cerezo-Mota, R., Cimadevilla, E., Cofiño, A. S., Di Luca, A., Faria, S. H., Gorodetskaya, I. V., et al. (2020). An update of ipcc climate reference regions for subcontinental analysis of climate model data: definition and aggregated datasets. *Earth System Science Data*, 12(4), 2959–2970.

Jahn, S., Gaythorpe, K. A., Wainwright, C. M., & Ferguson, N. M. (2025). Evaluation of the performance and utility of global gridded precipitation products for health applications and impact assessments in south america. *GeoHealth*, 9(6), e2024GH001260.

Jha, S., Gudmundsson, L., & Seneviratne, S. I. (2023). Partitioning the uncertainties in compound hot and dry precipitation, soil moisture, and runoff extremes projections in cmip6. *Earth's Future*, 11(3), e2022EF003315.

Jones, N. (2022). Rare 'triple'la niña climate event looks likely. *Nature*, 607(21), 10–1038.

Kendall, M. G. (1948). Rank correlation methods.

Kephart, J. L., Sánchez, B. N., Moore, J., Schinasi, L. H., Bakhtsiyarava, M., Ju, Y., Gouveia, N., Caiaffa, W. T., Dronova, I., Arunachalam, S., et al. (2022). City-level impact of extreme temperatures and mortality in latin america. *Nature medicine*, 28(8), 1700–1705.

Kim, W., Park, E., Jo, H.-W., Roh, M., Kim, J., Song, C., & Lee, W.-K. (2022). A meta-analytic review on the spatial and climatic distribution of meteorological drought indices. *Environmental Reviews*, 31(1), 95–110.

Kim, Y.-H., Min, S.-K., Zhang, X., Sillmann, J., & Sandstad, M. (2020). Evaluation of the cmip6 multi-model ensemble for climate extreme indices. *Weather and Climate Extremes*, 29, 100269.

Lagos-Zuniga, M., Balmaceda-Huarte, R., Regoto, P., Torrez, L., Olmo, M., Lyra, A., Pareja-Quispe, D., & Bettolli, M. L. (2024). Extreme indices of temperature and precipitation in south america: Trends and intercomparison of regional climate models. *Climate Dynamics*, 62(6), 4541–4562.

Lee, J., Kim, J., Sun, M.-A., Kim, B.-H., Moon, H., Sung, H. M., Kim, J., & Byun, Y.-H. (2020a). Evaluation of the korea meteorological administration advanced community earth-system model (k-ace). *Asia-Pacific Journal of Atmospheric Sciences*, 56(3), 381–395.

Lee, W.-L., Wang, Y.-C., Shiu, C.-J., Tsai, I.-c., Tu, C.-Y., Lan, Y.-Y., Chen, J.-P., Pan, H.-L., & Hsu, H.-H. (2020b). Taiwan earth system model version 1: description and evaluation of mean state. *Geoscientific Model Development*, 13(9), 3887–3904.

Leite-Filho, A. T., de Sousa Pontes, V. Y., & Costa, M. H. (2019). Effects of deforestation on the onset of the rainy season and the duration of dry spells in southern amazonia. *Journal of Geophysical Research: Atmospheres*, 124(10), 5268–5281.

Leonard, M., Westra, S., Phatak, A., Lambert, M., van den Hurk, B., McInnes, K., Risbey, J., Schuster, S., Jakob, D., & Stafford-Smith, M. (2014). A compound event framework for understanding extreme impacts. *Wiley Interdisciplinary Reviews: Climate Change*, 5(1), 113–128.

Li, L., Yu, Y., Tang, Y., Lin, P., Xie, J., Song, M., Dong, L., Zhou, T., Liu, L., Wang, L., et al. (2020). The flexible global ocean-atmosphere-land system model grid-point version 3 (fgoals-g3): Description and evaluation. *Journal of Advances in Modeling Earth Systems*, 12(9), e2019MS002012.

Li, W., Liu, X., & Sun, Q. (2025). Detectable anthropogenic expand of compound dry and hot events areas on global land. *Atmospheric Research*, (pp. 108219).

Libonati, R., Geirinhas, J. L., Silva, P. S., Russo, A., Rodrigues, J. A., Belém, L. B., Nogueira, J., Roque, F. O., DaCamara, C. C., Nunes, A. M., et al. (2022). Assessing the role of compound drought and heatwave events on unprecedented 2020 wildfires in the pantanal. *Environmental Research Letters*, 17(1), 015005.

Lovato, T., Peano, D., Butenschön, M., Materia, S., Iovino, D., Scoccimarro, E., Fogli, P., Cherchi, A., Bellucci, A., Gualdi, S., et al. (2022). Cmip6 simulations with the cmcc earth system model (cmcc-esm2). *Journal of Advances in Modeling Earth Systems*, 14(3), e2021MS002814.

Lyu, W., He, X., Liu, B., Qin, M., Chen, A., & Guan, H. (2025). On the synchronization of compound drought and heatwave events over global land regions. *Journal of Hydrology*, 654, 132836.

Mann, H. B. (1945). Nonparametric tests against trend. *Econometrica: Journal of the econometric society*, (pp. 245–259).

Manning, C., Widmann, M., Bevacqua, E., Van Loon, A. F., Maraun, D., & Vrac, M. (2019). Increased probability of compound long-duration dry and hot events in europe during summer (1950–2013). *Environmental Research Letters*, 14(9), 094006.

Marengo, J. A., Costa, M. C., Cunha, A. P., Espinoza, J.-C., Jimenez, J. C., Libonati, R., Miranda,

V., Trigo, I. F., Sierra, J. P., Geirinhas, J. L., et al. (2025). Climatological patterns of heatwaves during winter and spring 2023 and trends for the period 1979–2023 in central south america. *Frontiers in Climate*, 7, 1529082.

Marengo, J. A., Cunha, A. P., Cuartas, L. A., Deusdará Leal, K. R., Broedel, E., Seluchi, M. E., Michelin, C. M., De Praga Baião, C. F., Chuchón Angulo, E., Almeida, E. K., et al. (2021). Extreme drought in the brazilian pantanal in 2019–2020: Characterization, causes, and impacts. *Frontiers in Water*, 3, 639204.

Marengo, J. A., Cunha, A. P., Espinoza, J.-C., Fu, R., Schöngart, J., Jimenez, J. C., Costa, M. C., Ribeiro, J. M., Wongchuig, S., & Zhao, S. (2024). The drought of amazonia in 2023-2024. *American Journal of Climate Change*, 13(03), 567–597.

Marengo, J. A. & Espinoza, J. C. (2016). Extreme seasonal droughts and floods in amazonia: causes, trends and impacts. *International Journal of Climatology*, 36(3), 1033–1050.

Mauritsen, T., Bader, J., Becker, T., Behrens, J., Bittner, M., Brokopf, R., Brovkin, V., Claussen, M., Crueger, T., Esch, M., et al. (2019). Developments in the mpi-m earth system model version 1.2 (mpi-esm1. 2) and its response to increasing co2. *Journal of Advances in Modeling Earth Systems*, 11(4), 998–1038.

Mazdiyasni, O. & AghaKouchak, A. (2015). Substantial increase in concurrent droughts and heatwaves in the united states. *Proceedings of the National Academy of Sciences*, 112(37), 11484–11489.

McKee, T. B., Doesken, N. J., Kleist, J., et al. (1993). The relationship of drought frequency and duration to time scales. In *Proceedings of the 8th Conference on Applied Climatology*, volume 17 (pp. 179–183).: California.

Meng, Y., Hao, Z., Feng, S., Zhang, X., & Hao, F. (2022). Increase in compound dry-warm and wet-warm events under global warming in cmip6 models. *Global and Planetary Change*, 210, 103773.

Merz, N. & Zachariah, M. (2025). Understanding droughts under climate change in south america based on severity-duration-frequency curves and drought atlases. *Climatic Change*, 178(9), 163.

Miralles, D. G., Gentine, P., Seneviratne, S. I., & Teuling, A. J. (2019). Land–atmospheric feedbacks during droughts and heatwaves: state of the science and current challenges. *Annals of the New York Academy of Sciences*, 1436(1), 19–35.

Monteiro Dos Santos, D., de Oliveira, A. M., Duarte, E. S., Rodrigues, J. A., Menezes, L. S., Albuquerque, R., Roque, F. d. O., Peres, L. F., Hoelzemann, J. J., & Libonati, R. (2024a). Compound dry-hot-fire events connecting central and southeastern south america: an unapparent and deadly ripple effect. *npj Natural Hazards*, 1(1), 32.

Monteiro Dos Santos, D., Libonati, R., Garcia, B. N., Geirinhas, J. L., Salvi, B. B., Lima E Silva, E., Rodrigues, J. A., Peres, L. F., Russo, A., Gracie, R., et al. (2024b). Twenty-first-century demographic and social inequalities of heat-related deaths in brazilian urban areas. *PLoS one*, 19(1), e0295766.

Montiel, J. I. P., Epiayu, A. M. C., & Moscote, C. D. (2026). Evaluation of satellite precipitation products across climatic and topographic gradients in a basin in northern south america. *Environmental Challenges*, (pp. 101426).

Mukherjee, S. & Mishra, A. K. (2021). Increase in compound drought and heatwaves in a warming world. *Geophysical Research Letters*, 48(1), e2020GL090617.

Mukherjee, S., Mishra, A. K., Ashfaq, M., & Kao, S.-C. (2022). Relative effect of anthropogenic warming and natural climate variability to changes in compound drought and heatwaves. *Journal of Hydrology*, 605, 127396.

Müller, G. V., Lovino, M. A., Pierrestegui, M. J., Richter, P., Longo, M., & Tariq, A. (2025).

Regional warming and intensifying extremes: Past and future climate in the bajos submeridionales basin, argentina. *Earth Systems and Environment*, (pp. 1–22).

Nagy, G. J., Filho, W. L., Azeiteiro, U. M., Heimfarth, J., Verocai, J. E., & Li, C. (2018). An assessment of the relationships between extreme weather events, vulnerability, and the impacts on human wellbeing in latin america. *International journal of environmental research and public health*, 15(9), 1802.

Negron-Juarez, R., Wehner, M., Dias, M. A. F. S., Ullrich, P., Chambers, J. Q., & Riley, W. J. (2024). Coupled model intercomparison project phase 6 (cmip6) high resolution model intercomparison project (highresmip) bias in extreme rainfall drives underestimation of amazonian precipitation. *Environmental Research Communications*, 6(9), 091001.

Omay, P. O., Muthama, N. J., Oludhe, C., Kinama, J. M., Artan, G., & Atheru, Z. (2024). Projected changes in wet and dry extremes in the cmip6 multi-model ensemble over the igad region of eastern africa. *Discover Atmosphere*, 2(1), 11.

OMM (2022). *Estado del Clima en América Latina y el Caribe 2021*. Technical Report OMM-Nº 1295, Organización Meteorológica Mundial.

Oñate-Valdivieso, F., Uchuari, V., & Oñate-Paladines, A. (2020). Large-scale climate variability patterns and drought: a case of study in south–america. *Water Resources Management*, 34(6), 2061–2079.

Ortega, G., Arias, P. A., Villegas, J. C., Marquet, P. A., & Nobre, P. (2021). Present-day and future climate over central and south america according to cmip5/cmip6 models. *International Journal of Climatology*, 41(15), 6713–6735.

O'Neill, B. C., Kriegler, E., Ebi, K. L., Kemp-Benedict, E., Riahi, K., Rothman, D. S., Van Ruijven, B. J., Van Vuuren, D. P., Birkmann, J., Kok, K., et al. (2017). The roads ahead: Narratives for shared socioeconomic pathways describing world futures in the 21st century. *Global environmental change*, 42, 169–180.

Pak, G., Noh, Y., Lee, M. I., et al. (2021). Korea institute of ocean science and technology earth system model and its simulation characteristics. *Ocean Science Journal*, 56, 18–45.

Pan, R., Li, W., Wang, Q., & Ailiyaer, A. (2023). Detectable anthropogenic intensification of the summer compound hot and dry events over global land areas. *Earth's Future*, 11(6), e2022EF003254.

Panisset, J. S., Libonati, R., & Gouveia, C. M. P. (2018). Contrasting patterns of the extreme drought episodes of 2005. *Int. J. Climatol*, 38, 1096–1104.

Papalexiou, S. M., Rajulapati, C. R., Andreadis, K. M., Foufoula-Georgiou, E., Clark, M. P., & Trenberth, K. E. (2021). Probabilistic evaluation of drought in cmip6 simulations. *Earth's future*, 9(10), e2021EF002150.

Paredes Trejo, F. J., Alves Barbosa, H., Peñaloza-Murillo, M. A., Moreno, M. A., & Farias, A. (2016). Intercomparison of improved satellite rainfall estimation with chirps gridded product and rain gauge data over venezuela. *Atmósfera*, 29(4), 323–342.

Paredes-Trejo, F. J., Barbosa, H., & Kumar, T. L. (2017). Validating chirps-based satellite precipitation estimates in northeast brazil. *Journal of arid environments*, 139, 26–40.

Parsons, L. A. (2020). Implications of cmip6 projected drying trends for 21st century amazonian drought risk. *Earth's Future*, 8(10), e2020EF001608.

Penalba, O. C. & Rivera, J. A. (2013). Future changes in drought characteristics over southern south america projected by a cmip5 multi-model ensemble.

Penalba, O. C. & Rivera, J. A. (2016). Precipitation response to el niño/la niña events in southern south america–emphasis in regional drought occurrences. *Advances in Geosciences*, 42, 1–14.

Perkins, S. E. (2015). A review on the scientific understanding of heatwaves—their measurement, driving mechanisms, and changes at the global scale. *Atmospheric Research*, 164, 242–267.

Ramarao, M., Arunachalam, S., Sánchez, B. N., Schinasi, L. H., Bakhtsiyarava, M., Caiaffa, W. T., Dronova, I., O'Neill, M. S., Avila-Palencia, I., Gouveia, N., et al. (2024). Projected changes in heatwaves over central and south america using high-resolution regional climate simulations. *Scientific reports*, 14(1), 23145.

Reboita, M. S., de Souza Ferreira, G. W., Ribeiro, J. G. M., & Ali, S. (2024). Assessment of precipitation and near-surface temperature simulation by cmip6 models in south america. *Environmental Research: Climate*, 3(2), 025011.

Ridder, N., Ukkola, A., Pitman, A., & Perkins-Kirkpatrick, S. (2022). Increased occurrence of high impact compound events under climate change. *Npj Climate and Atmospheric Science*, 5(1), 3.

Ridder, N. N., Pitman, A. J., & Ukkola, A. M. (2021). Do cmip6 climate models simulate global or regional compound events skillfully? *Geophysical Research Letters*, 48(2), e2020GL091152.

Rivera, J. A., Arias, P. A., Sörensson, A. A., Zachariah, M., Barnes, C., Philip, S., Kew, S., Vautard, R., Koren, G., Pinto, I., et al. (2023). 2022 early-summer heatwave in southern south america: 60 times more likely due to climate change. *Climatic Change*, 176(8), 102.

Rivera, J. A. & Arnould, G. (2020). Evaluation of the ability of cmip6 models to simulate precipitation over southwestern south america: Climatic features and long-term trends (1901–2014). *Atmospheric Research*, 241, 104953.

Roberts, M. J., Baker, A., Blockley, E. W., Calvert, D., Coward, A., Hewitt, H. T., Jackson, L. C., Kuhlbrodt, T., Mathiot, P., Roberts, C. D., et al. (2019). Description of the resolution hierarchy of the global coupled hadgem3-gc3. 1 model as used in cmip6 highresmip experiments. *Geoscientific Model Development*, 12(12), 4999–5028.

Roberts, M. J., Camp, J., Seddon, J., Vidale, P. L., Hodges, K., Vannière, B., Mecking, J., Haarsma, R., Bellucci, A., Scoccimarro, E., et al. (2020). Projected future changes in tropical cyclones using the cmip6 highresmip multimodel ensemble. *Geophysical research letters*, 47(14), e2020GL088662.

Rodrigues, J. A., Viola, M. R., Alvarenga, L. A., de Mello, C. R., Chou, S. C., de Oliveira, V. A., Uddameri, V., & Morais, M. A. (2020). Climate change impacts under representative concentration pathway scenarios on streamflow and droughts of basins in the brazilian cerrado biome. *International Journal of Climatology*, 40(5), 2511–2526.

Ruiz-Vásquez, M., Arias, P. A., Martínez, J. A., & Espinoza, J. C. (2020). Effects of amazon basin deforestation on regional atmospheric circulation and water vapor transport towards tropical south america. *Climate Dynamics*, 54(9), 4169–4189.

Rusticucci, M. & Zazulie, N. (2021). Attribution and projections of temperature extreme trends in south america based on cmip5 models. *Annals of the New York Academy of Sciences*, 1504(1), 154–166.

Schlegel, R. W. & Smit, A. J. (2018). heatwaver: A central algorithm for the detection of heatwaves and cold-spells. *Journal of Open Source Software*, 3(27), 821.

Seland, Ø., Bentsen, M., Olivié, D., Toniazzo, T., Gjermundsen, A., Graff, L., Debernard, J., Gupta, A., He, Y., Kirkevåg, A., et al. (2020). Overview of the norwegian earth system model (noresm2) and key climate response of cmip6 deck, historical, and scenario simulations, geosci. model dev., 13, 6165–6200.

Sen, P. K. (1968). Estimates of the regression coefficient based on kendall's tau. *Journal of the American statistical association*, 63(324), 1379–1389.

Seneviratne, S., Nicholls, N., Easterling, D., Goodess, C., Kanae, S., Kossin, J., Luo, Y., Marengo, J., McInnes, K., Rahimi, M., et al. (2012). Changes in climate extremes and their impacts on the natural physical environment.

Seneviratne, S. I., Zhang, X., Adnan, M., Badi, W., Dereczynski, C., Di Luca, A., Ghosh, S.,

Iskandar, I., Kossin, J., Lewis, S., Otto, F., Pinto, I., Satoh, M., Vicente-Serrano, S. M., Wehner, M., & Zhou, B. (2021). Weather and climate extreme events in a changing climate. In V. Masson-Delmotte, P. Zhai, A. Pirani, S. L. Connors, C. Péan, S. Berger, N. Caud, Y. Chen, L. Goldfarb, M. I. Gomis, M. Huang, K. Leitzell, E. Lonnoy, J. B. R. Matthews, T. K. Maycock, T. Waterfield, O. Yelekçi, R. Yu, & B. Zhou (Eds.), *Climate Change 2021: The Physical Science Basis. Contribution of Working Group I to the Sixth Assessment Report of the Intergovernmental Panel on Climate Change* (pp. 1513–1766). Cambridge, United Kingdom and New York, NY, USA: Cambridge University Press.

Sharma, S. & Mujumdar, P. (2017). Increasing frequency and spatial extent of concurrent meteorological droughts and heatwaves in india. *Scientific reports*, 7(1), 15582.

Shi, Z., Jia, G., Zhou, Y., Xu, X., & Jiang, Y. (2021). Amplified intensity and duration of heatwaves by concurrent droughts in china. *Atmospheric Research*, 261, 105743.

Sierra, J. P., Arias, P. A., & Vieira, S. C. (2015). Precipitation over northern south america and its seasonal variability as simulated by the cmip5 models. *Advances in Meteorology*, 2015(1), 634720.

Silva, P. S., Libonati, R., Schmidt, I. B., Nogueira, J., & DaCamara, C. C. (2024). Climate change and fire: the case of cerrado, the brazilian savanna. *Climate Change and Regional Socio-Economic Systems in the Global South: Resilience Strategies for Sustainable Development*, (pp. 87–105).

Silverman, E. & Engström, J. (2025). Drought vulnerability in south america. *Water*, 17(15), 2332.

Stagge, J. H., Tallaksen, L. M., Gudmundsson, L., Van Loon, A. F., & Stahl, K. (2015). Candidate distributions for climatological drought indices (spi and spei). *International Journal of Climatology*, 35(13), 4027–4040.

Sun, Q., Miao, C., Duan, Q., Ashouri, H., Sorooshian, S., & Hsu, K.-L. (2018). A review of global precipitation data sets: Data sources, estimation, and intercomparisons. *Reviews of geophysics*, 56(1), 79–107.

Swart, N. C., Cole, J. N., Kharin, V. V., Lazare, M., Scinocca, J. F., Gillett, N. P., Anstey, J., Arora, V., Christian, J. R., Hanna, S., et al. (2019). The canadian earth system model version 5 (canesm5. 0.3). *Geoscientific Model Development*, 12(11), 4823–4873.

Tabari, H. & Willems, P. (2023). Global risk assessment of compound hot-dry events in the context of future climate change and socioeconomic factors. *Npj Climate and Atmospheric Science*, 6(1), 74.

Tatebe, H., Ogura, T., Nitta, T., Komuro, Y., Ogochi, K., Takemura, T., Sudo, K., Sekiguchi, M., Abe, M., Saito, F., et al. (2019). Description and basic evaluation of simulated mean state, internal variability, and climate sensitivity in miroc6. *Geoscientific Model Development*, 12(7), 2727–2765.

Taylor, K. E. (2001). Summarizing multiple aspects of model performance in a single diagram. *Journal of geophysical research: atmospheres*, 106(D7), 7183–7192.

Teodoro, P. E., Correa, C. C. G., Torres, F. E., Oliveira Junior, J. d., Silva Junior, C. d., Gois, G., & Delgado, R. C. (2015). Analysis of the occurrence of wet and drought periods using standardized precipitation index in mato grosso do sul state, brazil.

Tomasella, J., Cunha, A. P. M., Simões, P. A., & Zeri, M. (2023). Assessment of trends, variability and impacts of droughts across brazil over the period 1980–2019. *Natural Hazards*, 116(2), 2173–2190.

Valencia, S., Marin, D. E., Gomez, D., Hoyos, N., Salazar, J. F., & Villegas, J. C. (2023). Spatio-temporal assessment of gridded precipitation products across topographic and climatic gradients in colombia. *Atmospheric Research*, 285, 106643.

Van Loon, A. F. (2015). Hydrological drought explained. *Wiley Interdisciplinary Reviews: Water*,

2(4), 359–392.

Verdin, A., Funk, C., Peterson, P., Landsfeld, M., Tuholske, C., & Grace, K. (2020). Development and validation of the chirts-daily quasi-global high-resolution daily temperature data set. *Scientific Data*, 7(1), 303.

Vicente-Serrano, S. M., Beguería, S., & López-Moreno, J. I. (2010). A multiscalar drought index sensitive to global warming: the standardized precipitation evapotranspiration index. *Journal of climate*, 23(7), 1696–1718.

Vicente-Serrano, S. M. & López-Moreno, J. I. (2005). Hydrological response to different time scales of climatological drought: an evaluation of the standardized precipitation index in a mountainous mediterranean basin. *Hydrology and earth system sciences*, 9(5), 523–533.

Vieira, R. M. d. S. P., Tomasella, J., Cunha, A. P. M. d. A., Barbosa, A. A., Pompeu, J., Ferreira, Y., Santos, F. C., Alves, L. M., & Ometto, J. (2023). Socio-environmental vulnerability to drought conditions and land degradation: an assessment in two northeastern brazilian river basins. *Sustainability*, 15(10), 8029.

Volodin, E. M., Mortikov, E. V., Kostrykin, S. V., Galin, V. Y., Lykossov, V. N., Gritsun, A. S., Diansky, N. A., Gusev, A. V., & Iakovlev, N. G. (2018). Simulation of the modern climate using the inm-cm48 climate model. *Russian Journal of Numerical Analysis and Mathematical Modelling*, 33(6), 367–374.

Wainwright, C. M., Allan, R. P., & Black, E. (2022). Consistent trends in dry spell length in recent observations and future projections. *Geophysical Research Letters*, 49(12), e2021GL097231.

Wang, T., Tu, X., Singh, V. P., Chen, X., & Lin, K. (2021a). Global data assessment and analysis of drought characteristics based on cmip6. *Journal of Hydrology*, 596, 126091.

Wang, W., Wang, J., & Romanowicz, R. (2021b). Uncertainty in spi calculation and its impact on drought assessment in different climate regions over china. *Journal of Hydrometeorology*, 22(6), 1369–1383.

Wilhite, D. A. & Glantz, M. H. (1985). Understanding: the drought phenomenon: the role of definitions. *Water international*, 10(3), 111–120.

WMO (2024). *State of the Global Climate 2023*. Technical Report WMO-No. 1347, World Meteorological Organization.

WMO (2025). *State of Global Water Resources 2024*. Technical Report WMO-No. 1380, World Meteorological Organization.

Wu, H., Su, X., & Singh, V. P. (2021a). Blended dry and hot events index for monitoring dry-hot events over global land areas. *Geophysical Research Letters*, 48(24), e2021GL096181.

Wu, Y., Miao, C., Sun, Y., AghaKouchak, A., Shen, C., & Fan, X. (2021b). Global observations and cmip6 simulations of compound extremes of monthly temperature and precipitation. *GeoHealth*, 5(5), e2021GH000390.

Xu, F. & Luo, M. (2019). Changes of concurrent drought and heat extremes in the arid and semi-arid regions of china during 1961–2014. *Atmospheric Science Letters*, 20(12), e947.

Yang, J., Zhou, L., Wu, J., Wang, Z., Zhou, H., & Ma, Z. (2024). Effects of anthropogenic climate change on the compound drought and heat events in different agricultural regions of china. *Ecological Indicators*, 167, 112719.

Yang, T., Chen, B., Wang, S., Xu, X., Artaxo, P., Li, T., Peng, H., & Yu, X. (2025). Soil moisture dominates the severe decline in gross primary productivity during a 2023–2024 compound heatwave-drought event over the amazon. *Environmental Research Letters*, 20(3), 034024.

Yin, J., Gentine, P., Slater, L., Gu, L., Pokhrel, Y., Hanasaki, N., Guo, S., Xiong, L., & Schlenker, W. (2023). Future socio-ecosystem productivity threatened by compound drought–heatwave events. *Nature Sustainability*, 6(3), 259–272.

Yu, R. & Zhai, P. (2020). More frequent and widespread persistent compound drought and heat

event observed in china. *Scientific Reports*, 10(1), 14576.

Yukimoto, S., Kawai, H., Koshiro, T., Oshima, N., Yoshida, K., Urakawa, S., Tsujino, H., Deushi, M., Tanaka, T., Hosaka, M., et al. (2019). The meteorological research institute earth system model version 2.0, mri-esm2. 0: Description and basic evaluation of the physical component. *Journal of the Meteorological Society of Japan. Ser. II*, 97(5), 931–965.

Zargar, A., Sadiq, R., Naser, B., & Khan, F. I. (2011). A review of drought indices. *Environmental Reviews*, 19(NA), 333–349.

Zeng, J., Li, J., Lu, X., Wei, Z., Shangguan, W., Zhang, S., Dai, Y., & Zhang, S. (2022). Assessment of global meteorological, hydrological and agricultural drought under future warming based on cmip6. *Atmospheric and Oceanic Science Letters*, 15(1), 100143.

Zeng, Z., Wu, W., Peñuelas, J., Li, Y., Jiao, W., Li, Z., Ren, X., Wang, K., & Ge, Q. (2023). Increased risk of flash droughts with raised concurrent hot and dry extremes under global warming. *npj Climate and Atmospheric Science*, 6(1), 134.

Zhang, G., Wang, H., Gan, T. Y., Zhang, S., Shi, L., Zhao, J., Su, X., & Song, S. (2022a). Climate change determines future population exposure to summertime compound dry and hot events. *Earth's Future*, 10(11), e2022EF003015.

Zhang, Q., Yu, X., Qiu, R., Liu, Z., & Yang, Z. (2022b). Evolution, severity, and spatial extent of compound drought and heat events in north china based on copula model. *Agricultural Water Management*, 273, 107918.

Zhang, Y., Hao, Z., Feng, S., Zhang, X., & Hao, F. (2023). Changed relationship between compound dry-hot events and enso at the global scale. *Journal of Hydrology*, 621, 129559.

Zhao, C., Feng, Y., Wang, T., Liu, W., Wang, H., Liu, Y., & Sun, F. (2023). Projected changes in socioeconomic exposure to compound hot–dry/hot–wet days in china under cmip6 forcing scenarios. *Theoretical & Applied Climatology*, 154.

Ziehn, T., Chamberlain, M. A., Law, R. M., Lenton, A., Bodman, R. W., Dix, M., Stevens, L., Wang, Y.-P., & Srbinovsky, J. (2020). The australian earth system model: Access-esm1. 5. *Journal of Southern Hemisphere Earth Systems Science*, 70(1), 193–214.

Zscheischler, J., Westra, S., Van Den Hurk, B. J., Seneviratne, S. I., Ward, P. J., Pitman, A., AghaKouchak, A., Bresch, D. N., Leonard, M., Wahl, T., et al. (2018). Future climate risk from compound events. *Nature climate change*, 8(6), 469–477.

Supplementary material

Appendix A

Occurrence of hot, dry, and compound dry and hot events in Tropical South America: Observational Analysis (1981–2024)

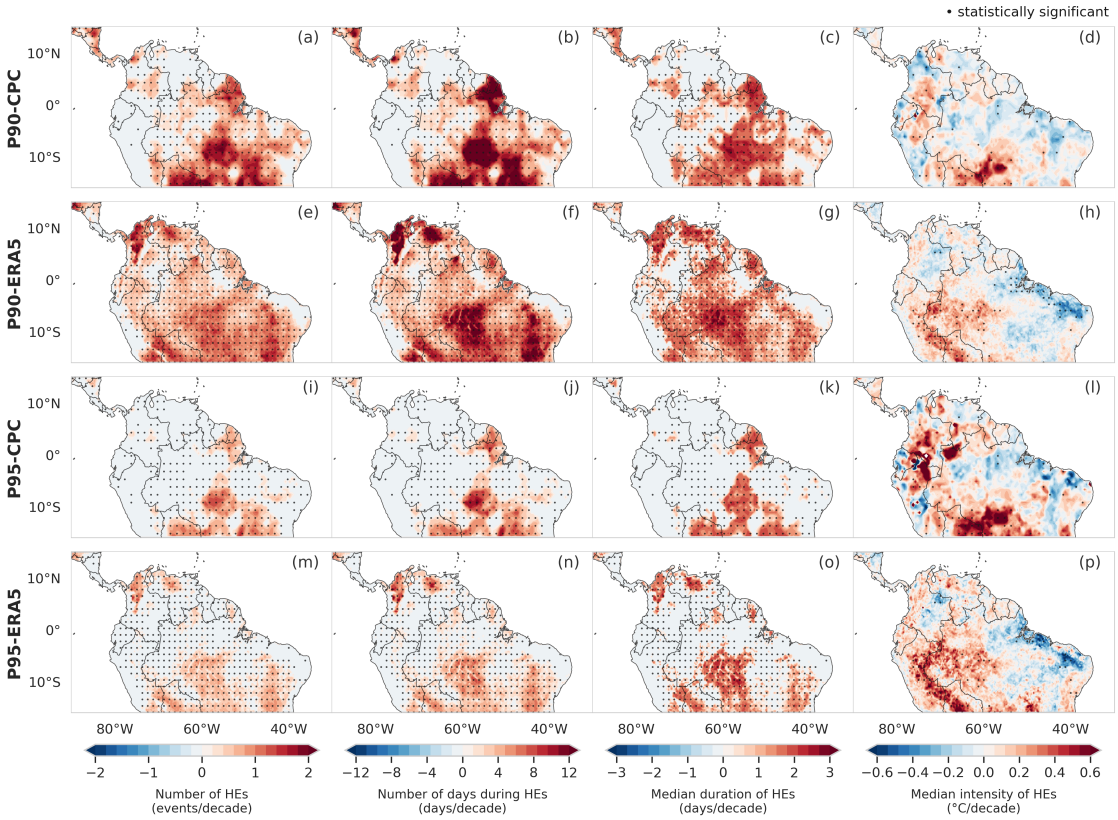

Figure A.1: Trends in the characteristics of Hot Events (HEs) over tropical South America during 1981–2024, based on CPC and ERA5 datasets using the 90th (P90) and 95th (P95) percentile thresholds. Statistically significant trends ($p < 0.05$) are marked with black dots.

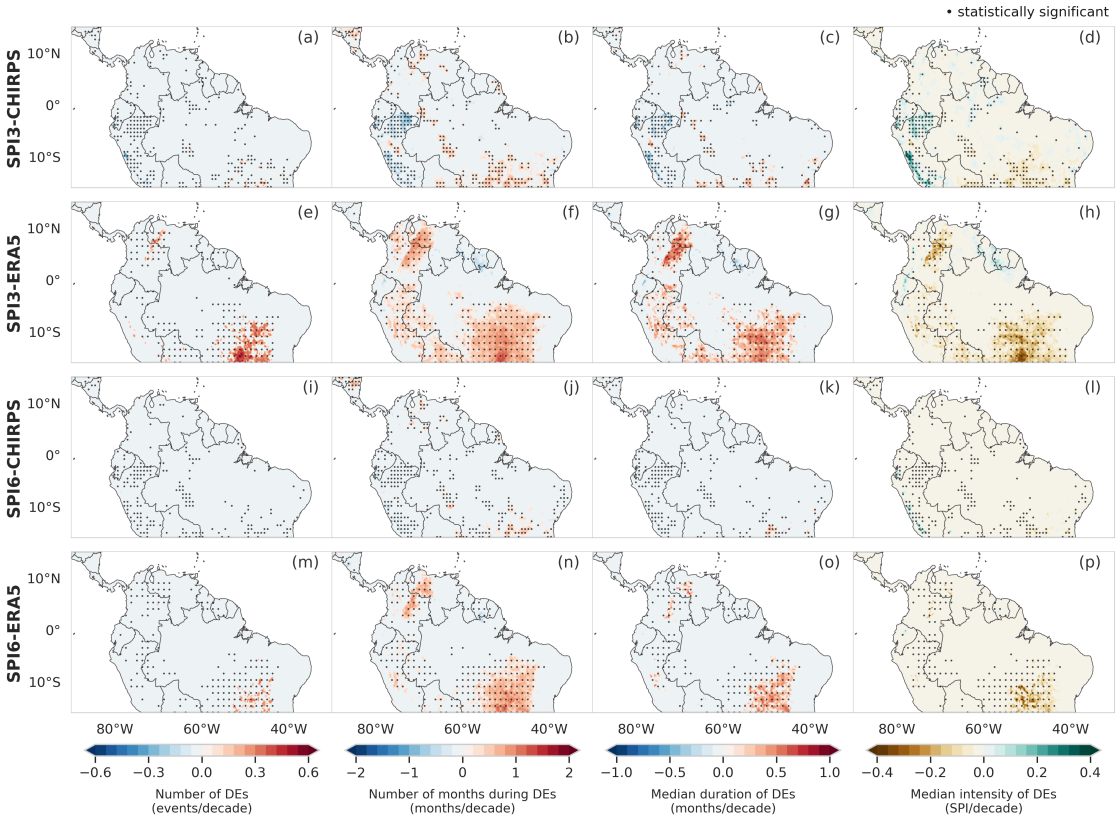

Figure A.2: Trends in the characteristics of Dry Events (DEs) over tropical South America during 1981–2024, based on CHIRPS and ERA5 datasets using the SPI3 and SPI6. Statistically significant trends ($p < 0.05$) are marked with black dots.

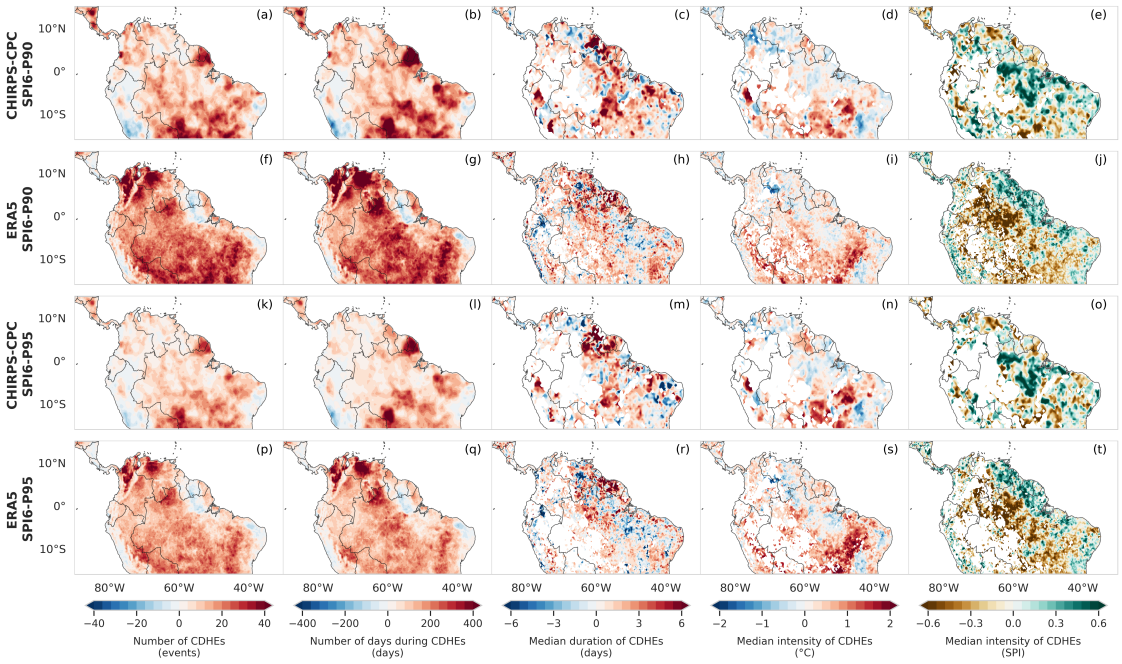

Figure A.3: Changes in the characteristics of Compound Dry and Hot Events (CDHEs) (SPI6-P90 and SPI6-P95) between 1981–2002 and 2003–2024 over tropical South America, based on CPC/CHIRPS and ERA5 datasets.

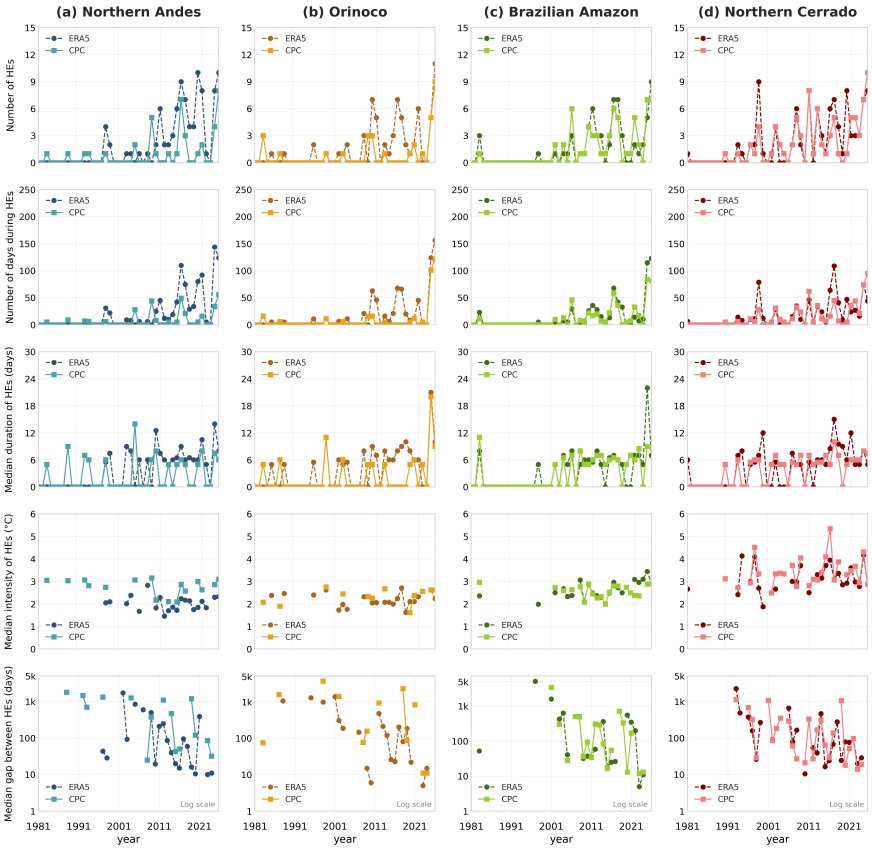

Figure A.4: Temporal Evolution of Hot Events (HEs) based on CPC and ERA5 datasets in a) northern Andes, b) Orinoco, c) Brazilian Amazon, and d) northern Cerrado during 1981–2024. The panel shows the HEs identified using the 95th (P95) percentile threshold.

Figure A.5: Temporal Evolution of Dry Events (DEs) based on CHIRPS v2 and ERA5 datasets in a) northern Andes, b) Orinoco, c) Brazilian Amazon, and d) northern Cerrado during 1981–2024. The panel shows the DEs identified using SPI6.

Figure A.6: Temporal Evolution of Compound Dry and Hot Events (CDHEs) based on CHIRPSv2/CPC and ERA5 datasets in a) northern Andes, b) Orinoco, c) Brazilian Amazon, and d) northern Cerrado during 1981–2024. The panel shows the events identified using SPI3-P95.

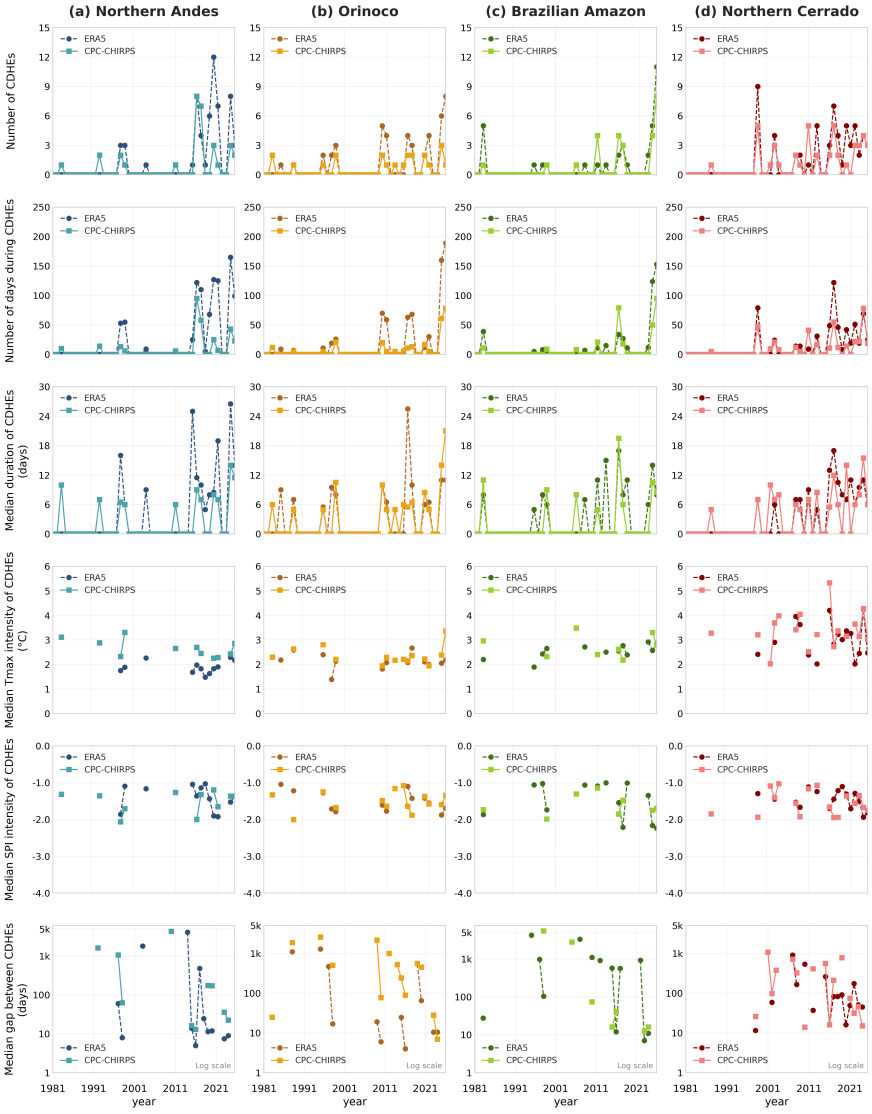

Figure A.7: Temporal Evolution of Compound Dry and Hot Events (CDHEs) based on CHIRPSv2/CPC and ERA5 datasets in a) northern Andes, b) Orinoco, c) Brazilian Amazon, and d) northern Cerrado during 1981–2024. The panel shows the events identified using SPI6-P90.

Figure A.8: Temporal Evolution of Compound Dry and Hot Events (CDHEs) based on CHIRPSv2/CPC and ERA5 datasets in a) northern Andes, b) Orinoco, c) Brazilian Amazon, and d) northern Cerrado during 1981–2024. The panel shows the events identified using SPI6-P95.

Appendix B

Assessing the performance of CMIP6/HighResMIP models in simulating hot, dry, and compound dry and hot events in Tropical South America (1983–2014)

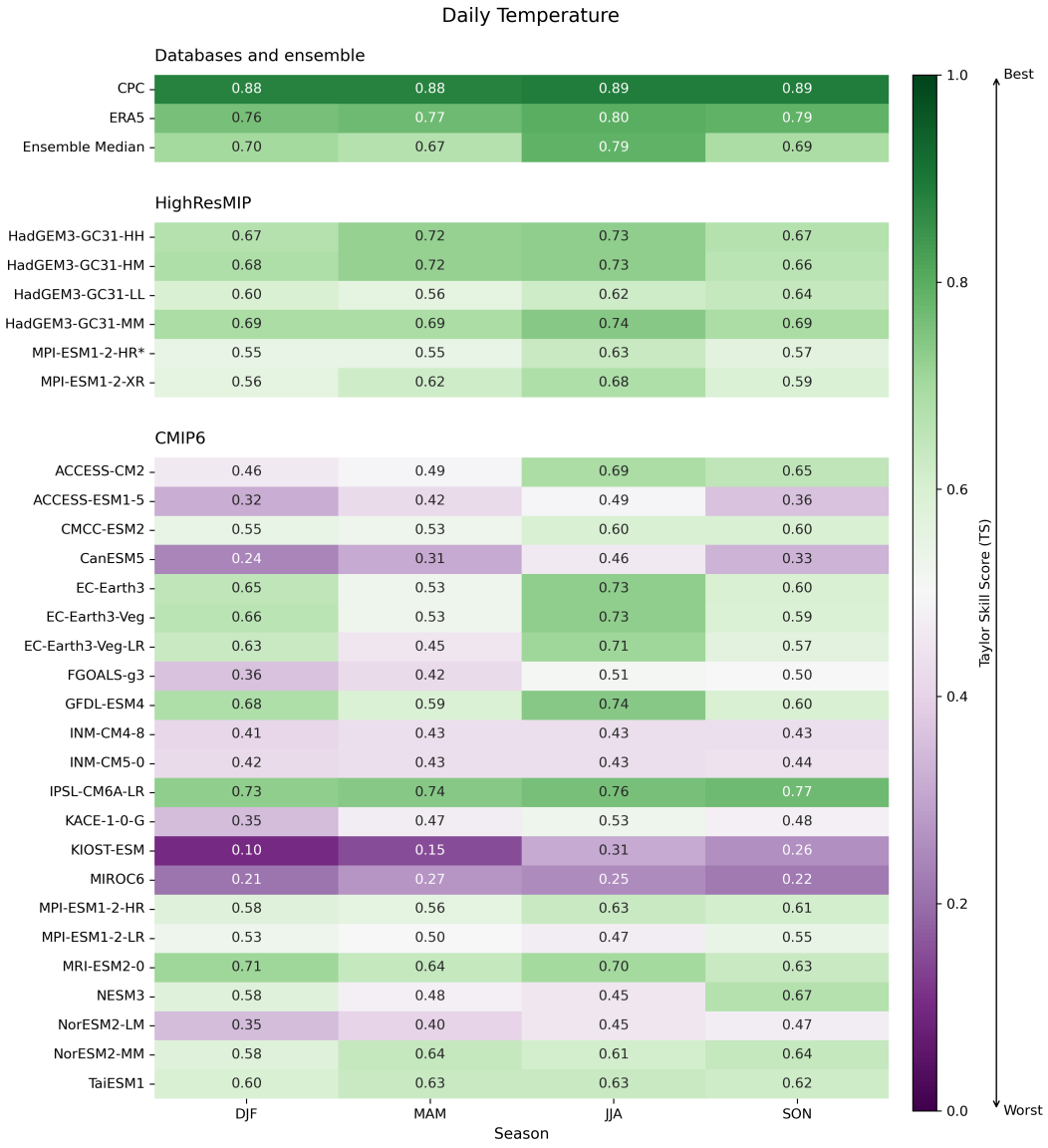

Figure B.1: Taylor Skill Score (TS) for the seasonal patterns of daily maximum temperature. Scores are shown for observational databases (CPC), ERA5, ensemble median, HighResMIP models, and CMIP6 models with respect to the reference dataset (CHIRTS). Higher values (green) indicate better model performance. Dark green (dark purple) indicates the best (worst) models.

Figure B.2: Taylor Skill Score (TS) for the seasonal patterns of daily precipitation. Scores are shown for observational databases (CHIRPS v3), ERA5, ensemble median, HighResMIP models, and CMIP6 models with respect to the reference dataset (CHIRTS). Higher values (green) indicate better model performance. Dark green (dark purple) indicates the best (worst) models.

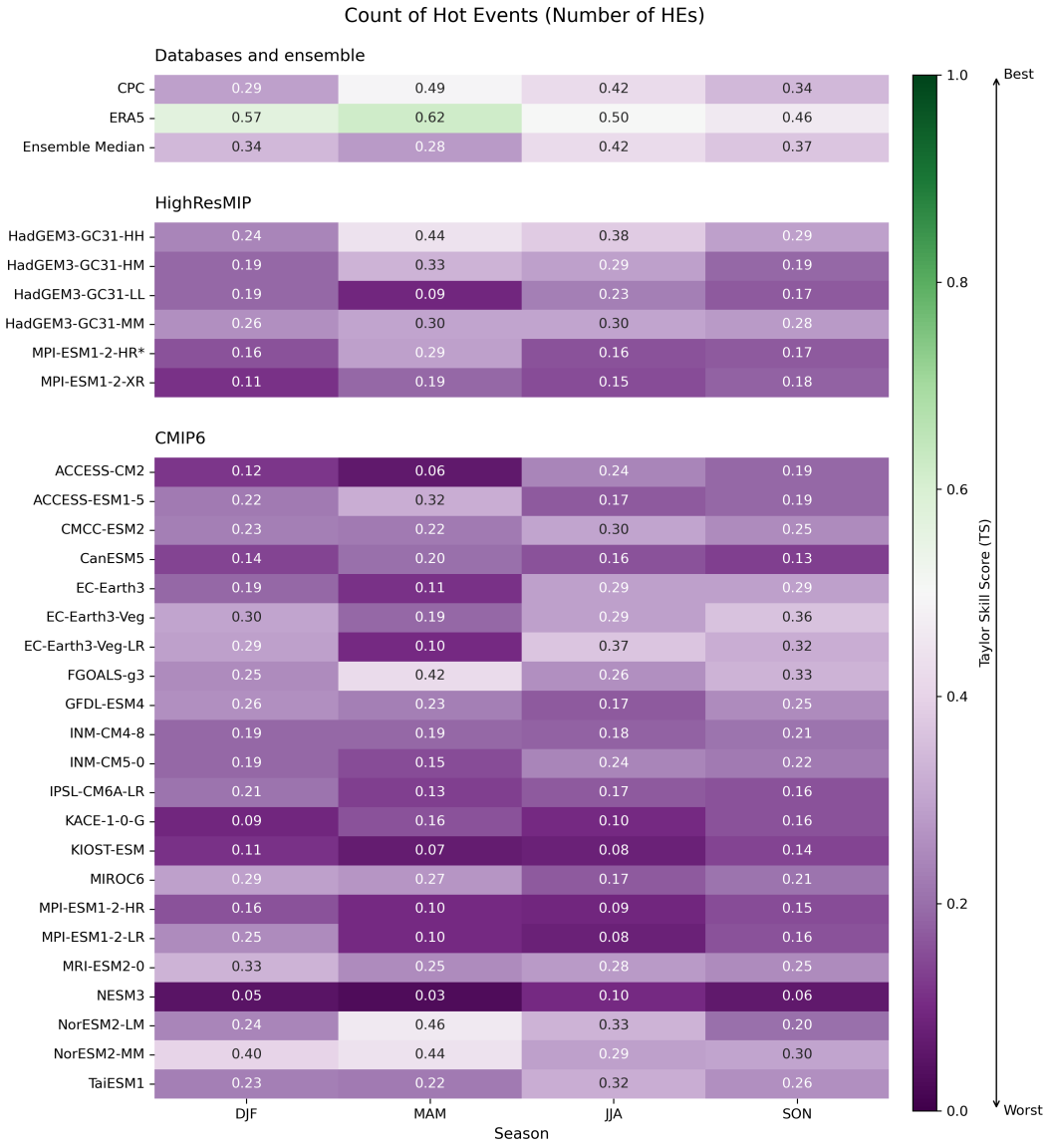

Figure B.3: Taylor Skill Score (TS) for the seasonal patterns of the number of hot events (HEs). Scores are shown for observational databases (CPC), ERA5, ensemble median, HighResMIP models, and CMIP6 models with respect to the reference dataset (CHIRTS). Higher values (green) indicate better model performance. Dark green (dark purple) indicates the best (worst) models.

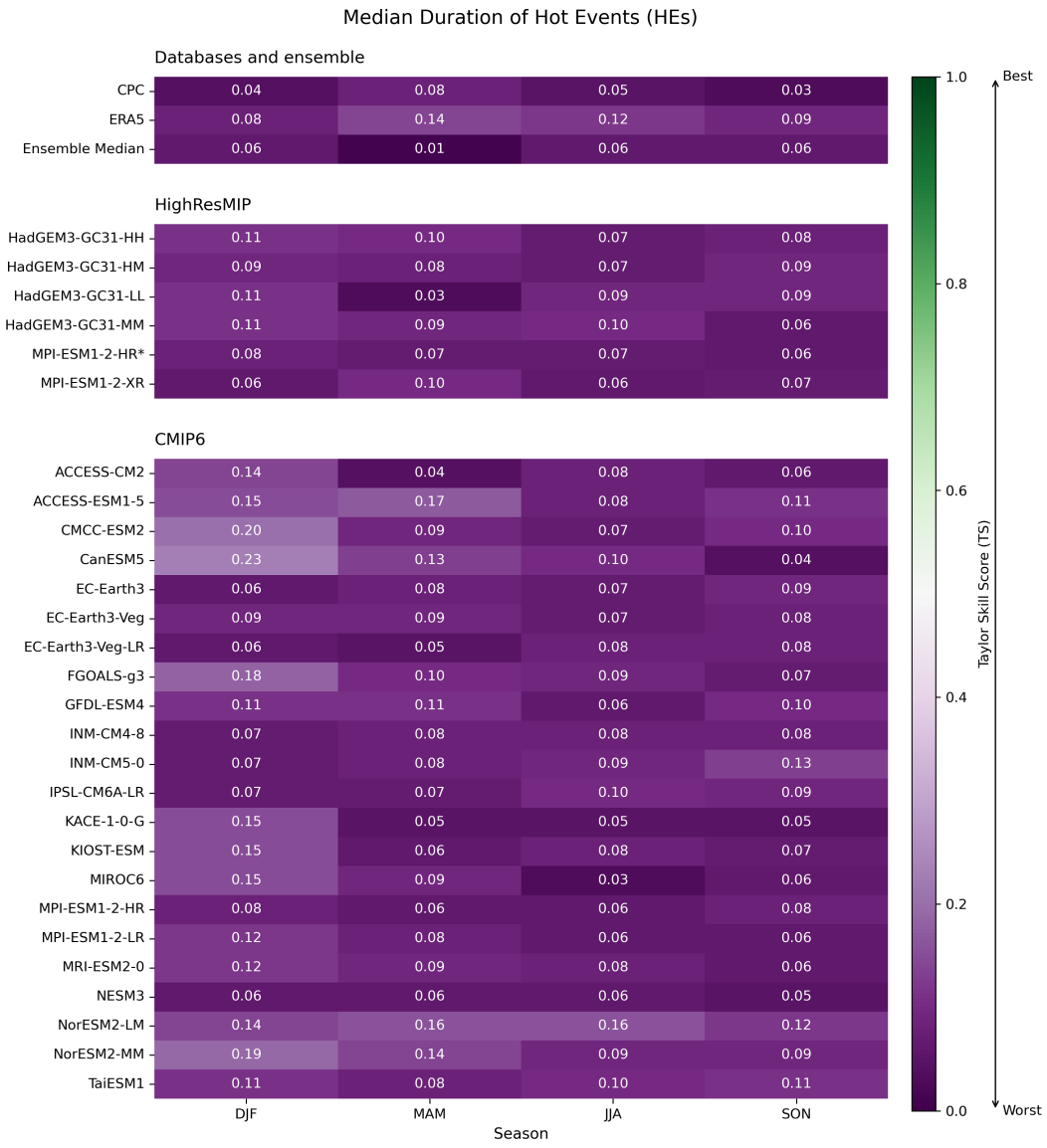

Figure B.4: Taylor Skill Score (TS) for the seasonal patterns of the median duration of hot events (HEs). Scores are shown for observational databases (CPC), ERA5, ensemble median, HighResMIP models, and CMIP6 models with respect to the reference dataset (CHIRTS). Higher values (green) indicate better model performance. Dark green (dark purple) indicates the best (worst) models.

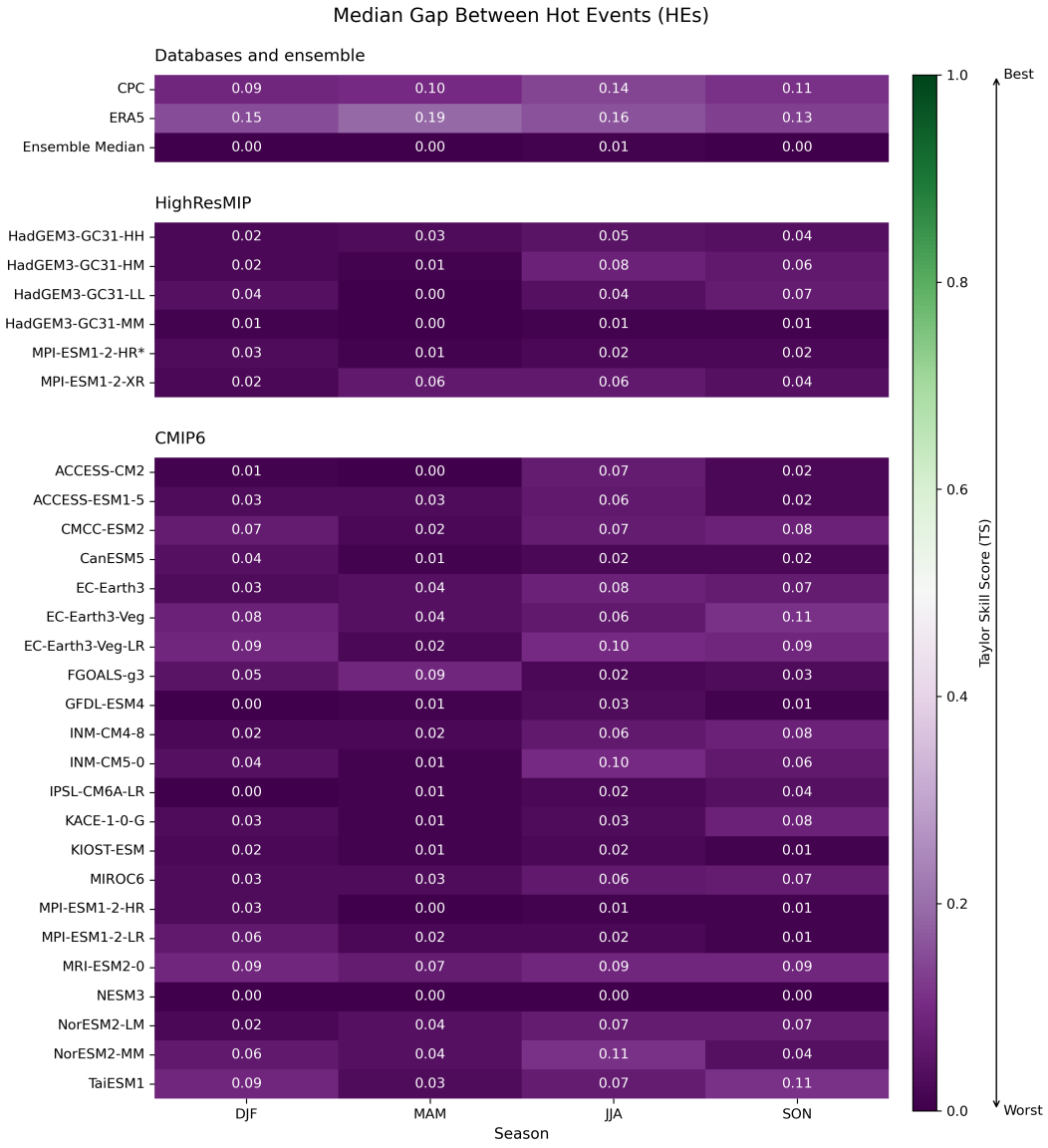

Figure B.5: Taylor Skill Score (TS) for the seasonal patterns of the median gap between hot events (HEs). Scores are shown for observational databases (CPC), ERA5, ensemble median, HighResMIP models, and CMIP6 models with respect to the reference dataset (CHIRTS). Higher values (green) indicate better model performance. Dark green (dark purple) indicates the best (worst) models.

Figure B.6: Taylor Skill Score (TS) for the seasonal patterns of the median intensity of hot events (HEs). Scores are shown for observational databases (CPC), ERA5, ensemble median, HighResMIP models, and CMIP6 models with respect to the reference dataset (CHIRTS). Higher values (green) indicate better model performance. Dark green (dark purple) indicates the best (worst) models.

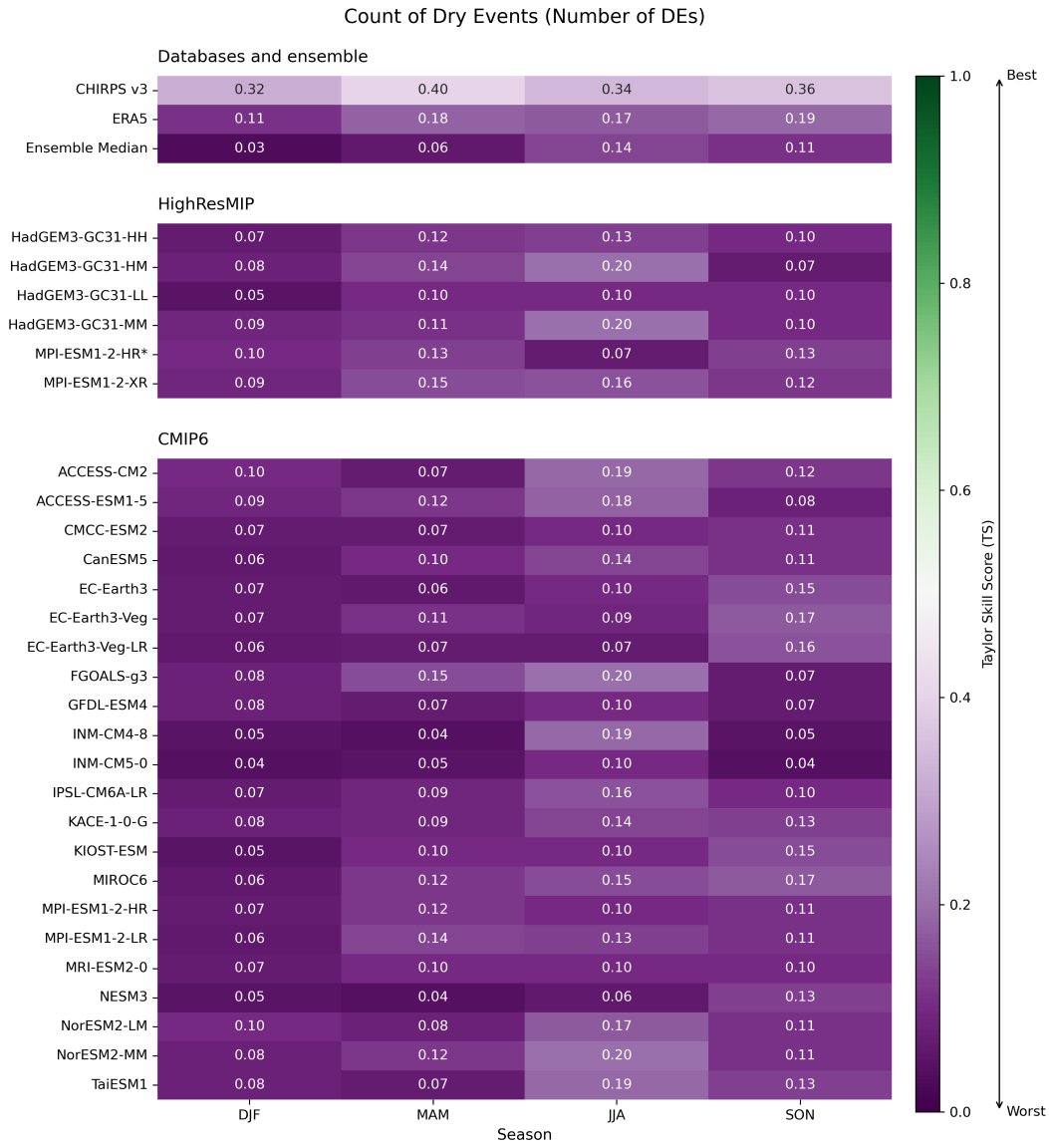

Figure B.7: Taylor Skill Score (TS) for the seasonal patterns of the number of dry events (DEs). Scores are shown for observational databases (CHIRPS v3), ERA5, ensemble median, HighResMIP models, and CMIP6 models with respect to the reference dataset (CHIRPS v2). Higher values (green) indicate better model performance. Dark green (dark purple) indicates the best (worst) models.

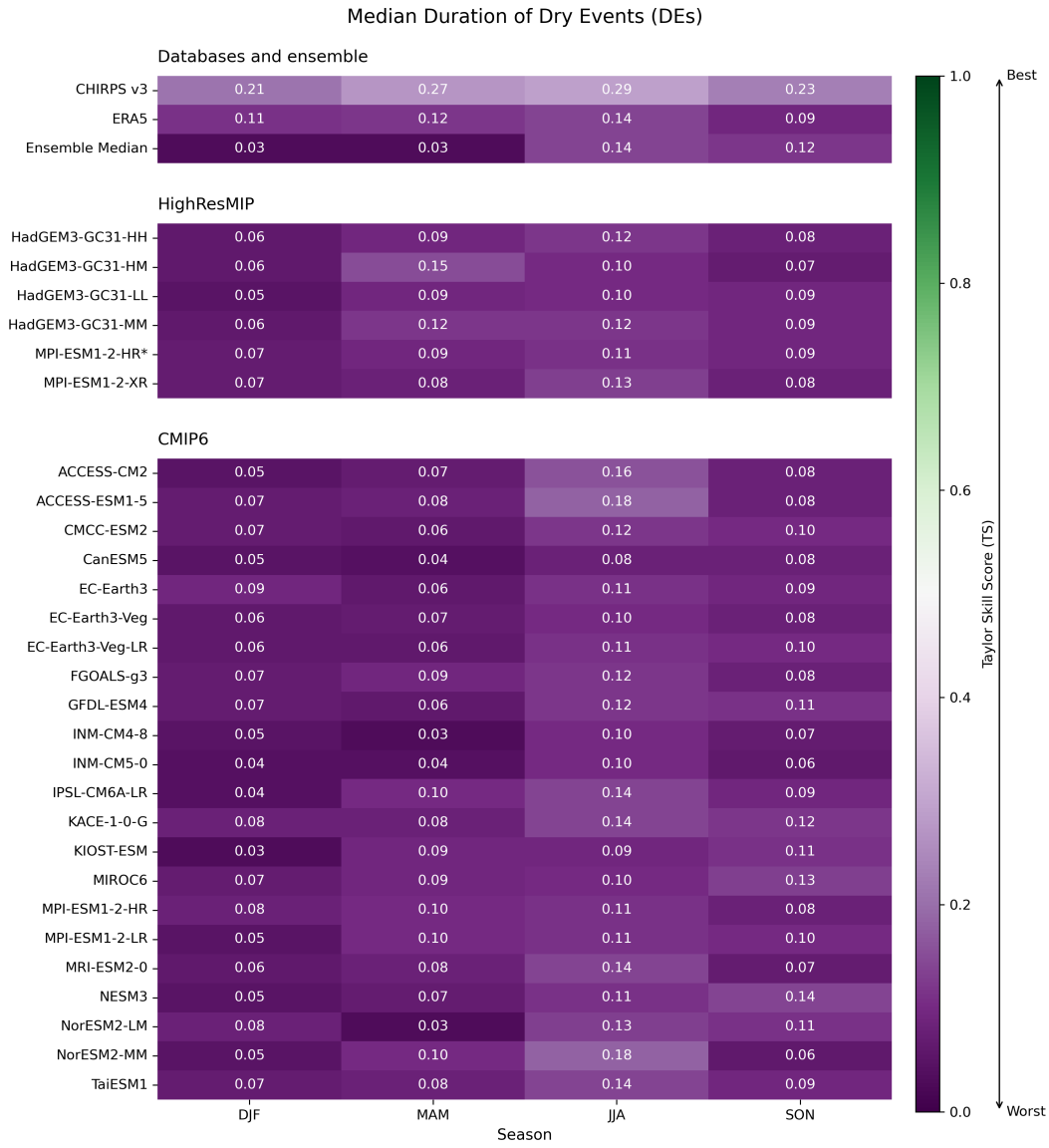

Figure B.8: Taylor Skill Score (TS) for the seasonal patterns of the median duration of dry events (DEs). Scores are shown for observational databases (CHIRPS v3), ERA5, ensemble median, HighResMIP models, and CMIP6 models with respect to the reference dataset (CHIRPS v2). Higher values (green) indicate better model performance. Dark green (dark purple) indicates the best (worst) models.

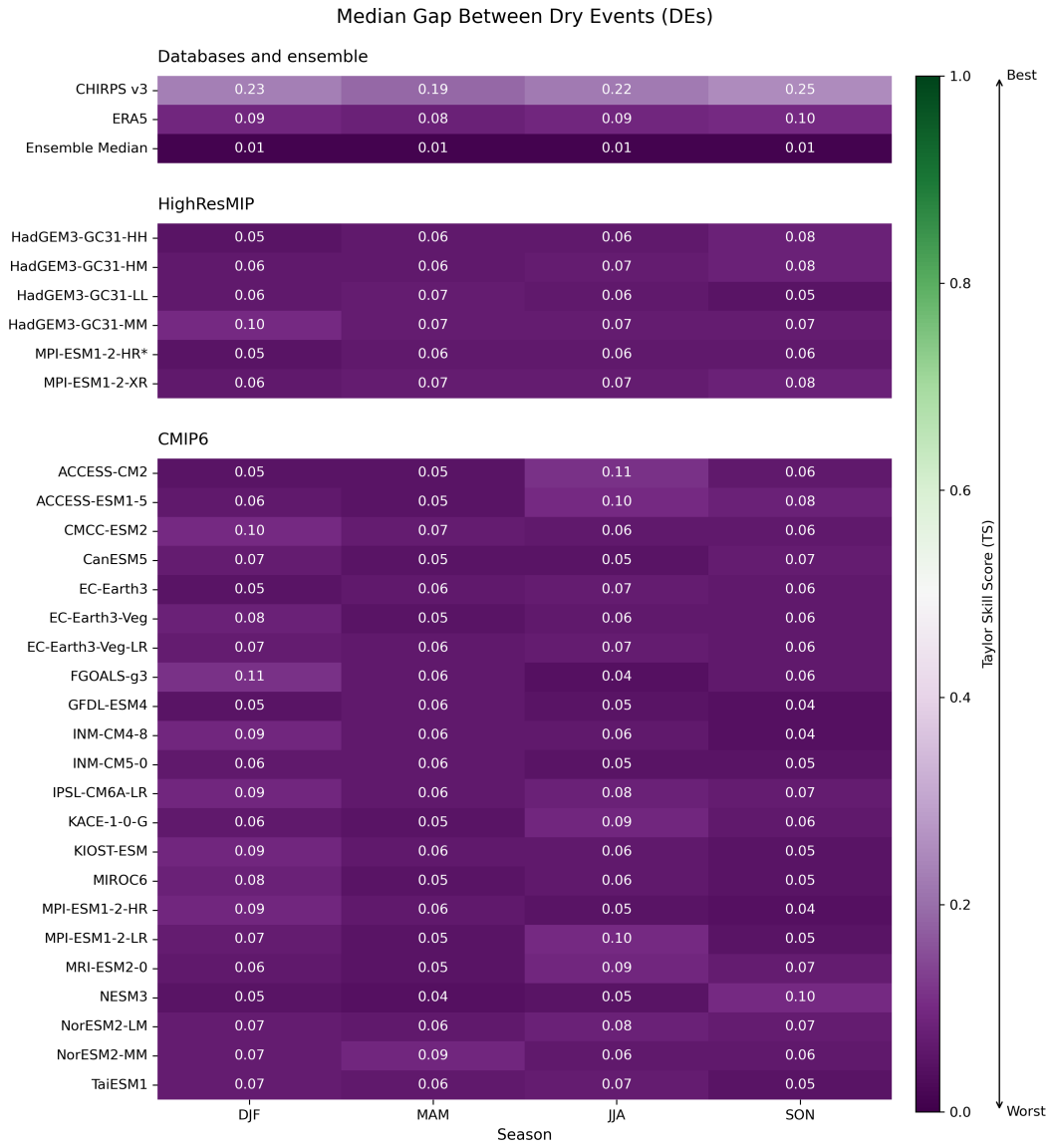

Figure B.9: Taylor Skill Score (TS) for the seasonal patterns of the median gap between dry events (DEs). Scores are shown for observational databases (CHIRPS v3), ERA5, ensemble median, HighResMIP models, and CMIP6 models with respect to the reference dataset (CHIRPS v2). Higher values (green) indicate better model performance. Dark green (dark purple) indicates the best (worst) models.

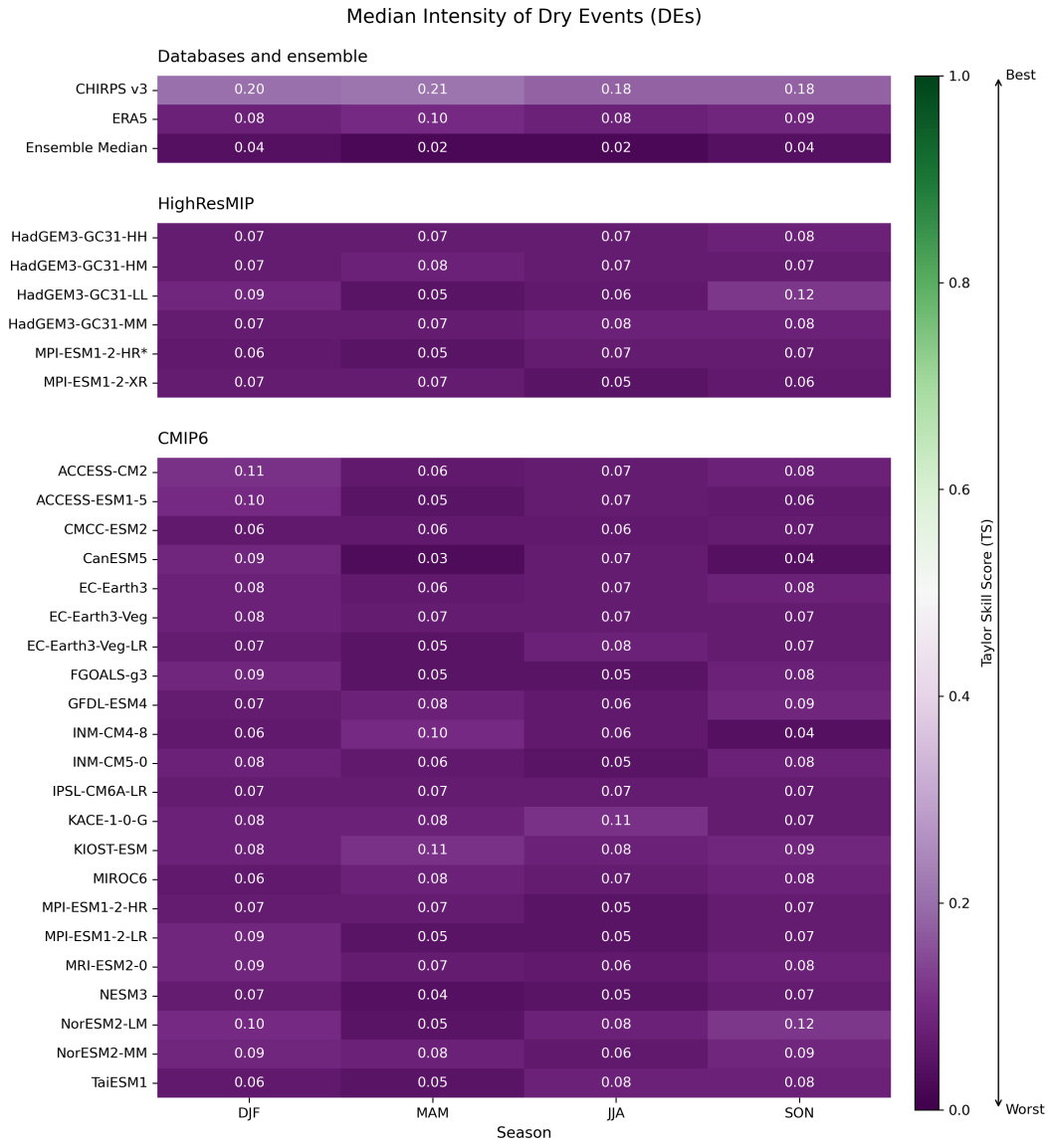

Figure B.10: Taylor Skill Score (TS) for the seasonal patterns of the median intensity of dry events (DEs). Scores are shown for observational databases (CHIRPS v3), ERA5, ensemble median, HighResMIP models, and CMIP6 models with respect to the reference dataset (CHIRPS v2). Higher values (green) indicate better model performance. Dark green (dark purple) indicates the best (worst) models.

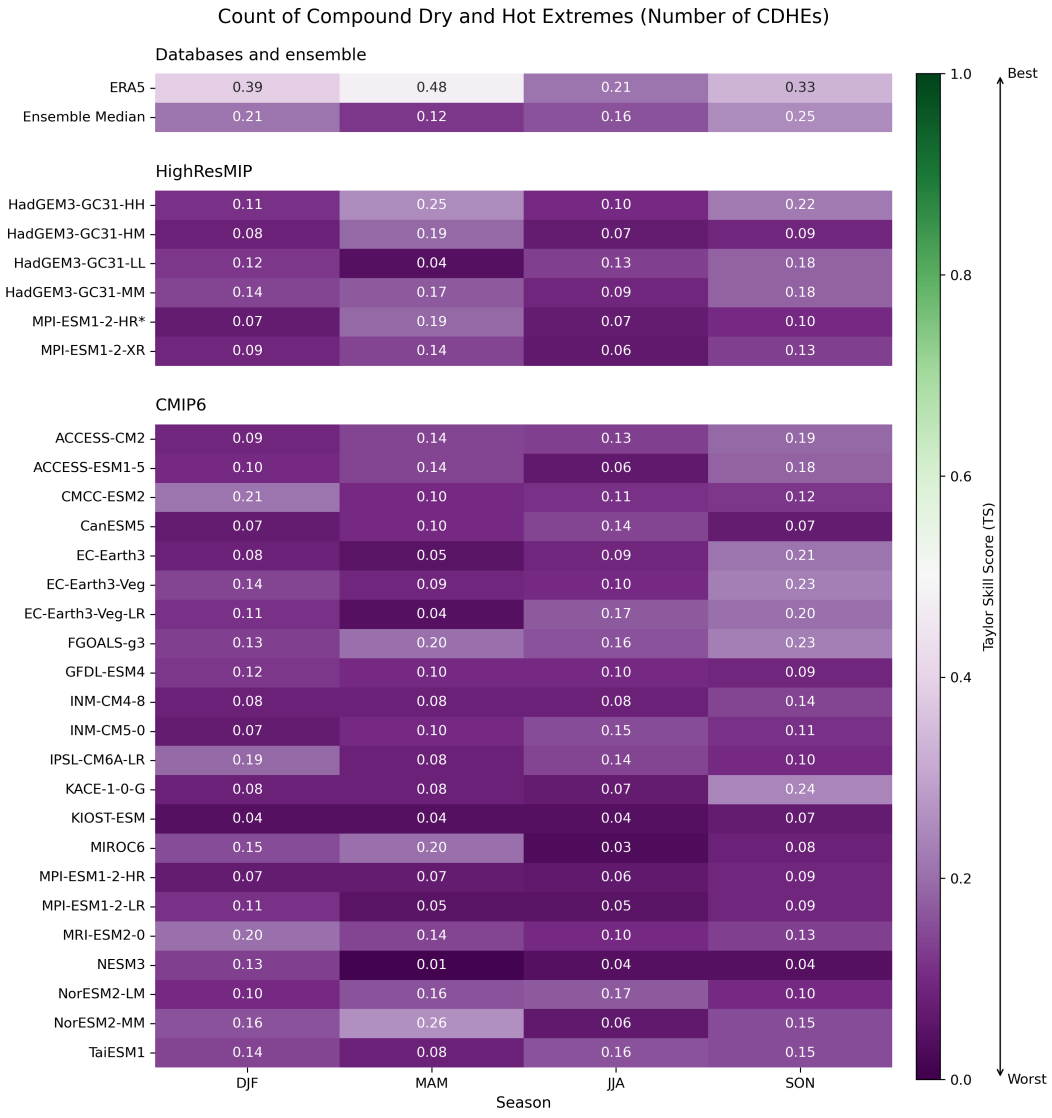

Figure B.11: Taylor Skill Score (TS) for the seasonal patterns of the number of compound dry and hot events (CDHEs). Scores are shown for ERA5, ensemble median, HighResMIP models, and CMIP6 models with respect to the reference dataset (CHIRPS v2/CHIRTS). Higher values (green) indicate better model performance. Dark green (dark purple) indicates the best (worst) models.

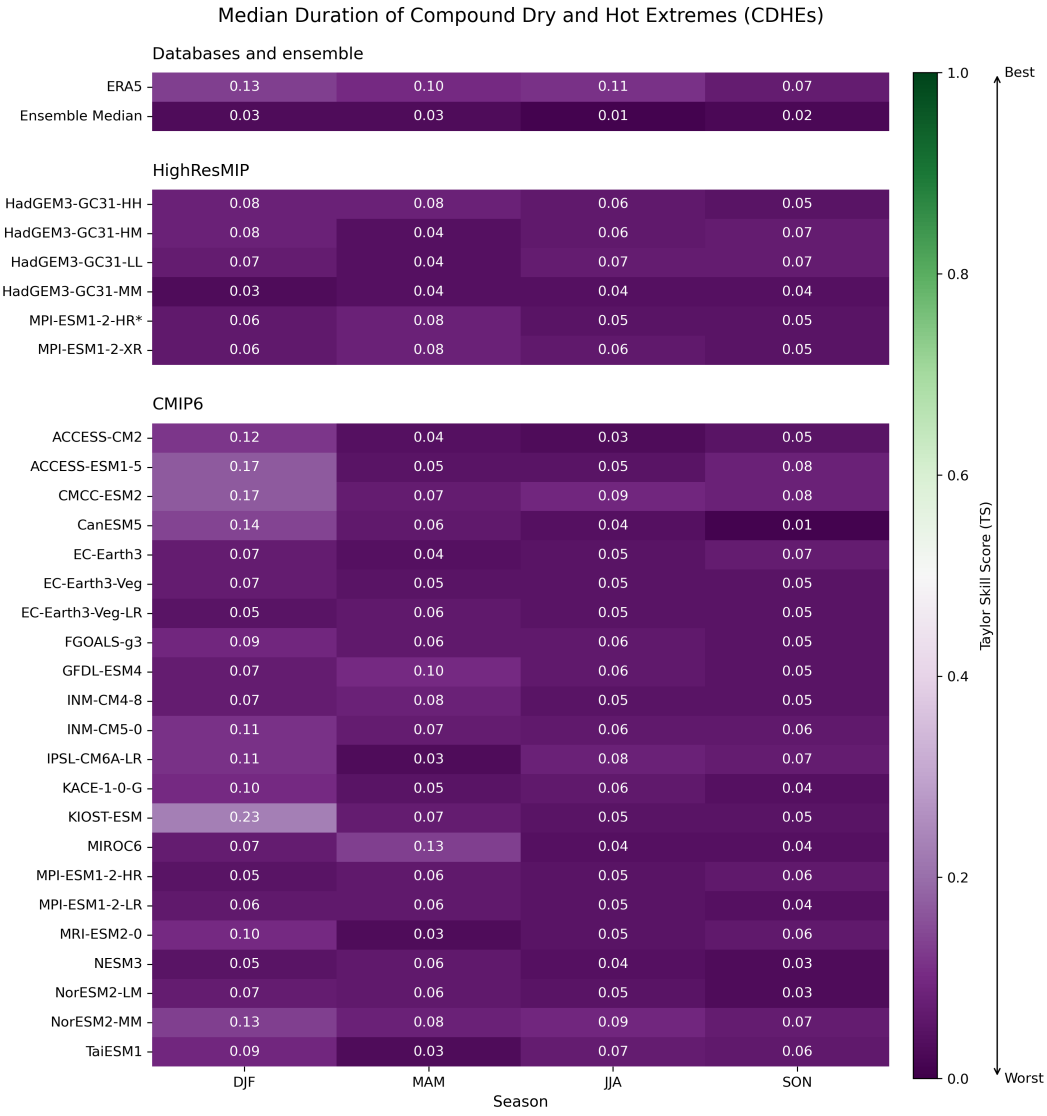

Figure B.12: Taylor Skill Score (TS) for the seasonal patterns of the median duration of compound dry and hot events (CDHEs). Scores are shown for ERA5, ensemble median, HighResMIP models, and CMIP6 models with respect to the reference dataset (CHIRPS v2/CHIRTS). Higher values (green) indicate better model performance. Dark green (dark purple) indicates the best (worst) models.

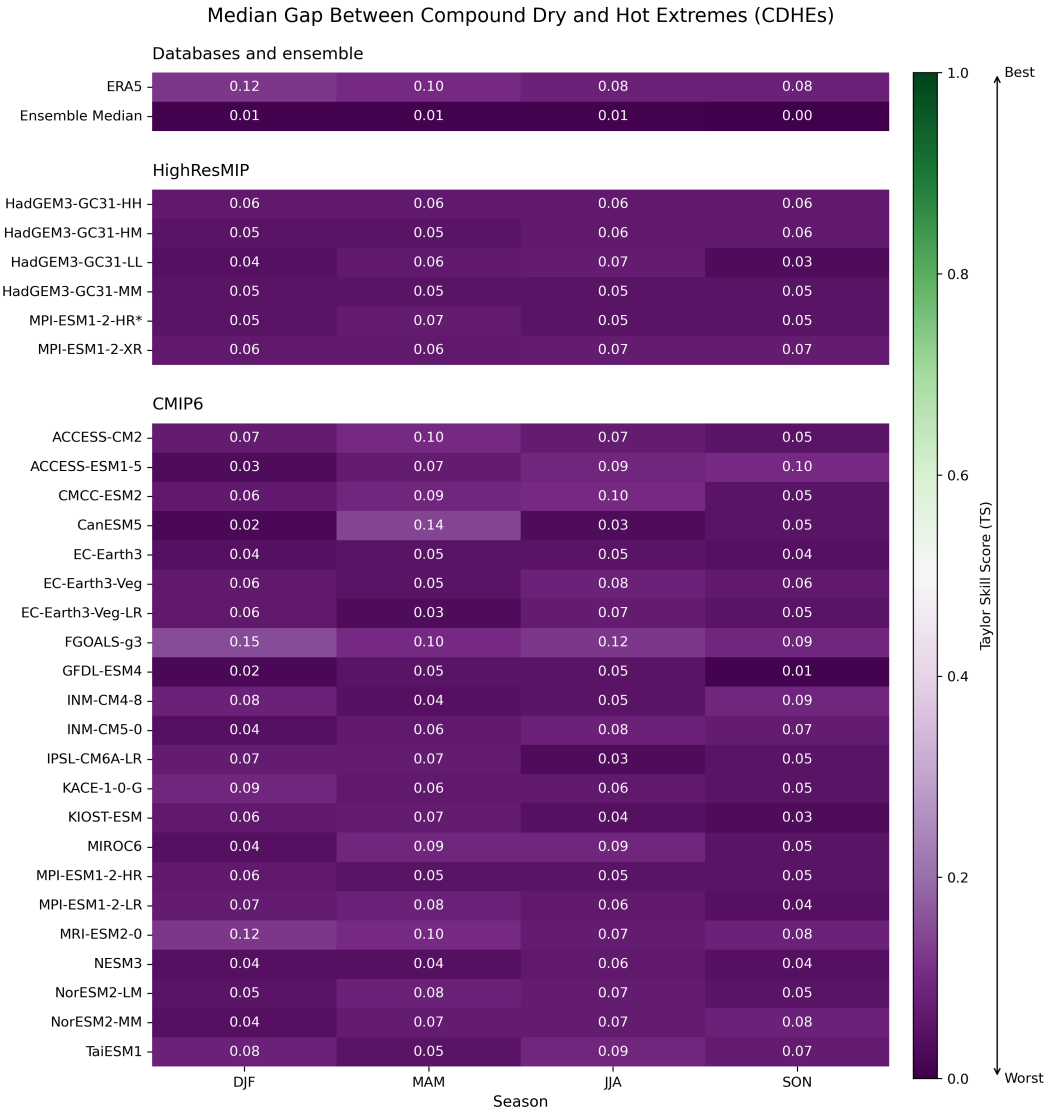

Figure B.13: Taylor Skill Score (TS) for the seasonal patterns of the median gap between compound dry and hot events (CDHEs). Scores are shown for ERA5, ensemble median, HighResMIP models, and CMIP6 models with respect to the reference dataset (CHIRPS v2/CHIRTS). Higher values (green) indicate better model performance. Dark green (dark purple) indicates the best (worst) models.

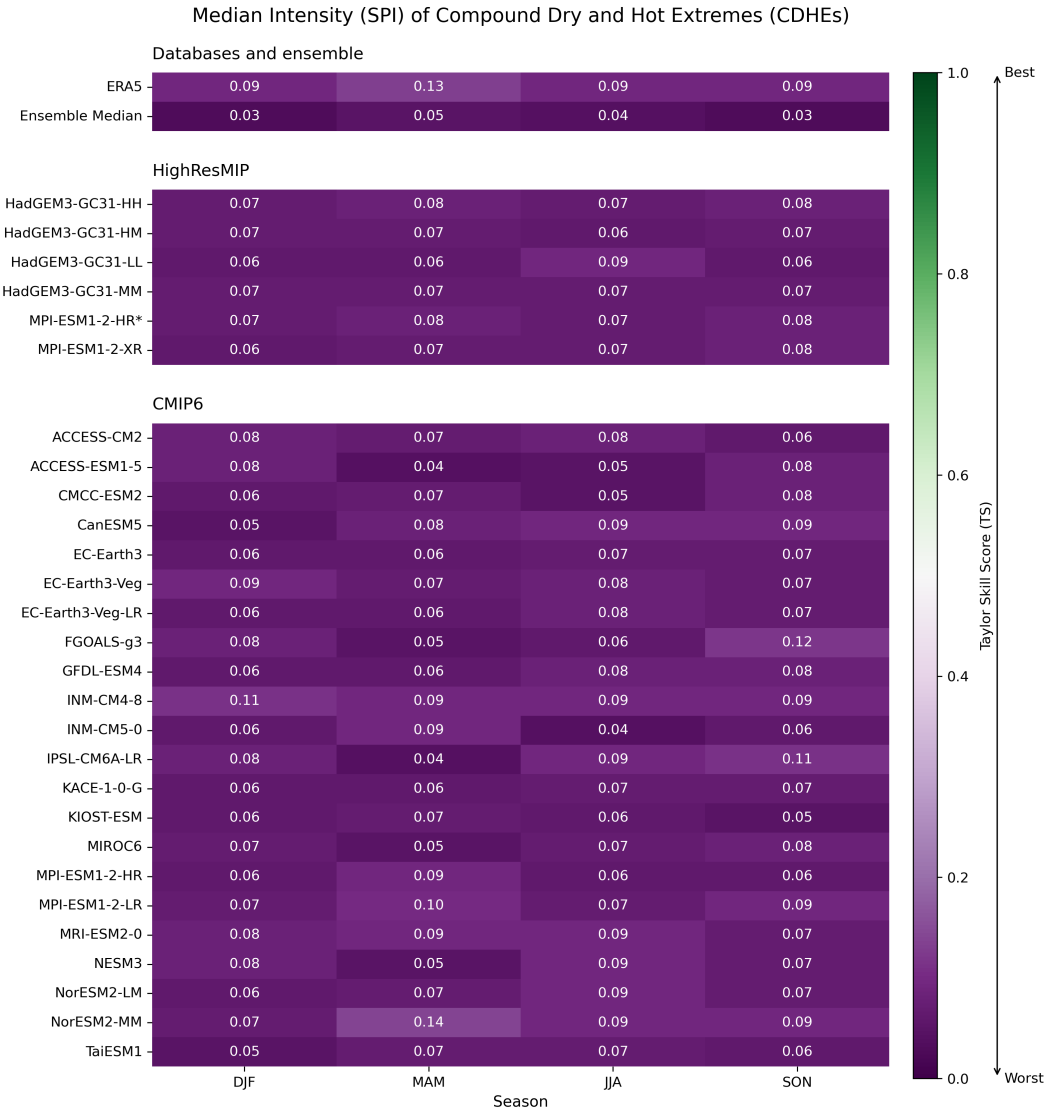

Figure B.14: Taylor Skill Score (TS) for the seasonal patterns of the median intensity of drought of compound dry and hot events (CDHEs). Scores are shown for ERA5, ensemble median, HighResMIP models, and CMIP6 models with respect to the reference dataset (CHIRPS v2/CHIRTS). Higher values (green) indicate better model performance. Dark green (dark purple) indicates the best (worst) models.

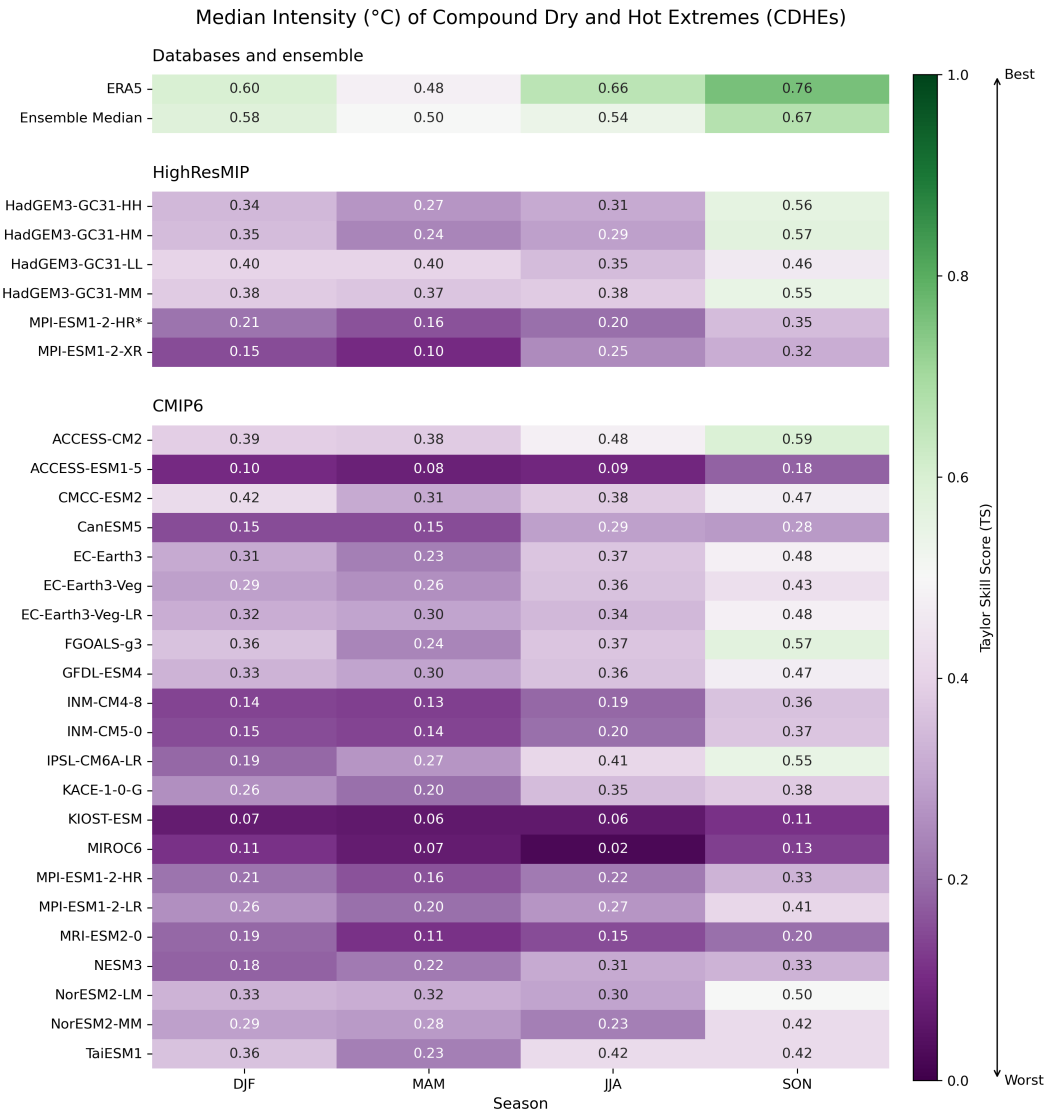

Figure B.15: Taylor Skill Score (TS) for the seasonal patterns of the median intensity of maximum temperature of compound dry and hot events (CDHEs). Scores are shown for ERA5, ensemble median, HighResMIP models, and CMIP6 models with respect to the reference dataset (CHIRPS v2/CHIRTS). Higher values (green) indicate better model performance. Dark green (dark purple) indicates the best (worst) models.

Appendix C

Projected changes in the characteristics of hot, dry, and compound dry-hot events under different climate change scenarios

Table C.1: Trends in characteristics of hot events (HEs) for the northern Andes, Orinoco, Brazilian Amazon, and northern Cerrado regions. Bold values with asterisk (*) denote statistically significant trends (Mann-Kendall test, $p < 0.05$). Negative values indicate decreasing trends. Trends were calculated for all scenarios over the period 2015–2100, except for highres-future, for which the analysis covers the period 2015–2050 due to its shorter temporal extent.

Region	Characteristics	SSP1-2.6	SSP2-4.5	SSP3-7.0	SSP5-8.5	highres-future
Brazilian Amazon	Number of HEs (events/decade)	**0.00***	0.00	**-0.46***	**-0.75***	**-1.67***
	Number of days during HEs (days/decade)	**10.36***	**28.33***	**38.50***	**40.28***	**84.32***
	Median duration of HEs (days/decade)	**0.33***	**1.09***	**2.32***	**2.05***	0.17
	Median intensity of HEs (°C/decade)	**0.05***	**0.14***	**0.23***	**0.34***	**0.15***
	Median gap between HEs (days/decade)	**-0.85***	**-1.60***	**-1.80***	**-1.59***	-1.08
Northern Andes	Number of HEs (events/decade)	**0.00***	**-0.43***	**-1.11***	**-1.21***	**-2.61***
	Number of days during HEs (days/decade)	**10.00***	**33.08***	**39.78***	**37.76***	**84.29***
	Median duration of HEs (days/decade)	**0.33***	**1.88***	**2.14***	0.00	1.32
	Median intensity of HEs (°C/decade)	**0.03***	**0.13***	**0.21***	**0.30***	**0.23***
	Median gap between HEs (days/decade)	**-0.80***	**-1.25***	**-1.47***	**-1.34***	**-2.28***
Northern Cerrado	Number of HEs (events/decade)	**0.25***	**0.00***	0.00	**-0.47***	0.00
	Number of days during HEs (days/decade)	**9.41***	**26.22***	**36.00***	**40.20***	**72.20***
	Median duration of HEs (days/decade)	**0.24***	**1.11***	**1.84***	**2.50***	**2.29***
	Median intensity of HEs (°C/decade)	**0.03***	**0.10***	**0.22***	**0.32***	**0.23***
	Median gap between HEs (days/decade)	**-1.95***	**-1.90***	**-2.26***	**-1.94***	**-4.72***
Orinoco	Number of HEs (events/decade)	**0.14***	0.00	**-0.77***	**-1.05***	**-1.25***
	Number of days during HEs (days/decade)	**9.09***	**30.60***	**39.38***	**38.05***	**85.49***
	Median duration of HEs (days/decade)	**0.29***	**1.51***	**2.95***	**2.86***	**2.18***
	Median intensity of HEs (°C/decade)	**0.03***	**0.11***	**0.22***	**0.35***	**0.31***
	Median gap between HEs (days/decade)	**-0.88***	**-1.58***	**-1.58***	**-1.40***	**-2.13***

Table C.2: Uncertainty in the estimated slopes of hot events (HEs) characteristics for the northern Andes, Orinoco, Brazilian Amazon, and northern Cerrado regions.

Region	Characteristics	SSP1-2.6	SSP2-4.5	SSP3-7.0	SSP5-8.5	highres-future
Brazilian Amazon	Number of HEs (events/decade)	[0.00, 0.26]	[0.00, 0.00]	[-0.64, -0.29]	[-0.88, -0.62]	[-2.63, -0.67]
	Number of days during HEs (days/decade)	[6.58, 13.89]	[26.17, 30.00]	[36.12, 40.88]	[37.32, 43.33]	[65.00, 101.29]
	Median duration of HEs (days/decade)	[0.15, 0.50]	[0.91, 1.25]	[2.00, 2.70]	[1.58, 2.63]	[-2.42, 3.40]
	Median intensity of HEs (°C/decade)	[0.03, 0.07]	[0.12, 0.15]	[0.21, 0.25]	[0.31, 0.38]	[0.05, 0.25]
	Median gap between HEs (days/decade)	[-1.32, -0.42]	[-2.00, -1.25]	[-2.16, -1.43]	[-1.85, -1.36]	[-2.79, 0.70]
Northern Andes	Number of HEs (events/decade)	[0.00, 0.17]	[-0.57, -0.30]	[-1.25, -0.91]	[-1.36, -1.05]	[-3.21, -1.92]
	Number of days during HEs (days/decade)	[6.76, 13.33]	[30.00, 36.03]	[36.03, 43.57]	[32.58, 42.21]	[69.41, 99.17]
	Median duration of HEs (days/decade)	[0.19, 0.47]	[1.61, 2.12]	[1.55, 2.78]	[-0.95, 1.11]	[0.00, 2.86]
	Median intensity of HEs (°C/decade)	[0.03, 0.04]	[0.12, 0.14]	[0.19, 0.22]	[0.28, 0.31]	[0.17, 0.28]
	Median gap between HEs (days/decade)	[-1.11, -0.53]	[-1.56, -0.96]	[-1.78, -1.20]	[-1.67, -1.09]	[-3.53, -1.36]
Northern Cerrado	Number of HEs (events/decade)	[0.00, 0.40]	[0.00, 0.26]	[0.00, 0.00]	[-0.71, -0.18]	[0.00, 1.00]
	Number of days during HEs (days/decade)	[7.00, 11.71]	[24.00, 28.39]	[34.29, 37.74]	[37.78, 42.50]	[58.33, 84.71]
	Median duration of HEs (days/decade)	[0.13, 0.35]	[0.94, 1.25]	[1.67, 2.06]	[2.33, 2.80]	[1.67, 3.33]
	Median intensity of HEs (°C/decade)	[0.02, 0.05]	[0.08, 0.12]	[0.19, 0.24]	[0.29, 0.35]	[0.10, 0.32]
	Median gap between HEs (days/decade)	[-2.60, -1.25]	[-2.17, -1.67]	[-2.61, -1.90]	[-2.50, -1.58]	[-6.52, -3.00]
Orinoco	Number of HEs (events/decade)	[0.00, 0.25]	[-0.17, 0.00]	[-0.94, -0.56]	[-1.18, -0.91]	[-2.00, -0.43]
	Number of days during HEs (days/decade)	[5.62, 12.50]	[28.12, 32.89]	[35.95, 42.50]	[34.00, 42.22]	[65.29, 100.36]
	Median duration of HEs (days/decade)	[0.14, 0.43]	[1.25, 1.74]	[2.50, 3.38]	[2.07, 3.68]	[0.65, 4.33]
	Median intensity of HEs (°C/decade)	[0.02, 0.04]	[0.10, 0.12]	[0.20, 0.24]	[0.32, 0.38]	[0.26, 0.37]
	Median gap between HEs (days/decade)	[-1.23, -0.52]	[-1.89, -1.28]	[-2.00, -1.30]	[-1.69, -1.13]	[-3.75, -1.00]

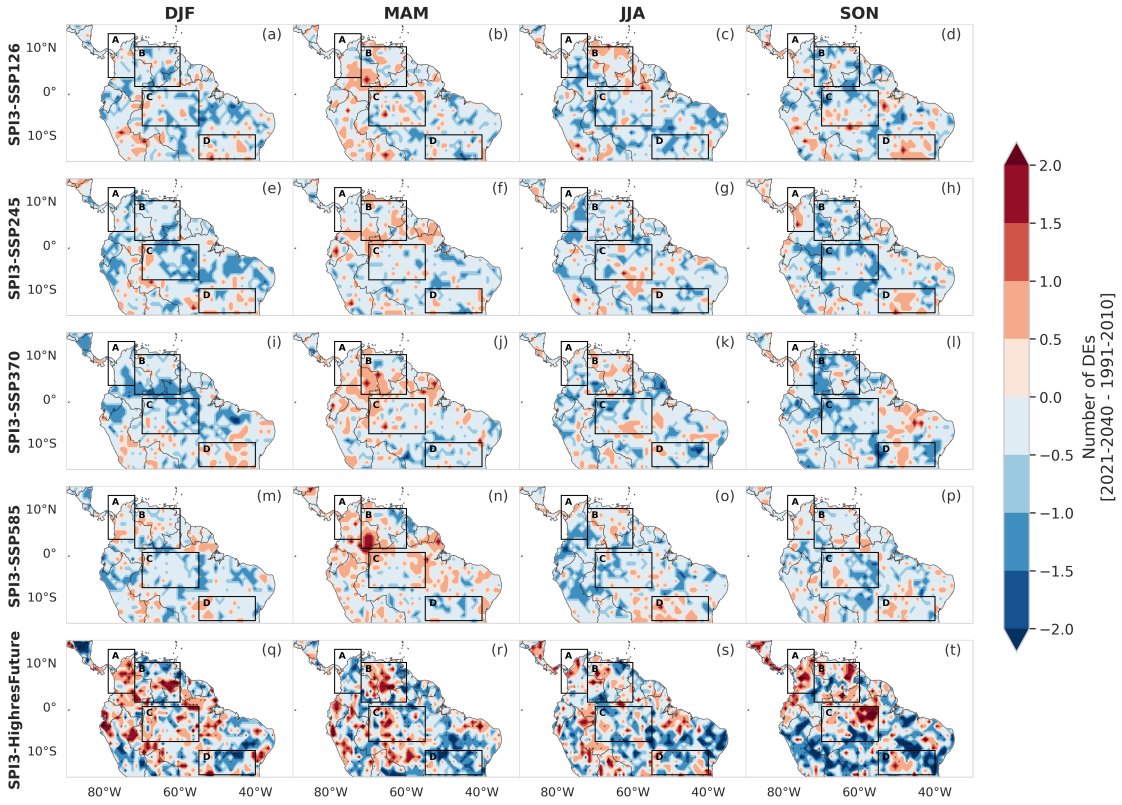

Figure C.1: Projected changes in the seasonal count of Dry Events (DEs) for the near-term period (2021–2040) based on the ensemble median under different emission scenarios: SSP1-2.6 (a–d), SSP2-4.5 (e–h), SSP3-7.0 (i–l), and SSP5-8.5 (m–p) from CMIP6, and HighresFuture (HighresFuture) (q–t) from HighResMIP. Dots indicate grid points where at least 80 % of the CMIP6 or HighResMIP models agree on the sign of the projected change. Black rectangles highlight the four subregions: (A) northern Andes, (B) Orinoco, (C) Brazilian Amazon, and (D) northern Cerrado. All spatial fields are shown at a common resolution of 1° × 1° (based on the second methodology (subsection 5.2.2)).

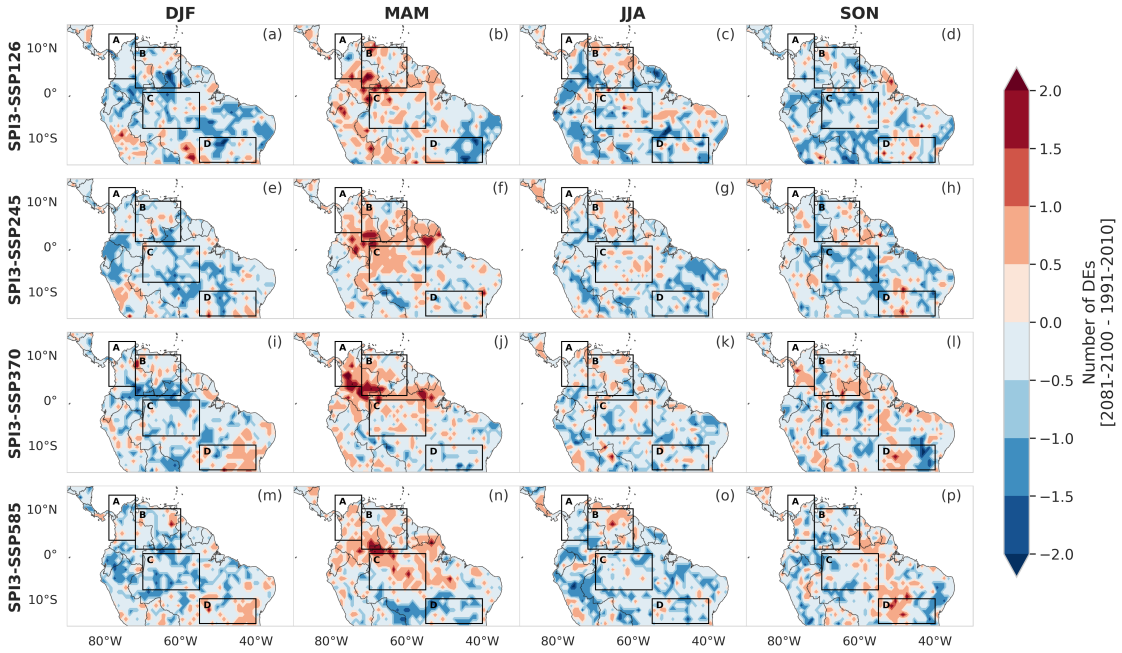

Figure C.2: Projected changes in the seasonal count of Dry Events (DEs) for the long-term period (2081–2100) based on the ensemble median under different emission scenarios: SSP1-2.6 (a–d), SSP2-4.5 (e–h), SSP3-7.0 (i–l), and SSP5-8.5 (m–p) from CMIP6. Dots indicate grid points where at least 80 % of the CMIP6 models agree on the sign of the projected change. Black rectangles highlight the four regions: (A) northern Andes, (B) Orinoco, (C) Brazilian Amazon, and (D) northern Cerrado. All spatial fields are shown at a common resolution of 1° × 1° (based on the second methodology (subsection 5.2.2)).

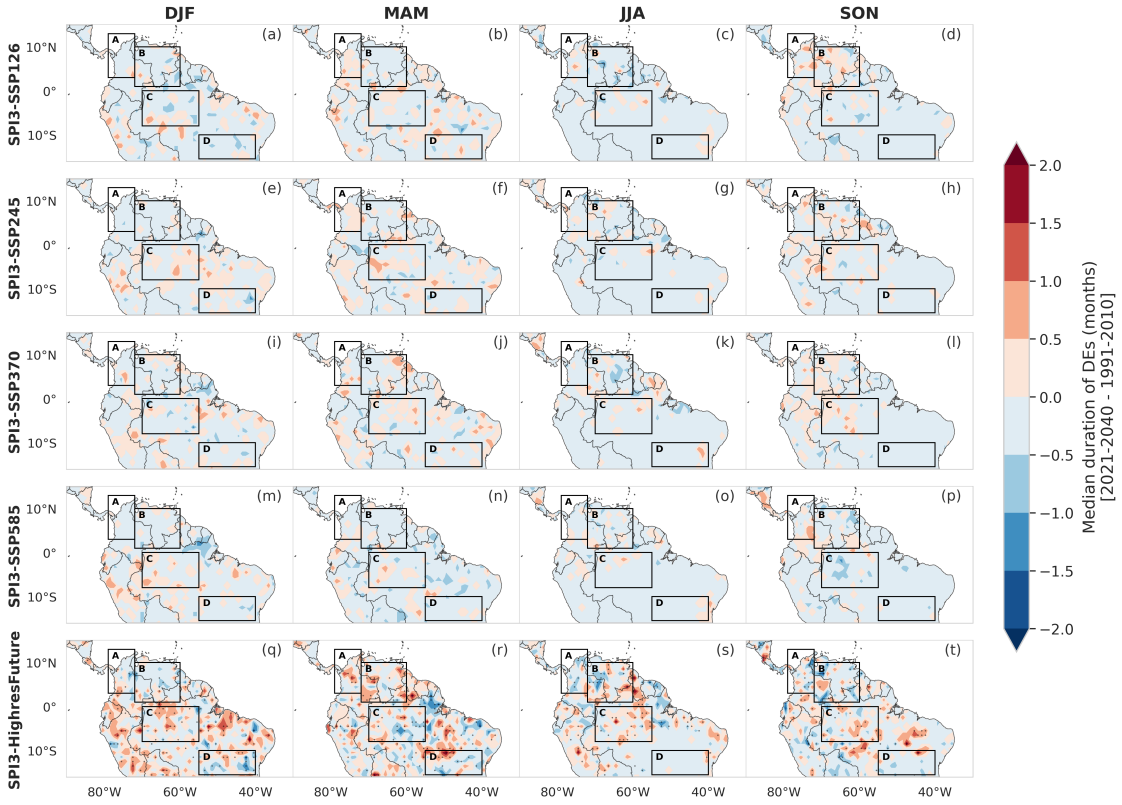

Figure C.3: Projected changes in the seasonal median duration (months) of Dry Events (DEs) for the near-term period (2021–2040) based on the ensemble median under different emission scenarios: SSP1-2.6 (a–d), SSP2-4.5 (e–h), SSP3-7.0 (i–l), and SSP5-8.5 (m–p) from CMIP6, and HighresFuture (HighresFuture) (q–t) from HighResMIP. Dots indicate grid points where at least 80 % of the CMIP6 or HighResMIP models agree on the sign of the projected change. Black rectangles highlight the four subregions: (A) northern Andes, (B) Orinoco, (C) Brazilian Amazon, and (D) northern Cerrado. All spatial fields are shown at a common resolution of 1° × 1° (based on the second methodology (subsection 5.2.2)).

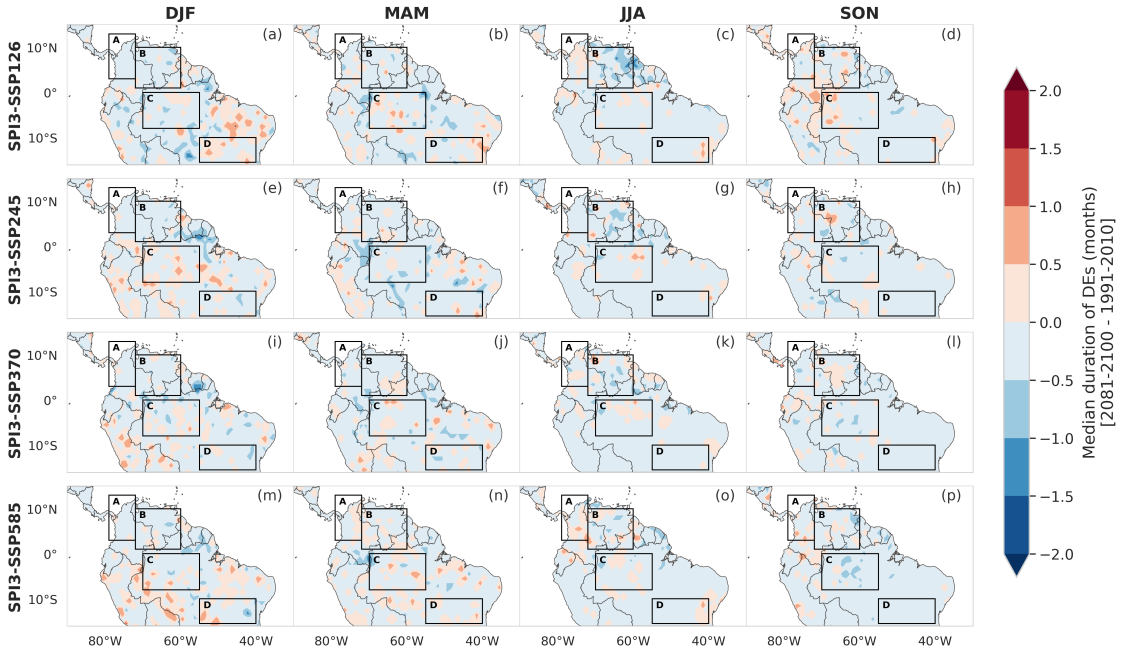

Figure C.4: Projected changes in the seasonal median duration (months) of Dry Events (DEs) for the long-term period (2081–2100) based on the ensemble median under different emission scenarios: SSP1-2.6 (a–d), SSP2-4.5 (e–h), SSP3-7.0 (i–l), and SSP5-8.5 (m–p) from CMIP6. Dots indicate grid points where at least 80 % of the CMIP6 models agree on the sign of the projected change. Black rectangles highlight the four regions: (A) northern Andes, (B) Orinoco, (C) Brazilian Amazon, and (D) northern Cerrado. All spatial fields are shown at a common resolution of 1° × 1° (based on the second methodology (subsection 5.2.2)).

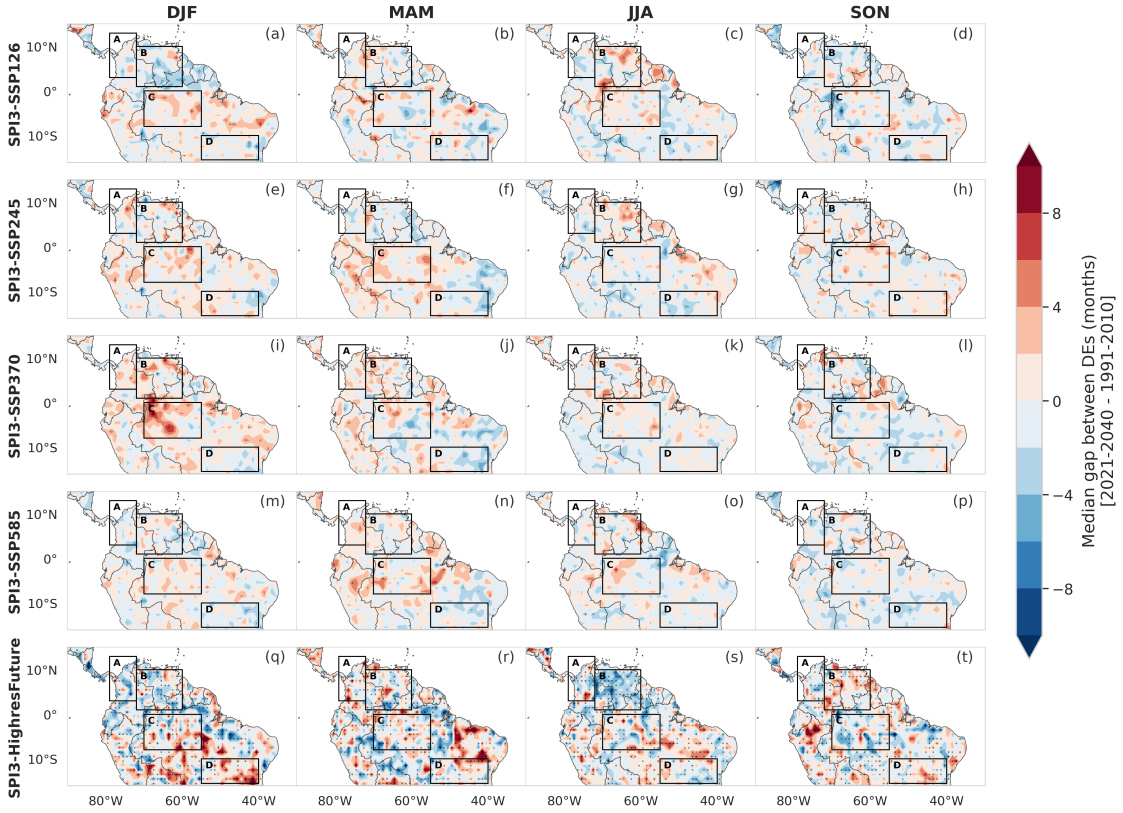

Figure C.5: Projected changes in the seasonal median gap (months) between Dry Events (DEs) for the near-term period (2021–2040) based on the ensemble median under different emission scenarios: SSP1-2.6 (a–d), SSP2-4.5 (e–h), SSP3-7.0 (i–l), and SSP5-8.5 (m–p) from CMIP6, and HighresFuture (HighresFuture) (q–t) from HighResMIP. Dots indicate grid points where at least 80 % of the CMIP6 or HighResMIP models agree on the sign of the projected change. Black rectangles highlight the four subregions: (A) northern Andes, (B) Orinoco, (C) Brazilian Amazon, and (D) northern Cerrado. All spatial fields are shown at a common resolution of 1° × 1° (based on the second methodology (subsection 5.2.2)).

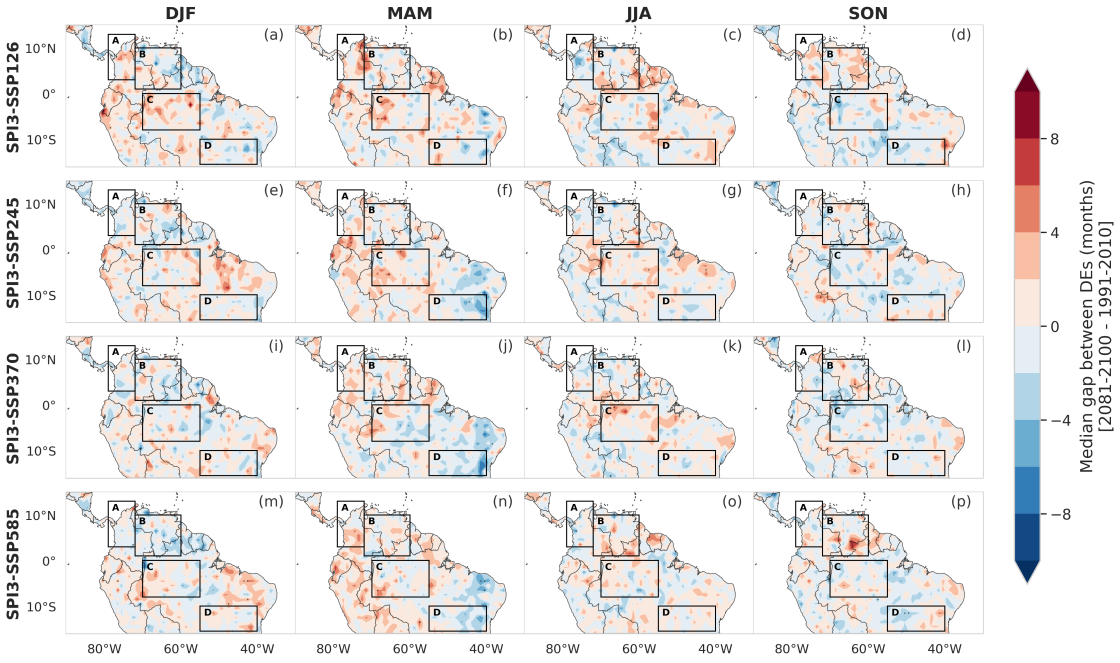

Figure C.6: Projected changes in the seasonal median gap (months) between Dry Events (DEs) for the long-term period (2081–2100) based on the ensemble median under different emission scenarios: SSP1-2.6 (a–d), SSP2-4.5 (e–h), SSP3-7.0 (i–l), and SSP5-8.5 (m–p) from CMIP6. Dots indicate grid points where at least 80 % of the CMIP6 models agree on the sign of the projected change. Black rectangles highlight the four regions: (A) northern Andes, (B) Orinoco, (C) Brazilian Amazon, and (D) northern Cerrado. All spatial fields are shown at a common resolution of 1° × 1° (based on the second methodology (subsection 5.2.2)).

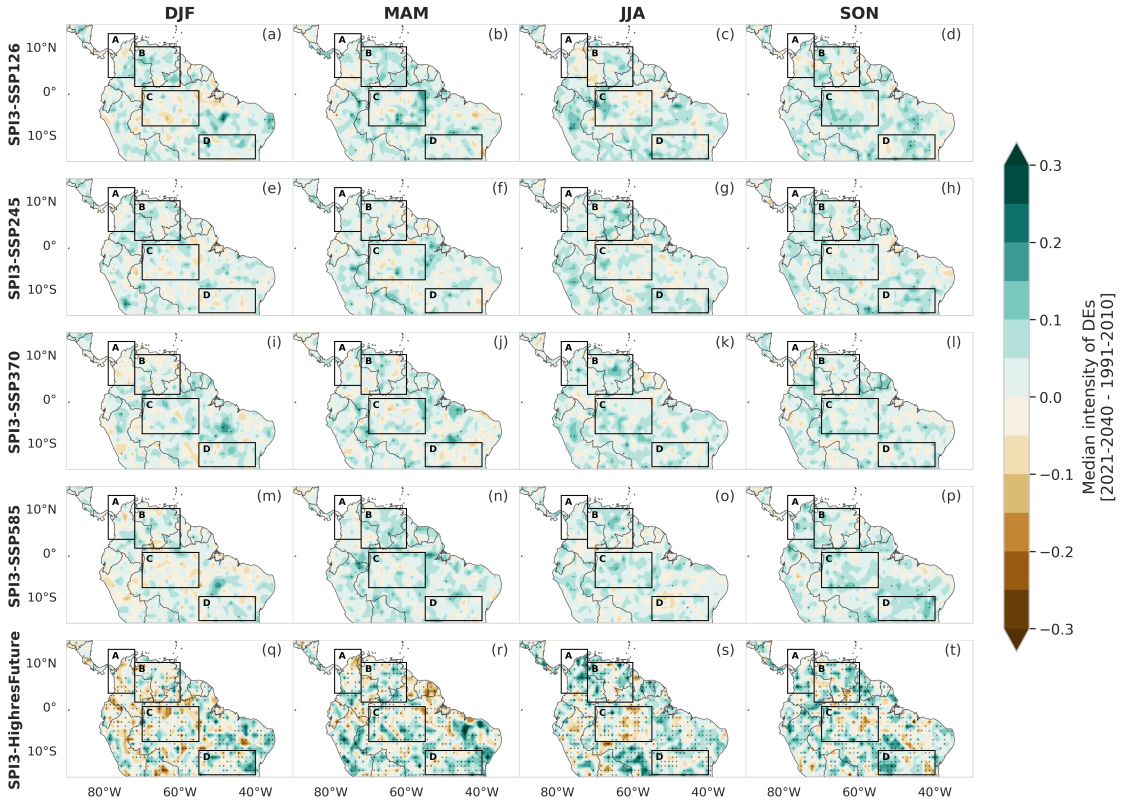

Figure C.7: Projected changes in the seasonal median intensity (SPI) of Dry Events (DEs) for the near-term period (2021–2040) based on the ensemble median under different emission scenarios: SSP1-2.6 (a–d), SSP2-4.5 (e–h), SSP3-7.0 (i–l), and SSP5-8.5 (m–p) from CMIP6, and HighresFuture (HighresFuture) (q–t) from HighResMIP. Dots indicate grid points where at least 80 % of the CMIP6 or HighResMIP models agree on the sign of the projected change. Black rectangles highlight the four regions: (A) northern Andes, (B) Orinoco, (C) Brazilian Amazon, and (D) northern Cerrado. All spatial fields are shown at a common resolution of 1° × 1° (based on the second methodology (subsection 5.2.2)).

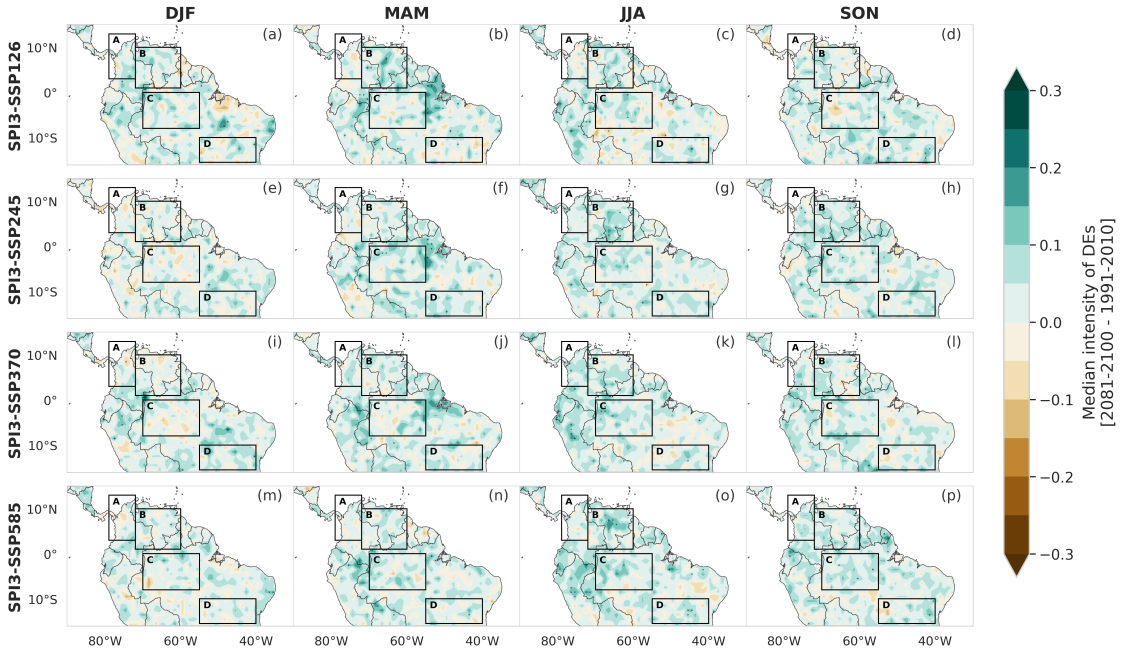

Figure C.8: Projected changes in the seasonal median intensity (SPI) of Dry Events (DEs) for the long-term period (2081–2100) based on the ensemble median under different emission scenarios: SSP1-2.6 (a–d), SSP2-4.5 (e–h), SSP3-7.0 (i–l), and SSP5-8.5 (m–p) from CMIP6. Dots indicate grid points where at least 80 % of the CMIP6 models agree on the sign of the projected change. Black rectangles highlight the four regions: (A) northern Andes, (B) Orinoco, (C) Brazilian Amazon, and (D) northern Cerrado. All spatial fields are shown at a common resolution of 1° × 1° (based on the second methodology (subsection 5.2.2)).

Table C.3: Trends in characteristics of dry events (DEs) for the northern Andes, Orinoco, Brazilian Amazon, and northern Cerrado regions. Bold values with asterisk (*) denote statistically significant trends (Mann-Kendall test, $p < 0.05$). Negative values indicate decreasing trends. Trends were calculated for all scenarios over the period 2015–2100, except for highres-future, for which the analysis covers the period 2015–2050 due to its shorter temporal extent.

Region	Characteristics	SSP1-2.6	SSP2-4.5	SSP3-7.0	SSP5-8.5	highres-future
Brazilian Amazon	Number of DEs (events/decade)	0.00	0.00	0.00	**0.00***	0.00
	Number of months during DEs (months/decade)	**0.00***	**0.16***	**0.35***	**0.41***	**0.62***
	Median duration of DEs (months/decade)	**0.00***	**0.12***	**0.20***	**0.21***	0.33
	Median intensity of DEs (SPI/decade)	-0.01	**-0.02***	**-0.03***	**-0.04***	**-0.08***
	Median gap between DEs (months/decade)	-0.07	**-0.24***	**-0.56***	**-0.55***	-0.70
Northern Andes	Number of DEs (events/decade)	0.00	0.00	**0.00***	**0.00***	**0.00***
	Number of months during DEs (months/decade)	0.00	0.00	**0.29***	**0.28***	**0.67***
	Median duration of DEs (months/decade)	0.00	0.00	**0.15***	**0.18***	**0.53***
	Median intensity of DEs (SPI/decade)	-0.01	**-0.01***	**-0.03***	**-0.04***	-0.03
	Median gap between DEs (months/decade)	0.36	0.00	**-0.49***	**-0.45***	-0.56
Northern Cerrado	Number of DEs (events/decade)	0.00	0.00	0.00	0.00	0.00
	Number of months during DEs (months/decade)	**0.00***	**0.00***	**0.26***	**0.37***	**0.45***
	Median duration of DEs (months/decade)	**0.00***	**0.00***	**0.19***	**0.24***	**0.16***
	Median intensity of DEs (SPI/decade)	-0.00	-0.01	**-0.03***	**-0.04***	-0.02
	Median gap between DEs (months/decade)	-0.15	**-0.18***	**-0.20***	**-0.22***	-0.48
Orinoco	Number of DEs (events/decade)	**0.00***	**0.00***	0.00	0.00	0.00
	Number of months during DEs (months/decade)	0.00	**0.20***	**0.56***	**0.60***	**0.91***
	Median duration of DEs (months/decade)	**0.00***	**0.11***	**0.35***	**0.34***	**0.53***
	Median intensity of DEs (SPI/decade)	-0.01	**-0.02***	**-0.04***	**-0.05***	**-0.05***
	Median gap between DEs (months/decade)	0.00	**-0.28***	**-0.66***	**-0.53***	-0.44

Table C.4: Uncertainty in the estimated slopes of dry events (DEs) characteristics for the northern Andes, Orinoco, Brazilian Amazon, and northern Cerrado regions.

Region	Characteristics	SSP1-2.6	SSP2-4.5	SSP3-7.0	SSP5-8.5	highres-future
Brazilian Amazon	Number of DEs (events/decade)	[0.00, 0.00]	[0.00, 0.00]	[0.00, 0.00]	[0.00, 0.00]	[0.00, 0.00]
	Number of months during DEs (months/decade)	[0.00, 0.13]	[0.00, 0.23]	[0.27, 0.42]	[0.34, 0.48]	[0.00, 1.03]
	Median duration of DEs (months/decade)	[0.00, 0.00]	[0.00, 0.18]	[0.14, 0.26]	[0.15, 0.26]	[0.00, 0.67]
	Median intensity of DEs (SPI/decade)	[-0.02, 0.00]	[-0.03, -0.02]	[-0.04, -0.02]	[-0.05, -0.04]	[-0.14, -0.02]
	Median gap between DEs (months/decade)	[-0.33, 0.10]	[-0.40, 0.00]	[-0.73, -0.36]	[-0.71, -0.38]	[-2.31, 0.28]
Northern Andes	Number of DEs (events/decade)	[0.00, 0.00]	[0.00, 0.00]	[0.00, 0.00]	[0.00, 0.00]	[0.00, 0.00]
	Number of months during DEs (months/decade)	[0.00, 0.00]	[0.00, 0.00]	[0.20, 0.37]	[0.20, 0.35]	[0.00, 1.00]
	Median duration of DEs (months/decade)	[0.00, 0.00]	[0.00, 0.00]	[0.00, 0.21]	[0.10, 0.24]	[0.00, 0.77]
	Median intensity of DEs (SPI/decade)	[-0.02, 0.00]	[-0.02, -0.00]	[-0.03, -0.02]	[-0.05, -0.04]	[-0.08, 0.04]
	Median gap between DEs (months/decade)	[0.00, 0.77]	[-0.19, 0.26]	[-0.69, -0.28]	[-0.62, -0.26]	[-2.50, 1.18]
Northern Cerrado	Number of DEs (events/decade)	[0.00, 0.00]	[0.00, 0.00]	[0.00, 0.00]	[0.00, 0.00]	[0.00, 0.00]
	Number of months during DEs (months/decade)	[0.00, 0.15]	[0.00, 0.15]	[0.18, 0.33]	[0.30, 0.44]	[0.00, 0.83]
	Median duration of DEs (months/decade)	[0.00, 0.00]	[0.00, 0.09]	[0.14, 0.23]	[0.19, 0.29]	[0.00, 0.50]
	Median intensity of DEs (SPI/decade)	[-0.01, 0.00]	[-0.01, 0.00]	[-0.03, -0.02]	[-0.04, -0.03]	[-0.07, 0.04]
	Median gap between DEs (months/decade)	[-0.36, 0.00]	[-0.32, 0.00]	[-0.34, -0.06]	[-0.37, 0.00]	[-1.67, 0.71]
Orinoco	Number of DEs (events/decade)	[0.00, 0.00]	[0.00, 0.00]	[0.00, 0.00]	[0.00, 0.00]	[0.00, 0.00]
	Number of months during DEs (months/decade)	[0.00, 0.00]	[0.00, 0.28]	[0.49, 0.65]	[0.53, 0.67]	[0.00, 1.43]
	Median duration of DEs (months/decade)	[0.00, 0.08]	[0.00, 0.18]	[0.29, 0.41]	[0.28, 0.42]	[0.00, 1.00]
	Median intensity of DEs (SPI/decade)	[-0.02, 0.00]	[-0.02, -0.01]	[-0.05, -0.03]	[-0.06, -0.04]	[-0.11, -0.00]
	Median gap between DEs (months/decade)	[-0.19, 0.19]	[-0.48, -0.05]	[-0.83, -0.48]	[-0.68, -0.39]	[-2.14, 0.31]

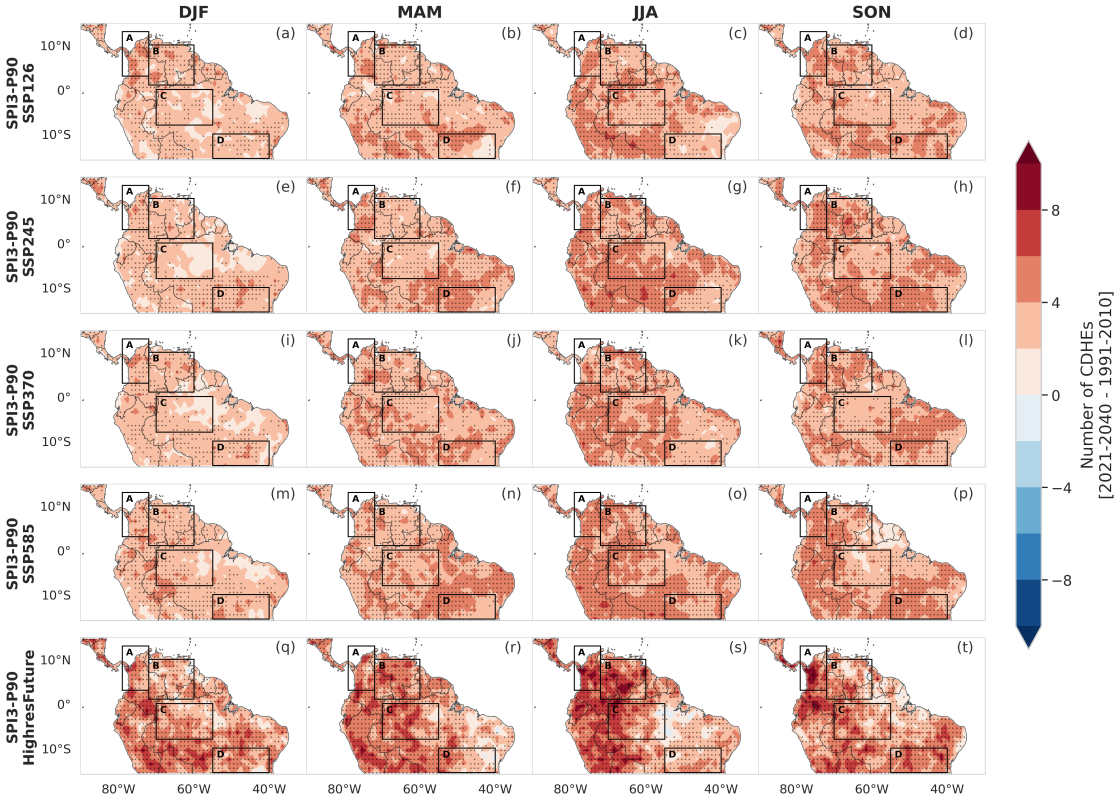

Figure C.9: Projected changes in the seasonal count of Compound Dry and Hot Events (CDHEs) for the near-term period (2021–2040) based on the ensemble median under different emission scenarios: SSP1-2.6 (a–d), SSP2-4.5 (e–h), SSP3-7.0 (i–l), and SSP5-8.5 (m–p) from CMIP6, and HighresFuture (HighresFuture) (q–t) from HighResMIP. Dots indicate grid points where at least 80 % of the CMIP6 or HighResMIP models agree on the sign of the projected change. Black rectangles highlight the four subregions: (A) northern Andes, (B) Orinoco, (C) Brazilian Amazon, and (D) northern Cerrado. All spatial fields are shown at a common resolution of 1° × 1° (based on the second methodology (subsection 5.2.2)).

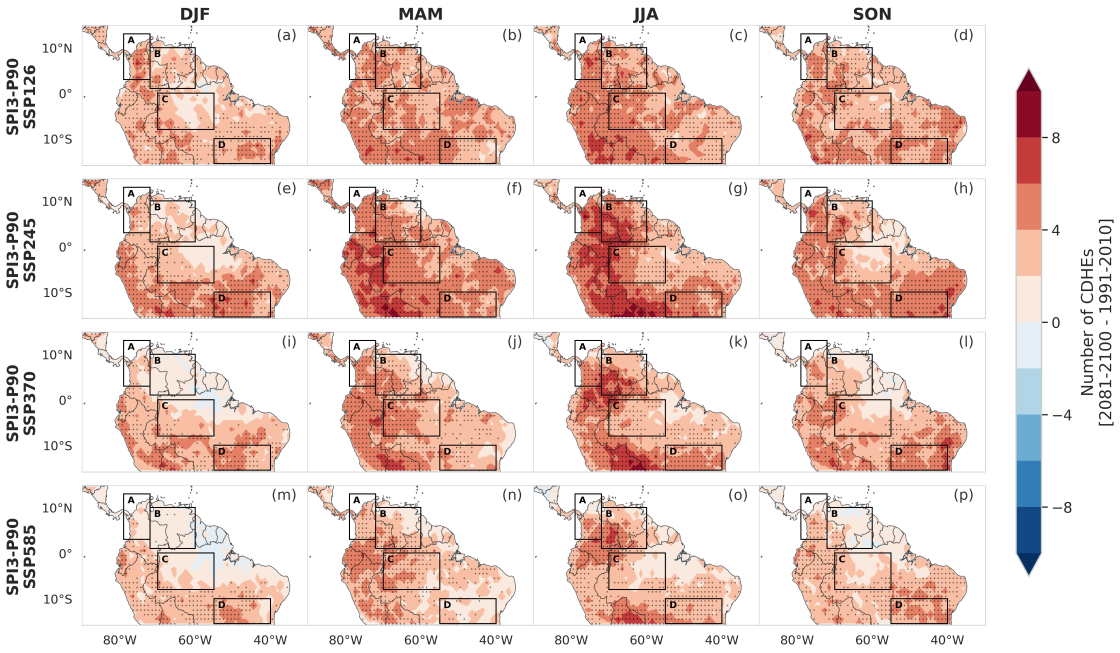

Figure C.10: Projected changes in the seasonal count of Compound Dry and Hot Events (CDHEs) for the long-term period (2081–2100) based on the ensemble median under different emission scenarios: SSP1-2.6 (a–d), SSP2-4.5 (e–h), SSP3-7.0 (i–l), and SSP5-8.5 (m–p) from CMIP6. Dots indicate grid points where at least 80 % of the CMIP6 models agree on the sign of the projected change. Black rectangles highlight the four regions: (A) northern Andes, (B) Orinoco, (C) Brazilian Amazon, and (D) northern Cerrado. All spatial fields are shown at a common resolution of 1° × 1° (based on the second methodology (subsection 5.2.2)).

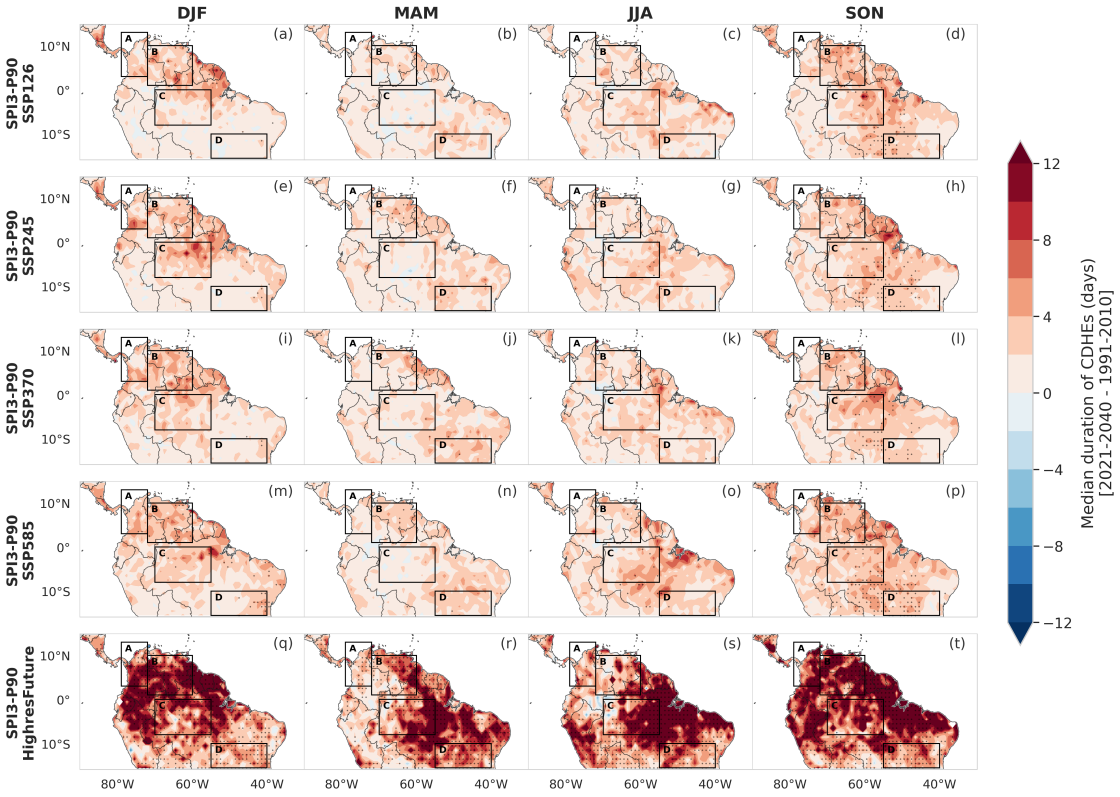

Figure C.11: Projected changes in the seasonal median duration (days) of Compound Dry and Hot Events (CDHEs) for the near-term period (2021–2040) based on the ensemble median under different emission scenarios: SSP1-2.6 (a–d), SSP2-4.5 (e–h), SSP3-7.0 (i–l), and SSP5-8.5 (m–p) from CMIP6, and HighresFuture (HighresFuture) (q–t) from HighResMIP. Dots indicate grid points where at least 80 % of the CMIP6 or HighResMIP models agree on the sign of the projected change. Black rectangles highlight the four regions: (A) northern Andes, (B) Orinoco, (C) Brazilian Amazon, and (D) northern Cerrado. All spatial fields are shown at a common resolution of 1° × 1° (based on the second methodology (subsection 5.2.2)).

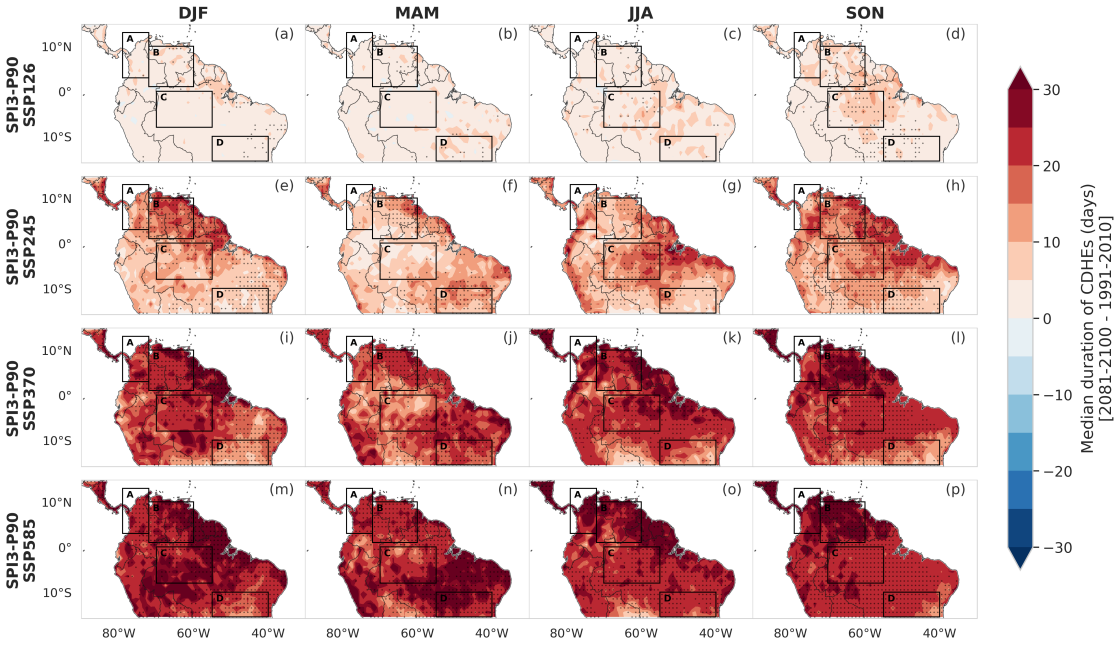

Figure C.12: Projected changes in the seasonal median duration (days) of Compound Dry and Hot Events (CDHEs) for the long-term period (2081–2100) based on the ensemble median under different emission scenarios: SSP1-2.6 (a–d), SSP2-4.5 (e–h), SSP3-7.0 (i–l), and SSP5-8.5 (m–p) from CMIP6. Dots indicate grid points where at least 80 % of the CMIP6 models agree on the sign of the projected change. Black rectangles highlight the four regions: (A) northern Andes, (B) Orinoco, (C) Brazilian Amazon, and (D) northern Cerrado. All spatial fields are shown at a common resolution of 1° × 1° (based on the second methodology (subsection 5.2.2)).

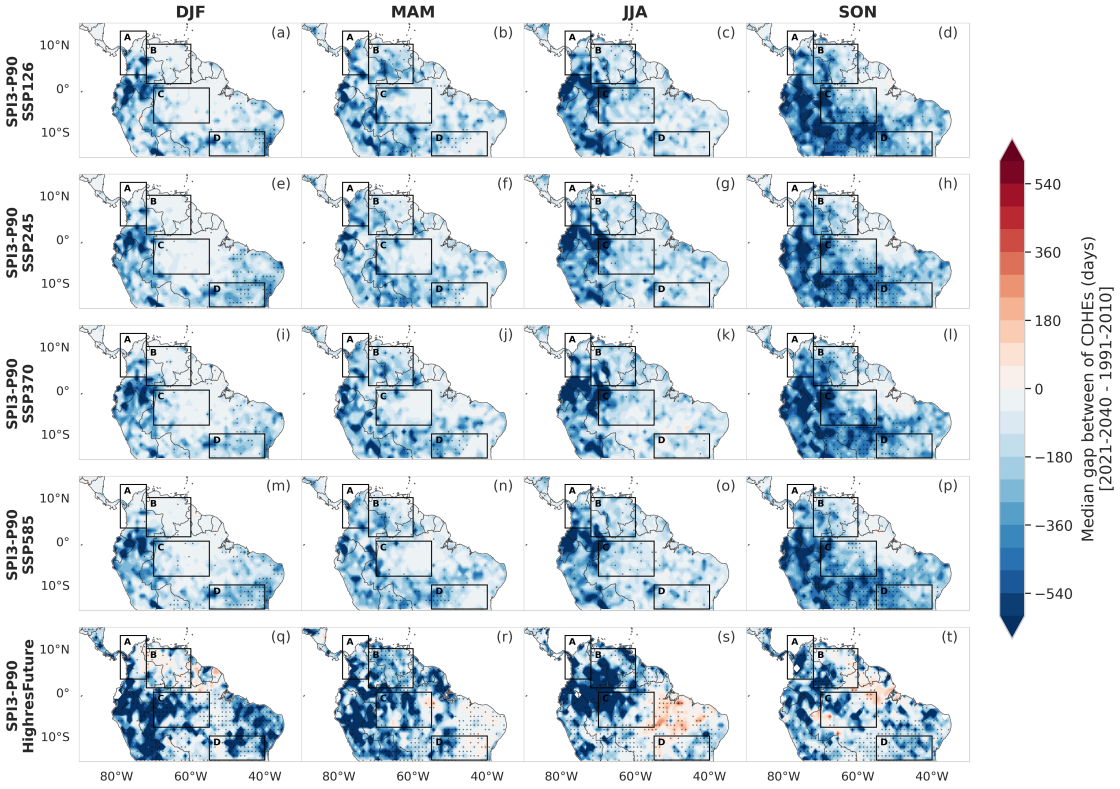

Figure C.13: Projected changes in the seasonal median gap (days) between Compound Dry and Hot Events (CDHEs) for the near-term period (2021–2040) based on the ensemble median under different emission scenarios: SSP1-2.6 (a–d), SSP2-4.5 (e–h), SSP3-7.0 (i–l), and SSP5-8.5 (m–p) from CMIP6, and HighresFuture (HighresFuture) (q–t) from HighResMIP. Dots indicate grid points where at least 80 % of the CMIP6 or HighResMIP models agree on the sign of the projected change. Black rectangles highlight the four regions: (A) northern Andes, (B) Orinoco, (C) Brazilian Amazon, and (D) northern Cerrado. All spatial fields are shown at a common resolution of 1° × 1° (based on the second methodology (subsection 5.2.2)).

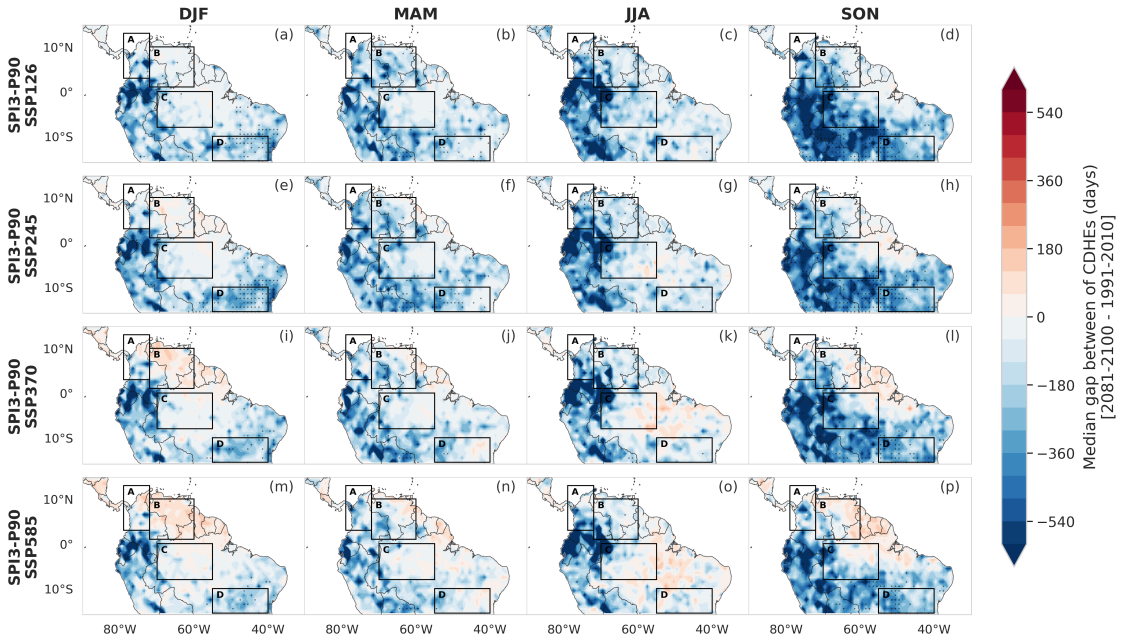

Figure C.14: Projected changes in the seasonal median gap (days) between Compound Dry and Hot Events (CDHEs) for the long-term period (2081–2100) based on the ensemble median under different emission scenarios: SSP1-2.6 (a–d), SSP2-4.5 (e–h), SSP3-7.0 (i–l), and SSP5-8.5 (m–p) from CMIP6. Dots indicate grid points where at least 80 % of the CMIP6 models agree on the sign of the projected change. Black rectangles highlight the four regions: (A) northern Andes, (B) Orinoco, (C) Brazilian Amazon, and (D) northern Cerrado. All spatial fields are shown at a common resolution of 1° × 1° (based on the second methodology (subsection 5.2.2)).

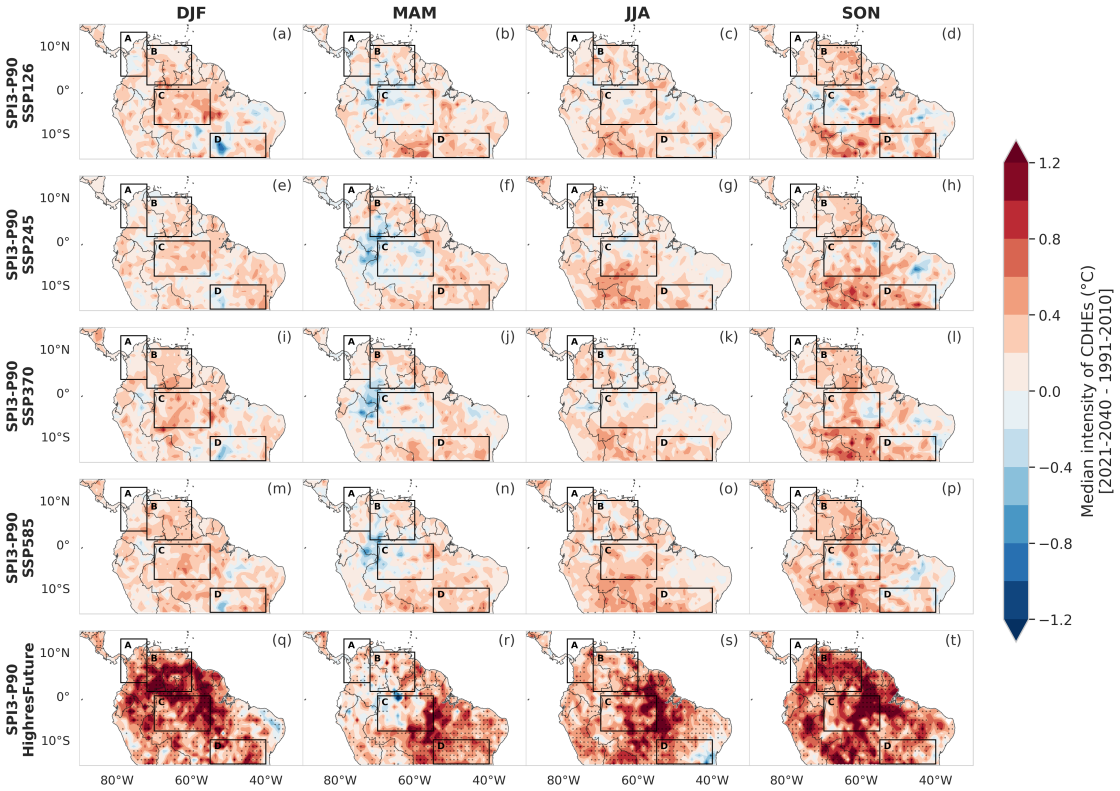

Figure C.15: Projected changes in the seasonal median intensity (°C) of Compound Dry and Hot Events (CDHEs) for the near-term period (2021–2040) based on the ensemble median under different emission scenarios: SSP1-2.6 (a–d), SSP2-4.5 (e–h), SSP3-7.0 (i–l), and SSP5-8.5 (m–p) from CMIP6, and HighresFuture (HighresFuture) (q–t) from HighResMIP. Dots indicate grid points where at least 80 % of the CMIP6 or HighResMIP models agree on the sign of the projected change. Black rectangles highlight the four regions: (A) northern Andes, (B) Orinoco, (C) Brazilian Amazon, and (D) northern Cerrado. All spatial fields are shown at a common resolution of 1° × 1° (based on the second methodology (subsection 5.2.2)).

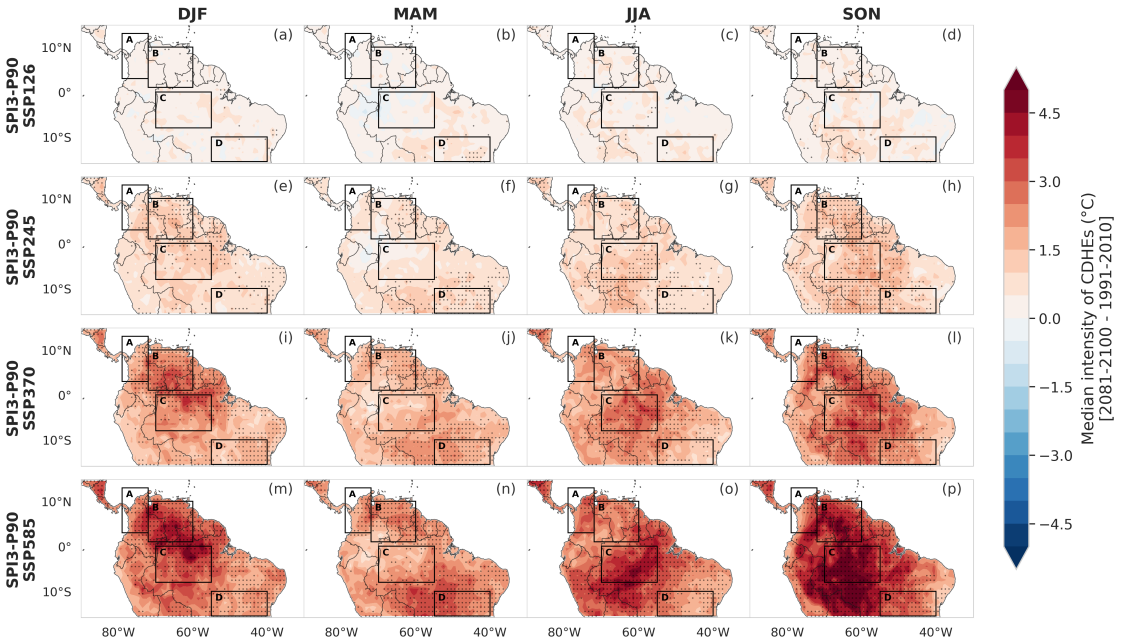

Figure C.16: Projected changes in the seasonal median intensity (°C) of Compound Dry and Hot Events (CDHEs) for the long-term period (2081–2100) based on the ensemble median under different emission scenarios: SSP1-2.6 (a–d), SSP2-4.5 (e–h), SSP3-7.0 (i–l), and SSP5-8.5 (m–p) from CMIP6. Dots indicate grid points where at least 80 % of the CMIP6 models agree on the sign of the projected change. Black rectangles highlight the four regions: (A) northern Andes, (B) Orinoco, (C) Brazilian Amazon, and (D) northern Cerrado. All spatial fields are shown at a common resolution of 1° × 1° (based on the second methodology (subsection 5.2.2)).

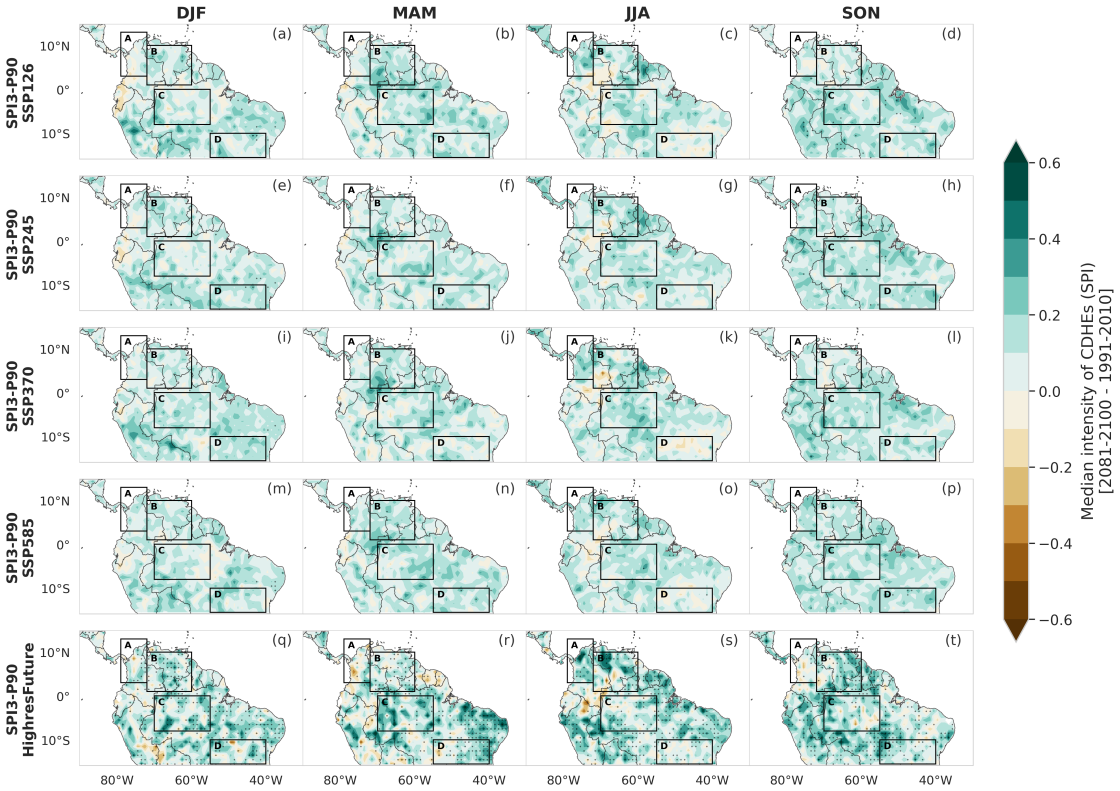

Figure C.17: Projected changes in the seasonal median intensity (SPI) of Compound Dry and Hot Events (CDHEs) for the near-term period (2021–2040) based on the ensemble median under different emission scenarios: SSP1-2.6 (a–d), SSP2-4.5 (e–h), SSP3-7.0 (i–l), and SSP5-8.5 (m–p) from CMIP6, and HighresFuture (HighresFuture) (q–t) from HighResMIP. Dots indicate grid points where at least 80 % of the CMIP6 or HighResMIP models agree on the sign of the projected change. Black rectangles highlight the four regions: (A) northern Andes, (B) Orinoco, (C) Brazilian Amazon, and (D) northern Cerrado. All spatial fields are shown at a common resolution of 1° × 1° (based on the second methodology (subsection 5.2.2)).

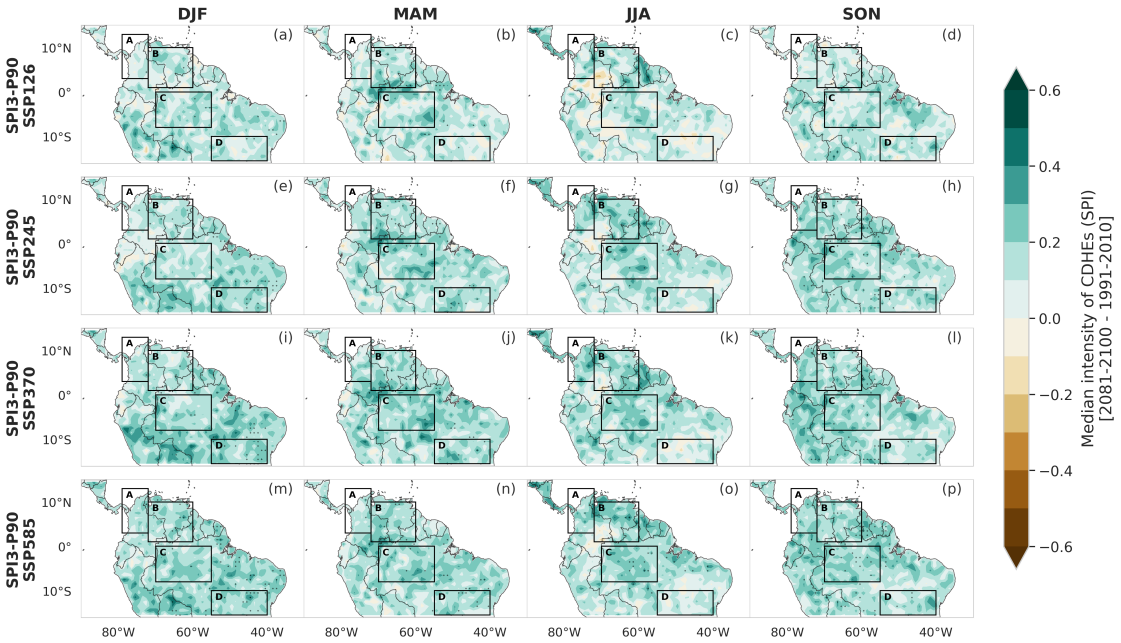

Figure C.18: Projected changes in the seasonal median intensity (SPI) of Compound Dry and Hot Events (CDHEs) for the long-term period (2081–2100) based on the ensemble median under different emission scenarios: SSP1-2.6 (a–d), SSP2-4.5 (e–h), SSP3-7.0 (i–l), and SSP5-8.5 (m–p) from CMIP6. Dots indicate grid points where at least 80 % of the CMIP6 models agree on the sign of the projected change. Black rectangles highlight the four regions: (A) northern Andes, (B) Orinoco, (C) Brazilian Amazon, and (D) northern Cerrado. All spatial fields are shown at a common resolution of 1° × 1° (based on the second methodology (subsection 5.2.2)).

Table C.5: Trends in characteristics of compound dry and hot events (CDHEs) for the northern Andes, Orinoco, Brazilian Amazon, and northern Cerrado regions. Bold values with asterisk (*) denote statistically significant trends (Mann-Kendall test, $p < 0.05$). Negative values indicate decreasing trends. Trends were calculated for all scenarios over the period 2015–2100, except for highres-future, for which the analysis covers the period 2015–2050 due to its shorter temporal extent.

Region	Characteristics	SSP1-2.6	SSP2-4.5	SSP3-7.0	SSP5-8.5	highres-future
Brazilian Amazon	Number of CDHEs (events/decade)	0.00	**0.00***	0.00	**0.00***	0.00
	Number of days during CDHEs (days/decade)	**2.50***	**9.23***	**14.47***	**18.89***	**25.90***
	Median duration of CDHEs (days/decade)	**0.68***	**3.00***	**5.26***	**8.75***	**10.71***
	Median intensity of CDHEs (°C/decade)	**0.06***	**0.20***	**0.35***	**0.53***	**0.72***
	Median intensity of CDHEs (SPI/decade)	-0.01	**-0.01***	**-0.02***	**-0.04***	-0.05
	Median gap between CDHEs (days/decade)	3.30	2.40	**8.80***	**11.89***	25.32
Northern Andes	Number of CDHEs (events/decade)	0.00	0.00	**0.00***	0.00	**0.00***
	Number of days during CDHEs (days/decade)	0.00	**3.90***	**12.34***	**12.65***	**24.12***
	Median duration of CDHEs (days/decade)	0.00	**1.89***	**5.74***	**7.59***	**12.62***
	Median intensity of CDHEs (°C/decade)	**0.05***	**0.15***	**0.30***	**0.43***	**0.47***
	Median intensity of CDHEs (SPI/decade)	-0.00	-0.00	**-0.02***	**-0.04***	-0.02
	Median gap between CDHEs (days/decade)	8.21	**25.00***	**15.41***	**15.93***	29.17
Northern Cerrado	Number of CDHEs (events/decade)	**0.00***	**0.00***	0.00	0.00	0.00
	Number of days during CDHEs (days/decade)	**3.50***	**8.22***	**14.17***	**16.83***	**19.14***
	Median duration of CDHEs (days/decade)	**0.59***	**1.46***	**3.41***	**5.54***	**5.17***
	Median intensity of CDHEs (°C/decade)	0.02	**0.15***	**0.27***	**0.43***	**0.49***
	Median intensity of CDHEs (SPI/decade)	-0.00	-0.00	**-0.02***	**-0.03***	0.03
	Median gap between CDHEs (days/decade)	-3.04	**-2.50***	0.00	**5.97***	-13.48
Orinoco	Number of CDHEs (events/decade)	0.00	0.00	0.00	**0.00***	0.00
	Number of days during CDHEs (days/decade)	**2.11***	**10.00***	**21.58***	**24.53***	**34.64***
	Median duration of CDHEs (days/decade)	**0.61***	**3.39***	**9.46***	**12.50***	**12.30***
	Median intensity of CDHEs (°C/decade)	**0.07***	**0.17***	**0.34***	**0.48***	**0.61***
	Median intensity of CDHEs (SPI/decade)	-0.00	**-0.01***	**-0.03***	**-0.04***	**-0.06***
	Median gap between CDHEs (days/decade)	**6.91***	**13.91***	**11.55***	**11.67***	**27.35***

Table C.6: Uncertainty in the estimated slopes of compound dry and hot events (CDHEs) characteristics for the northern Andes, Orinoco, Brazilian Amazon, and northern Cerrado regions.

Region	Characteristics	SSP1-2.6	SSP2-4.5	SSP3-7.0	SSP5-8.5	highres-future
Brazilian Amazon	Number of CDHEs (events/decade)	[0.00, 0.00]	[0.00, 0.00]	[0.00, 0.00]	[0.00, 0.00]	[0.00, 0.00]
	Number of days during CDHEs (days/decade)	[1.15, 4.07]	[7.75, 10.49]	[12.89, 16.00]	[17.27, 20.49]	[16.15, 38.18]
	Median duration of CDHEs (days/decade)	[0.40, 1.01]	[2.50, 3.44]	[4.55, 6.14]	[7.50, 10.00]	[5.00, 17.00]
	Median intensity of CDHEs (°C/decade)	[0.01, 0.10]	[0.17, 0.22]	[0.32, 0.38]	[0.48, 0.57]	[0.58, 0.90]
	Median intensity of CDHEs (SPI/decade)	[-0.02, 0.00]	[-0.02, -0.00]	[-0.03, -0.01]	[-0.04, -0.03]	[-0.13, 0.02]
	Median gap between CDHEs (days/decade)	[-0.17, 9.10]	[-3.43, 8.05]	[4.41, 12.81]	[7.70, 14.88]	[-15.56, 49.02]
Northern Andes	Number of CDHEs (events/decade)	[0.00, 0.00]	[0.00, 0.00]	[0.00, 0.00]	[0.00, 0.00]	[0.00, 0.36]
	Number of days during CDHEs (days/decade)	[0.00, 1.75]	[2.46, 5.28]	[10.53, 14.29]	[11.05, 14.11]	[14.29, 32.22]
	Median duration of CDHEs (days/decade)	[0.00, 0.33]	[1.18, 2.73]	[5.00, 6.80]	[6.25, 9.00]	[7.69, 18.80]
	Median intensity of CDHEs (°C/decade)	[0.03, 0.07]	[0.14, 0.17]	[0.27, 0.32]	[0.41, 0.45]	[0.38, 0.59]
	Median intensity of CDHEs (SPI/decade)	[-0.01, 0.01]	[-0.01, 0.01]	[-0.03, -0.01]	[-0.05, -0.03]	[-0.09, 0.05]
	Median gap between CDHEs (days/decade)	[-0.44, 16.58]	[17.81, 31.67]	[9.48, 20.06]	[9.73, 21.40]	[-4.38, 66.76]
Northern Cerrado	Number of CDHEs (events/decade)	[0.00, 0.19]	[0.00, 0.13]	[0.00, 0.00]	[0.00, 0.00]	[0.00, 0.59]
	Number of days during CDHEs (days/decade)	[2.08, 4.86]	[7.02, 9.51]	[12.92, 15.36]	[15.56, 17.96]	[10.00, 27.74]
	Median duration of CDHEs (days/decade)	[0.34, 0.82]	[1.21, 1.79]	[3.00, 3.89]	[5.00, 6.43]	[2.86, 8.00]
	Median intensity of CDHEs (°C/decade)	[-0.01, 0.06]	[0.11, 0.18]	[0.24, 0.31]	[0.38, 0.47]	[0.34, 0.68]
	Median intensity of CDHEs (SPI/decade)	[-0.01, 0.00]	[-0.01, 0.01]	[-0.02, -0.01]	[-0.04, -0.02]	[-0.03, 0.08]
	Median gap between CDHEs (days/decade)	[-8.81, 0.79]	[-5.56, 0.00]	[-3.00, 2.88]	[2.31, 9.21]	[-43.18, 9.50]
Orinoco	Number of CDHEs (events/decade)	[0.00, 0.00]	[0.00, 0.00]	[0.00, 0.00]	[0.00, 0.00]	[0.00, 0.42]
	Number of days during CDHEs (days/decade)	[0.67, 3.60]	[8.31, 11.71]	[19.64, 23.23]	[22.33, 26.80]	[18.33, 50.00]
	Median duration of CDHEs (days/decade)	[0.25, 0.91]	[2.86, 3.87]	[8.00, 11.07]	[11.21, 13.75]	[6.25, 23.64]
	Median intensity of CDHEs (°C/decade)	[0.04, 0.09]	[0.15, 0.19]	[0.31, 0.36]	[0.44, 0.52]	[0.50, 0.73]
	Median intensity of CDHEs (SPI/decade)	[-0.01, 0.01]	[-0.02, -0.00]	[-0.04, -0.02]	[-0.05, -0.03]	[-0.12, -0.00]
	Median gap between CDHEs (days/decade)	[0.79, 13.15]	[9.11, 18.44]	[7.65, 15.00]	[8.31, 14.50]	[6.82, 51.39]